KERNFORSCHUNGSZENTRUM

KARLSRUHE

September 1973 KFK 1834

Projekt Schneller Brüter

Analysis of Hypothetical Accidents for SNR-300

G. Heusener, G. Kessler, H. Lauber

GESELLSCHAFT
FÜR
KERNFORSCHUNG M.B.H.

KARLSRUHE

KERNFORSCHUNGSZENTRUM KARLSRUHE

März 1973 KFK 1834

Projekt Schneller Brüter

Analysis of hypothetical accidents for SNR-300

G. Heusener G. Kessler H. Lauber

in collaboration with:

G.J. Fischer, W.R. Bohl, D.H. Cho, F.E. Dunn,
J.F. Jackson, S. Fistedis, A. Machertas,
M. Stevenson, J.R. Travis

Argonne National Laboratory, Argonne,Ill.,USA

K.Doerbecker, H. Lange

Interatom, Bensberg

Gesellschaft für Kernforschung mbH, Karlsruhe

Abstract

Possible effects of extremely hypothetical accident chains are investigated and discussed for the definition of a design basis of the containment system of the DeBeNeLux-Fast-Prototype-Reactor SNR-3oo. Two accident chains are analysed in detail:

- pump coast down with simultaneous failure of the two independent scram systems
- reactivity accidents with simultaneous failure of the two independent scram systems

The accident coarse is followed up to the point were pressure loads are imposed on the reactor tank systems after core disassembly and very rapid energy transfer from hot molten and vapourized fuel to sodium. Maximum strains and stresses in the tank system are calculated and discussed.

Zusammenfassung

Mögliche Auswirkungen extrem hypothetischer Unfallketten werden für den DeBeNeLux-Schnellbrüter Prototyp Reaktor SNR-3oo untersucht und diskutiert , um eine Basis für die Containment-Auslegung zu definieren. Im einzelnen werden zwei Unfallketten analysiert:

- Pumpenausfall mit gleichzeitigem Versagen der zwei unabhängigen Abschaltsysteme
- Reaktivitätsunfall mit gleichzeitigem Versagen der zwei unabhängigen Abschaltsysteme

Der Unfallverlauf wird bis zu dem Zeitpunkt verfolgt, wo das Reaktortanksystem mit Druckbelastungen nach vorhergehender Corezerstörung und sehr schnellem Wärmeübergang von sehr heißem, geschmolzenem und verdampftem Brennstoff an Natrium beaufschlagt wird. Die dabei auftretenden maximalen Spannungen und Dehnungen im Tanksystem werden berechnet und diskutiert.

Preface

The present study was initiated by an exchange of letters between Dr. E.E. Kintner, USAEC/RDT, Dr. R.V. Laney, ANL and Dr. W. Häfele, GfK on an exchange of information concerning results of the analysis of hypothetical accidents and their impact on the definition of the containment design basis for SNR-300.

The calculations were performed at ANL in collaboration between GfK/Interatom and the Reactor Safety and Analysis Division of ANL during October and November 1971. The results were analysed at GfK during 1972. A few additional comparing calculations had to be performed with the codes ARES, DRAP and HEINKO at Interatom in spring 1972.

TABLE OF CONTENTS

LIST OF FIGURES

LIST OF FIGURES (continued)

LIST OF FIGURES (continued)

LIST OF FIGURES (continued)

LIST OF FIGURES (continued)

LIST OF FIGURES (continued)

1 INTRODUCTION

Safe and reliable design of fast reactors ensures accident prevention by a multitude of redundant and diverse trips (first level of incident control). Hence severe accidents can only occur if several of the safety devices fail independent of each other, either simultaneously or one after the other. Since the probability of this kind of failure is extremely low, this type of accident is called hypothetical /1, 2, 3/.

Despite the low probability of occurence, the possible consequences of major hypothetical accidents have to be safely controled in SNR-3oo through special design measures in the construction of the reactor vessel, the primary cooling circuits and the concrete containment (second level of incident control). Thus any major activity release to the outside of the containment is prevented, even for major hypothetical accidents /fig. 1/.

In order to assess the basis for calculations of the design measures required for the reactor vessel and the containment system, all hypothetical incidents that can be imagined have to be investigated with respect to their accident course and consequences /4, 5, 6/. In the licensing procedure of SNR-3oo, two accident chains turned out to be important:

- failure of primary coolant pumps accompanied by the simultaneous failure of the primary and secondary shut down system
- addition of positive reactivity, accompanied by the simultaneous failure of the primary and secondary shut down system.

In the former case, a failure of all three primary coolant pumps is postulated. In order to initiate this hypothetical accident, the following safety devices of the first level of incident control would have to fail simultaneously or successively:

(1) After a decrease in the coolant flow through the core at steady state power, the primary and secondary scram system, actuated by the increasing ratio between neutron flux and primary sodium flow exceeding its limiting value would have to fail. With the coolant flow decreasing at constant power, the core coolant outlet temperature would increase steadily, taking approximately 5 sec to reach the sodium boiling temperature.

(2) The primary and secondary scram systems actuated by the mean core outlet temperature exceeding its limited value would have to fail.

(3) After this intitial phase of approximately 5 sec, in which there could be a certain probability for the operator to initiate a manual scram, the coolant surrounding the most highly rated fuel elements would start boiling. Under certain conditions, fuel pins with high burnup would fail also and release fission gas. In this way, reactivity changes and increases in the neutron flux would be caused through the sodium void effect which:
(4) would actuate the primary and secondary scram system by exceeding the limiting value of the neutron flux in the power range. For SNR-3oo this scram initiation would be reached at 112 % of the design power for the primary shut down system and at 12o % of the design power for the secondary shut down system. Another o.2 sec would pass until the shut down rods of the primary and secondary systems would drop. As will be shown below, a power peak caused by sodium boiling would be accommodated by the doppler effect and most probably it would be possible to shut down the reactor in time, by the secondary shut down system.

Only if this fourth and last double barrier (primary and secondary shut down systems) of the first level of engineered safeguards should also fail, will there be sodium boiling in the entire reactor core with dryout of the sodium film at the cladding surface, melt down of the cladding, melting of the fuel with subsequent slumping and finally core disassembly caused by a Bethe-Tait-excursion.

For the second accident chain the following safety devices would have to fail simultaneously or consecutively: After introduction of a positive reactivity ramp there will be an increase in neutron flux and scram will be initiated by exceeding the limiting value in the power range. This scram initiation would be reached at 112 % of the design power for the primary shut down system and at 12o % for the secondary shut down system. At positive reactivity ramps smaller than approximately 5 to 8 $/sec both the absorber rods of the primary and of the secondary shut down system would be actuated in time. As soon as the super prompt critical conditions had been reached, the doppler coefficient would limit the increase in power /7,8/ and the shut down rods would safely scram the reactor /2,3,9/. This fact has been demonstrated convincingly by the super prompt critical experiments with SEFOR /7,8,1o,11,12/.

Only if this scram initiation should fail for both shut down systems, which are designed with a high degree of diversity and redundancy, the following chain of events would occur very rapidly:

- fuel melting, fuel pin failure with subsequent thermal interaction between the molten fuel and the sodium, sodium expulsion from the coolant channel and a positive sodium void reactivity effect that could lead to an increased positive ramp insertion.

However, three main cases must be distinguished:

α) for very small positive ramps of reactivity introduction there will always be sodium boiling in the cooling channel before a sufficient cross section of fuel is molten causing failure and a subsequent fuel-coolant interaction. This makes the course of the accident in principle, similar to that of the pump failure case, and, in addition the safety barriers 2) to 4) discussed above would have to fail as well. The initial phase up to the point of sodium boiling would of course be shorter in this case.

β) for larger reactivity ramps, the range up to a few $/sec, there would be fuel melting, fuel pin failure with a subsequent thermal interaction between the molten fuel and the sodium. This would very quickly cause either additional superposition of positive ramp contributions and initiate disassembly or shut the reactor down earlier by causing negative ramp contribution through fuel movement /13/.

γ) for reactivity ramps larger than 1o $/sec, the reaction times of the primary and secondary shut down systems are too long. Even if the scram would be actuated, the chain of events resulting in subsequent fuel pin failure would occur so rapidly, that core disassembly with a simultaneous thermal interaction between molten fuel and the sodium will have been completed before the shut down rods would even become operative.

Large positive reactivity contributions with ramps of incident initiation in excess of 1o $/sec have been identified for SNR-3oo so far for only a small number of theoretically constructed cases, such as:

- a coherent argon gas bubble migrating through the center of the core. This would generate maximum reactivity ramps of 55 $/sec. However, SNR-3oo has a gas separator running gas bubbles through the radial blanket area. In addition hydraulic tests performed on FFTF have shown that major gas bubbles are decomposed into a number of individual little bubbles in the inlet plenum /14/.

-ejection of an absorber rod preceded by a separation between the absorber rod and the guide mechanisms followed by a total blockage of the coolant channel with subsequent sodium boiling. This accident is prevented in SNR-3oo by a special design of the absorber guide rods /3/.

- local blockage in a fuel element with subsequent boiling, fuel melting and a thermal interaction between molten fuel and sodium which could result in a propagation of the damage from subassembly to subassembly. Whether this so called single-subassembly event is at all capable of generating ramps in excess of 1o $ is still the subject of an experimental program. All calculations performed so far seem to indicate the opposite /3/.

The detailed chain of events for the first accident chain (pump failure) are investigated and discussed in sections 4.1.1 and 4.1.2 of this report. Results are reported for both a fresh core and a so called equilibrium core. The case of a reactivity ramp rate of 5 $/sec with subsequent fuel pin failure and sodium expulsion due to the thermal interaction between molten fuel and coolant will be described in section 4.1.3 below. As in /4/, this case of a reactivity ramp rate of 5 $/sec is intended to serve only as a characteristic example of the course of an incident in this ramp range. Hence, it is not based on a realistic accident initiation. The case of the expulsion of an absorber rod after preceding total blocking of the coolant channel and the case of a coherent argon gas bubble are without any significance to SNR-3oo.
Nevertheless, the expulsion of an absorber rod has been analysed and will be described in section 4.1.4.

Fig. 1 Levels of incident control

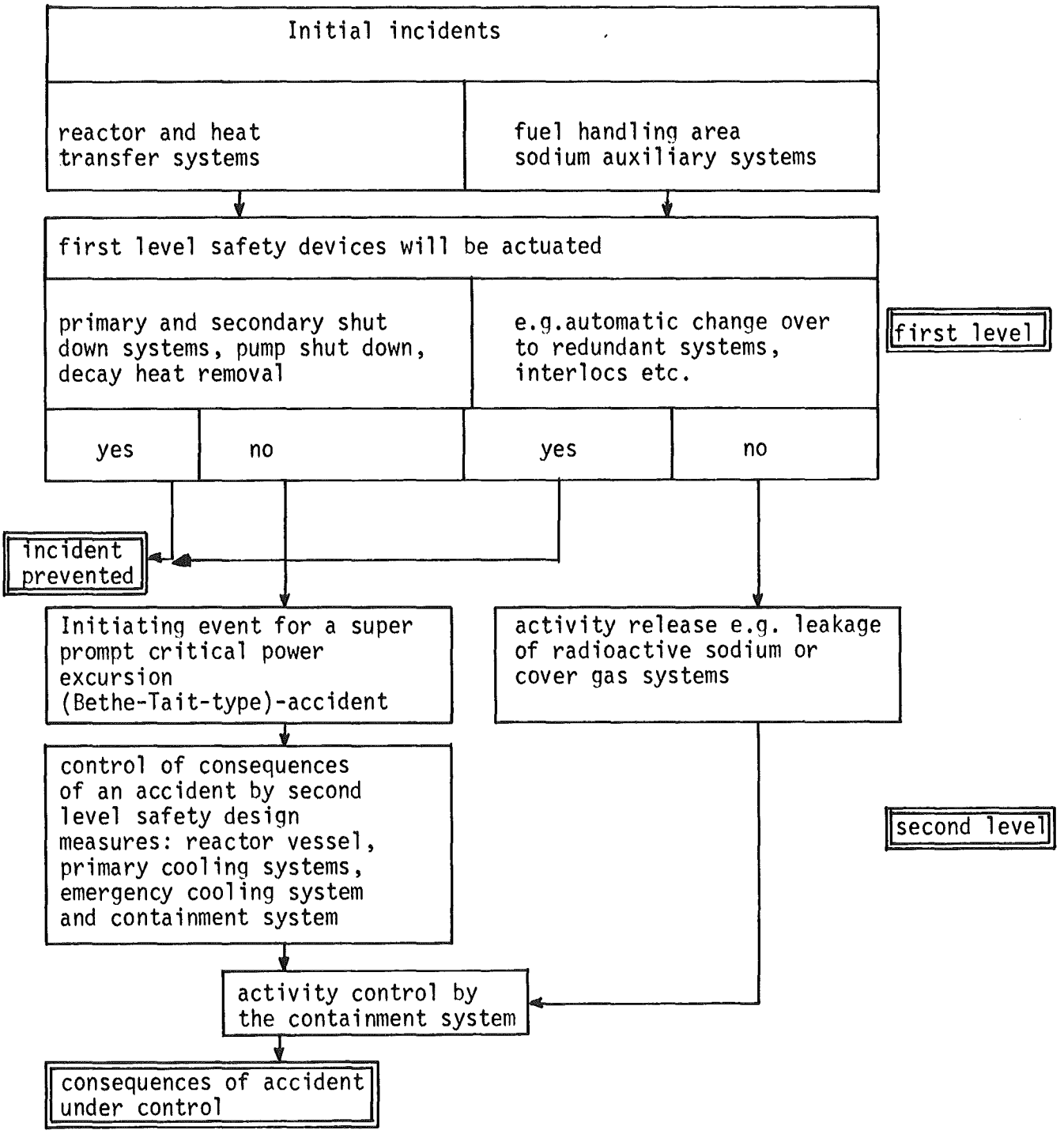

2. ANALYTICAL METHODS AND COMPUTER CODES

Analytical methods and computer codes used to describe the phenomena occuring in the reactor core and reactor vessel, during four different accident phases are shown in fig. 2.1. The four different accident phases to be described are:

- accident events in the predisassembly phase
- core disassembly phase
- energy release during core disassembly and energy transfer from hot molten fuel to sodium
- mechanical effects and deformations of the reactor vessel

The events occuring during the predisassembly phase are described by the SAS2A-code / 15,16, 17, 18, 19, 2o, 21/ in which the initiating hypothetical incidents are given as input. SAS2A then calculates the reactivity, power and temperature as a function of time taking into account fuel pin failure, sodium boiling and fuel pin slumping /22, 23/.

At a sufficiently high fuel temperature and shortly in advance of super prompt criticality, all data for reactivity, power, temperature field and core compositions are passed on from SAS2A to the VENUS-code /24, 25, 26/. VENUS calculates the pressure buildup in the fuel as a consequence of rising fuel temperatures and determines the material displacement. It also accounts for the negative doppler-coefficient.

During and after core disassembly, thermal energy can be transfered from hot molten fuel to sodium leading to a conversion into mechanical energy. These events of energy transfer and of the vapour pressure buildup are described by the fuel coolant interaction model of D.H. Cho and R.W. Wright /21/. This rapid pressure buildup within the core zone results in strains and stresses within the elastic-mechanical system represented by the sodium filled reactor vessel containing a shield tank, a perforated plate and the vessel cover being clamped down by strainbolts. Deformations and stresses within this system are calculated by the codes REXCO-H /27, 28/ ARES, DRAP and HEINKO /29, 3o, 55/.

After absorption of the mechanical energy within the tank system, partly molten fuel, together with sodium will remain in the reactor vessel. Cooling of these molten core masses is a long time problem and will not be dealt with in this report /3/.

2.1 Course of accident during the predisassembly phase - SAS2A-Code

SAS2A is a multichannel dynamics code using point kinetics and consists of individual modules to calculate

- neutron kinetics
- temperature field in the fuel, cladding, coolant and structural material
- sodium boiling and ejection from coolant channels
- stresses and strains in the fuel cladding
- fuel pin slumping
- feedback effects

The reactor core can be represented by a maximum of ten coolant channels. Each channel consists of a fuel pin and its respective coolant and structural material. Axially, the channel may be subdivided into a maximum of 3o sections. Radially, up to 1o temperature points are calculated in the fuel pellet, three in the cladding, and one mean temperature for coolant and structural material. For the heat transfer in the gap between the fuel and the cladding, heat transfer coefficients depending on temperature and contact pressure are used. Heat transfer by radiation is also included /15, 17/.

Sodium boiling and ejection phenomena from coolant channels are described by the multiple boiling model of F. Dunn /16,17 /. This boiling model can also take into account sudden fission gas releases from failing fuel pins which may occur shortly before or during sodium boiling. Introducing a certain sodium superheat, this multiple bubble model describes the formation and dynamic behavior of sodium vapour bubbles in cooling channels accounting for sodium superheat. Pressure gradients within individual vapour bubbles and dryout of a thin sodium film at the cladding are included
On the basis of the transient fuel and cladding temperatures, the stresses and deformations within the fuel pin cladding can be determined by the model of K. Watanabe /18/.
After fuel pin failure, molten fuel may contact the sodium still contained in the coolant channel. Energy transfer between molten fuel and sodium may give rise to buildup of sodium vapour pressure and to axial movement of sodium and fuel. This energy transfer is described by the model of Cho-Wright /21/.
Melting of the fuel pin cladding after dryout of the sodium film and subsequent melting of the fuel may ultimately result in fuel slumping. This slumping process and the positive changes of reactivity it causes, are described by the model of W. Bohl /22, 23/.

SAS2A simulates and calculates the course of accidents in the predisassembly phase up to the time at which the fuel temperatures are so high and the net reactivity is so close to super prompt criticality that core disassembly is imminent.

2.2 Course of accident during the disassembly phase - VENUS-Code

SAS2A then transfers the space dependent temperature-, density-, and coolant void data as well as transition conditions for power, concentrations of delayed neutron emitters, net reactivity, and the reactivity ramp to the VENUS-code /24/. VENUS calculates the time dependent 2-dimensional temperature-, pressure-, density-, and fuel displacement fields within the reactor core for a maximum number of 53o mesh points and 2o material zones. VENUS is able to take into account both sodium-in and sodium-out equations of state for the individual material zones as well as effects of porosities and fission gas on the equation of state for fuel /25/.

A model similar to that developed by Cho-Wright /21/ is used in VENUS to describe accident events during disassembly in which energy transfer from molten fuel to sodium can occur. This can lead to subsequent additional pressure buildup, as well as sodium and fuel movements. Prefered directions of movement, which are given by the structure of the subassembly, are also treated in VENUS /26/.

The disassembly phase is terminated within a few msec by the negative doppler coefficient and the effects on reactivity resulting from material displacements. Final results of disassembly calculations with VENUS are a space dependent pressure and temperature field and the thermal energy released during the disassembly accident. With these data in hand it is then possible to determine the mass of molten fuel.

2.3 Energy release during and after core disassembly

After termination of a nuclear excursion by core disassembly, mechanical work can be performed by either expansion of evaporated fuel or expansion of sodium and sodium vapor after the available thermal energy has been transfered from the molten fuel to the surrounding sodium.

The possible mechanical work is determined by a theoretical model in which molten fuel is mixed with sodium assuming a certain time constant for mixing and dispersion of the molten fuel. The fuel, consisting of small particles with a specific particle density distribution, transfers thermal energy to the surrounding liquid sodium. In this way, sodium is heated up and evaporates in a very short time. As a consequence, pressure builds up in the mixing zone. The liquid sodium resting on top of this mixing zone will be moved. This process is also described by the model of Cho and Wright /21/.

2.4 Mechanical effects and deformations of the reactor vessel system

On the basis of the conceptual model described above and the results of the pressure time history within the mixing zone, strains and stresses in the vessel system are determined by means of the codes REXCO-H /27, 28/ ARES /29/, DRAP /3o/ and HEINKO /55/.
REXCO-H /27, 28/ and ARES /29/ are two-dimensional codes which calculate the hydrodynamic and the elastic-plastic propagation of shock waves from the core region and their effects on the surrounding materials, and steel structures. A difference is made between hydrodynamic areas containing only liquids or gases and areas consisting of steel structures. The hydrodynamic areas are considered as compressible liquids, while the theory of thin shells is used to describe the elastic-plastic behavior of the steel structures. The partial differential equations of hydrodynamics and strength are solved by finite element methods in a Lagrange formalism. Any shock waves that mightoccur are taken into account by introduction of an artificial viscosity using the method of von Neumann. Starting with given boundary conditions and suitable equations of state for the individual materials, the local displacements, material velocities, pressures, specific energies, material densities and expansions are calculated as functions of time on the basis of the given initial pressure and energy distribution. Through the introduction of yield and rupture criteria, and the correction of stress tensors, ARES can also be used to deal with steel structures which are either plastically strained, show embrittlement phenomena or may be subject to rupture.

REXCO-H and ARES, however, are used only to describe the dynamic behavior in the initial range up to a few 1o's of msec, since the numerical methods used require rezoning of the mesh grid and long computer times. For longer time periods, liquid movements in the reactor vessel are to be described and friction effects are to be taken into account. Therefore, it is advisable to apply such codes as HEINKO /55/ and DRAP /3o/. These codes cover the range up to several hundreds of msec with tolerable computer times. HEINKO is a one-dimensional code which numerically solves the compressible hydrodynamics equations by means of the method of characteristics.
To calculate nonsteady state flow phenomena in the reactor vessel, it is possible to take into account friction losses due to structures and the elasticity of the shield tank. For the studies described in this report, HEINKO was used mainly to calculate the stress in the perforated dip plate of SNR-3oo due to incoming shock waves. The necessary input data were taken from calculations with REXCO-H, which is unable to deal exactly with the flow phenomena and friction effects caused by the perforated dip plate.

DRAP is a quasi-two-dimensional code describing dynamical processes within the reactor vessel by solving the incompressible hydrodynamic equations. In this case, the events in the core region can be simulated by giving an equation of state H (p,v) = o, and defined initial and boundary conditions for pressure and volume. The reaction bubble of the core region performs mechanical work by way of expansion, thereby accelerating the liquid sodium in the radial and axial directions. Losses of pressure due to friction caused by flow movement through tank components, such as the shield tank and the dip plate, are taken into account. The nonsteady state pressure distribution in sodium has an effect on the steel structures whose stresses and strains are determined by taking into account elastic-plastic behavior of the material. The main application of this code, in addition to the calculation of stresses and strains in the shield tank and the reactor vessel, is the optimization of the conditions of perforation of the dip plate.
This is to reduce the water hammer effect acting upon the top of the vessel. In addition, it is possible to determine the stress acting on the stretch bolts of the top plug. These stretch bolts are stressed on the one hand by the transfer of the liquid friction acting upon the perforated dip plate and by the compression of the inert gas due to the sodium flow in the upper direction. The advantages and disadvantages of the codes in this last phase of an accident are summarized in table 2.1.

Table 2.1

Comparison of the characteristics of the HEINKO, ARES, REXCO-H and DRAP-codes

	HEINKO	ARES	REXCO-H	DRAP
Characteristics				
mathematical methods	method of charact.	Lagrange-mesh	Lagrange-mesh	Runge-Kutta
geometry	1-dim.	2-dim.	2-dim.	2-dim.
sodium is taken into account as being	compress.	compress.	compress.	incompress.
rezoning required	no	yes	yes	no
comparison of computer time	2o min+ for 5oo msec real time	3oo-5oo longer than HEINKO	3oo-5oo longer than HEINKO	comparable to HEINKO

+ on a CDC 64oo

Fig. 2: Information Flow during hypothetical accident calculations

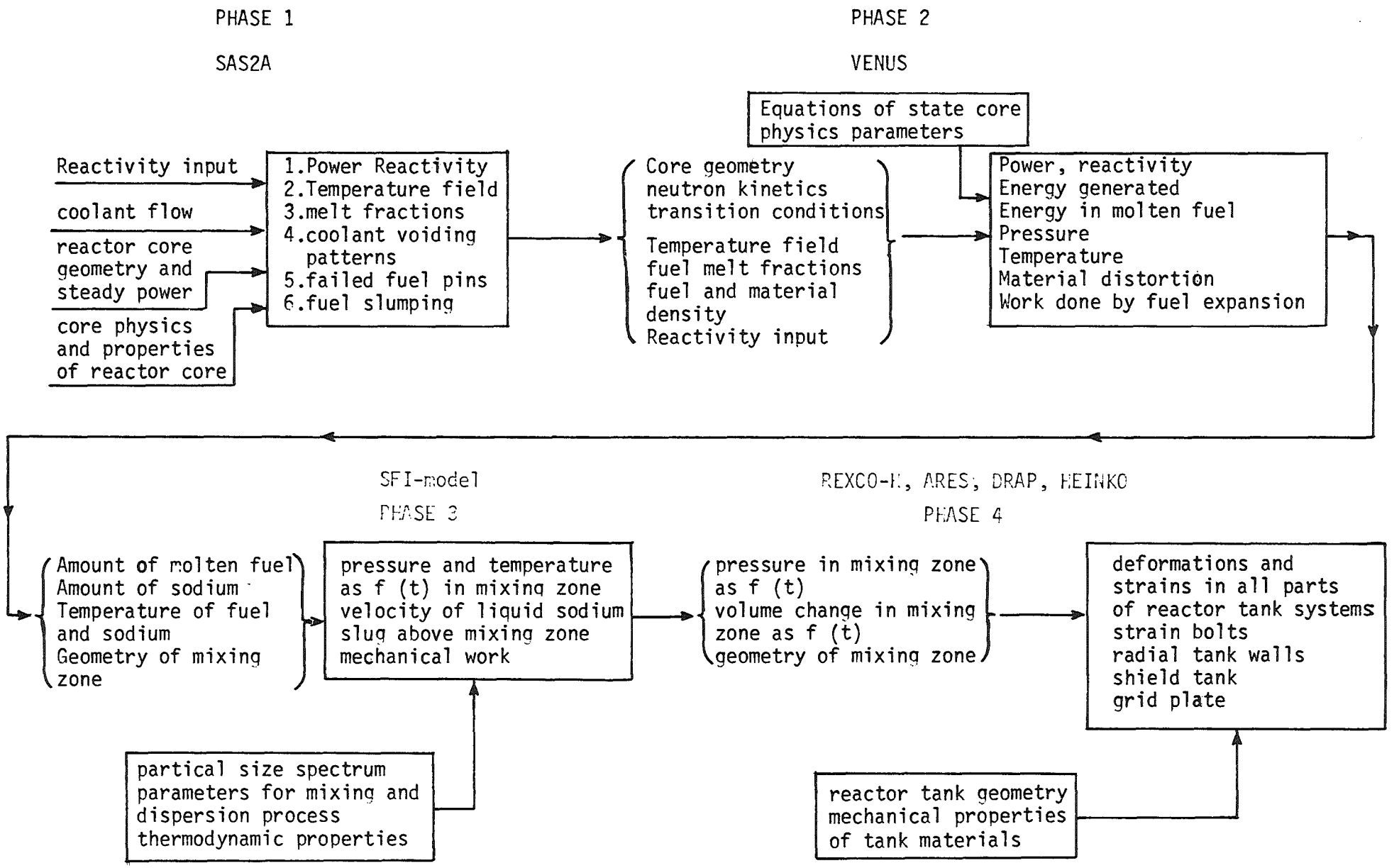

3. DESCRIPTION OF SNR 3oo AND INPUT CALCULATIONS

The core of SNR-3oo has a thermal reactor power of 73o MW. This thermal power is supplied to 3 steam generators via 3 primary and 3 secondary circuits. Twelve steam generators generate steam at 17o atm and 5oo^{o}C. The electrical power is 3oo MW.

The reactor core consists of two zones of different enrichment and 151 fuel elements, each containing 169 fuel rods filled with PuO_2-UO_2-pellets. Six shut down rods and 12 shim control rods provide the necessary negative reactivity for 2 independent scram systems. The core with blankets, is arranged in a double walled reactor vessel with a triple rotating plug for refueling. The reactor vessel and the primary circuit system are surrounded by an inner concrete containment filled with nitrogen. This inner containment in turn is surrounded by an outer containment /2, 3, 31/.

Fig. 3.1 shows the reactor core and its subdivision into annular channels used for SAS2A calculations. A total of 5 annular channels were selected for the inner core zone, 3 annular channels for the outer core zone and 1 annular channel for the radial blanket. The annular ring of fuel elements located at the transition from the inner to the outer core zone contains fuel elements of the inner and outer core zone. It is therefore represented by 2 separate annular channels making 1o annular channels in all. The axial subdivision of an annular zone with its break down into zones for fuel pins, cooling channel, and structural material is shown by fig. 3.2.

The resultant mesh grid for SAS2A calculations is shown in fig. 3.3. The radial break down for calculating the temperature field in the fuel pellet, cladding, coolant channel and structural material is evident from fig. 3.4.

For VENUS calculations the mesh grid shown in fig. 3.5 was used, with the finer VENUS mesh grid being superimposed on top of the coarser SAS2A mesh grid. For the two-dimensional diffusion calculations determining the input data for SAS2A and VENUS, an even finer break down of mesh points, superimposed on the VENUS mesh was selected. Fig. 3.6 shows the idealised geometry of the vessel structure for REXCO calculations.

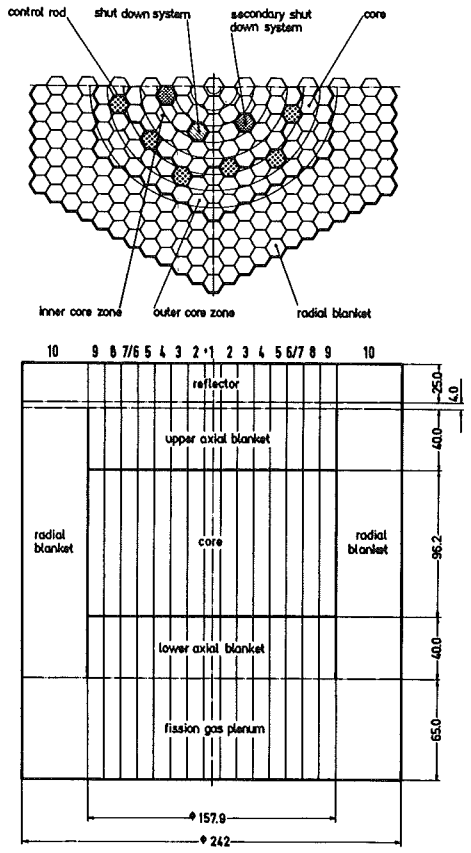

Fig. 3.1 **Core crossection of SNR 300**
Channels used in the SAS2A calculations

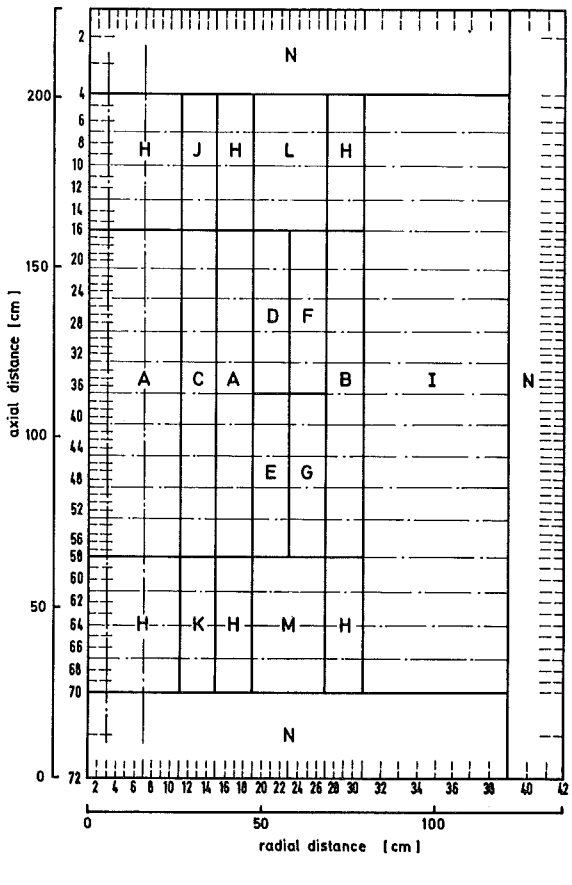

—·— Mesh grid used in SAS2A calculations

Fig. 3.3 Material zones and geometry used in the diffusion calculations

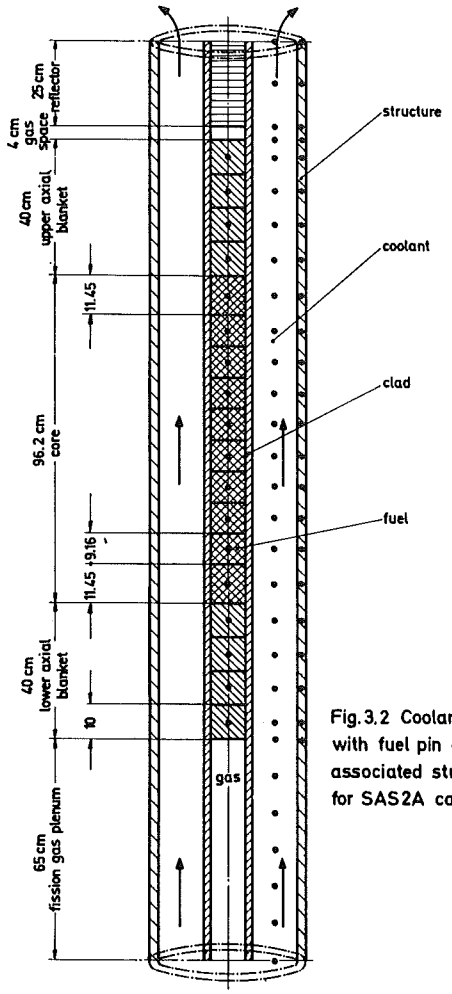

Fig. 3.2 Coolant channel with fuel pin and associated structure for SAS2A calculations

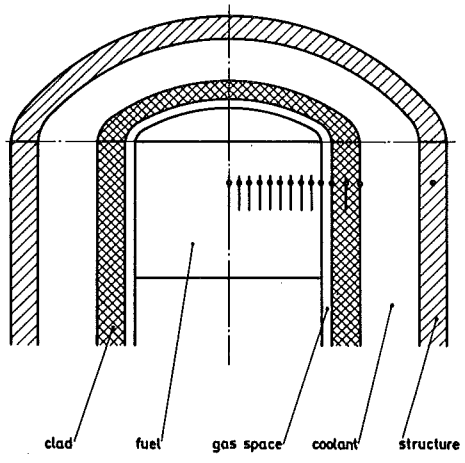

Fig. 3.4
Model for calculation of the temperature field in fuel, clad, coolant and structure

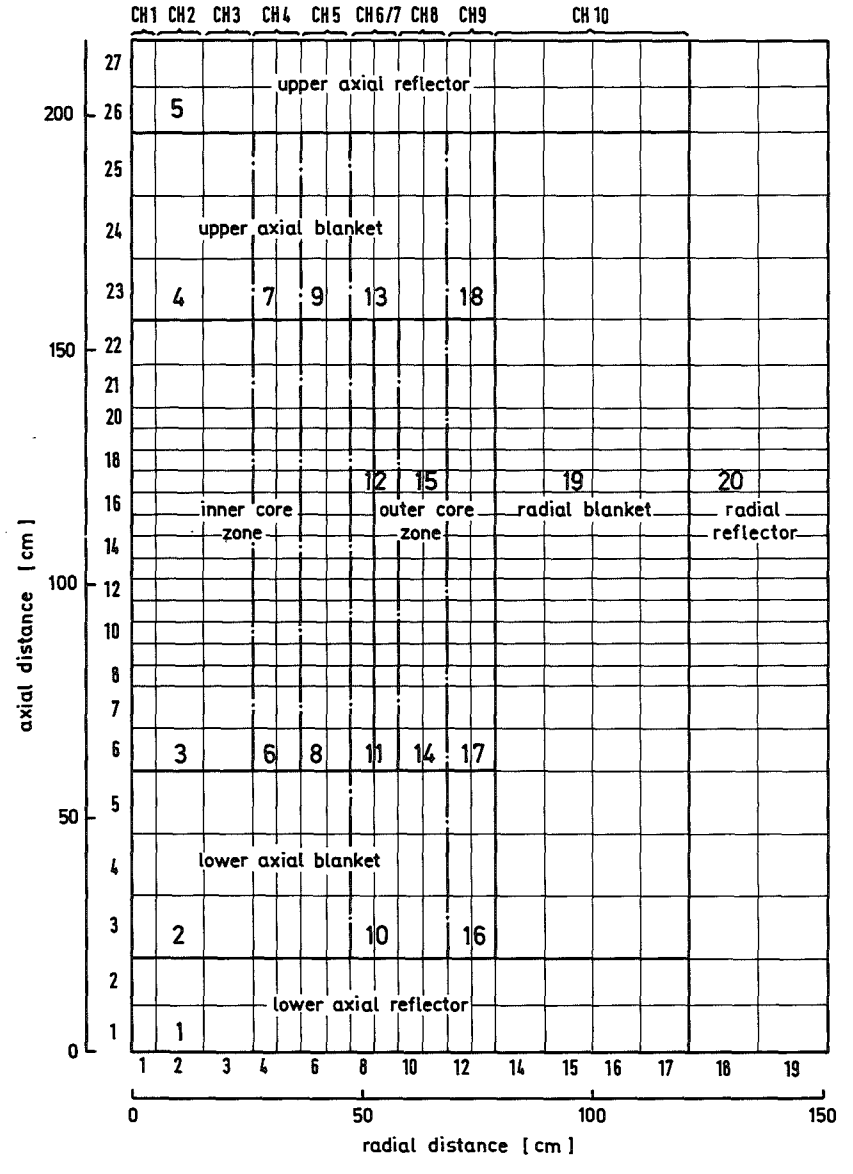

Fig. 3.5 Mesh grid and regions used in VENUS calculations

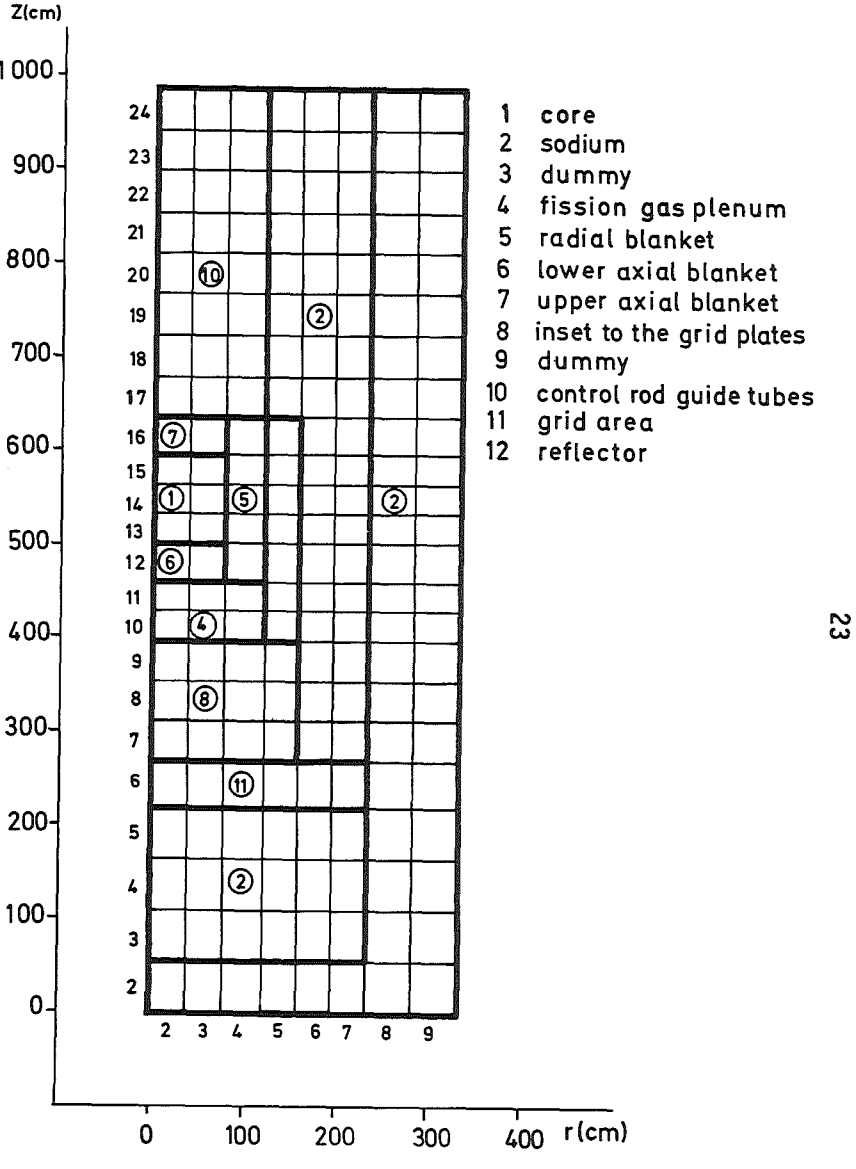

Mesh grid used in REXCO calculation: (vessel model 1)

Fig. 3.6

3.1 Geometrical and nuclear input data

In order to have a consistent data set for the nuclear properties of SNR-3oo, 2-dimensional diffusion and perturbation calculations were performed for the "clean" reactor core (fresh core).

3.1.1 Description of core structure

Fig. 3.1 shows the assignment of fuel element positions in the first and second enrichment zones, respectively. For power flattening reasons the core has 2 enrichment zones. The radial blanket consists of 228 blanket elements. The thickness of the upper and lower axial blankets is 4o cm each. To determine the material compositions, all elements of a hexagonal ring were smeared on a circular ring as outlined in fig. 3.1. In so doing, it was assumed that the shut down rods were located in the upper axial blanket whereas the shim rods reached down to the middle of the core. The material distribution in the reactor obtained with these assumptions is represented in fig. 3.3. Table 3.1.1 indicates the volume fractions of the individual mixtures.

Table 3.1.1 Composition of material zones according to fig. 3.1

Symbol	Composition of mixture	steel	Na	fuel	absorber	Pu-enrichment /at/%/
A	core zone 1	o.2o2	o.478	o.32o	-	22.3
B	core zone 2	o.2o2	o.478	o.32o	-	32.2
C	core zone 1, follower	o.187	o.599	o.214	-	22.3
D	core zone 1, core zone 2, absorber	o.212	o.469	o.256	o.o63	24.7
E	core zone 1, core zone 2, follower	o.194	o.55o	o.256	-	24.7
F	core zone 2, absorber	o.21o	o.471	o.267	o.o52	32.2
G	core zone 2, follower	o.195	o.538	o.267	-	32.2
H	axial blanket	o.2o2	o.478	o.32o	-	o
I	radial blanket	o.233	o.312	o.455	-	o
J	axial blanket, absorber	o.218	o.464	o.214	o.1o4	o
K	axial blanket, follower	o.188	o.599	o.214	-	o
L	axial blanket, absorber	o.211	o.47o	o.262	o.o57	o
M	axial blanket, follower	o.194	o.544	o.262	-	o
N	reflector	o.2	o.8	-	-	o

The diffusion and perturbation calculations were performed with a two-dimensional code using 26 energy groups. The mesh grid used is shown in fig. 3.3. The group constants were determined by means of the Karlsruhe MOXTOT-group set /32/.
The most important input quantities to the diffusion calculations are summarized in table 3.1.2.

Table 3.1.2 Summary of input data for the diffusion calculations

Geometry:		
core diameter	(cm)	157.9
core height	(cm)	96.24
thickness of radial blanket	(cm)	42
thickness of axial blanket	(cm)	4o
volume fractions	see table 3.1.1	
fuel density:		
core (% TD)		8o
axial blanket (%TD)		9o
radial blanket (%TD)		9o
enrichment	see table 3.1.1	
Pu-composition:		
Pu 239/Pu 24o/Pu 241/Pu 242		o.75/o.22/o.25/o.oo5
fuel:	PuO_2-UO_2	
absorber:	B_4C	
fuel temperature: (^oK):	1473	

3.1.2 Core physics parameters

3.1.2.1 Doppler coefficient

For the accident analysis the doppler coefficient must be calculated with respect to the following two problems:

α) the absolute magnitude of the doppler coefficient under operating conditions with its dependence on fuel temperature and sodium content of the core

β) the local distribution of the doppler coefficient

Magnitude of the doppler coefficient as a function of fuel temperature and the sodium content of the core

To determine the temperature dependence of the doppler coefficient diffusion calculations were performed at three different fuel temperatures: 300°K, 1473°K and 2100°K. In addition the sodium fraction in the core was changed. The following three cases were studied:

case 1: the whole core is filled with sodium

case 2: the core is completely voided up to a radius of 57.42 cm, the remaining part of the core as well as the axial and the radial blankets are filled with sodium

case 3: the entire core and the axial blanket are voided; the radial blanket is filled with sodium.

Table 3.1.3 shows the differences in k_{eff} obtained in these calculations.

Table 3.1.3 differences in k_{eff} at 3 fuel temperatures and various sodium contents in the fuel

	case 1	case 2	case 3
T_{fuel}	k_{eff} (T) - k_{eff} (1473)	k_{eff} (T) - k_{eff} (1473)	k_{eff} (T) - k_{eff} (1473)
300	0.0084	0.0062	0.0053
1473	0	0	0
2100	-0.0016	-0.0013	-0.0011

It is assumed that the dependence of the doppler coefficient on temperature can be represented by a relationship of the kind:

$$\frac{1}{k}\frac{\partial k}{\partial T} = A \times T^{-1} + B \times T^{-1,5}$$

The values for the constants A and B resulting from the diffusion calculations are indicated in table 3.1.4. In addition, the resultant average doppler constant for a fuel temperature of $1473^{o}K$ is given:

$$\frac{1}{k}\frac{\partial k}{\partial T} \times T = DC\ (1473) = A + \frac{B}{\sqrt{1473}}$$

Table 3.1.4 coefficients of temperature dependence of the doppler coefficient:

$$\frac{1}{k}\frac{\partial k}{\partial T} = A \times T^{-1} + B \times T^{-1,5}$$

DC (1473): average doppler constant at $T = 1473^{o}C$

	case 1	case 2	case 3
A	-3.3626×10^{-3}	-3.3205×10^{-3}	-2.7859×10^{-3}
B	-4.8124×10^{-2}	-1.4461×10^{-2}	-1.4359×10^{-2}
DC (1473)	-4.62×10^{-3}	-3.70×10^{-3}	-3.13×10^{-3}

Local distribution of the doppler coefficient

Perturbation calculations were performed for each of the 3 cases mentioned above to determine the local distribution of the doppler coefficient. For each of the mesh points used in diffusion calculations, the reactivity was calculated for a local increase in the fuel temperature of $100^{o}K$. The starting point was the nominal operating temperature of $1473^{o}K$.

A pure 1/T-behavior was assumed to determine the doppler constant. Table 3.1.5 shows a comparison of the doppler constants as resulting from the diffusion calculations for the whole reactor with those determined by perturbation calculations. Moreover, the doppler constants are broken down into fractions of the core, the axial and the radial blankets.

Table 3.1.5 doppler constants ($\frac{\partial k}{k} / \frac{\partial T}{T} \times 10^3$) for the individual reactor zones as determined by perturbation calculations

	case 1		case 2		case 3	
	Diff.	Pert.	Diff.	Pert.	Diff.	Pert.
total reactor	-4.62	-5.o	-3.7	-3.6	3.13	-3.o
core	-	-3.7	-	-2.1	-	-1.7
rad.blanket	-	-o.8o	-	-o.88	-	-o.91
ax. blanket	-	-o.5o	-	-o.62	-	-o.39

Input data for SAS2A and VENUS-calculations

In SAS2A, a 1/T-behavior of the doppler coefficient can be assumed. For each channel the values of the doppler constants must be indicated, both for the case of sodium being in or out of the channel. In addition, the relative fraction of the doppler constant for the total channel must be indicated for each axial segment. For this purpose, the results of the perturbation calculations (cases 1 and 3) were used. The data employed are indicated in table 3.1.6 for each channel. The relative fractions of the axial segments are shown in table 3.1.6.a.

In VENUS it is possible to account for deviations from the 1/t-behavior of the doppler coefficient. Therefore, the values indicated in table 3.1.4 including the $T^{-1.5}$ term were used. Depending upon the conditions of the core just before beginning of disassembly, (either filled with sodium, partly or totally voided), the results of cases 1, 2 or 3 were applied. The relative fractions of the VENUS-regions defined in fig. 3.5 are indicated in table 3.1.7.

Table 3.1.6 values of the doppler constants for each channel as used in SAS2A calculations

channel	$\frac{\partial k}{k} / \frac{\partial T}{T} \times 10^3$ sodium in	$\frac{\partial k}{k} / \frac{\partial T}{T} \times 10^3$ sodium out
1	-0.563	-0.0259
2	-0.4351	-0.1983
3	-0.8041	-0.3508
4	-0.6708	-0.2752
5	-0.9609	-0.4489
6	-0.3970	-0.2010
7	-0.1323	-0.0670
8	-0.3802	-0.2112
9	-0.3794	-0.3072
10	-0.8078	-

Table 3.1.6.a: relativ fraction (%) of a segment of the doppler constants of the channel (SAS2A input)

0.02	0.02	0.01	0.00	0.00	0.00	0.00	0.00	0.01	0.01	
0.15	0.13	0.06	0.01	0.02	0.02	0.02	0.02	0.06	0.06	upper axial
0.72	0.62	0.32	0.01	0.15	0.11	0.11	0.13	0.33	0.24	blanket
2.66	2.43	1.60	0.66	0.96	0.63	0.63	1.77	1.61	0.91	
4.06	3.90	3.38	2.65	2.16	0.71	0.71	0.44	0.71	2.99	
5.52	5.46	5.28	4.84	3.62	1.23	1.23	0.89	2.88	4.51	
7.79	7.75	7.64	7.16	5.39	1.87	1.87	1.38	4.36	6.79	
9.91	9.09	9.85	9.39	7.26	2.67	2.67	2.03	6.10	9.26	Core
11.48	11.50	11.57	11.32	9.59	4.78	4.04	4.04	8.60	11.68	
11.26	12.22	12.43	12.59	12.76	12.67	12.67	12.15	12.46	13.55	
11.76	11.85	12.18	12.66	14.05	17.12	17.12	16.90	14.32	14.05	
10.35	10.45	10.82	11.44	13.05	16.56	16.56	16.48	13.49	12.84	
8.26	8.37	8.71	9.32	10.70	13.78	13.78	13.74	11.04	10.26	
7.09	7.19	7.48	8.13	9.31	12.24	12.24	12.17	9.18	8.23	
5.57	5.66	5.92	6.61	7.45	10.62	10.62	12.93	9.65	3.17	lower
1.86	1.90	2.04	2.34	2.61	3.72	3.72	4.45	3.13	1.06	axial
0.50	0.52	0.57	0.66	0.73	1.03	1.03	1.21	0.84	0.31	blanket
0.12	0.12	0.13	0.15	0.17	0.23	0.23	0.27	0.19	0.09	
CH 1	2	3	4	5	6	7	8	9	10	

Table 3.1.7: Doppler Weighting Factors used in VENUS-calculations

Region	case 1	case 2	case 3
1	o	o	o
2	o.o559	o.o717	o.o51o
3	o.2298	o.1498	o.1638
4	o.oo63	o.oo89	o.oo77
5	o	o	o
6	o.1195	o.o755	o.o792
7	o.oo1o	o.oo15	o.oo16
8	o.1681	o.1259	o.1265
9	o.oo22	o.oo34	o.oo35
1o	o.o3o8	o.o433	o.o313
11	o.o763	o.o73o	o.o576
12	o.o118	o.o137	o.o143
13	o.oo15	o.oo27	o.oo33
14	o.o541	o.o633	o.o45o
15	o.oo66	o.oo92	o.oo84
16	o.o1o4	o.o154	o.o151
17	o.o636	o.o925	o.o84o
18	o.oo15	o.oo27	o.oo35
19	o.o162	o.2476	o.3o43
2o	o	o	o

3.1.2.2 Sodium void reactivities

The sodium void reactivities were determined by diffusion calculations in which the sodium was removed from core-areas having various sizes. Three cases, as defined in section 3.1.2.1, were investigated. In addition, perturbation calculations were performed to determine the local distribution of sodium void reactivities caused by a 1%-change of the sodium content. These values were determined for each mesh point used in the diffusion calculations.
Table 3.1.8 shows a comparison of the reactivities determined by diffusion and by perturbation calculations. It is seen that the sodium void reactivities obtained from perturbation calculations are more pessimistic than the values obtained from diffusion calculations. Therefore, the values determined by means of perturbation theory were used for the SAS2A-calculations. In doing so, it was assumed that in the areas in which there are control rod positions only the sodium contained in the fuel elements is removed. The values used in the SAS2A calculations are indicated in table 3.1.9. Accordingly, the maximum positive sodium void reactivity is 3.5 $.

Table 3.1.8 Comparison of sodium void reactivities determined by diffusion and perturbation calculations

case	description	Δk_{Diff}	Δk_{Pert}
2	core partially voided axial: total radial: up to R = 57.4 cm blankets filled with sodium	0.0075	0.0078
3	core totally voided axial blanket: totally voided radial blanket: filled with sodium	-0.0029	-0.0015

Table 3.1.9 sodium void reactivity ($\Delta k/_k \times 10^4$) for each segment (SAS2A-input)

-0.00	-0.02	-0.02	-0.01	-0.02	-0.01	-0.00	-0.01	-0.01	-0.00	upper axial blanket
-0.01	-0.05	-0.07	-0.02	-0.05	-0.02	-0.01	-0.02	-0.03	-0.01	
-0.03	-0.19	-0.33	-0.14	-0.29	-0.11	-0.04	-0.12	-0.18	-0.05	
-0.10	-0.75	-1.36	-0.98	-1.48	-0.52	-0.17	-0.64	-0.92	-0.17	
-0.15	-0.17	-2.09	-2.58	-2.50	-0.55	-0.18	-0.79	-0.32	-0.93	
-0.02	-0.17	-0.50	-1.07	-0.44	-0.81	-0.27	-0.78	-1.93	-1.28	
0.10	0.70	0.90	0.19	1.45	2.23	0.74	2.32	-1.96	-1.81	
0.22	1.57	2.33	1.53	3.45	3.63	1.21	3.76	-2.16	-2.40	Core
0.30	2.23	3.50	2.67	5.07	4.18	1.39	3.91	-3.01	-3.07	
0.34	2.53	4.06	3.27	5.77	2.99	1.00	1.62	-4.69	-3.67	
0.31	2.32	3.78	3.04	5.30	2.42	0.81	0.66	-5.57	-3.92	
0.22	1.60	2.61	1.89	3.61	1.30	0.43	-0.52	-5.38	-3.70	
0.07	0.50	0.76	0.04	0.94	-0.37	-0.12	-2.15	-5.78	-3.08	
-0.14	-1.04	-1.81	-2.66	-2.86	-2.97	-0.99	-5.14	-6.83	-2.53	
-0.11	-0.86	-1.43	-2.14	-2.27	-2.11	-0.70	-3.23	-2.91	-0.82	lower axial blanket
-0.03	-0.20	-0.35	-0.75	-0.61	-0.65	-0.22	-0.97	-0.75	-0.20	
-0.01	-0.05	-0.10	-0.26	-0.18	-0.20	-0.07	-0.28	-0.19	-0.04	
-0.00	-0.03	-0.06	-0.12	-0.10	-0.09	-0.03	-0.11	-0.07	-0.01	

CH	1	2	3	4	5	6	7	8	9	10

Table 3.1.10: Total material worth ($\partial k/_k \times 10^3$) for each segment (SAS2A input)

0.00	0.01	0.01	0.01	0.01	0.01	0.00	0.01	0.01	0.00	
0.00	0.02	0.04	0.02	0.04	0.02	0.01	0.02	0.02	0.01	upper axial blanket
0.01	0.08	0.16	0.09	0.16	0.07	0.02	0.07	0.09	0.04	
0.03	0.25	0.54	0.45	0.67	0.25	0.08	0.30	0.41	0.18	
0.26	2.00	3.55	3.46	4.62	2.38	0.79	3.42	3.60	0.57	
0.27	2.04	3.67	3.41	4.98	2.71	0.90	4.17	4.60	0.71	
0.32	2.45	4.46	4.01	6.28	3.56	1.19	5.77	6.52	0.94	
0.36	2.82	5.15	4.53	7.49	4.47	1.49	7.58	8.66	1.22	
0.40	3.07	5.63	4.85	8.32	5.57	1.82	9.73	10.90	1.56	
0.41	3.17	5.81	4.93	8.47	6.25	2.08	11.80	12.80	1.90	
0.40	3.10	5.68	4.84	8.25	6.14	2.05	12.03	13.28	2.07	Core
0.37	2.89	5.29	4.63	7.75	5.82	1.94	11.27	12.32	2.02	
0.34	0.29	4.72	4.36	6.99	5.27	1.76	9.71	10.27	1.76	
0.36	2.80	5.04	4.98	7.52	5.63	1.88	9.49	9.29	1.55	
0.02	0.13	0.14	0.62	0.27	0.59	0.20	1.09	1.08	0.53	lower axial blanket
0.01	0.04	0.05	0.29	0.11	0.23	0.08	0.39	0.31	0.14	
0.00	0.02	0.03	0.13	0.07	0.10	0.03	0.14	0.10	0.03	
0.00	0.02	0.03	0.07	0.06	0.05	0.02	0.06	0.04	0.01	

CH	1	2	3	4	5	6	7	8	9	10

3.1.2.3 Total material worth reacitivty

Total material worth reactivities were determined for each mesh point by means of perturbation calculations. In doing so, the B_4C contained in the reactor core was not accounted for in the SAS2A input calculations.
Fig. 3.7 shows the local distribution of the total material worth reactivities. Table 3.1.1o indicates these values for each of the mesh points used in the SAS2A-calculations. In the VENUS-calculations, the displacement reactivity is calculated from the total material worth reactivities. Since in this case it must be assumed that also the control rods will be displaced, the absorber materials were taken into account in determining the material worth reactivities.

3.1.2.4 Kinetic parameters

The value obtained for the prompt neutron life time is

$$l_p = 4.67 \times 10^{-7} \text{ sec}$$

For calculating the delayed neutron fractions and delay constants, data obtained from reference /33/ were used. The integral values used in SAS2A and VENUS are indicated in table 3.1.1.1.

Table 3.1.1.1 fractions and delay constant of delayed neutron groups

group	$\beta_{i_{eff}}$	$\lambda_{i_{eff}}$
1	7.838×10^{-5}	1.29×10^{-2}
2	6.626×10^{-4}	3.11×10^{-2}
3	5.828×10^{-4}	1.34×10^{-1}
4	1.083×10^{-3}	3.31×10^{-1}
5	4.743×10^{-4}	1.26
6	1.574×10^{-4}	3.21
SUM	3.038×10^{-3}	

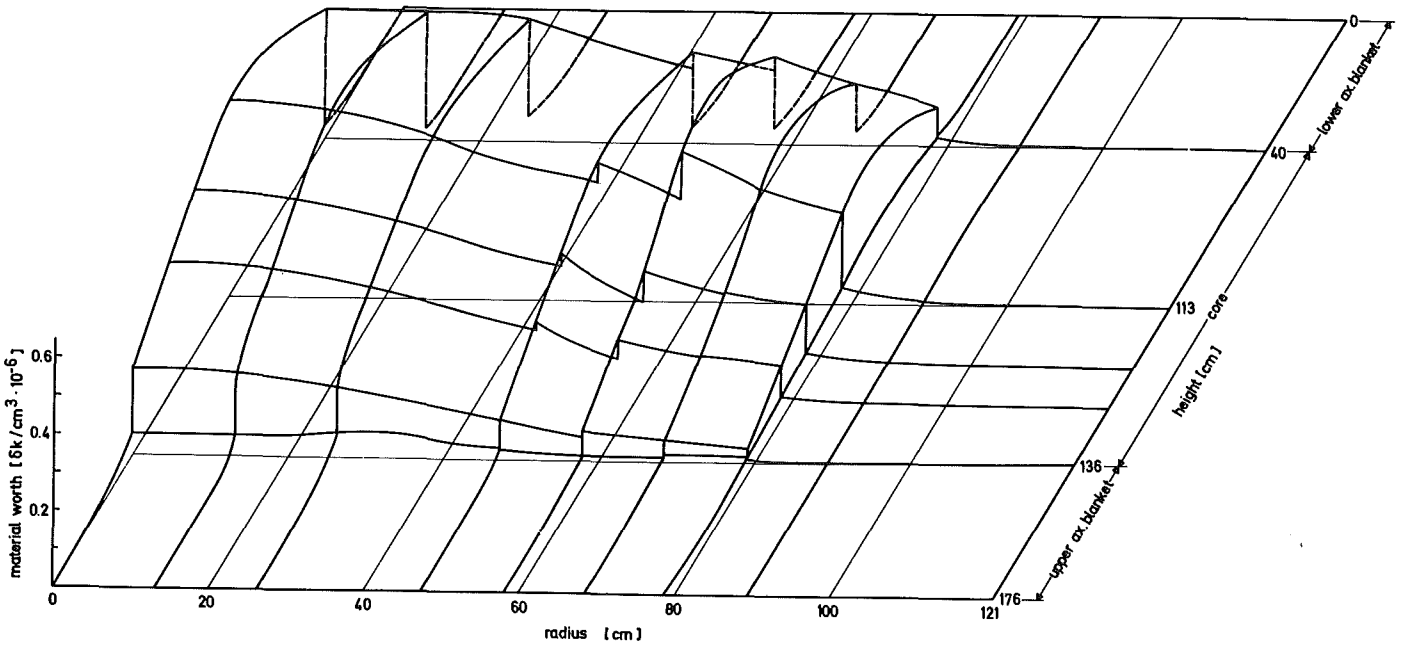

Fig. 3.7 Material reactivity worth distribution as function of reactor radius and height

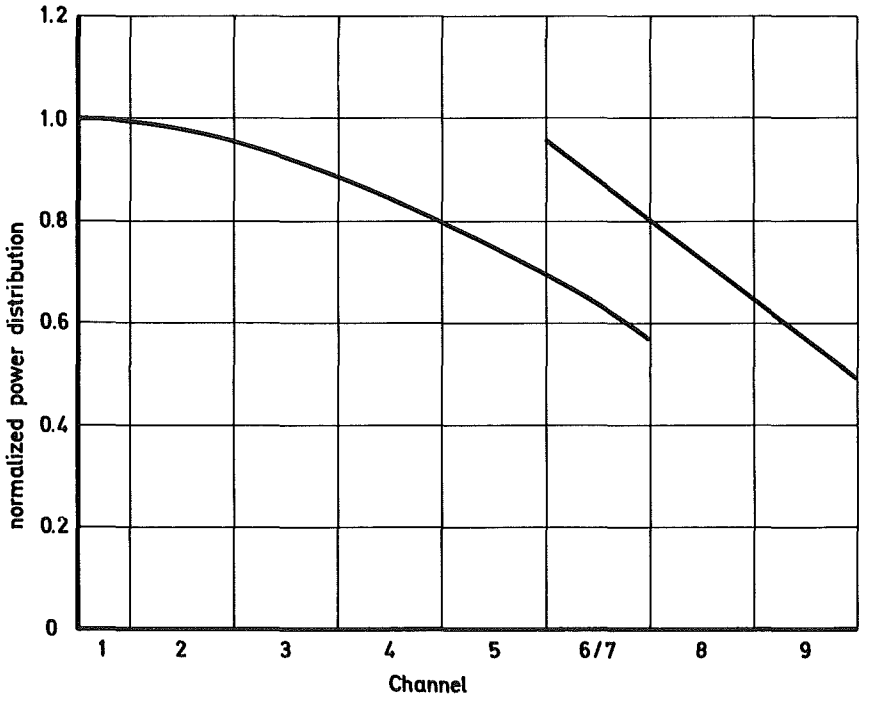

Fig. 3.8 Radial power distribution (PRSHAP)

3.1.2.5 Power distribution

The following definitions are used in the SAS2A input lists to describe the power distribution:

a) radial power distribution

$$PRSHAP\ (ICH) = \frac{\bar{p}\ (ICH)}{\bar{p}\ (1)}$$

with

$\bar{p}$ (ICH) = average power of a fuel pin in the ICH channel

b) axial power distribution

$$PSHAPE\ (J, ICH) = \frac{P\ (J, ICH)}{P_{max}\ (ICH)}$$

with P (J, ICH) power of a fuel pin in segment J of channel ICH

P_{max} (ICH) maximum of values p (J, ICH) in channel ICH

The values used for PRSHAP and PSHAPE are indicated in tables 3.1.12 and 3.1.13. In addition, fig. 3.8 shows the radial power curve in a normalized representation. With this power distribution, a thermal reactor power of 73o MW is achieved with a maximum linear rating of 448 W/cm in the pins.

Channel	PRSHAP (ICH)
1	1.o
2	o.9778
3	o.9221
4	o.8475
5	o.7465
6	o.6191
7	o.877o
8	o.721o
9	o.5657
1o	o.o244

Table 3.1.12: radial power distribution PRSHAP

Table 3.1.13: Normalized axial power distribution PSHAPE (SAS2A-input)

0.00	0.00	0.00	0.00	0.00	0.00	0.00	0.00	0.00	0.03	upper axial blanket
0.01	0.01	0.00	0.00	0.00	0.00	0.00	0.00	0.00	0.05	
0.01	0.01	0.01	0.01	0.01	0.01	0.01	0.01	0.01	0.11	
0.06	0.06	0.05	0.05	0.05	0.04	0.04	0.04	0.04	0.22	
0.59	0.58	0.57	0.54	0.51	0.45	0.45	0.53	0.46	0.48	
0.66	0.66	0.65	0.63	0.59	0.52	0.52	0.51	0.54	0.56	
0.80	0.79	0.78	0.76	0.72	0.64	0.64	0.63	0.67	0.70	
0.90	0.90	0.89	0.88	0.84	0.76	0.76	0.74	0.79	0.82	
0.97	0.97	0.97	0.96	0.93	0.87	0.87	0.86	0.89	0.92	
1.00	1.00	1.00	0.99	0.97	0.97	0.97	0.97	0.98	0.99	
0.98	0.98	0.99	0.99	1.00	1.00	1.00	1.00	1.00	1.00	
0.91	0.91	0.92	0.93	0.95	0.95	0.95	0.96	0.95	0.95	
0.80	0.80	0.81	0.82	0.84	0.95	0.85	0.85	0.85	0.83	
0.75	0.76	0.77	0.79	0.80	0.81	0.81	0.81	0.80	0.76	
0.08	0.08	0.08	0.08	0.08	0.08	0.08	0.07	0.07	0.38	lower axial blanket
0.02	0.02	0.02	0.02	0.02	0.02	0.02	0.01	0.01	0.20	
0.01	0.01	0.01	0.01	0.01	0.01	0.01	0.01	0.01	0.10	
0.00	0.00	0.00	0.00	0.00	0.00	0.00	0.00	0.00	0.06	
CH 1	2	3	4	5	6	7	8	9	10	

3.2 Thermal and mechanical properties of fuel pin and coolant

The best experimental data regarding fuel, cladding and coolant were taken from the most recent literature available.

a) thermal conductivity of PuO_2-UO_2.
For the thermal conductivity of PuO_2-UO_2 pellets in breeder fuel pins with low and high burnup, the data by Kämpf /34, 35/ and the results of inpile measurements by Craig and Baily /36, 37/ were used.

b) heat transfer coefficient between fuel and cladding.
Heat transfer coefficient between fuel and cladding can be taken into account in SAS2A by considering a variable gas gap thickness, and taking into account the thermal radiation between the pellet and the cladding. For SAS2A, the inpile measurements by Craig and Baily /38/ were mainly used.

c) sodium, steel and UO_2-PuO_2 materials data.
The data for the density ρ, specific heat c_p, linear coefficient of expansion, melting temperature, latent heat of melting, fractional linear change due to melting, poisson ratio, youngs modulus for fuel and bulk modulus for liquid fuel were taken from /39, 4o, 41, 42, 43, 44, 45, 46/. The main data is summarized in tables 3.2.1, 3.2.2, 3.2.3, 3.2.4.

d) sodium superheat.
Sodium superheat ΔT is dependent on the heat flux, coolant velocity, oxide level, and the surface roughness of the fuel pin. A survey of the experimental results published shows that the measured values of superheating vary greatly /47, 48, 49, 5o/. For SAS2A calculations, sodium superheating of $5o^{o}C$ is regarded as a meaningful mean value /3/.

Table 3.2.1 Geometry of core coolant channel

fuel pellet outer radius	o.255 (cm)
clad inner radius	o.262 (cm)
clad outer radius	o.3oo (cm)
structural thickness	o.28 (cm)
structure coolant surface area ratio	o.1o82
volume fraction of coolant	o.496
coolant inlet temperature	$377^{o}C$
coolant exit temperature	$546^{o}C$
coolant exit pressure	1.8 at

Table 3.2.2: Material properties

Fuel	
melting temperature	$2767^{o}C$
latent heat of melting	28o Joules/gr
coefficient of linear expansion of solid	$1.o8 \times 1o^{-5}\ {}^{o}C^{-1}$
coefficient linear expansion of liquid	$3.ox1o^{-5}\ {}^{o}C^{-1}$
fractional linear expansion due to melting	o.o3
youngs modulus	$1.ox1o^{12}$ Dynes/cm^2
Cladding	
melting temperature	$1375^{o}C$
coefficient of linear expansion	$1.8x1o^{-5}\ {}^{o}C^{-1}$
specific heat density	4.73 Joules/$cm^3\ {}^{o}C$
thermal conductivity	o.196 W/cm ^{o}C
poisson ratio	o.3
Coolant	
specific heat	1.265 Joules/gr ^{o}C
degrees of superheat	$5o^{o}C$
initial film thickness	o.o15 (cm)
Structure	
coefficient of linear expansion	$1.8 \times 1o^{-5}\ {}^{o}C^{-1}$
thermal conductivity	o.196 W/cm ^{o}C
specific heat density	4.73 Joules/$cm^3\ {}^{o}C$

Table 3.2.3: Fuel thermal conductivity

temperature (^{o}C)	conductivity (W/cm ^{o}C)
8oo	o.o27
1ooo	o.o245
12oo	o.o225
14oo	o.o215
16oo	o.o21o
18oo	o.o21o
2ooo	o.o215
22oo	o.o22o
24oo	o.o22o
26oo	o.o225
28oo	o.o225
29oo	o.o226

Table 3.2.4: Fuel specific heat

temperature (^{o}C)	specific heat (Joule/gr ^{o}C)
6oo	o.31o
993	o.318
1289	o.329
1485	o.345
178o	o.388
1977	o.43o
2174	o.484
2371	o.548
2567	o.621
2764	o.7o1

4. ANALYSIS OF CHARACTERISTIC HYPOTHETICAL ACCIDENTS

In section 1 the mechanisms for initiation were briefly discussed for different characteristic hypothetical incidents. In this section, the most important results of SAS2A- and VENUS-calculations will be reported for the following hypothetical accident chains:

a) pump coast down with simultaneous failure of the primary and secondary shut down systems for

   α) a fresh core of SNR-3oo

   β) an equilibrium core of SNR-3oo with a maximum burnup of 55.ooo MWd/to

b) a reactivity accident with an initial reactivity ramp of 5 $/sec and simultaneous failure of the primary and secondary shut down systems

c) a reactivity accident with a very steep reactivity ramp of about 25 $/sec, simulating the ejection of an absorber rod.

4.1 Description of the course of accident

As described in section 1 four trip sets of the primary and secondary shut down systems, with the redundancy and diversity inherent in their design, must fail successively to allow core disassembly. The chain of events begins with the failure of all three primary pumps, for instance, after a break down of the entire electrical supply. This causes the coolant flow to drop to approximately 5 % of the nominal flow within about 2o sec (fig. 4.1). Since the shut down systems fail to scram, the reactor power remains constant, at 723 MWth.

The sequence of events during the flow coast down accident is characterized by two particular cases. Since they may produce different results, they will be dealt with individually in sections 4.1.1 and 4.1.2. These cases are:

a) pump failure accompanied by subsequent sodium boiling, fuel slumping and core disassembly (fresh core)

b) pump failure, accompanied by failure of the fuel pins, fission gas release, sodium boiling, fuel slumping and core disassembly (equilibrium core).

4.1.1 Flow coast down accident in a fresh core

Core physics and material data for the fresh reactor core, the subdivision of the reactor core into 1o annular channels and the mesh grid used for the SAS2A- and VENUS calculations were described in section 3. An axial expansion of 3o% of the theoretically possible value is assumed for the fresh fuel.

Fig. 4.1.1a shows the reactor power as function of time from the onset of the accident up to the abrupt discontinuation of power production following core disassembly. During the first 4 seconds, the coolant flow decreases continously to some 25 % of the nominal flow (fig. 4.1). The reactor power remains constant for the time being and then starts to decrease gradually because an increase of coolant, cladding and fuel temperatures causes the entire net reactivity to become negative (fig. 4.1.1.b). In this phase the coolant temperature rises very quickly, reaching approximately 9oo^{o}C in the central fuel element at the upper axial end of the core (fig. 4.1.1c). The coolant temperatures, in the annular channels 2 through 8, show a similar behavior, depending on the throttling of the coolant at the inlet of the fuel element and the radial power distribution in the core. As can be seen from fig. 4.1.1d, the fuel temperatures change only slightly since the reactor power decreases slightly, whereas the temperatures of the coolant and cladding increase.
At 4.85 sec after the beginning of the accident, the sodium temperature has reached 1oo7^{o}C at the upper axial core end of the central fuel element. Hence, under the assumption of 5o^{o}C sodium superheat, sodium boiling is initiated (fig. 4.1.1e and 4.1.1f). Since the coolant flow is still above 2o% of the initial nominal flow, the sodium vapour bubble moves mainly in the upper axial blanket area causing a negative sodium void reactivity effect. Shortly afterwards (4.85 s and 4.97 s respectively), sodium boiling starts also in annular channels 2 and 3 with an expansion of the sodium vapour bubble into the upper axial blanket (fig. 4.1.1h). The total sodium void reactivity and the total net reactivity then become negative. Consequently there is a slight reduction of the reactor power (fig. 4.1.1a and 4.1.1b). Approximately 5.o5 s after initiation of the accident, the sodium vapour bubbles in the central annular channel 1, 2 and 3 penetrate into the reactor core from the top to the bottom (fig. 4.1.1e, 4.1.1.h). At 5.11 s and 5.12 s after initiation of the accident, annular channels 4 and 7 follow with sodium boiling (fig. 4.1.1.h) and together with the annular channels 1 to 3 generate a positive sodium void reactivity ramp of 2.5 $/sec (fig. 4.1.1b). This causes the reactor power to rise to 3 to 5 times the nominal power. The fuel temperature initially begins to rise only slowly (fig. 4.1.1d).

At 5.36 and 5.44 s after initiation of the accident, the annular channels 5 and 8, which are further away from the center, start to show sodium boiling in the upper core and the axial blanket areas (fig. 4.1.1h). This again makes a negative reactivity contribution which once more limits and changes the power increase at about 5.5o sec (fig. 4.1.1a). At that time, no pellet of the reactor core has as yet reached fuel melting temperatures (fig. 4.1.1d and 4.1.1g): i.e., the potential in terms of negative doppler reactivity of the reactor core is still fully available. Annular channels 1, 2 and 3 and essentially also channels 4 and 7 are filled with sodium vapour after this phase (fig. 4.1.1h). The boundary areas of these sodium vapour bubbles oscillate at the bottom edge of the core and the end of the upper axial blanket, respectively, at a frequency of approximately 5 Hz; in the further course of the accident they hardly make any other contributions to the positive sodium void reactivity ramps (fig. 4.1.1e and 4.1.1f). Now the main contributions to the sodium void reactivity ramps come from annular channels 5 and 8 after another increase in the power level after 5.61 sec, mainly from annular channel 6 (fig. 4.1.1h). Between 5.61 and 5.66 sec there is a stronger positive sodium void reactivity ramp of approximately 7 $ /sec. The reactor core becomes superprompt critical for the first time at approximately 5.67 sec. However, the sharp power peak generated is accommodated by the negative doppler coefficient and the negative sodium void reactivity contribution of the annular channel 9, which now also starts boiling (fig. 4.1.1a and 4.1.1b). The negative reactivity contribution of annular channel 9, which is comprised of 42 fuel elements, is sufficient to change the total sodium void reactivity contribution of channels 1 to 8 (core and upper axial blanket) from a total of 1.6 $ to a total of 1.1 $ within a few milliseconds (fig. 4.1.1b).
As a consequence of the penetration of the sodium vapour bubble of annular channel 9 into the axial center of the core (negative sodium void reactivity contribution) (fig. 4.1.1h), there is even a strong negative reactivity ramp for the overall sodium void reactivity in the further course of the accident (fig. 4.1.1b).

After this short power peak the fuel temperatures have increased rapidly. In the most highly rated annular channels 1, 2, 3, 4, 5, 7 and 8 the fuel within the fuel pins has melted to a maximum of 35% of the fuel pin cross section (fig. 4.1.1d, 4.1.1g, 4.1.1k). The central temperature of the fuel pins in annular channels 1, 2, 3, 5, 7 in part, already exceeds the melting point of the fuel (fig. 4.1.1k). However, the positive sodium void reactivity ramp and the positive sodium void reactivity increment are not sufficient to initiate disassembly.

The total net reactivity (fig. 4.1.1.b) again drops below o.9 $. In large areas of the reactor core, such as the annular channels 6 and 9, the central temperatures of the fuel pellets in the center of the core have not yet reached the melting point (fig. 4.1.1.k).

Now different reactivity effects begin to play a role. From fig. 4.1.1.e and 4.1.1.f it is seen that approximately o.4 sec after initiation of boiling the sodium film of about 0.15 mm thickness which adhered to the cladding of the fuel element during the boiling expulsion begins to dry out. This very rapidly causes the cladding temperatures (fig. 4.1.1.i) to rise up to the melting point (1375°C), and gradually the fuel element cladding melts over its entire axial core length (fig. 4.1.1.e, 4.1.1.f, 4.1.1.i, 4.1.1.g, 4.1.1.k). Since the total reactor power is still in the range of 3o-8o times the nominal power, the radial cross section of the fuel pins in the axial core center will melt further within a very short time. There will then be fuel slumping as a function of the radial power profile (4.1.1.a and b).

The fuel slumping model developed by W. Bohl /22/ was used in the SAS2A calculations. According to this model, fuel slumping begins in an annular channel if the cladding has melted after sodium boiling ejection and dry out of the sodium film and approximately 6o to 8o% of the areal cross section of the fuel pin has melted. This model is based on very conservative assumptions. Because of the relatively flat axial power profile the above conditions are reached almost simultaneously by a fuel zone of 3o cm length in the SNR-3oo fuel element. It is assumed that afterwards, the fuel element section hanging over this molten zone drops down into the molten zone because of its weight and at the same time molten fuel may enter the lower fuel element region.

Fuel slumping begins in the individual annular channels in this time sequence:

annular channel	initiation of fuel slumping
1	5.678 sec
2	5.681 "
3	5.685 "
7	5.698 "
4	5.7o4 "
8	5.724 "
5	5.727 "
6	5.743 "

Superposition of the positive reactivity contributions caused by fuel slumping in the individual annular channels results in the overall reactivity curve with time, shown in fig. 4.1.1b and 4.1.1l for fuel slumping. Superposition of the contributions from negative doppler feedback and expansion reactivities, positive sodium void reactivity and positive slumping reactivity will make the reactor core superprompt critical again after approximately 5.37 msec. As the fuel temperatures will very quickly reach values in excess of 3500^{o}C in the most highly rated channels, coupling between SAS2A and VENUS is made at 5.745 sec.

Fig. 4.1.1m supplements fig. 4.1.1b and 4.1.1l by showing the time curve of the positive reactivity contributions of sodium void and fuel slumping in the transition to the disassembly phase. The positive reactivity ramp at the beginning of the disassembly phase amounts to 25 $/sec. It is generated mainly by fuel slumping. There is a very sharp power peak which is shown in fig. 4.1.1a and 4.1.1n (different scales).
The fuel temperatures increase very rapidly, generating not only the continued buildup of the negative doppler feedback reactivity (fig. 4.1.1o), but, after approximately 5.746 sec, above all, a very strongly negative displacement reactivity contribution (fig. 4.1.1p). This very quickly causes the net reactivity to decrease to values below -3 $ (fig. 4.1.1m and 4.1.1q). The reactor power very quickly drops below the original nominal power. Power production is stopped abruptly.

On the whole, an additional 1490 MWsec of thermal energy is released during this short disassembly phase of approximately 8 msec (fig. 4.1.1r). This is now stored in the further increase in the fuel temperature (fig.4.1.1t), buildup of fuel pressure (fig. 4.1.1s), and additional fuel melting. In the center of the core fuel vapour temperatures reach approximately 5000^{o}K and fuel vapour pressures reach approximately 50 atm (table 4.1.4A and 4.1.1B).
As is shown in tables 4.1.1A and 4.1.1B in the outer core region the fuel is only molten to some extent. In annular channel 9 (fig. 4.1.1k) and the lower and upper axial core regions of annular channels 2 to 8 the fuel cladding is still intact even after the disassembly phase; the radial cross section of the fuel pin has melted only partially.

In the axial and radial blanket zones there has been neither fuel melting nor melt down of the cladding. All the annular channels, except for the lower core regions of annular channels 6 and 9 are without sodium (fig. 4.1.1.g). Hence, there can be no immediate energy transfer from hot molten fuel to the sodium. A total of 2100 kg of fuel has melted completely and is no longer present in the original fuel pin and pellet geometries, respectively.

The further course of the accident is discussed in section 5.1 together with the flow coast down accident for the equilibrium core.

T_{max} = 5o4o°K ≙ 5o4 at Mesh Point /14,1/

22	3o3	3o3	3o3	3o3	3o3	3o2	299	281	278	29o	284	255	249
21	4o5	4o3	399	311	3o8	3o3	3o3	3o3	3o3	3o3	3o3	3o3	293
2o	436	434	429	4o5	4o2	31o	3o6	3o3	3p3	3o7	3p3	3o3	3o3
19	456	454	448	419	416	32o	315	3o8	3o3	32o	311	3o3	3o3
18	473	471	465	433	429	428	323	319	313	326	317	3o3	3o3
17	488	485	479	444	44o	4o8	4o2	327	321	331	322	3o3	3o3
16	498	495	488	452	447	415	4o9	396	39o	41o	4oo	3o3	3o3
15	5o3	5o1	493	458	453	42o	413	399	392	415	4o5	3o3	3o3
14	5o8	5o1	493	459	453	422	414	4oo	393	417	4o8	3o3	3o3
13	5o1	498	49o	458	452	421	413	399	392	417	41o	3o3	3o3
12	492	49o	482	451	446	416	4o7	395	387	413	4o5	3o3	3o3
11	482	479	471	443	437	4o9	4o1	39o	383	4o7	4oo	3o3	3o3
1o	466	463	456	429	423	398	39o	381	374	396	389	3o3	3o3
9	449	446	439	414	4o8	386	378	371	364	384	378	3o3	3o3
8	427	424	418	395	39o	372	365	358	353	368	363	3o3	3o3
7	393	391	385	3o3	3o3	3o3	3o3	3o3	3o3	3o3	3o3	3o3	3oo
6	3o3	3o3	3o3	3o3	3o3	285	281	27o	267	263	281	241	238
	1	2	3	4	5	6	7	8	9	1o	11	12	13

Table 4.1.1A Flow coast down I

Temperatures in each mesh of the core at the end of the disassembly phase.
For definition of the meshes see fig. 3.5.

P_{max} = 5o.8 bar ≙ 5o8 at Mesh Point /14,1/

22	3	5	2	1o	o	o	o	o	o	o	o	o	o
21	4o	42	3o	12	3	2	o	o	o	o	o	o	o
2o	1o9	112	84	43	28	9	o	o	o	o	o	o	o
19	172	172	135	77	46	21	2	o	o	o	o	o	o
18	255	245	214	12o	116	34	1o	4	o	o	o	o	o
17	257	335	286	114	1oo	64	28	8	1o	11	8	3	o
16	445	418	355	144	211	84	36	23	18	39	27	4	o
15	5o7	477	4o4	166	166	97	43	27	29	44	32	9	o
14	5o8	477	4o1	172	161	99	44	28	31	49	36	11	o
13	476	446	374	17o	183	92	42	27	3o	49	37	12	o
12	396	37o	3o9	14o	119	77	36	23	26	41	32	1o	3
11	3o9	288	239	127	131	58	28	18	2o	34	27	o	o
1o	215	2o8	161	98	61	39	19	13	14	22	19	2	o
9	139	138	1o4	58	37	22	11	8	8	14	11	o	o
8	86	88	64	32	19	11	6	4	4	7	6	o	o
7	28	29	2o	7	2	1	o	o	o	o	o	o	o
6	1	2	1	o	o	o	o	o	o	o	o	o	o
	1	2	3	4	5	6	7	8	9	1o	11	12	13

Table 4.1.1B Flow coast down I (fresh core)

Pressures in each mesh of the core at the end of the disassembly phase

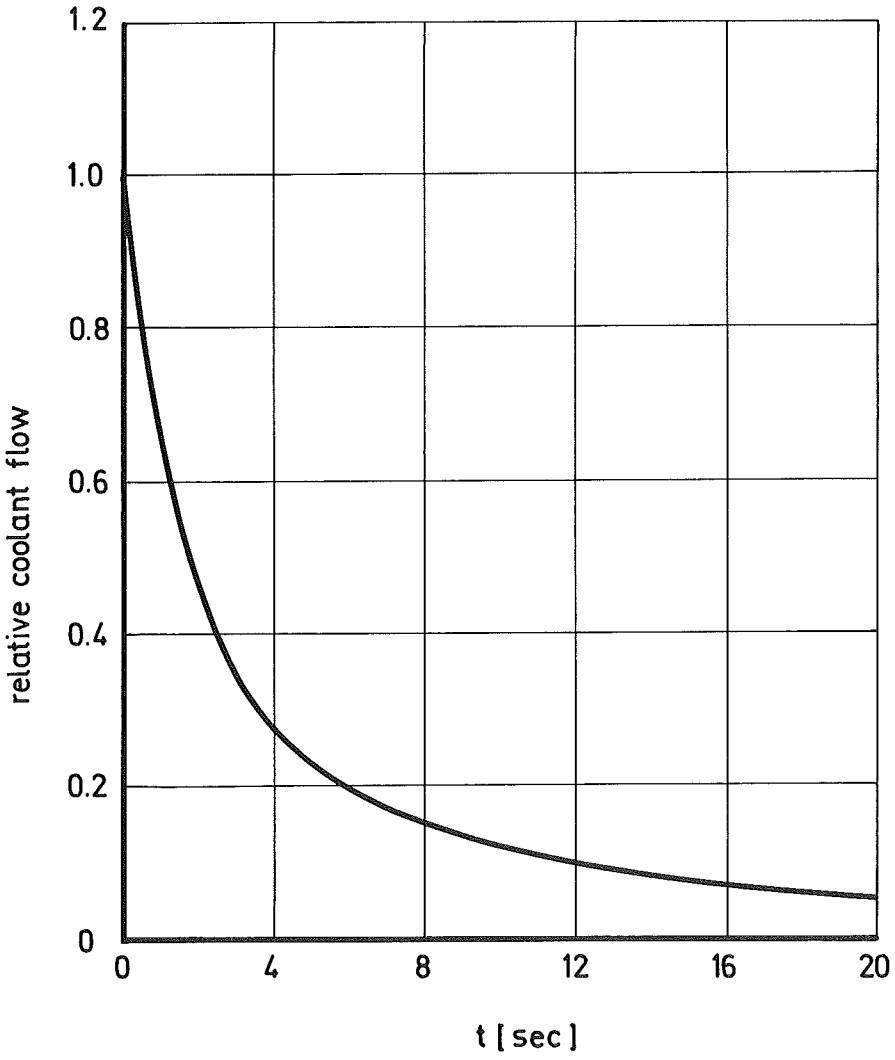

Fig. 4.1 Coolant flow as function of time
(Pump coast down)

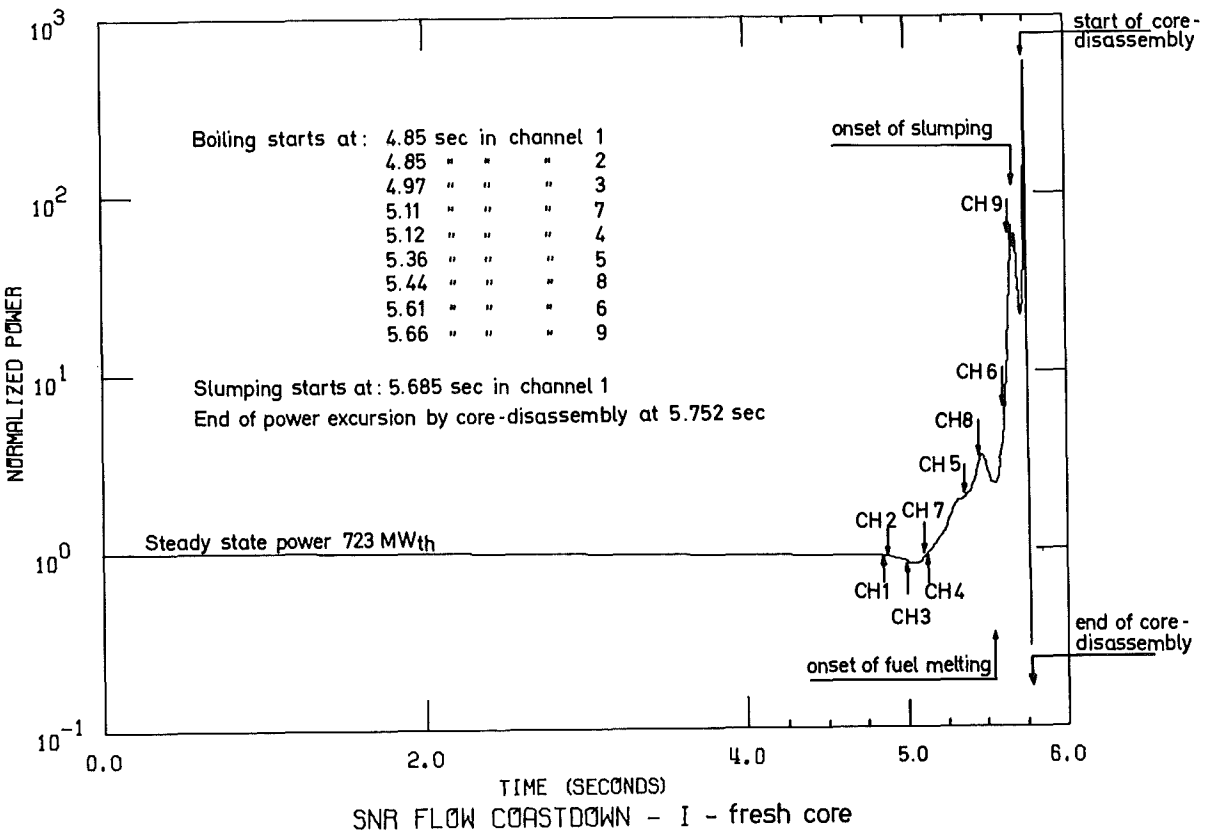

Fig. 4.1.1.a Normalized power as function of time

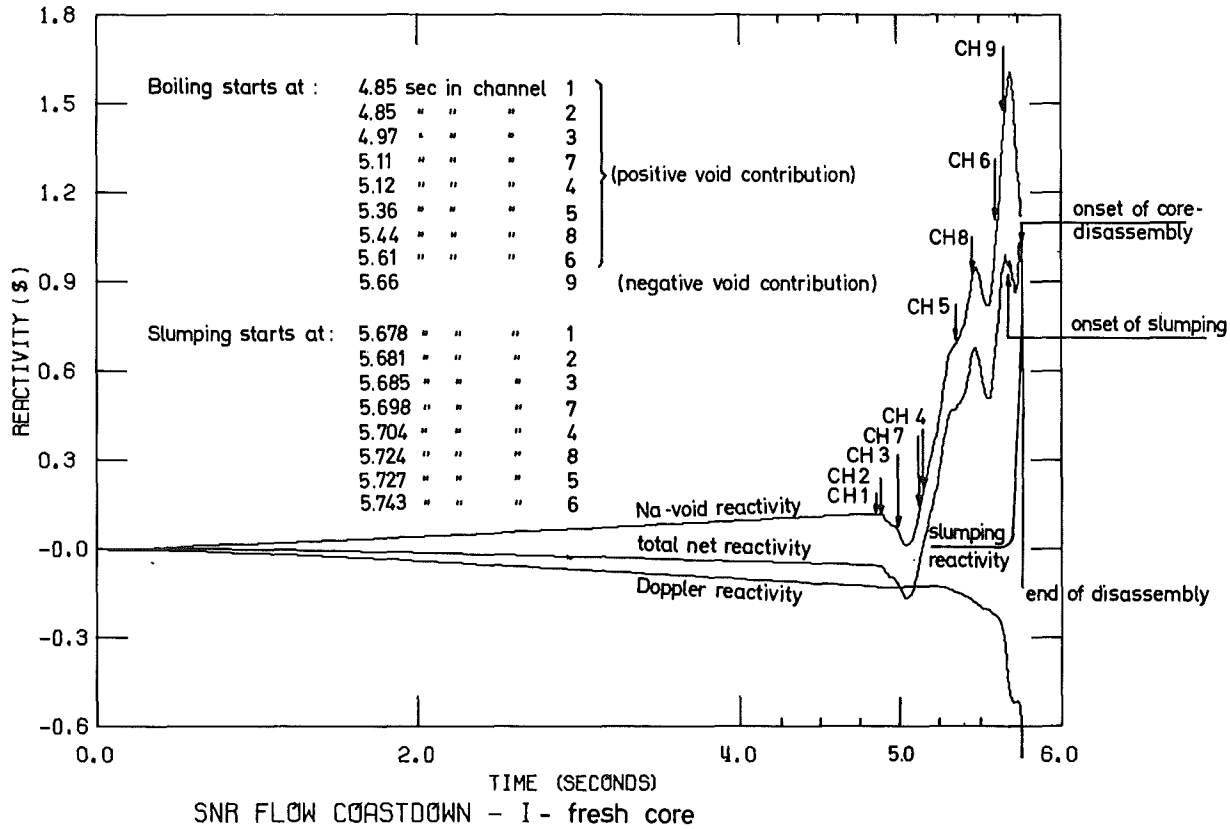

Fig. 4.1.1.b Reactivity as function of time

Fig.4.1.1.c Coolant temperature in channel 1
Flow coast down I (fresh core)

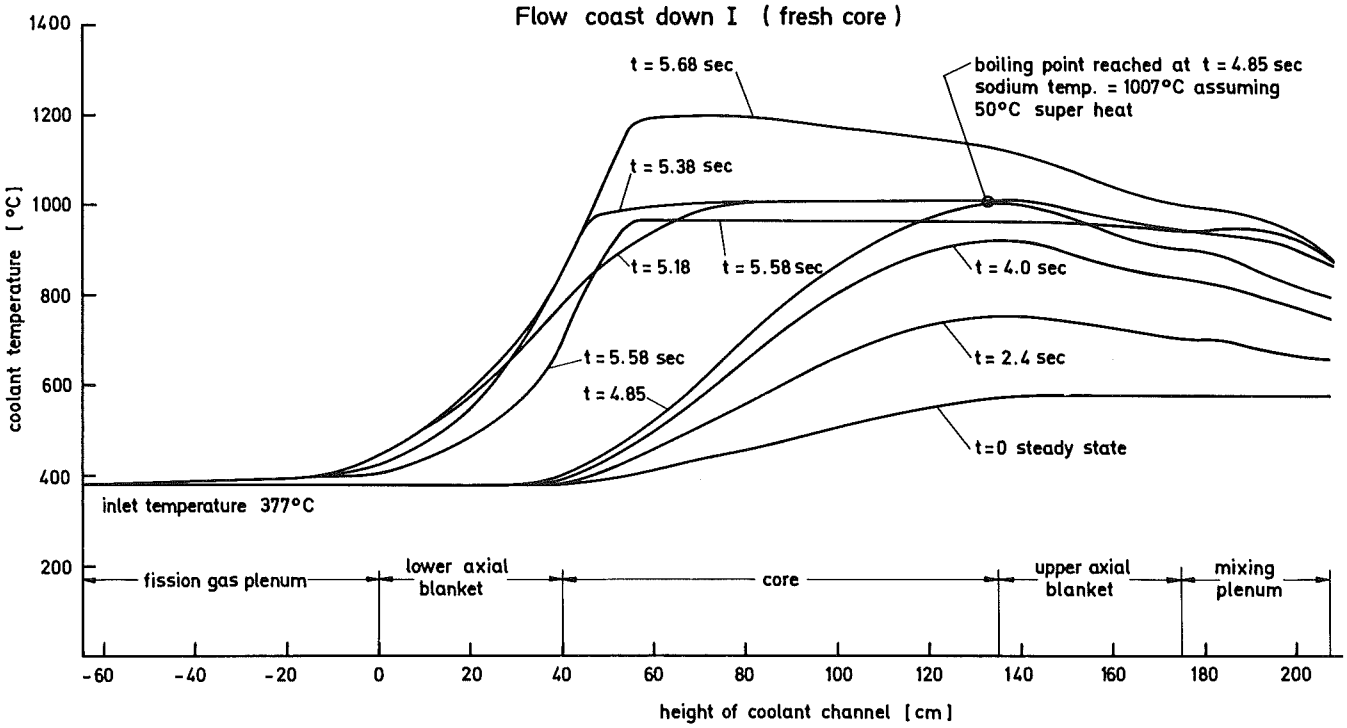

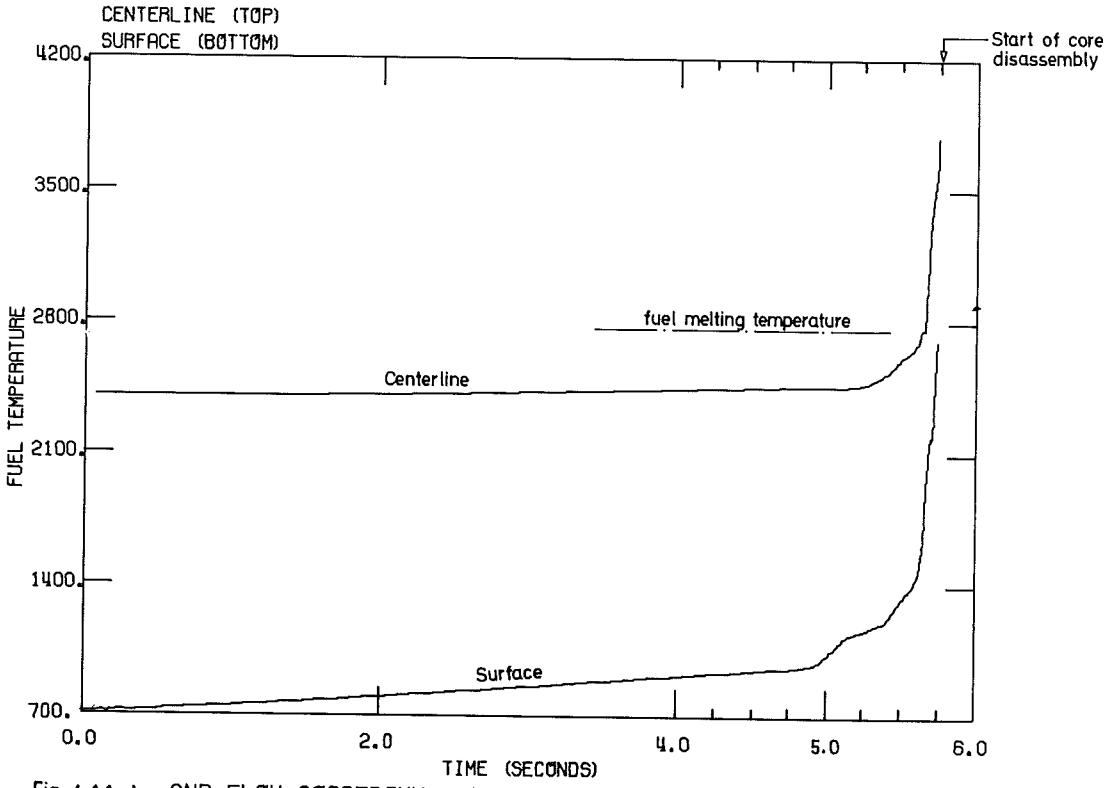

Fig. 4.1.1.d. SNR FLOW COASTDOWN - I , CHANNEL 1 MIDPLANE
Fuel temperatures as a function of time

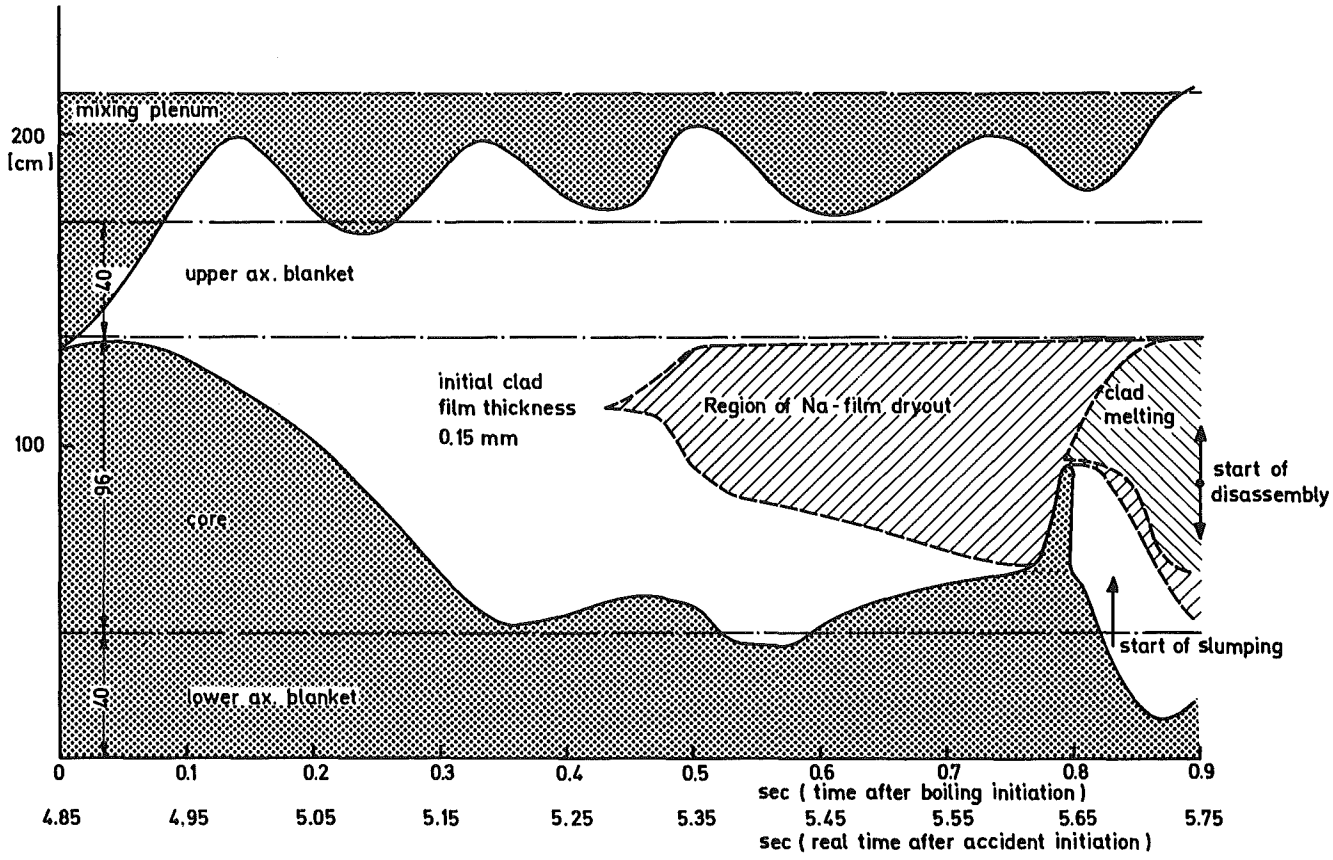

Fig.4.1.1.e Flow coast down (fresh core)
Voiding pattern of channel 1

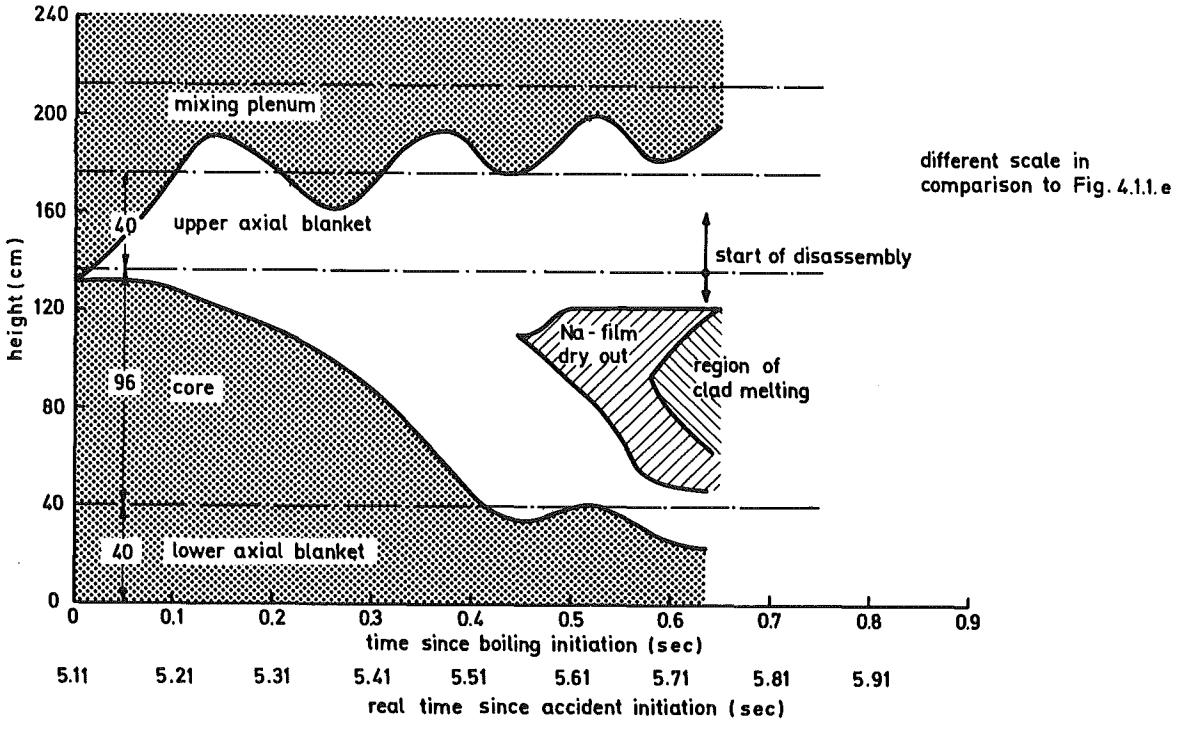

Fig.4.1.1.f Flow coast down I (fresh core)
Voiding pattern of channel 7

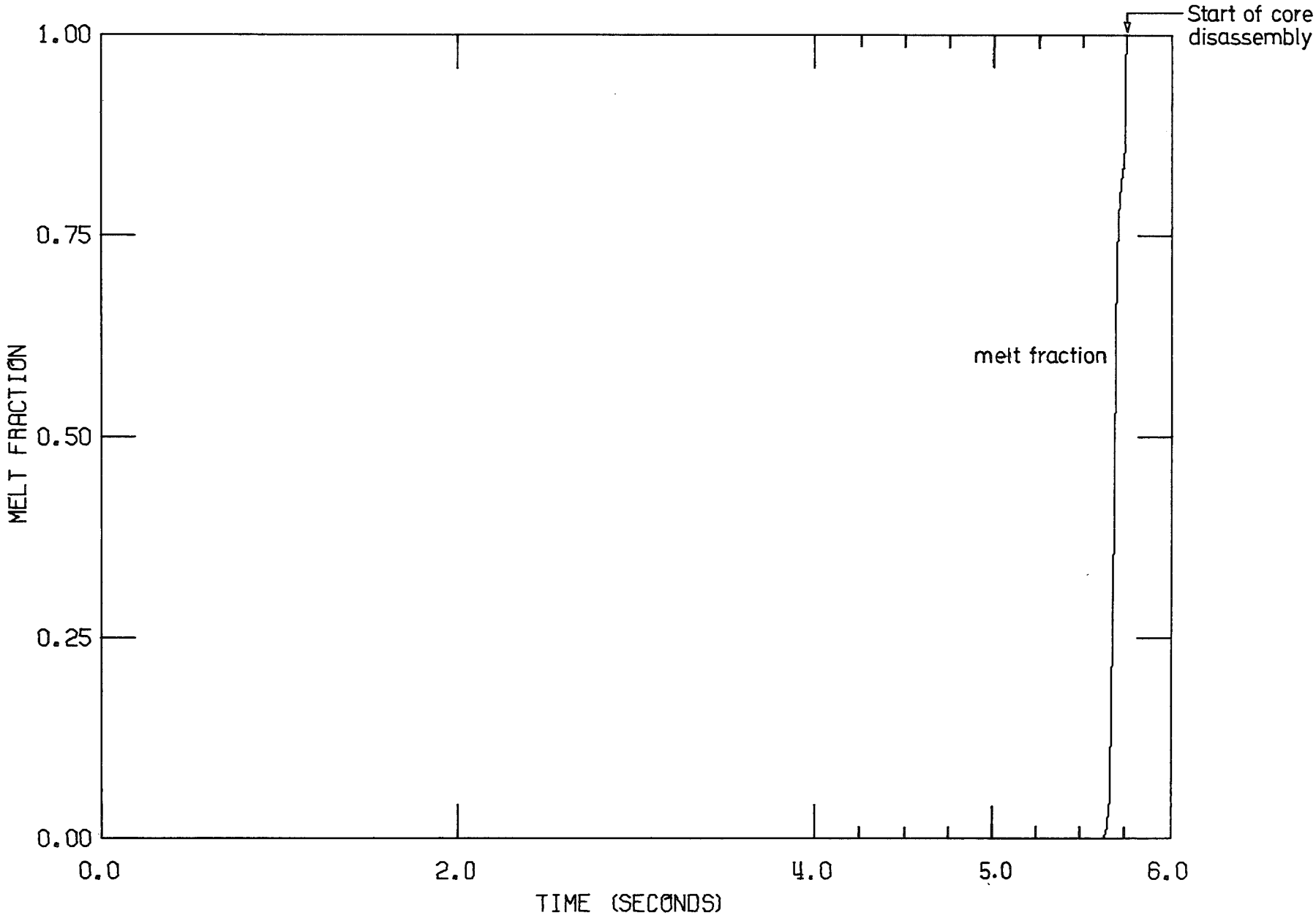

Fig. 4.11.g. SNR FLOW COASTDOWN – I , CHANNEL 1 MIDPLANE
Melt fraction as a function of time

Fig. 4.1.1.h Boiling pattern during predisassembly phase
Flow coast down I (fresh core)

No boiling until 4.85 sec
after accident initiation

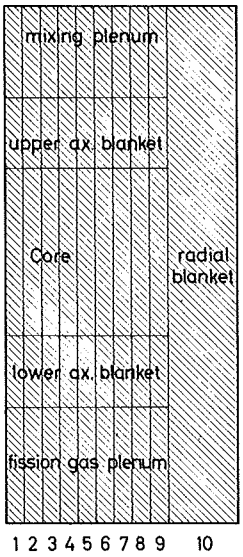

time : 5.18 sec
after accident initiation

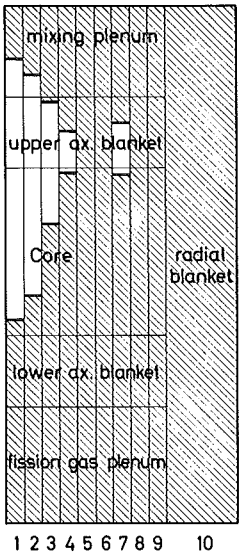

time : 5.38 sec
after accident initiation

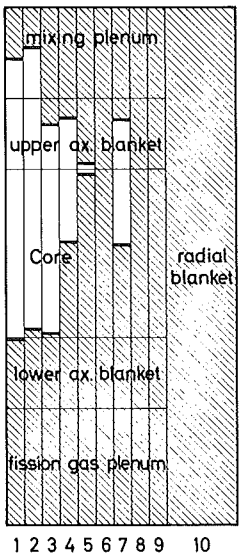

time : 5.48 sec
after accident initiation

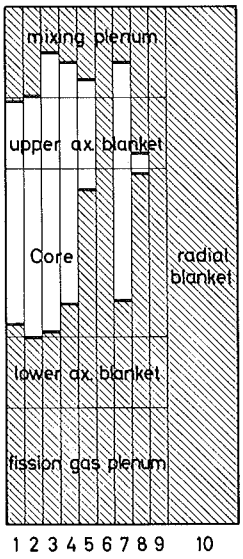

time : 5.58 sec
after accident initiation

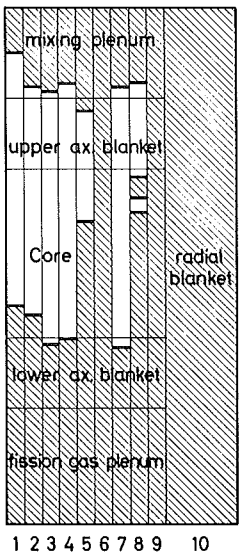

time : 5.68 sec
after accident initiation

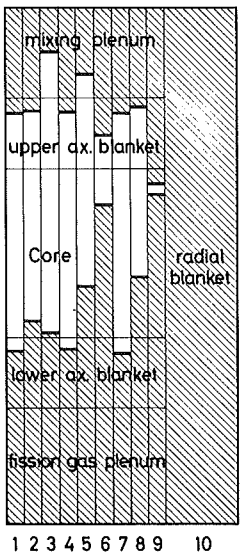

time : 5.72 sec
after accident initiation

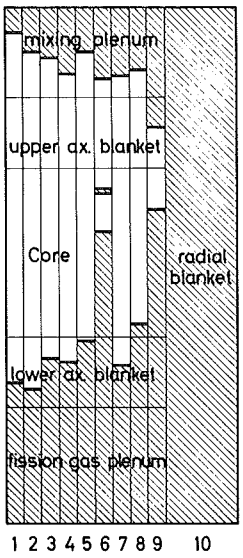

time : 5.744 sec
after accident initiation
just before begin of disassembly

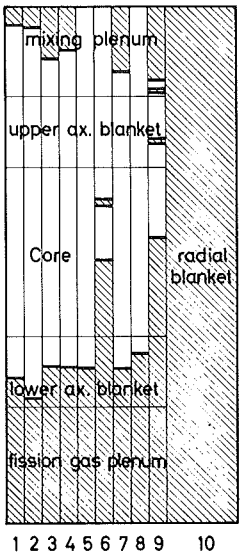

Fig. 4.11.i Outer clad temperature in channel 1

Flow coast down I (fresh core)

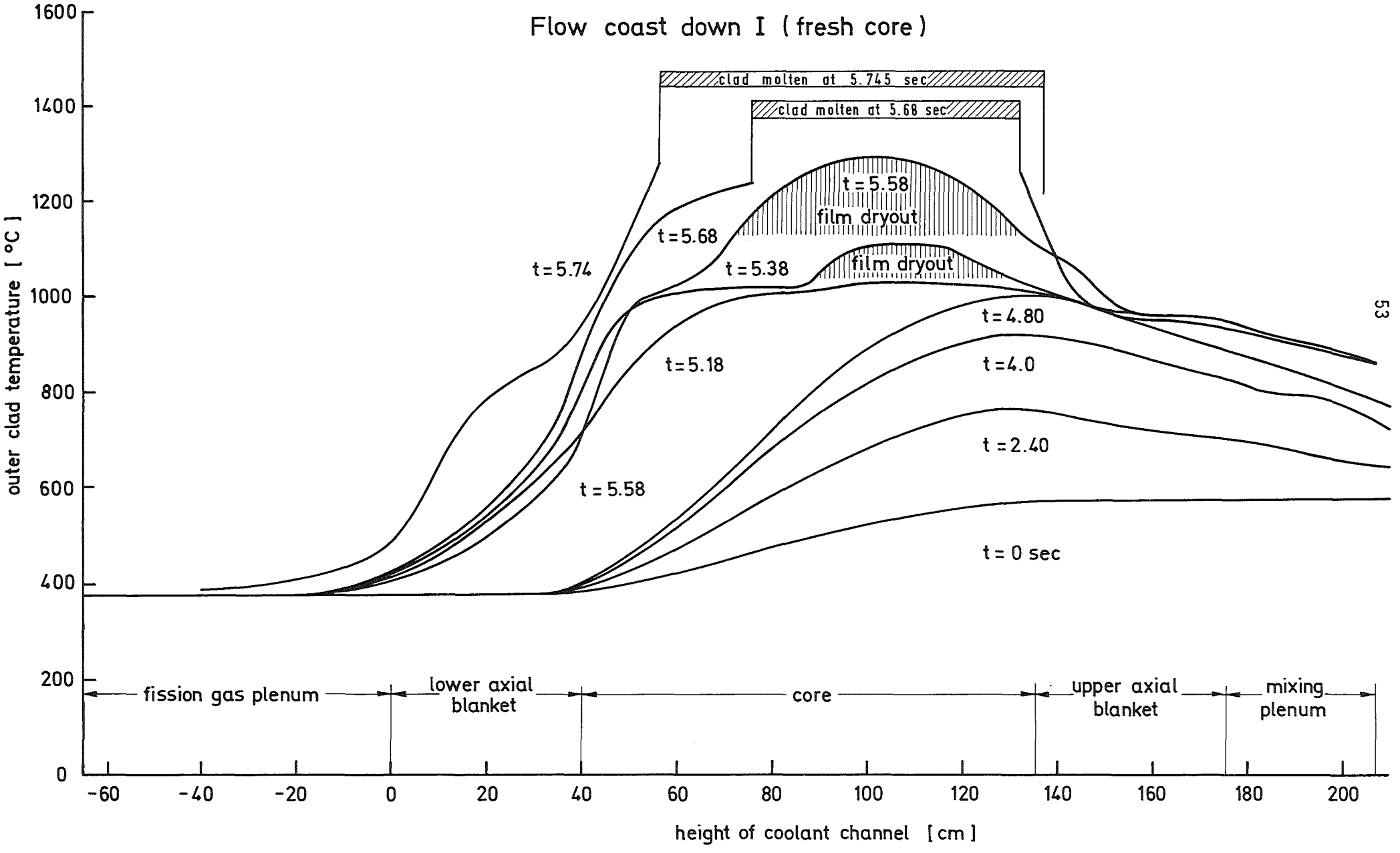

Fig. 4.1.1.k Fuel- and cladding-temperatures (midplane) as a function of time
Flow coast down I (fresh core)

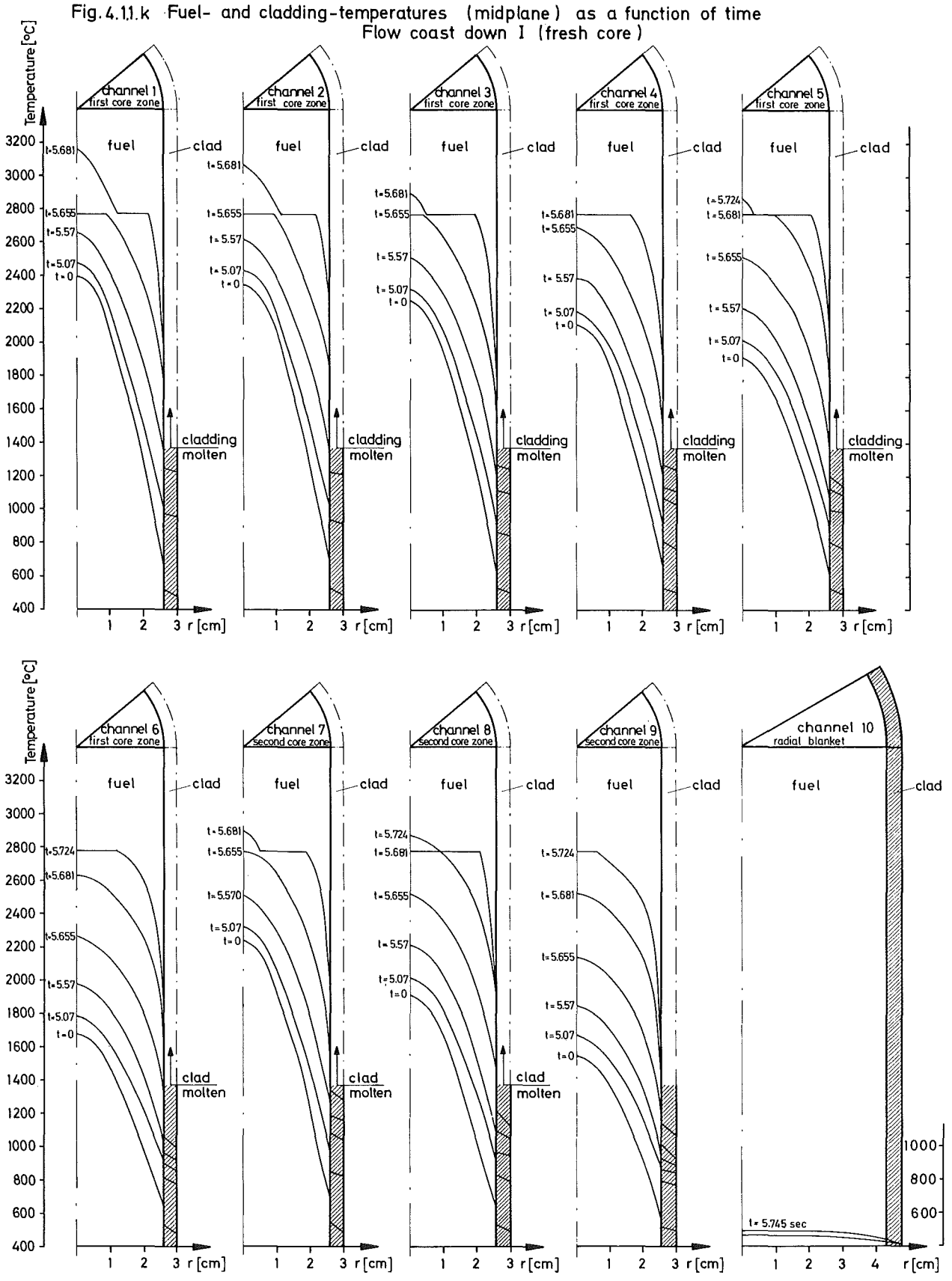

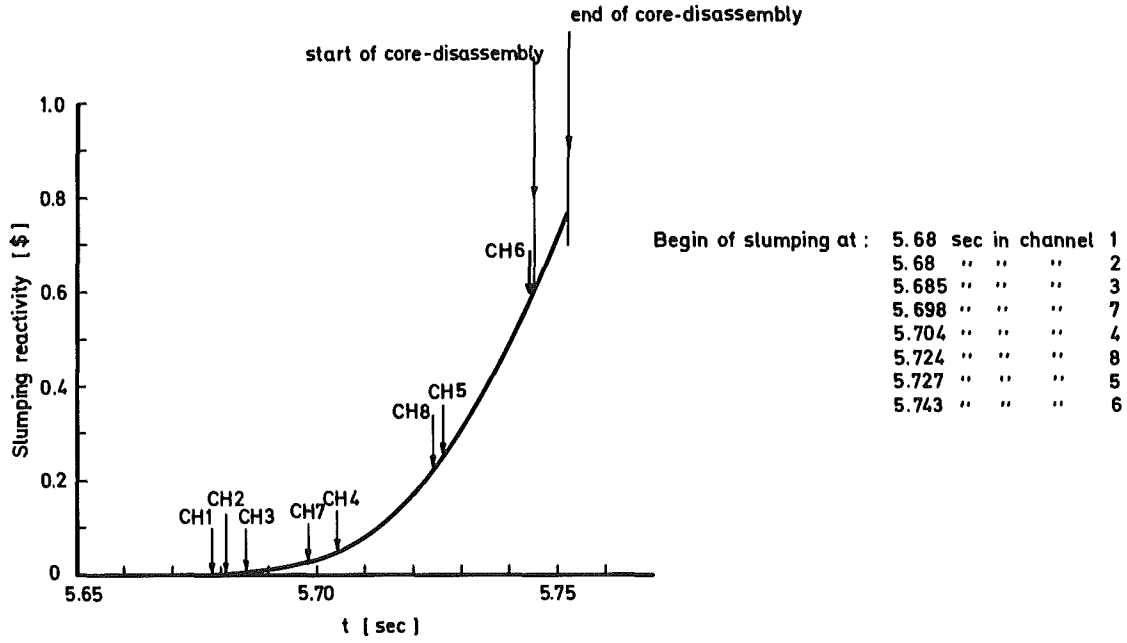

Fig.4.1.1.l Fuel slumping reactivity as function of time

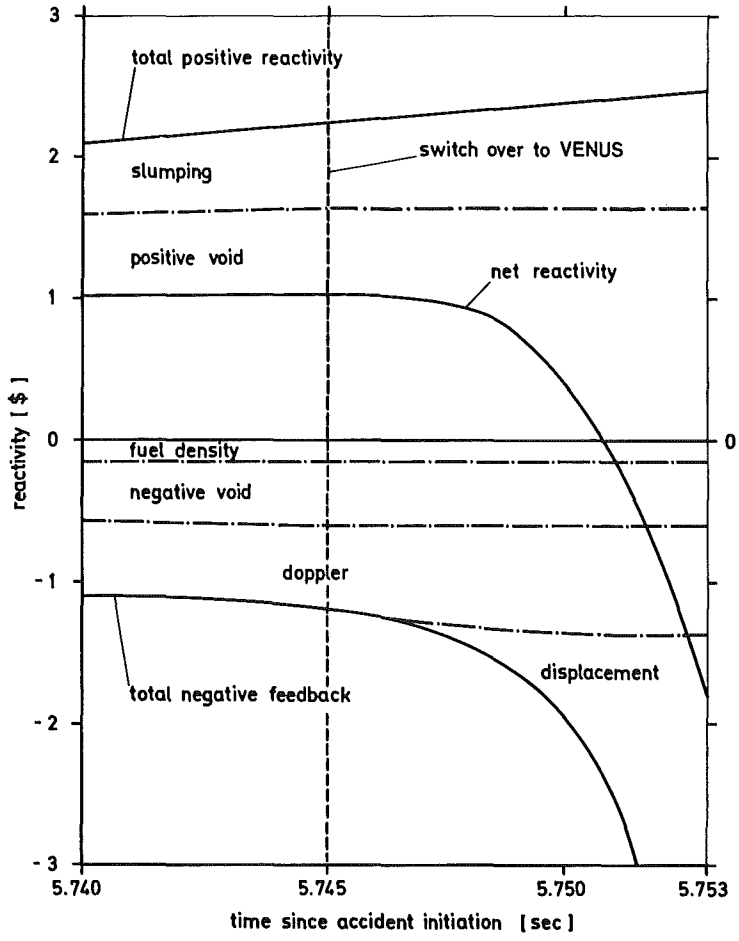

Fig.4.1.1.m Flow coast down I (fresh core)
Reactivities immediately before and during the disassembly phase

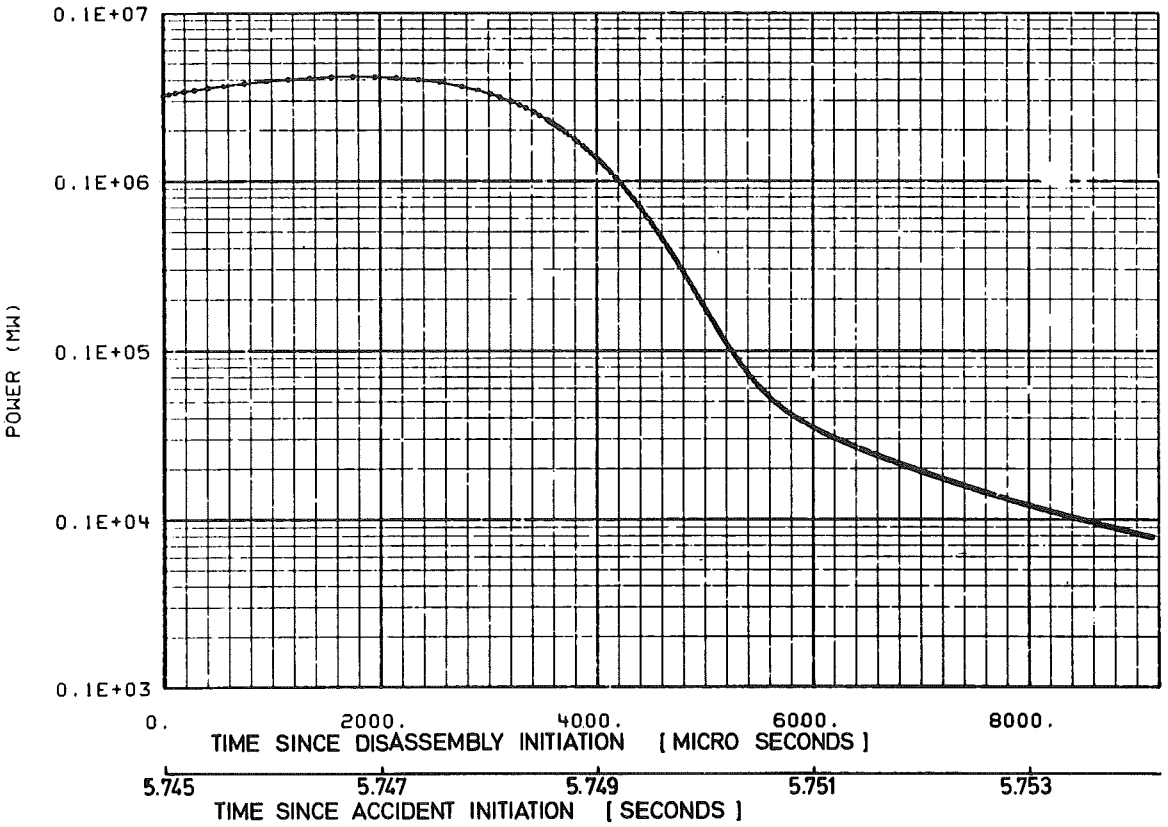

FIG. 4.11.n. FLOW COAST DOWN I
POWER AS FUNCTION OF TIME DURING THE DISASSEMBLY PHASE

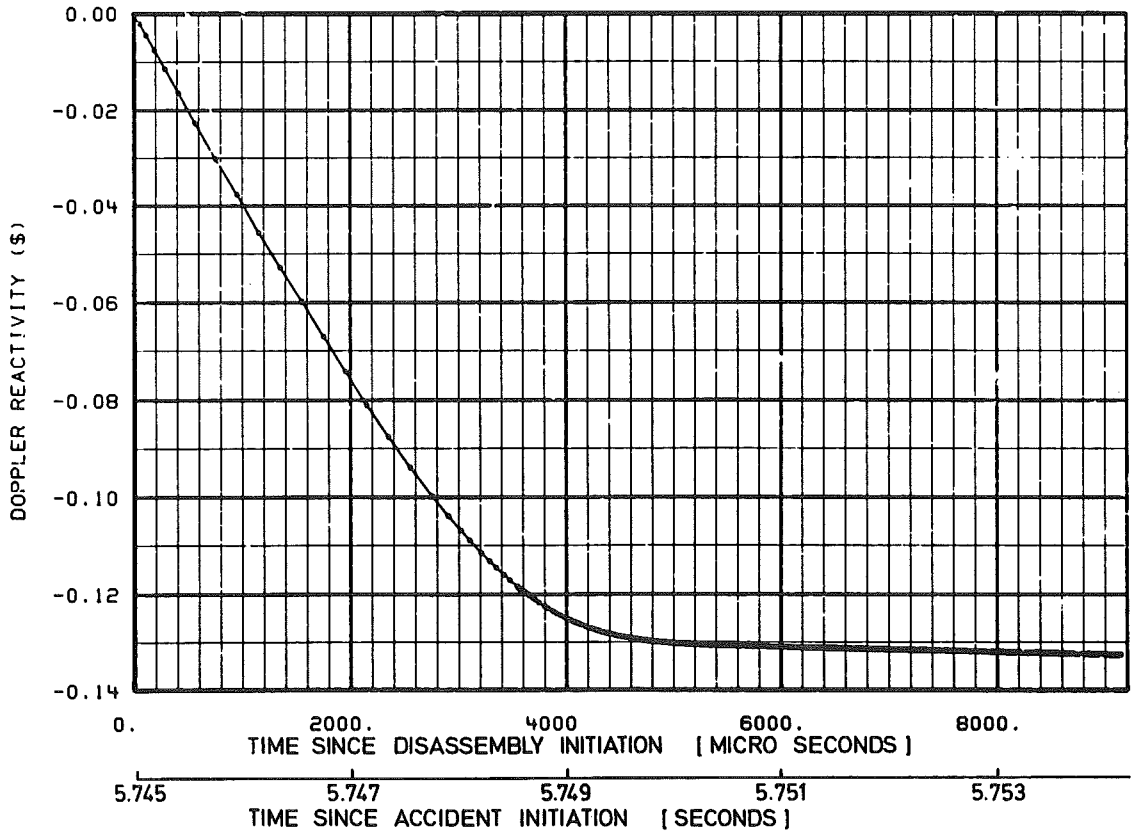

FIG. 4.11.o FLOW COAST DOWN I
DOPPLER FEEDBACK AS FUNCTION OF TIME DURING THE DISASSEMBLY PHASE

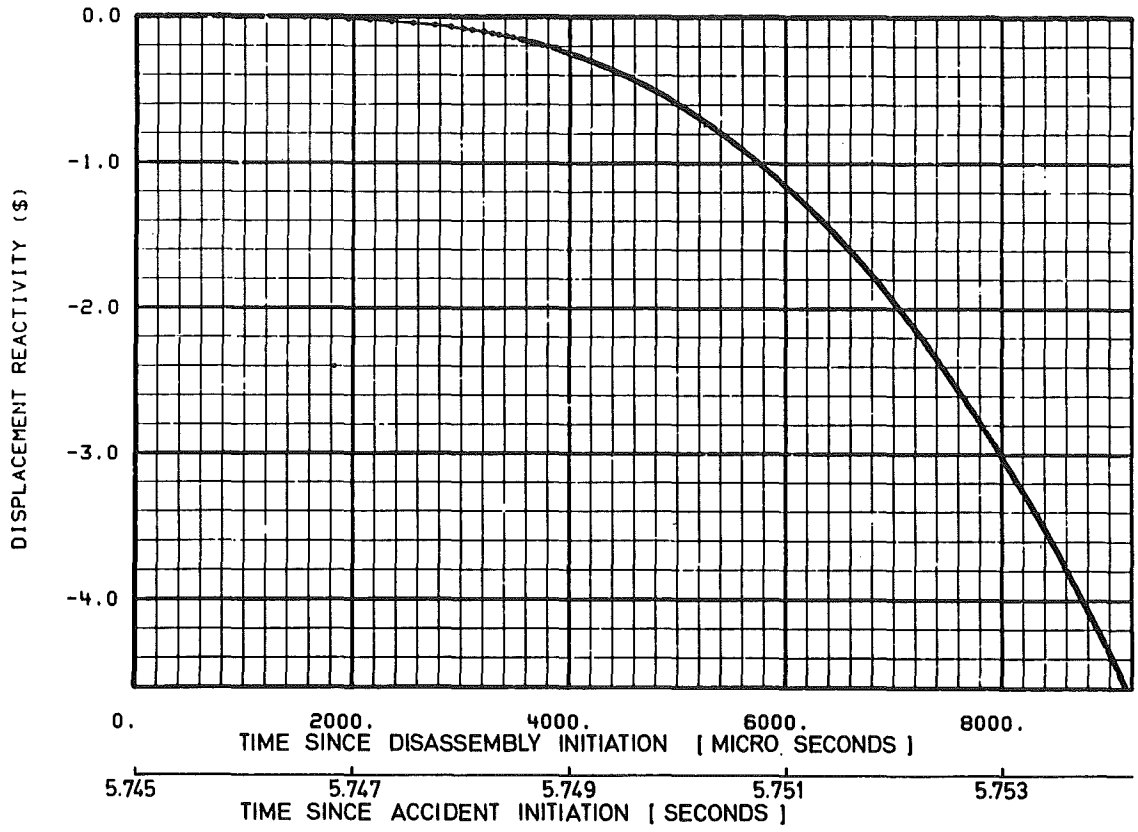

FIG. 4.11.p FLOW COAST DOWN I
DISPLACEMENT REACTIVITY AS FUNCTION OF TIME DURING THE DISASSEMBLY PHASE

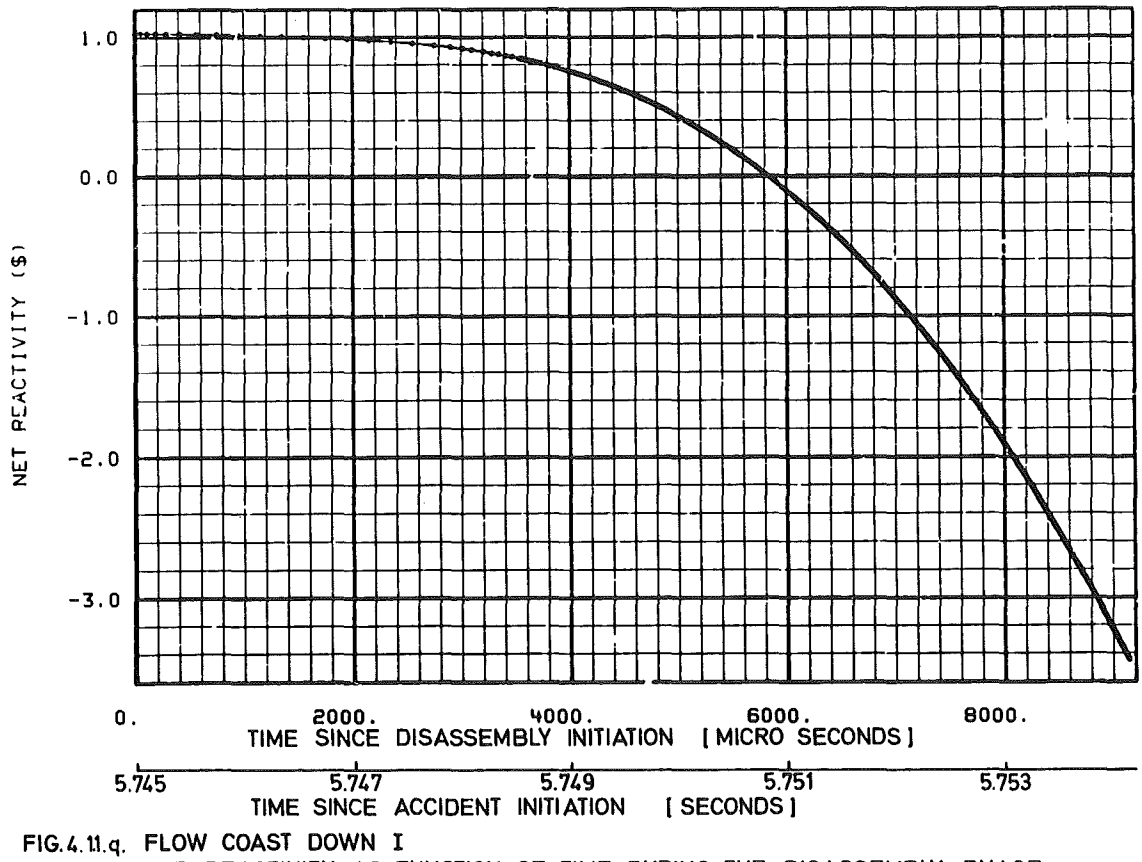

FIG. 4.11.q. FLOW COAST DOWN I
NET REACTIVITY AS FUNCTION OF TIME DURING THE DISASSEMBLY PHASE

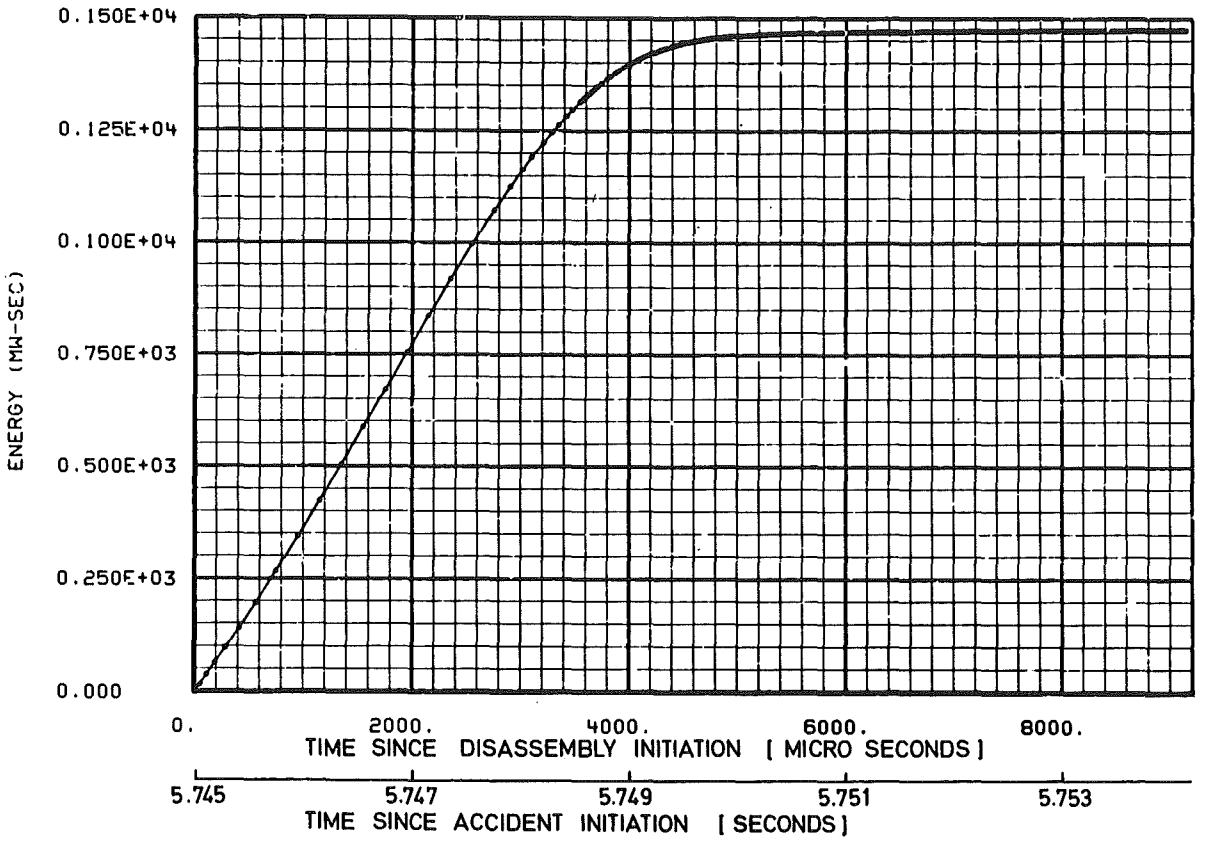

FIG. 4.11.r FLOW COAST DOWN I (FRESH CORE)
THERMAL ENERGY RELEASE DURING THE DISASSEMBLY PHASE

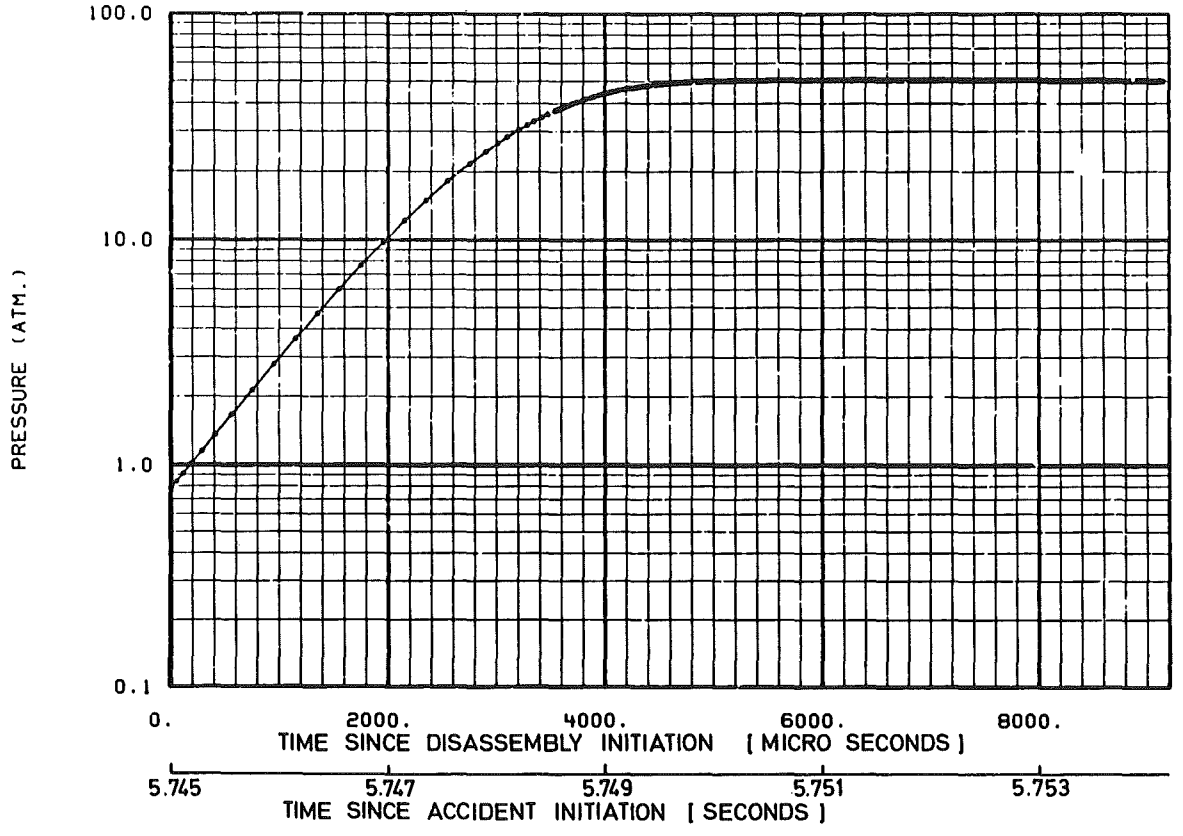

FIG. 4.11.s FLOW COAST DOWN I
PRESSURE AT THE CENTRE OF THE CORE AS FUNCTION OF TIME
DURING THE DISASSEMBLY PHASE

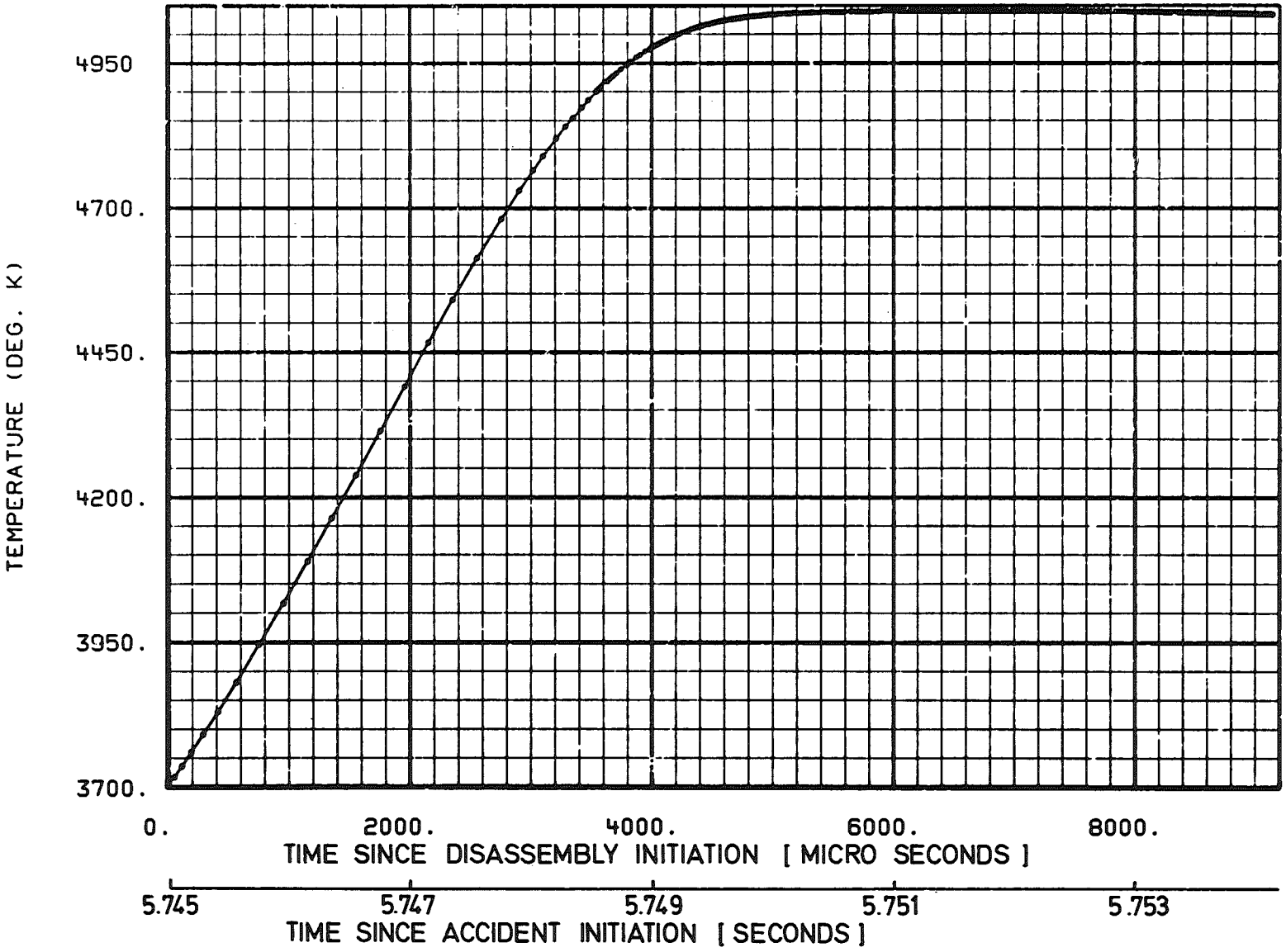

FIG. 4.11.t FLOW COAST DOWN I
TEMPERATURE AT THE CENTRE OF THE CORE AS FU] OF TIME
DURING THE DISASSEMBLY PHASE

4.1.2 Flow coast down accident in an equilibrium core

In contrast to the flow coast down accident for a fresh core (section 4.1.1) it is possible that in a core with a high burnup, fission gas is released when fuel pins fail. This generates larger gas bubbles in the core coolant channels and also positive reactivity effects with a subsequent power excursion. In a fuel element of SNR-3oo, the fission gas plenum is arranged underneath the lower axial blanket, contrary to the FFTF-design /4/. Over the entire course of the accident, up to the point of disassembly, the cladding temperatures (fig. 4.1.1h and 4.1.2i) remain less then 45o^{o}C in this area. For the fission gas plenum, cladding temperatures that would result in failure of the cladding are not reached. Moreover, the fission gas plenum of each fuel pin is reinforced with a support tube; hence, a rupture of the external cladding tube would only give rise to a gradual fission gas release through an orifice of the inner support tube. Therefore, this case will not be considered here /3/. There is a small fission gas plenum of 4 cm length above the upper axial blanket in the SNR-3oo fuel element. Since only a small amount of fission gas can be stored there, only little fission gas would be released in case of a rupture of the cladding tube. This fission gas could give rise to minor negative reactivity effects in the upper blanket region.
High cladding temperatures are reached in the core area approximately 3 sec after initiation of the accident. In this connection, minor quantities of fission gas may be released. A release of major fission gas quantities from this area is improbable because fission gas will collect mainly in the fission gas plenum by a process of diffusion.
In order to study the effects of major fission gas releases during hypothetical accident, it was assumed that the cladding of the fuel pin would fail at cladding temperatures of 86o^{o}C at the upper core end and 75o^{o}C in the core center respectively /3/. Under the assumption of 7% fission gas retention in the fuel pellet all fission gas existing in the core area would then instantaneously escape through a small opening of 2 mm diameter in the cladding into the cooling channel. For the dynamics of the gas bubbles in the cooling channel, experimental and theoretical results by Chawla and Hoglund /71/ were applied.For the SAS2A- and VENUS calculations, all core physics and material data outlined in section 3 were referred to the conditions of the high-burnup equilibrium core; in particular, the doppler constant was changed so that the value of 3.2 x 1o^{-3}, indicated in /3/, was attained for the equilibrium core. Axial fuel expansion was neglected.

Fig. 4.1.2a shows the time curve of reactor power from the initiation of the accident up to the abrupt discontinuation of power production following core disassembly. In the first 3 sec the coolant flow continuously decreases to approximately 3o% of the nominal flow (fig. 4.1). The reactor power remains relatively constant (fig. 4.1.2a) because the sodium void and doppler reactivities mutually compensate each other by the increasing coolant and fuel temperatures (fig. 4.1.2b). At the same time, the temperature of the fuel pin cladding increases quickly, reaching approximately 86o°C, after 3.2 sec in the central fuel element close to the upper axial core end (fig. 4.1.2h). The fuel temperature, as is evident from fig. 4.1.2d, undergoes only a slight change up to that time.
After reaching failure temperature for the cladding (75o°C in the center of the core, 86o°C at the upper core end), fission gas is released in the central channel (fig. 4.1.2e). According to the same criteria, fission gas release follows shortly afterwards in annular channels 2 to 9 (fig. 4.1.2.a, 4.1.2.b, 4.1.2.g). Since the gas bubbles expand in the axial center of the core, there is a succesion of positive reactivity ramps (fig. 4.1.2.b), all of which are limited to $ o.8 though. This causes the reactor power to rise to about 4-5 times the nominal value within a short time. The gas bubbles migrate upward in the channels (fig. 4.1.2e, 4.1.2.g), which causes the sodium void reactivity to decrease again. After 3.71 sec fission gas is released also in the outermost channel 9. The voiding pattern now generated in the reactor core and in the axial blanket results in a steep decrease of the net reactivity (fig. 4.1.1.b).

In this way, the reactor power even decreases for a short time to less than the steady state initial power (fig. 4.1.2.a).The central fuel temperature of the most highly rated central channel 1 increases to approximately 27oo°C (fig. 4.1.2.d). However, the melting temperature of the fuel has not been reached at any point in the reactor core at that time (fig. 4.1.2.f).

As a consequence of the increased power production during the fission gas release phase, the fuel pin cladding and coolant temperatures have increased more rapidly, and after 3.8o5 sec (fig. 4.1.2.a) there is boiling at the upper axial core end of the central fuel element (fig. 4.1.2.c) if the assumption of 5o°C sodium superheating (fig. 4.1.2.e) is also made.
Because at that time the coolant flow is still in excess of 25% of the initial nominal flow, the sodium vapour bubble generated first moves mainly in the upper axial blanket area, generating a negative sodium void reactivity effect here.

The fission gas bubble, existing at that time in the upper mixing plenum, is compressed by the dynamics of the liquid column on top of the sodium vapour bubble and expelled from the fuel element (fig. 4.1.3.e). Shortly afterwards (fig. 4.1.2.a), the same phenomena occurs in annular channels 2, 3, 4 and 7.
The expansion and movement of the sodium vapour bubbles into the upper axial blanket (fig. 4.1.2.b) causes the sodium void and the overall net reactivities to become negative, bringing about another short time decrease of power (fig. 4.1.2.a).

After slightly unstable boiling and the generation of several single bubbles, the vapour bubbles penetrate into the reactor core from top to bottom in annular channels 1, 2, 3, 4, 7 (fig. 4.1.3.e, 4.1.2.g),generating a positive reactivity ramp of about 4 $/sec (fig. 4.1.2.b). This causes the reactor power to rise again to approximately 3 times the nominal power. As a consequence of incipient sodium boiling in annular channels 5 and 8, however, (4.22 sec and 4.29 sec after initiation of the accident) this positive sodium void ramp is first limited, and the reactor power slightly decreases again (fig. 4.1.2.a, 4.1.2.b). At that time the sodium film adhering to the fuel pin cladding begins to dryout in the central channels (fig. 4.1.2.e) and the cladding temperatures (fig. 4.1.2.h) rapidly rise in this area. The fuel temperature again increases gradually (fig. 4.1.2.d). However, the point of fuel melt down is not yet reached (fig. 4.1.2.f). Annular channels 1, 2, and 3, and by and large, the annular channels 4 and 7 are already full of vapour after this phase (fig. 4.1.2.g). The boundary areas of these sodium vapour bubbles oscillate at the lower edge of the core as well as at the end of the upper axial blanket. This occurs at a frequency of approximately 5 Hz and hardly makes any further contributions to the positive sodium void reactivity ramps in the further course of the accident (fig. 4.1.2.b, 4.1.2.e, 4.1.2.g). Now the main contributions to the sodium void reactivity ramps come from annular channels 5 and 8, after a further increase in power (at 4.61 sec) mainly from annular channel 6 (fig. 4.1.2.b and 4.1.2.g). After 4.5 sec there is a more strongly positive sodium void reactivity ramp of 7 $/sec. This causes the reactor core to become super prompt critical (fig. 4.1.2.b), generating a very steep increase in power (fig. 4.1.2.a).

Now the fuel temperatures increase very rapidly (fig. 4.1.2.d), reaching the melting point and causing 6o to 8o% of the cross sectional area of the fuel pin to melt within a very short period of time (fig. 4.1.2.f). Again, fuel slumping occurs in accordance with the assumptions of the concept model of W. Bohl /22/.

Because of the rapid increase in power fuel slumping is initiated in the individual annular channels in very rapid succession:

annular channel	beginning of fuel slumping
1	4.672 sec
2	4.673
3	4.674
7	4.677
4	4.679
8	4.683
5	4.686

However, fuel slumping itself is a relatively slow process, hence, only the beginning of the fuel slumping event makes a contribution to the overall reactivity in the time scale of the processes now underway in the individual annular channels. Superposition of the positive reactivity contributions in the individual annular channels result in the overall reactivity curve shown in fig. 4.1.2.b, 4.1.2.k and 4.1.2.l. As a result of superposition of all reactivity contributions, the reactor core finally enters the disassembly phase with a positive reactivity ramp of 25 $/sec (coupling of SAS2A and VENUS).
Contrary to the case of the fresh core accident, the reactor core, because of the higher temperature level reached earlier, enters the disassembly phase as a result of the superposition of a sodium void reactivity and a fuel slumping reactivity ramp. The reactor power continues to rise for some time (fig. 4.1.2.m), but is then accommodated very rapidly by the negative doppler feedback (fig. 4.1.2.b, 4.1.2.l and 4.1.2.n) and, above all, by the very strong negative displacement reactivity (fig. 4.1.2.l,4.1.2.o).
The net reactivity (fig. 4.1.2.l, 4.1.2.p) decreases very rapidly and the reactor power very quickly decreases below the initial nominal power of 723 MWth (fig. 4.1.2.a). The energy production is stopped abruptly.

On the whole, an additional 12oo MWsec of thermal energy is released within this very short disassembly phase of approximately 7 msec (fig.4.1.2.q). This thermal energy is stored in a further increase in the fuel temperature (fig. 4.1.2.s), the fuel pressure (fig. 4.1.2.r) and additional fuel melting.

Fuel vapour pressures of 3o atm are reached in the center of the core (table 4.1.2A and table 4.1.2B).
As is evident from tables 4.1.2A and 4.1.2B, fuel is also molten in the central plane of the outer core regions. In annular channel 9 (fig. 4.1.2.i) and the lower and upper axial core regions of annular channels 2 through 8, the fuel cladding however, is still intact, even after disassembly; the radial cross section of the fuel pin is only partly molten. In the axial and radial blanket zones there has been neither fuel melt down or melt down of the can. All annular channels except for channels 6 and 9 are without any sodium (fig. 4.1.2.g).

On the whole, 21oo kg of fuel are completely molten and are no longer present in the original fuel pin or pellet geometries. The further course of the accident is discussed in section 5 together with the flow coast down accident for a fresh core.

T_{max} = 4788 ≙ 478 at Mesh Point /14,1/

22	3o3	3o3	3o3	3o3	3o3	291	289	271	268	278	274	247	241
21	381	38o	376	3o3	3o3	3o3	3o3	3o3	3o3	3o3	324	292	284
2o	415	413	4o9	386	383	3o3	3o3	3o3	3o3	3o3	3o3	3o3	3o3
19	433	431	427	398	394	3o7	3o3	3o3	3o3	369	362	3o3	3o3
18	449	447	442	41o	4o7	385	381	3o3	3o3	375	368	3o3	3o3
17	463	461	455	421	418	392	387	312	3o7	386	372	3o3	3o3
16	471	469	463	429	425	398	393	38o	375	393	384	3o3	3o3
15	477	475	469	435	431	4o4	398	384	378	396	388	3o3	3o3
14	487	476	47o	437	433	4o6	3oo	385	379	4oo	392	3o3	3o3
13	477	475	468	437	432	4o7	4oo	39o	383	4o1	395	3o3	3o3
12	47o	468	462	431	426	4o2	396	386	38o	397	392	3o3	3o3
11	462	459	453	424	419	397	39o	382	376	393	388	3o3	3o3
1o	448	445	439	411	4o7	386	382	37o	365	383	378	3o3	3o3
9	432	43o	424	398	394	375	369	362	356	372	368	3o3	3o3
8	411	4o9	4o4	382	378	363	357	35o	346	359	355	3o3	3o3
7	381	379	374	3o3	3o3	3o3	3o3	3o3	3o3	3o3	3o3	3oo	296
6	3o3	3o3	3o3	297	294	282	279	267	264	279	277	239	237
	1	2	3	4	5	6	7	8	9	1o	11	12	13

Table 4.1.2A Flow coast down II (equilibrium core)

Temperatures in each mesh of the core after the end of the disassembly phase

P_{max} = 28.4 bar ≙ 284 at Mesh Point /14,1/

22	o	o	o	o	o	o	o	o	o	o	o	o	o
21	14	15	11	3	o	o	o	o	o	1	o	o	o
2o	49	49	38	18	13	1	o	o	o	4	o	o	o
19	84	83	67	33	21	7	1	o	o	7	5	o	o
18	133	127	1o8	53	17	12	o	1	9	7	7	o	o
17	192	181	156	77	49	26	16	4	4	12	9	o	o
16	239	226	194	1o1	64	35	2o	12	1o	2o	14	o	o
15	277	261	224	12o	77	39	24	14	13	13	17	o	o
14	284	268	229	126	8o	44	15	16	14	26	2o	o	o
13	275	258	22o	121	7o	41	26	18	15	27	21	o	o
12	223	219	186	1o1	66	38	22	16	14	24	19	o	o
11	186	175	148	76	52	28	18	13	11	2o	16	o	o
1o	127	121	99	52	34	19	13	8	7	12	11	o	o
9	8o	76	61	3o	21	11	7	5	4	8	7	o	o
8	45	46	34	16	11	6	4	3	2	4	3	o	o
7	14	14	1o	2	o	o	o	o	o	o	o	o	o
6	o	o	o	o	o	o	o	o	o	o	o	o	o
	1	2	3	4	5	6	7	8	9	1o	11	12	13

Table 4.1.2B Flow coast down II (equilibrium core)

Pressures in each mesh of the core after the end of the disassembly phase

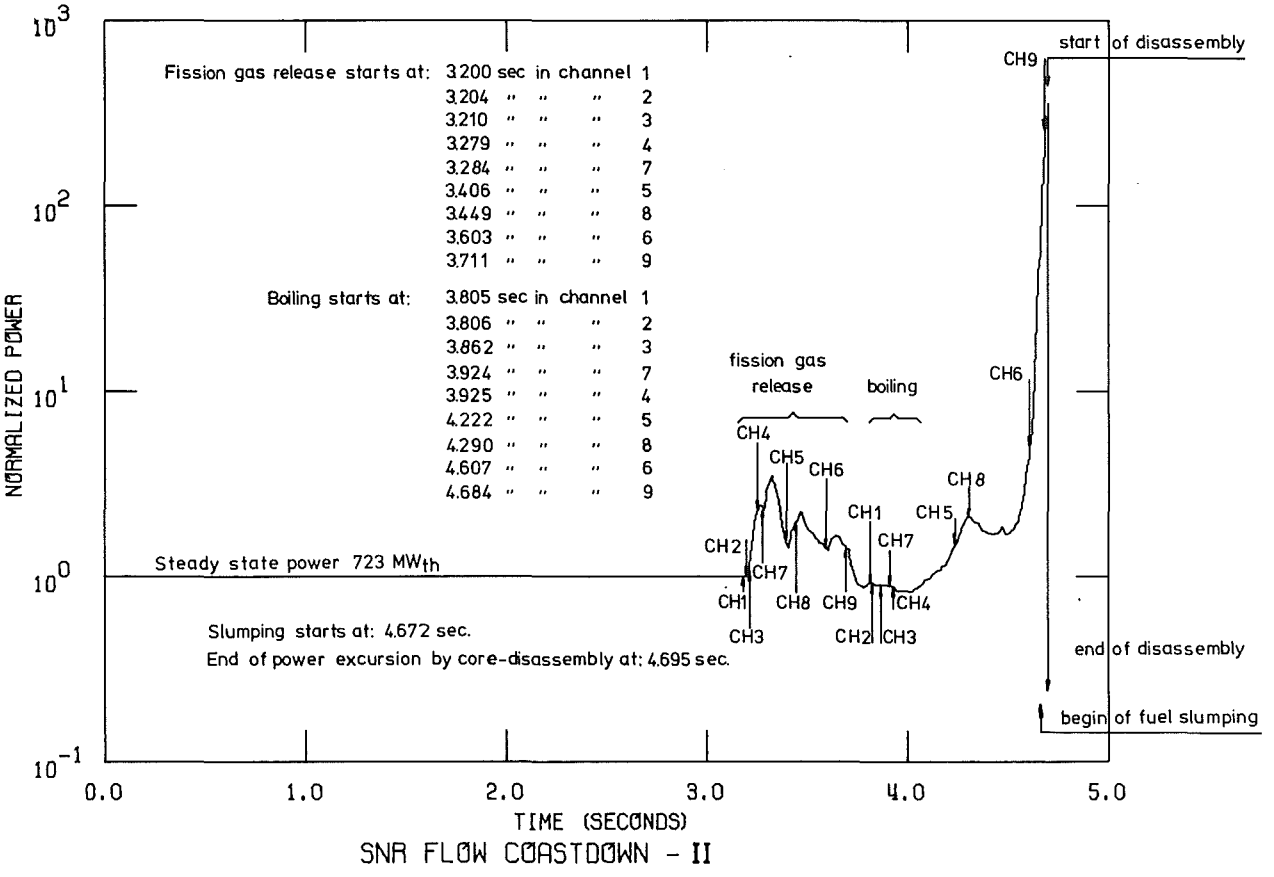

Fig.4.1.2.a Normalized power as function of time

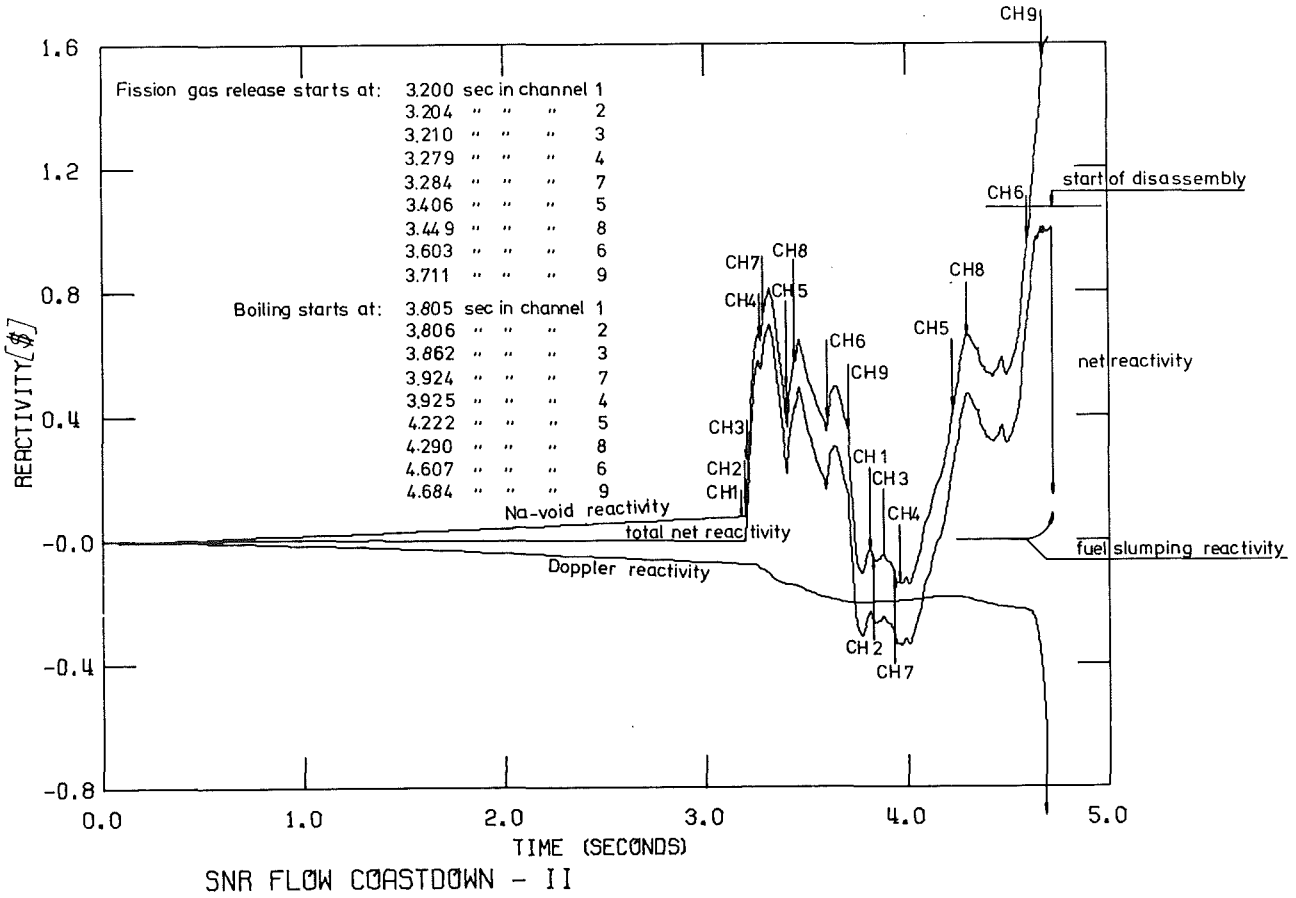

Fig.4.1.2b Reactivity as function of time

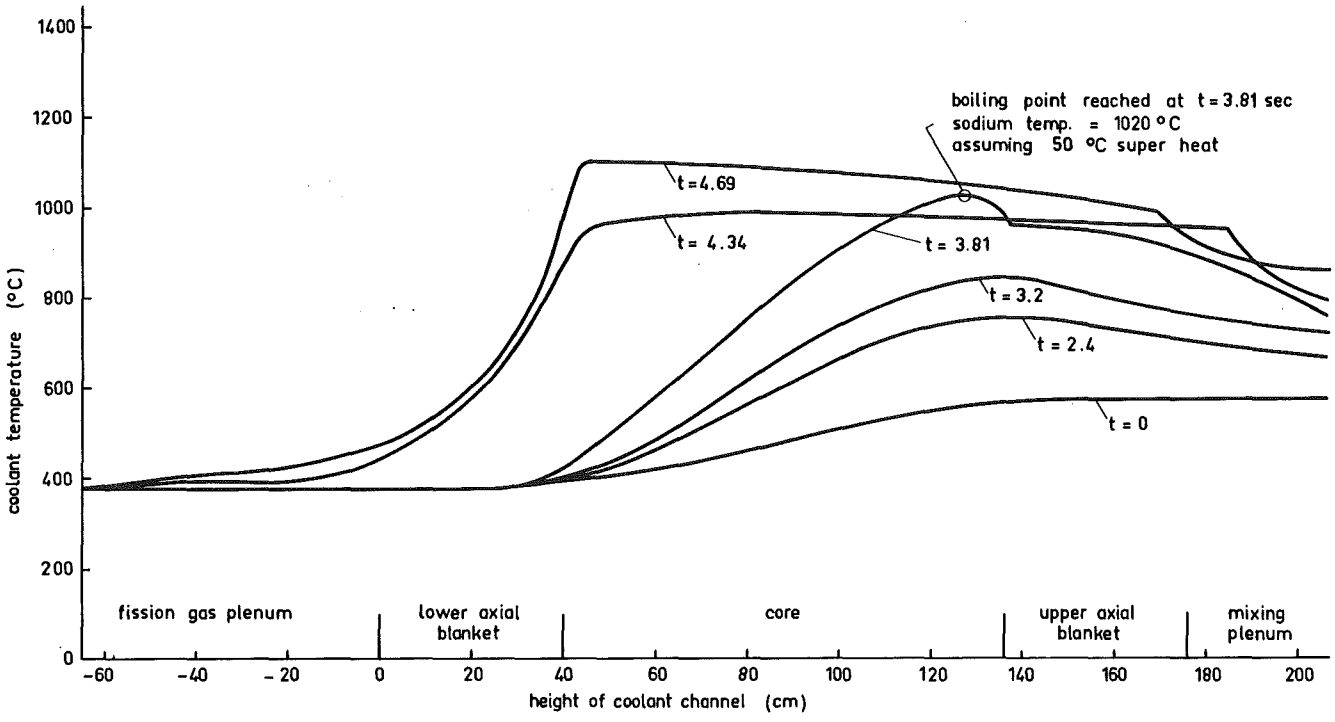

Fig. 4.1.2.c Flow coast down II
Coolant temperature in channel 1

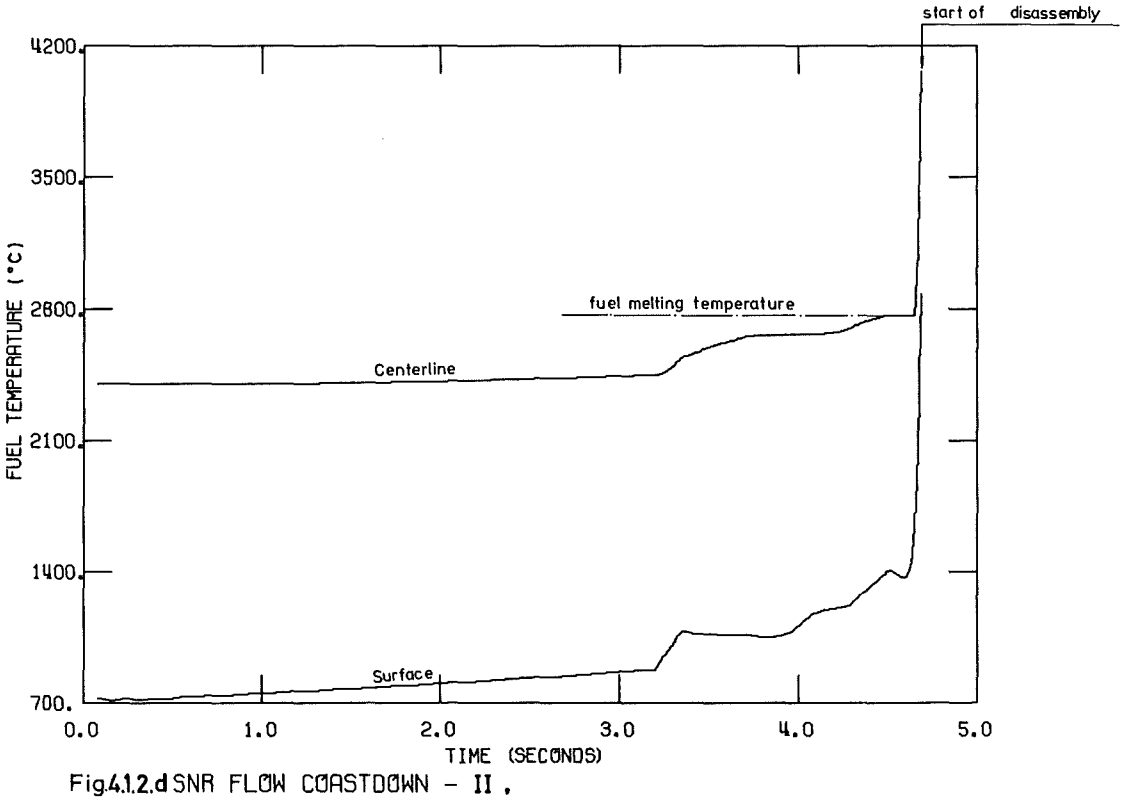

Fig.4.1.2.d SNR FLOW COASTDOWN - II ,
FUEL TEMPERATURE (CHANNEL 1 MIDPLANE) AS A FUNCTION OF TIME

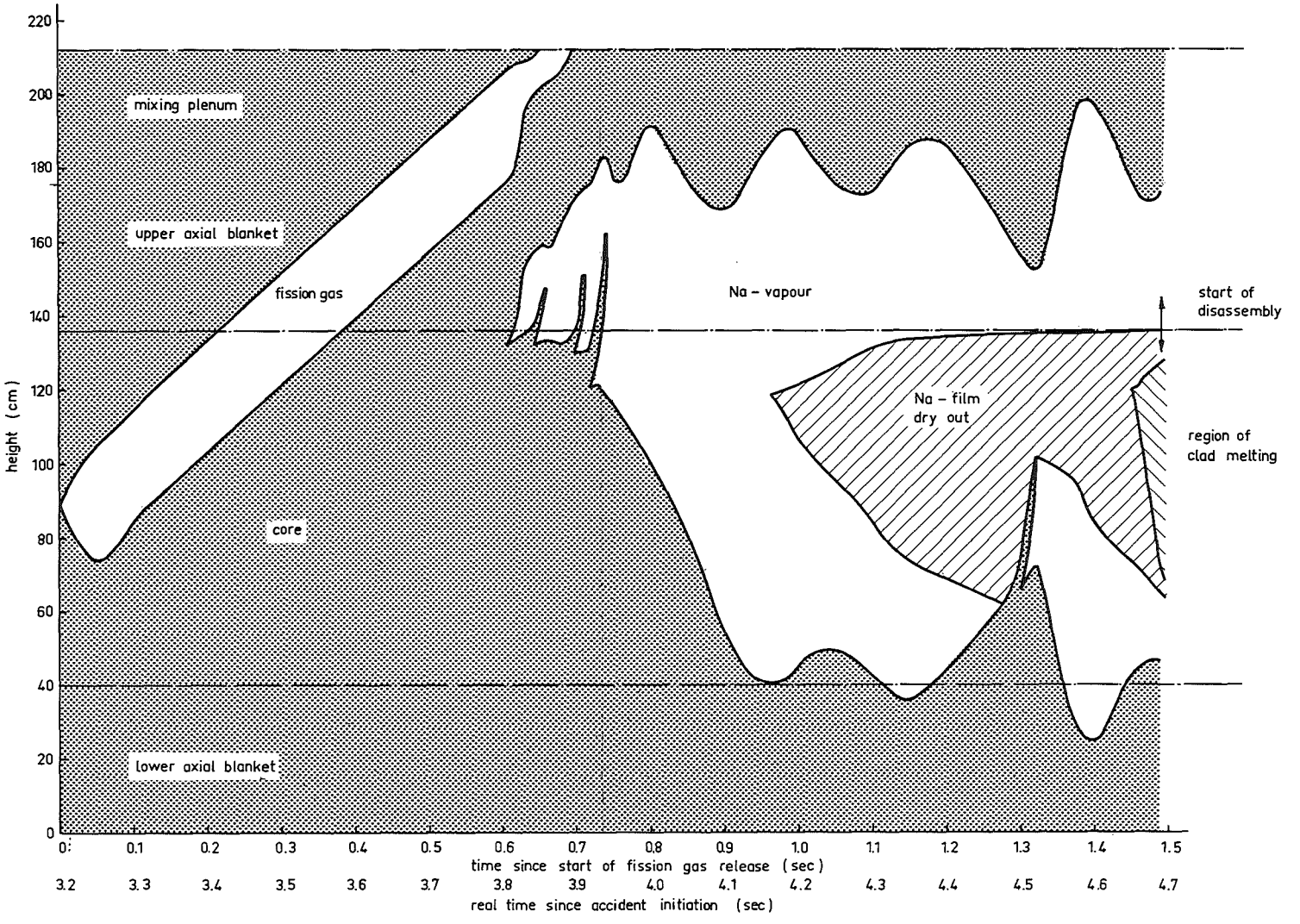

Fig. 4.1.2.e Fission gas release and Na boiling pattern in channel 1
Flow coast down II

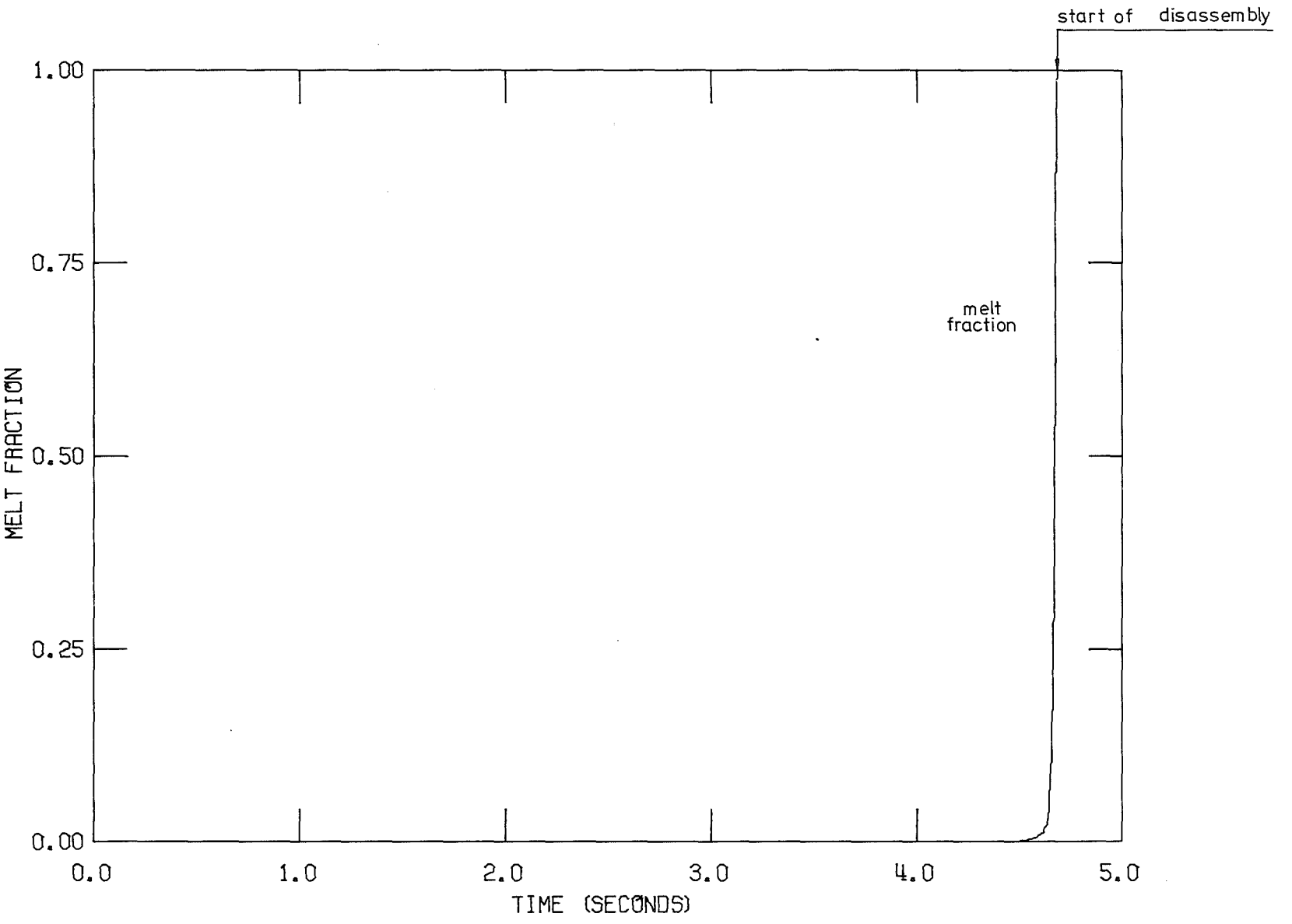

Fig.4.1.2.f SNR FLOW COASTDOWN – II

MELT FRACTION (CHANNEL 1 MIDPLANE) AS A FUNCTION OF TIME

FIG. 4.1.2.g Fission gas release and boiling pattern during predisassembly phase

Flow coast down II (equilibrium core)

No fission gas release until
time : 3.200 sec
after accident initiation

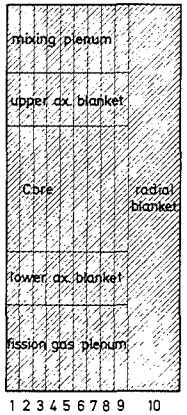

time : 3.245 sec
after accident initiation

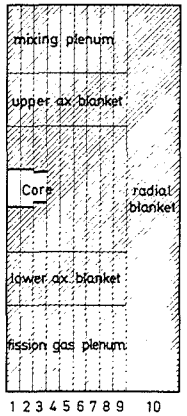

time : 3.337 sec
after accident initiation

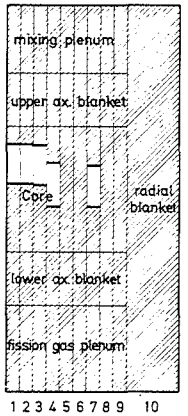

time : 3.515 sec
after accident initiation

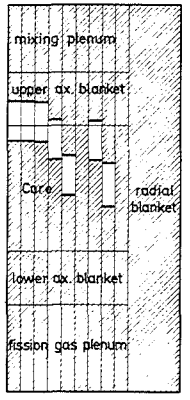

time : 3.680 sec
after accident initiation

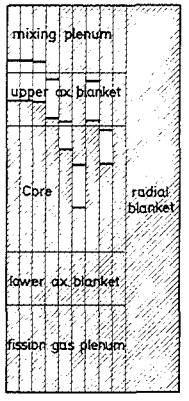

time : 3.750 sec
after accident initiation

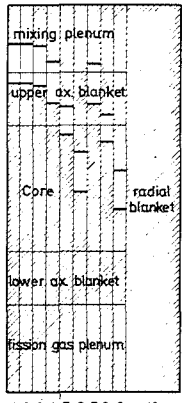

time : 3.788 sec
after accident initiation

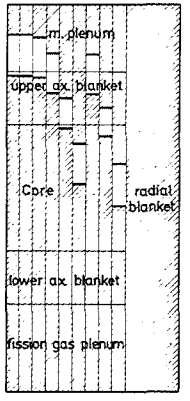

time : 3.825 sec
after accident initiation

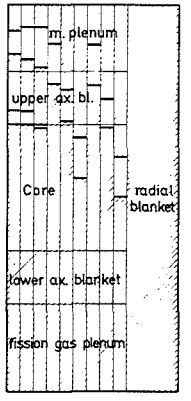

time : 3.935 sec
after accident initiation

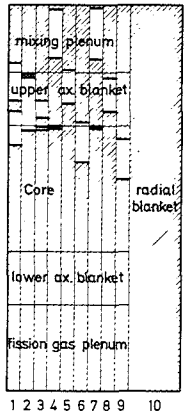

time : 3.978 sec
after accident initiation

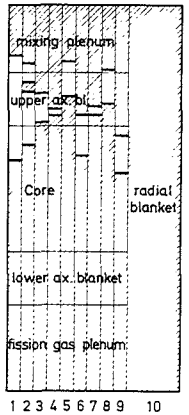

time : 4.486 sec
after accident initiation

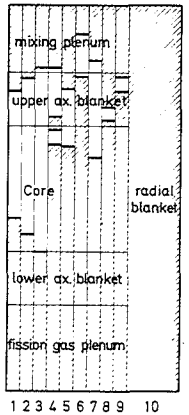

time : 4.528 sec
after accident initiation

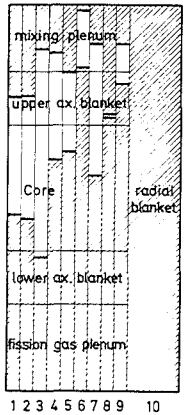

time : 4.600 sec
after accident initiation

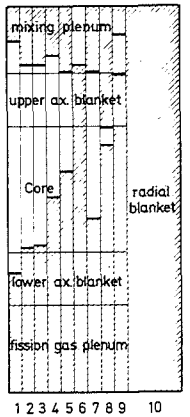

time : 4.626 sec
after accident initiation

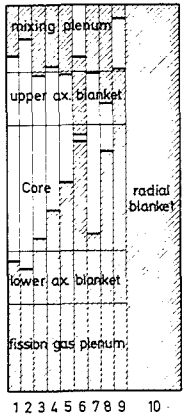

time : 4.671 sec
after accident initiation

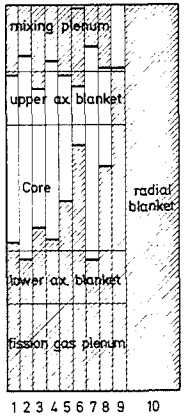

time : 4.687 sec
after accident initiation
just before begin of disassembly

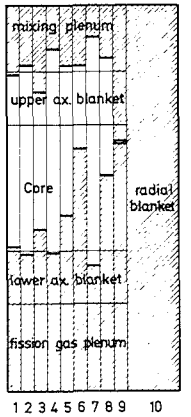

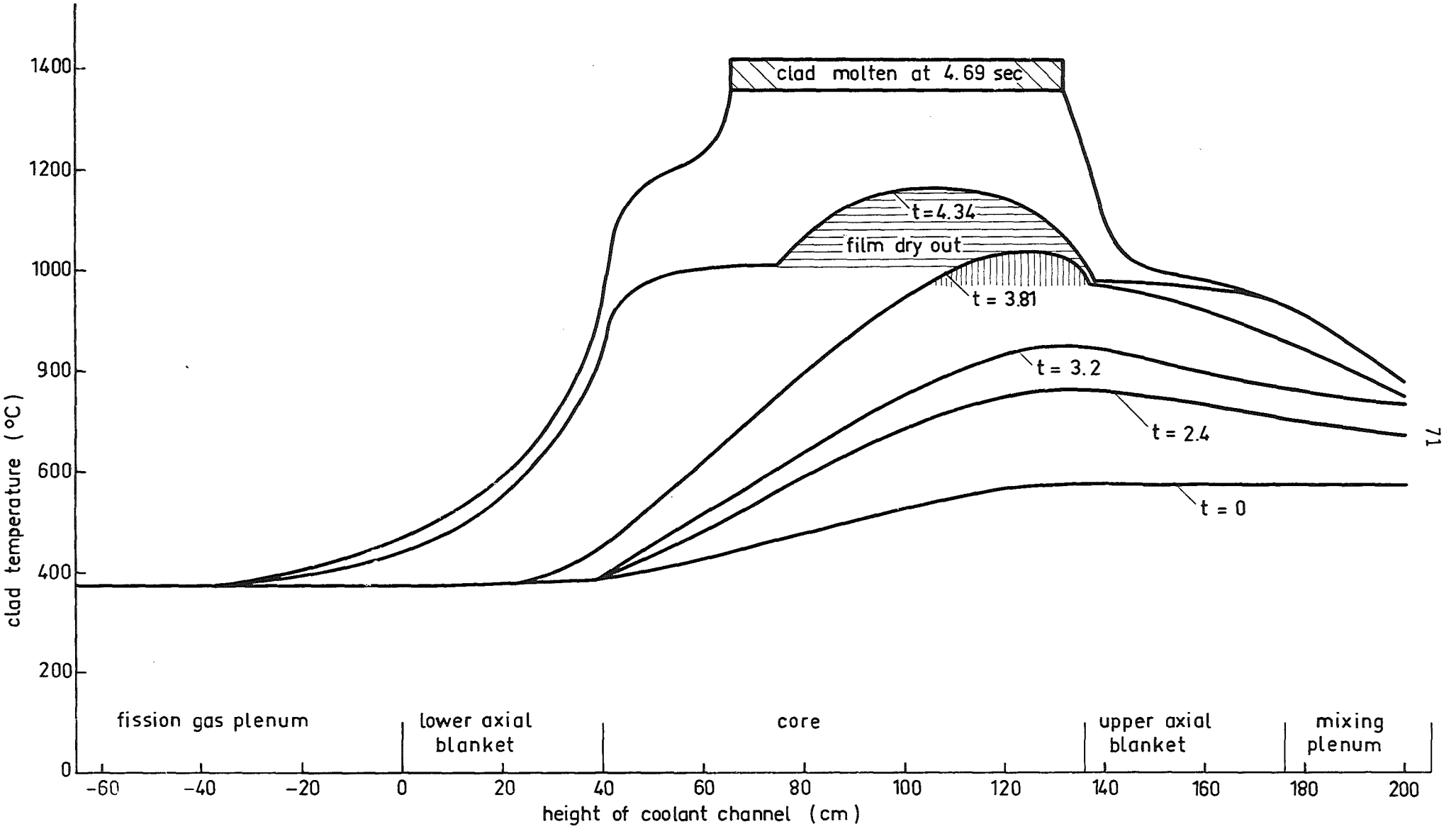

Fig. 4.1.2.h Flow coast down II

Outer clad temperature in channel 1

Fig. 4.1.2.i Fuel temperatures as a function of time
Flow coast down II

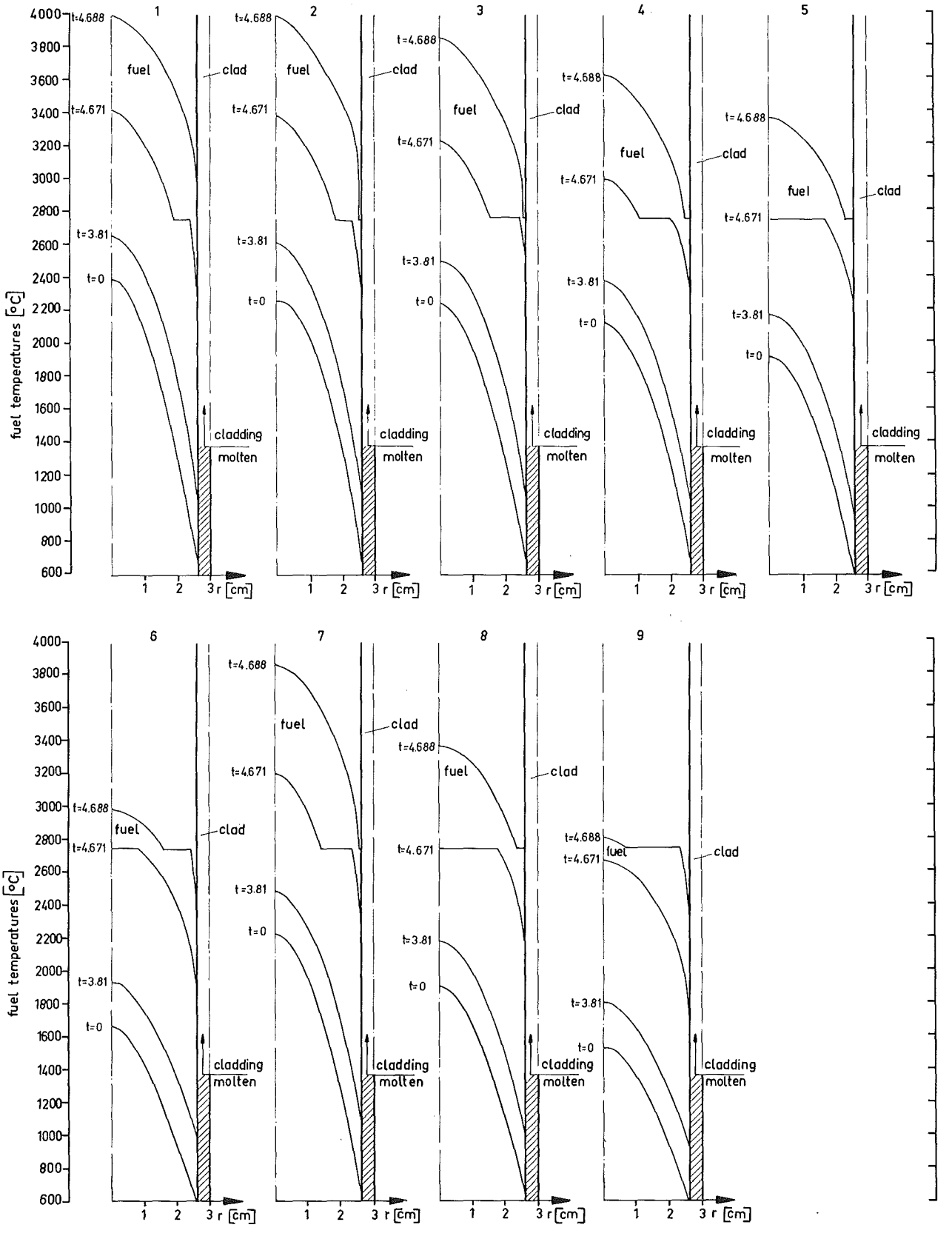

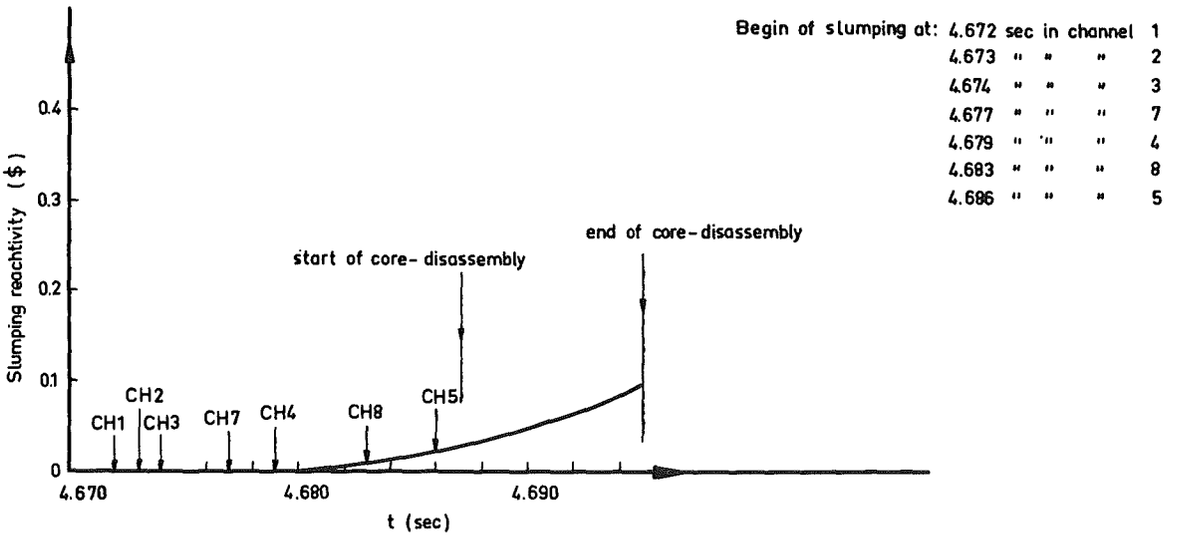

Fig. 4.1.2.k Fuel slumping reactivity as function of time
Flow coast down II - equilibrium core

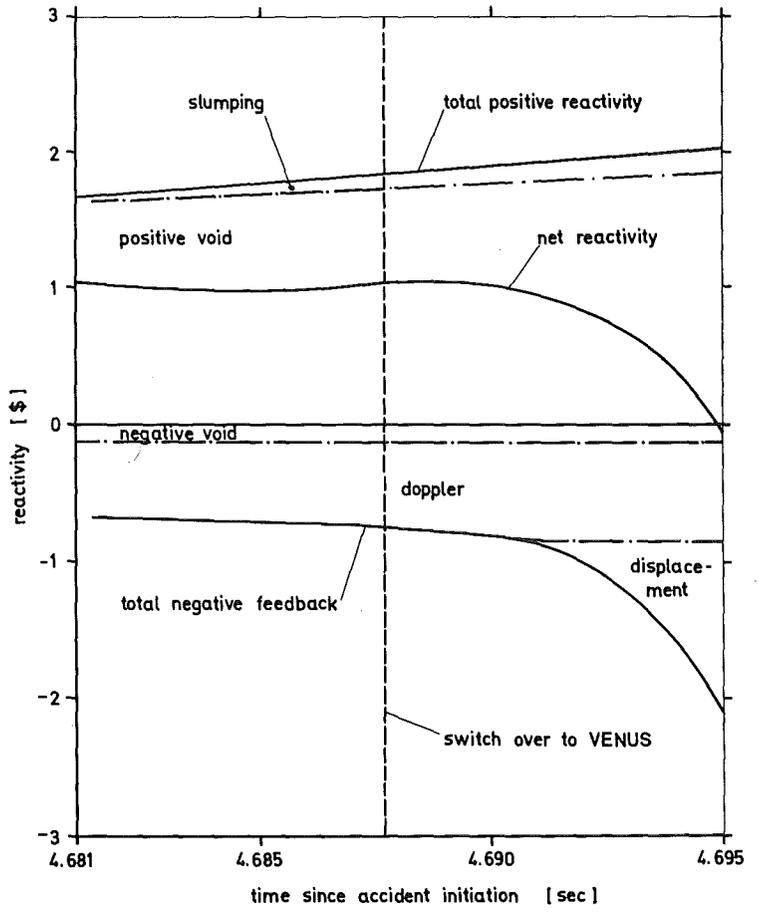

Fig. 4.1.2.l Flow coast down II
Reactivities immediately before and
during the disassembly phase

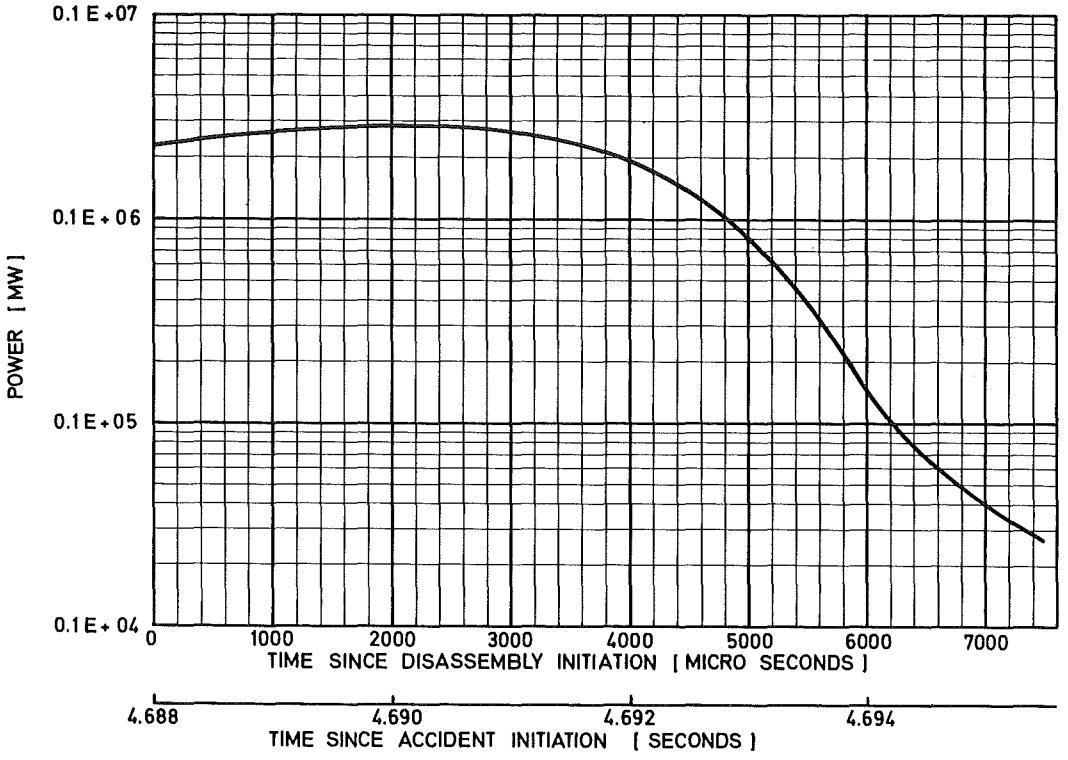

FIG. 4.1.2.m FLOW COAST DOWN II
POWER AS FUNCTION OF TIME DURING THE DISASSEMBLY PHASE

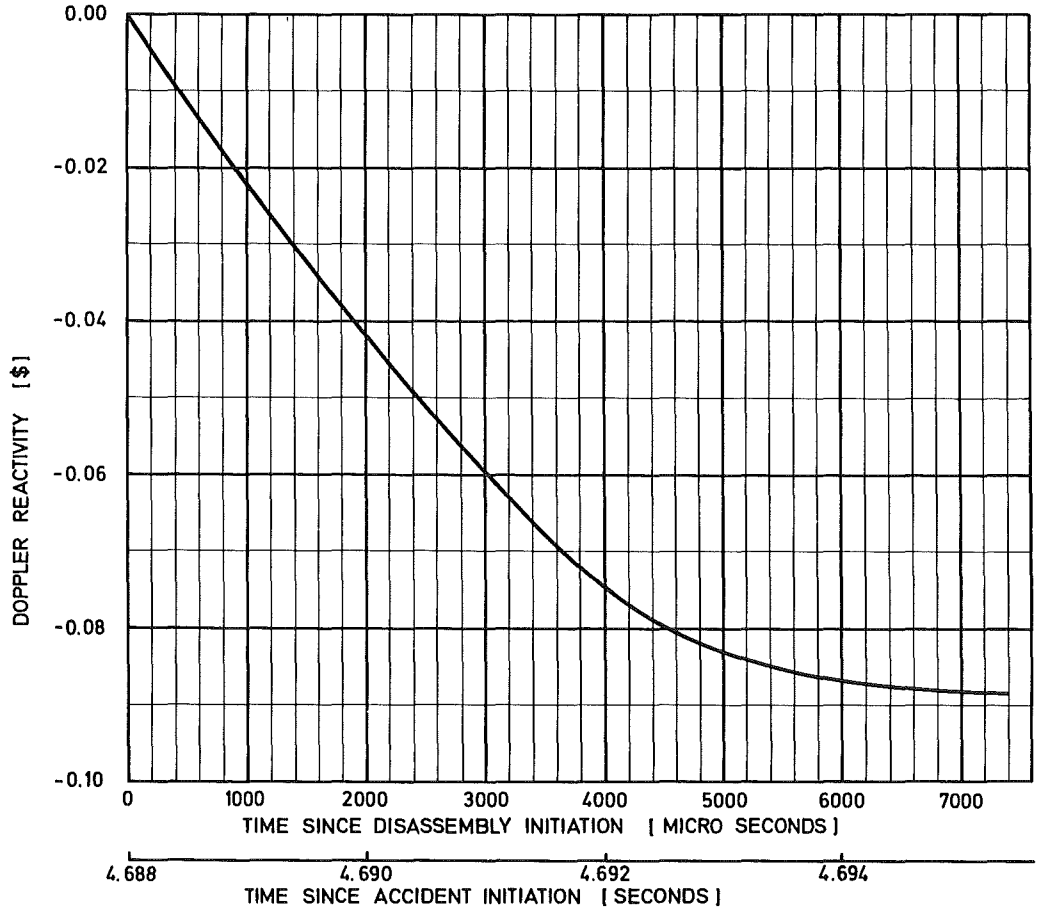

FIG. 4.1.2.n FLOW COAST DOWN II
DOPPLER FEEDBACK AS FUNCTION OF TIME DURING THE DISASSEMBLY PHASE

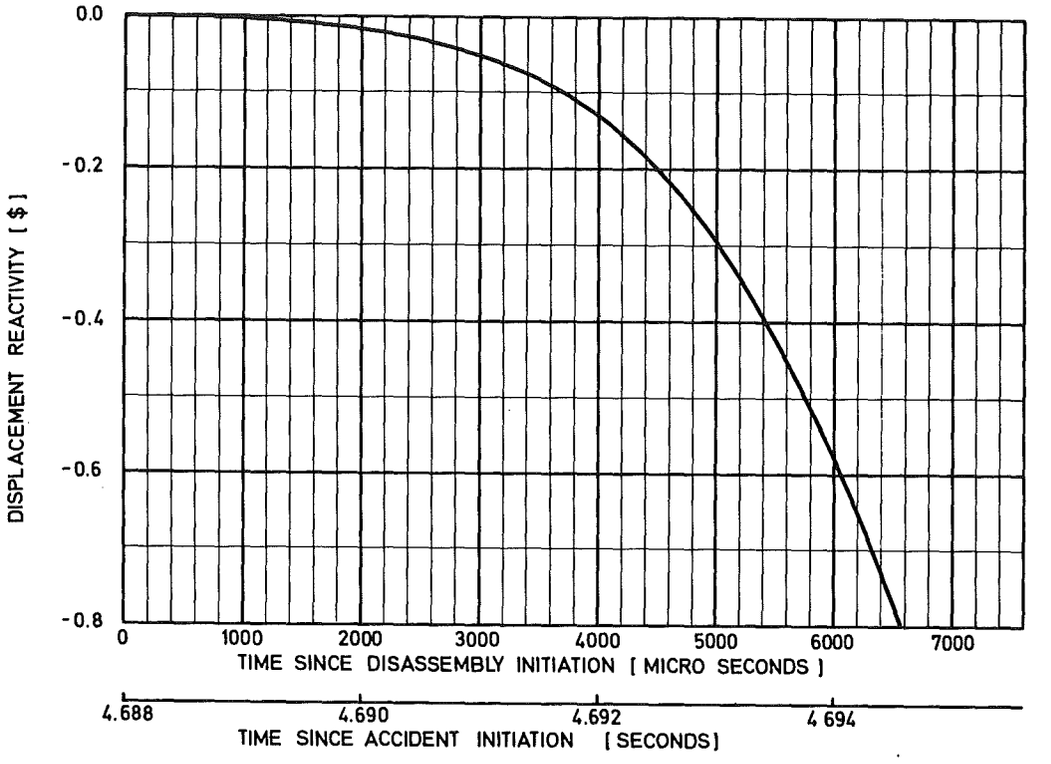

FIG. 4.1.2.o FLOW COAST DOWN II
DISPLACEMENT REACTIVITY AS FUNCTION OF TIME DURING THE DISASSEMBLY PHASE

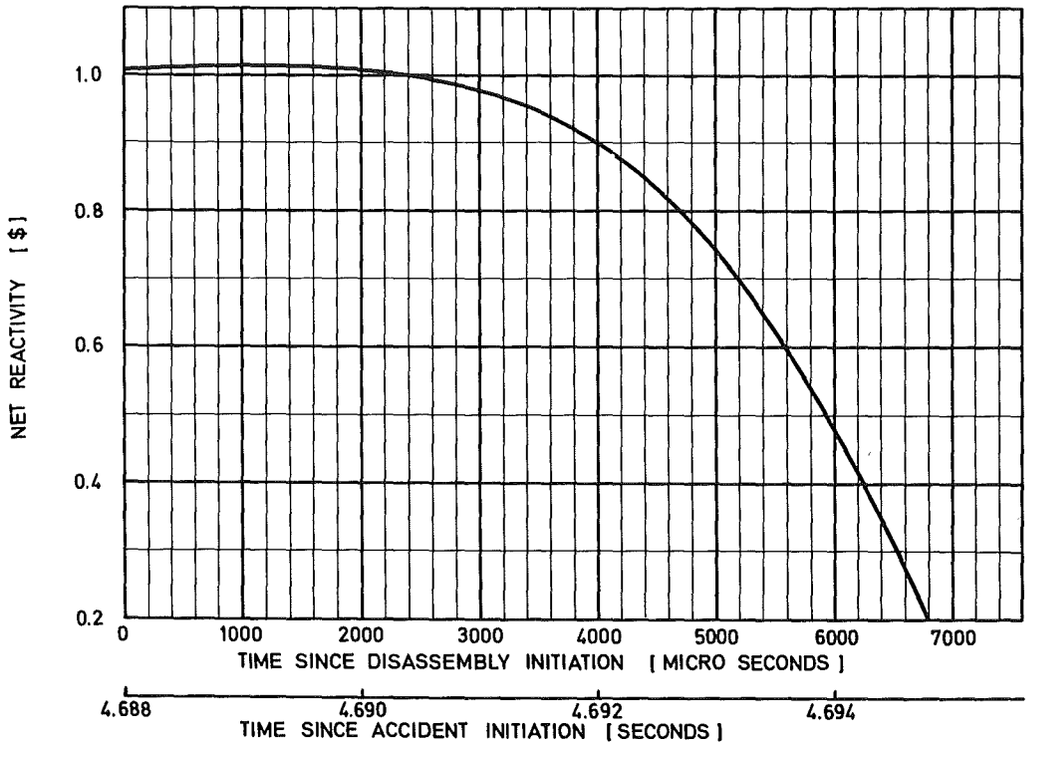

FIG. 4.1.2.p FLOW COAST DOWN II
NET REACTIVITY AS FUNCTION OF TIME DURING THE DISASSEMBLY PHASE

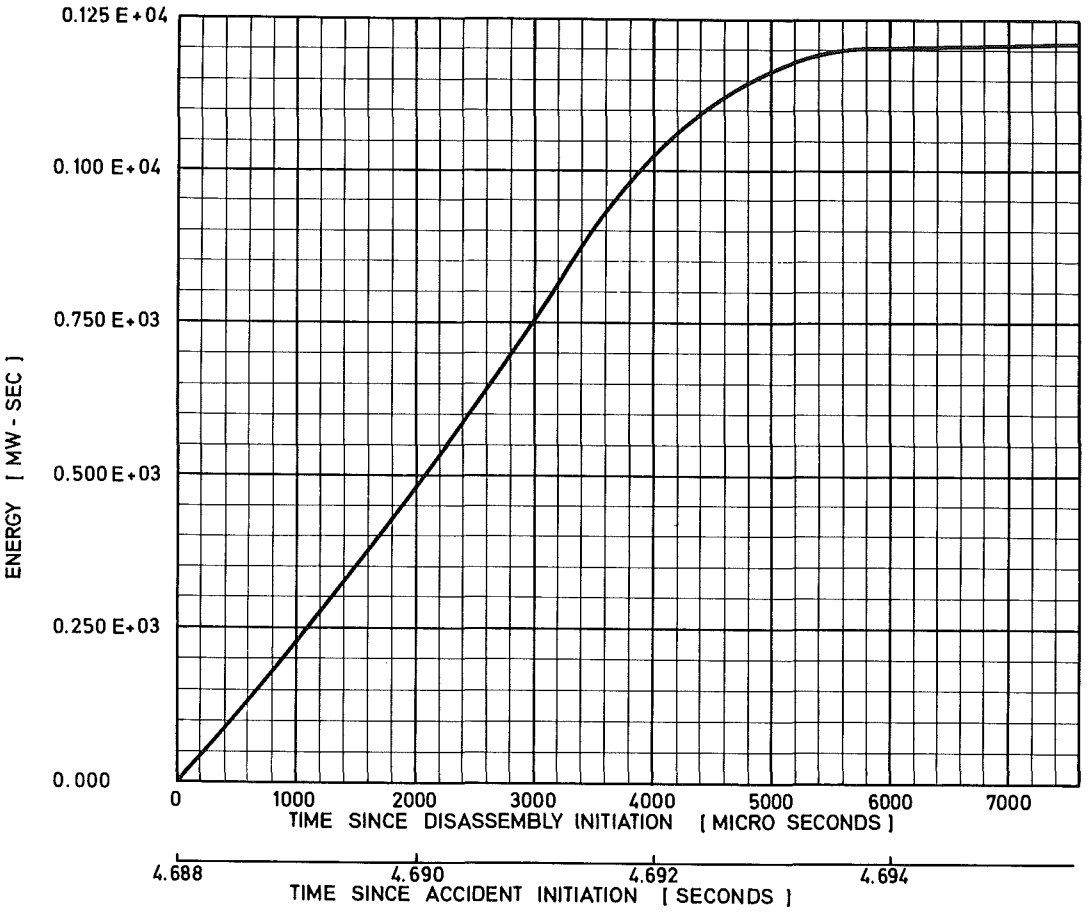

FIG. 4.1.2.q FLOW COAST DOWN II
THERMAL ENERGY RELEASE DURING THE DISASSEMBLY PHASE

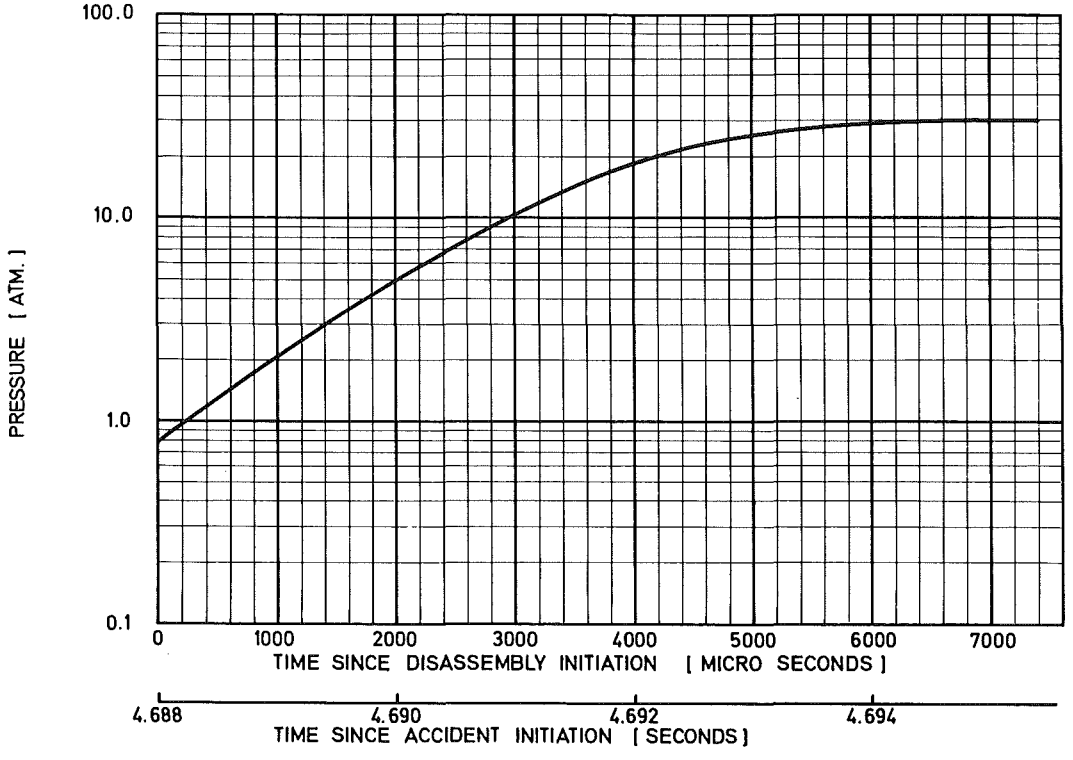

FIG. 4.1.2.r FLOW COAST DOWN II
PRESSURE AT THE CENTRE OF THE CORE AS FUNCTION OF TIME
DURING THE DISASSEMBLY PHASE

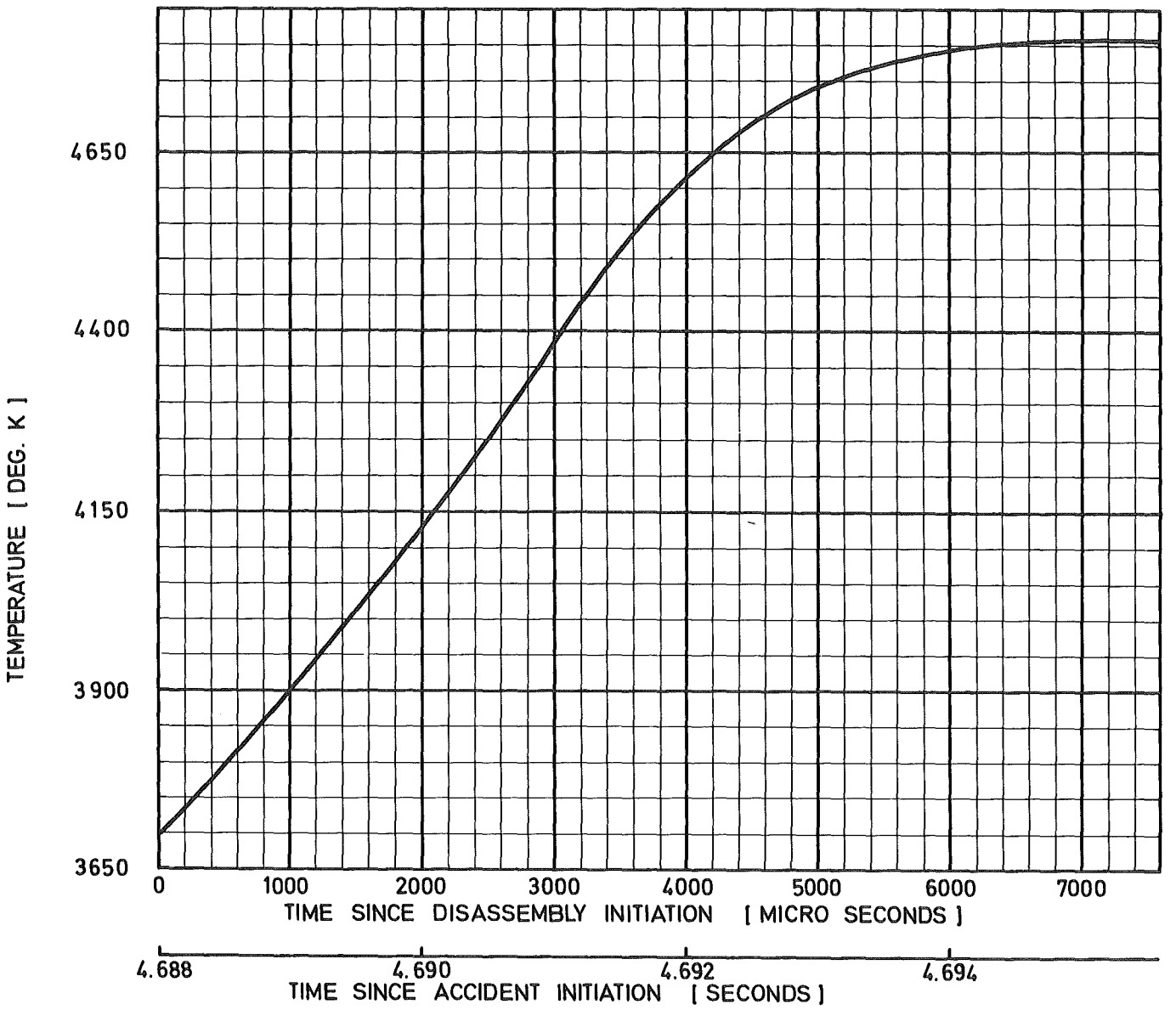

FIG. 4.1.2.s FLOW COAST DOWN II
TEMPERATURE AT THE CENTRE OF THE CORE AS FUNCTION OF TIME
DURING THE DISASSEMBLY PHASE

4.1.3 Reactivity accident (5 $/sec)

It has been stated in section 1 that the introduction of a reactivity ramp of 5 $/sec in SNR 3oo is not due to a particular sequence of events. It is merely characteristic of a whole range of hypothetical incidents in which the initiating reactivity ramp can be superimposed by positive reactivity contributions during the predisassembly phase. Under very conservative assumptions, these positive reactivity contributions could be built-up subsequently by failing fuel pins and consecutive thermal interactions between molten fuel and sodium, causing sodium voiding of coolant channels. The initiating reactivity ramp of 5 $/sec is simply postulated to study the coarse of the accident for this characteristic range of hypothetical ramp accidents.

The core physics data and materials properties used for the SAS2A and VENUS calculations have been described in sections 2 and 3 above. Fig. 4.1.3.b shows the reactivity curve up to the end of the disassembly phase. Approximately 1.66 $ of inserted reactivity is introduced within o.33 sec. Within the initial o.3 sec the reactor power increases to approximately 7o-times the nominal power (fig. 4.1.3.a). The fuel temperatures increase relatively rapidly, reaching the melting temperature of the fuel at the center of the fuel pins of the central annular channel after o.246 sec (fig. 4.1.3.c and 4.1.3.d). The building up of negative doppler feedback keeps the total net reactivity below prompt critical up to about o.32 sec. At o.318 sec, however, approximately 5o% of the areal cross section of the fuel pin in the central annular channels 1 and 2 has melted (fig. 4.1.3.d). The central temperature has risen to about 31oo^{o}C (fig. 4.1.3.c, 4.1.3.g). By contrast, the coolant and cladding temperatures in the center of the core are still approximately 77o^{o}C and 8oo^{o}C, respectively (fig. 4.1.3.e and 4.1.3.f). The point of sodium boiling in the individual annular channels is not reached.

Now the conservative assumption is made that under these temperature conditions, the fuel pin will rupture over a length of 3o cm in the center of the core. The total amount of molten fuel existing in the fuel pin over this length is then assumed to mix with all the sodium existing in the coolant channel. A mixing and dispersion time constant of approximately 1o msec is assumed. The fuel particles are assumed to have the particle size distributions measured in the ANL-experiments to date /53/.

After a very short phase of heat transfer from the fuel particles to liquid sodium, there is sodium vapour formation and pressure buildup. Subsequent pressure relief, causes expulsion of the liquid columns on top of and below the 3o cm reaction zone (fig. 4.1.3.h). This dilutes the coolant and contributes to positive sodium void reactivity. For calculation of the sodium vapour pressure buildup and the velocities of the sodium columns on top of the reaction zone the model of Cho-Wright /21/ was used. The movement of fuel particles into areas of less importance is excluded in order to keep the basis of the assumptions made as conservative as possible.
A movement of fuel particles into areas of lower importance can influence the further coarse of the accident considerably and result in even negative ramp contributions, as shown in /13/, /23/, /51/. However, since no experimental verification of these models accounting for axial movements of fuel particles is available yet, the above conservative assumptions are chosen, although they overestimate the real coarse of accident considerably. On the basis of these criteria, the fuel pins in the individual annular channels will fail in the following sequence:

annular channel 1 at o.3181 sec
2 at o.3181
3 at o.3238
7 at o.3238
4 at o.3265

The successive initiation of sodium voiding in annular channels 1, 2, 3 and 7 will very quickly build up positive reactivity ramp contributions which (fig. 4.1.3.b) lead to super prompt criticality and to a very sharp power peak accompanied by a transition into the disassembly phase (fig. 4.1.3.a).

For the calculations with SAS2A, the predisassembly phase was continued to shortly before core disassembly, in order to include all positive reactivity ramp contributions due to sodium voiding. In this case, the maximum positive reactivity ramp (sodium void plus initiation reactivity) before the onset of core disassembly is approximately 55 $/sec (fig. 4.1.3.b and 4.1.3.i). Core disassembly starts at o.33o4 sec. The doppler and displacement feedbacks cause the overall net reactivity to decrease below - 1 $ very quickly (fig. 4.1.3.b, 4.1.3.i, 4.1.3.l, 4.1.3.m, 4.1.3.n).

As a consequence the reactor power drops abruptly (fig. 4.1.3.a, 4.1.3.k) and energy generation is stopped.

Because of bursting pins during disassembly, there is also a thermal interaction between molten fuel and sodium during the short disassembly phase, slight fuel chilling and a moderate increase in the doppler feedback curve towards the end of the disassembly process (fig. 4.1.3.l).

On the whole, an additional 2o8o MWsec of thermal energy is released during the short disassembly phase of 2.3 msec (fig. 4.1.3.o). This is stored in a further increase in the fuel temperature (fig.4.1.3.q), buildup of fuel pressure (fig. 4.1.3.p), and additional fuel melting. In the center of the core fuel temperatures of 52oo^{o}K and fuel vapour pressures of 14o atm are reached (table 4.1.3A and 4.1.3B). Approximately 2515 kg of fuel are molten or have evaporated in the core region, which are capable of transfering energy to the sodium coolant. In the axial and radial blankets, there has been no melting of cladding or fuel, even during the disassembly phase. In core regions with fuel temperatures above the melting point, there is a thermal interaction between molten fuel and sodium. The further coarse of the accident will be described in section 5.

T_{max} = 526o^{o}K ≅ 526 at Mesh Point /14,1/

22	3o3	3o3	3o3	3o3	3o3	3o2	298	279	274	288	281	247	238
21	354	352	347	33o	327	3o3	3o3	3o3	3o3	3o3	3o3	3o2	289
2o	432	43o	424	351	356	33o	325	3o6	3o3	323	313	3o3	3o3
19	449	447	439	413	4o8	343	337	321	315	339	328	3o3	3o3
18	464	461	453	419	414	351	345	336	329	35o	338	3o3	3o3
17	498	487	479	428	422	359	351	346	338	358	346	312	3o3
16	5o2	499	49o	435	429	419	411	352	344	362	349	318	3o4
15	517	514	5o5	437	432	418	4o9	356	346	418	4o6	322	3o9
14	526	522	512	438	432	419	4o9	392	383	4o9	398	321	31o
13	5o2	498	487	434	429	417	4o6	386	377	4o5	395	319	3o9
12	476	472	463	429	423	412	4o1	374	365	398	389	315	3o5
11	466	462	454	421	415	4o4	393	382	372	392	383	315	3o5
1o	453	45o	441	4o9	4o3	394	383	381	372	381	374	3o3	3o3
9	437	434	425	396	39o	386	376	362	354	37o	363	3o3	3o3
8	417	414	4o6	383	377	321	313	31o	31o	3o3	362	356	3o3
7	339	337	33o	313	3o9	3o3	3o3	3o3	3o3	3o3	3o3	3o3	3o3
6	3o3	3o3	3o3	3o3	3o3	293	288	277	273	29o	286	248	3o3
	1	2	3	4	5	6	7	8	9	1o	11	12	13

Table 4.1.3.A 5 $/sec Reactivity Ramp

Temperatures in each mesh of the core after the end of the disassembly phase

P_{max} = 2534 bar ≅ 253 at Mesh Point /11,1/

22	o	16	14	37	43	8	o	o	o	o	o	o	o
21	o	29	8	38	o	o	o	o	34	31	19	35	o
2o	o	o	62	o	33	2o	43	38	23	33	32	7	o
19	14	7	19	o	1o	1o	13	23	o	33	o	o	o
18	86	69	11	7	29	16	87	o	4	23	o	23	o
17	158	1o9	7o	7o	33	29	79	56	11	o	17	28	51
16	129	149	8o	44	35	33	2	56	35	14	33	o	12
15	158	143	69	16	72	49	74	22	24	3o	11	57	1o
14	162	27	16	43	39	18	55	1	o	25	64	5	o
13	228	14	12	31	19	2o	64	34	28	2	24	48	1
12	158	248	29	38	18	63	3	24	68	2	28	o	1
11	253	119	51	2	3	25	8	24	2	2	48	o	51
1o	163	15o	95	13	3	9	5	8	13	21	22	45	39
9	117	111	11o	83	17	28	3	o	o	1	21	1o	13
8	26	23	34	1	35	2	3	74	45	39	33	45	8
7	17	36	46	12	28	29	46	o	45	1	o	o	o
6	o	o	19	o	o	54	14	22	o	35	31	18	o
	1	2	3	4	5	6	7	8	9	1o	11	12	13

Table 4.1.3.B 5 $/sec Reactivity Ramp
Pressures in each mesh of the core after the end of the disassembly phase

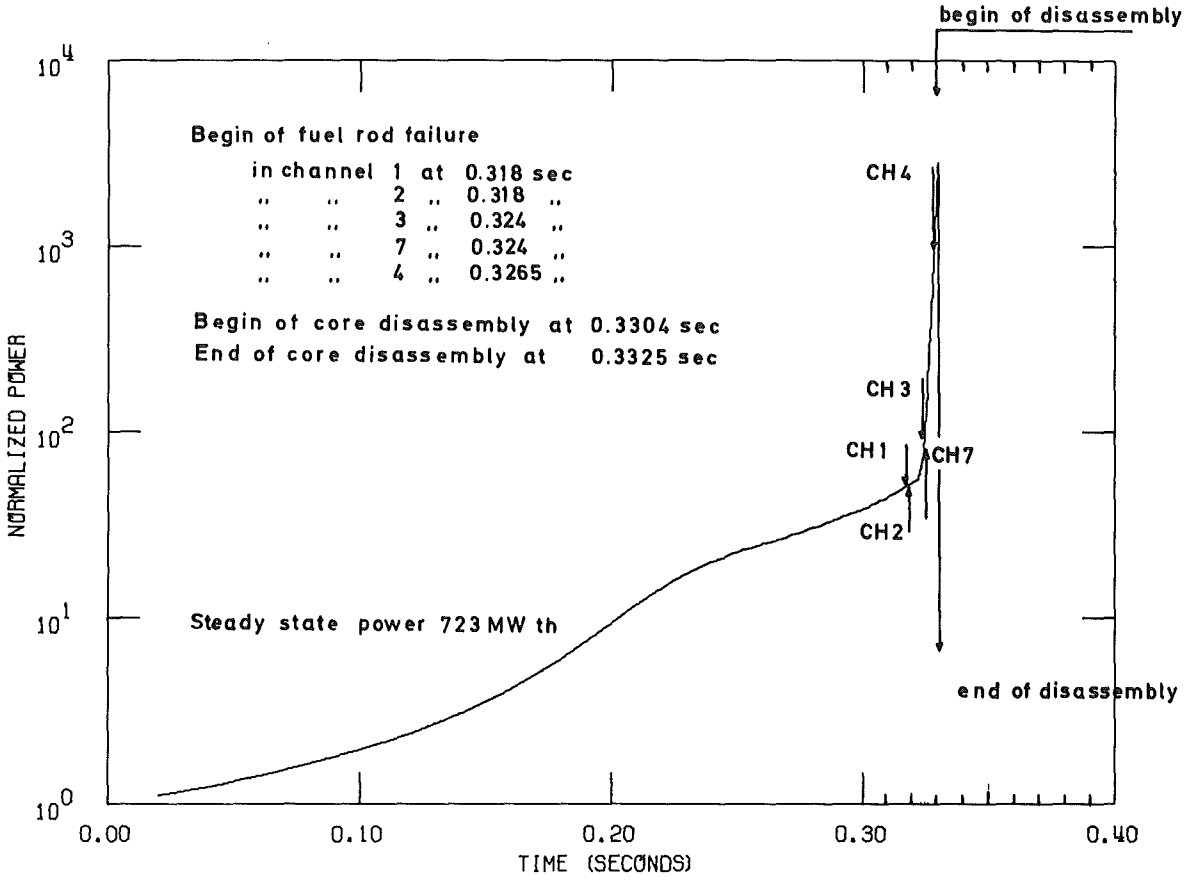

$5 REACTIVITY RAMP

Fig. 4.1.3.a Normalized power as function of time

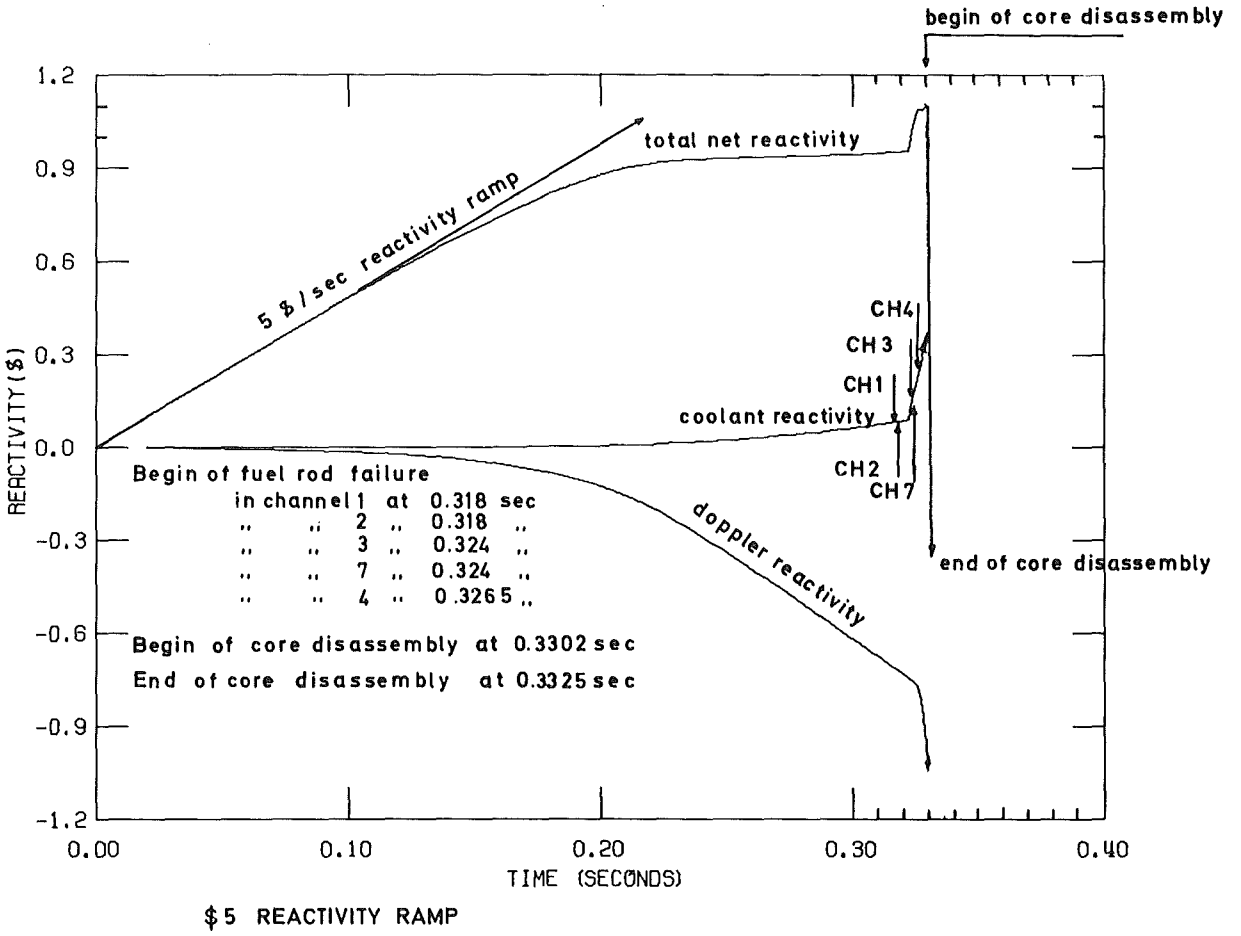

$5 REACTIVITY RAMP

Fig. 4.1.3.b Reactivity as a function of time

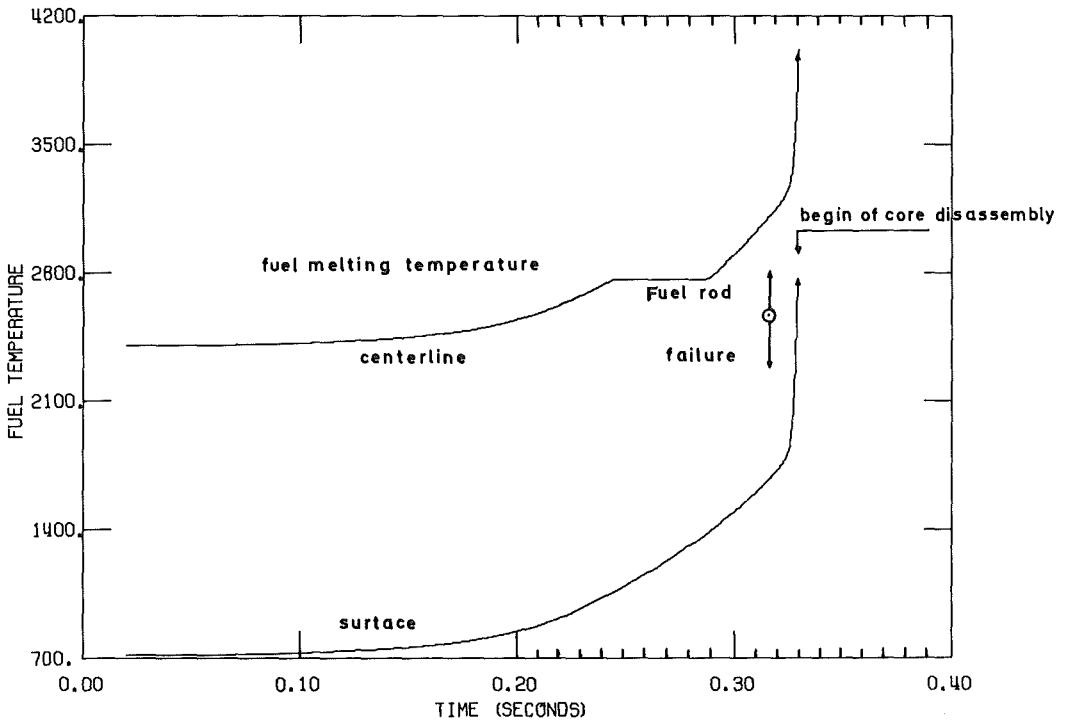

Fig.4.1.3.c 5 $/sec Reactivity Ramp - Case
Fuel temperature as a function of time - Channel 1 - midplane

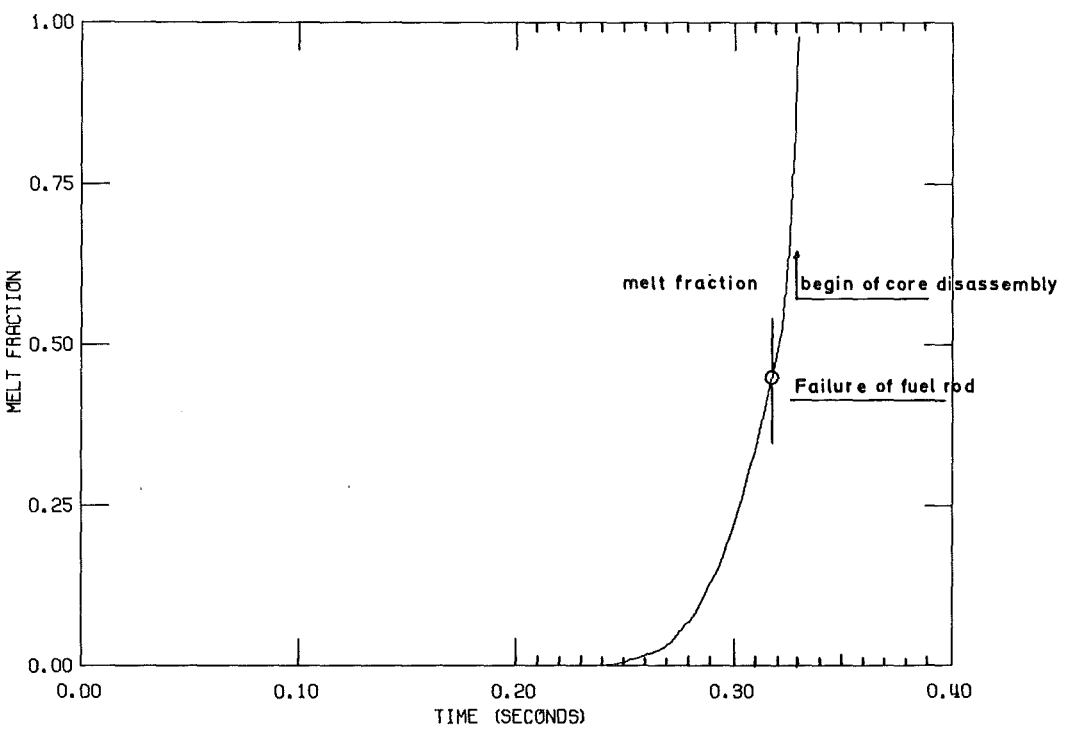

Fig. 4.13.d $5 REACTIVITY RAMP
Melt fraction as a function of time - channel 1 midplane

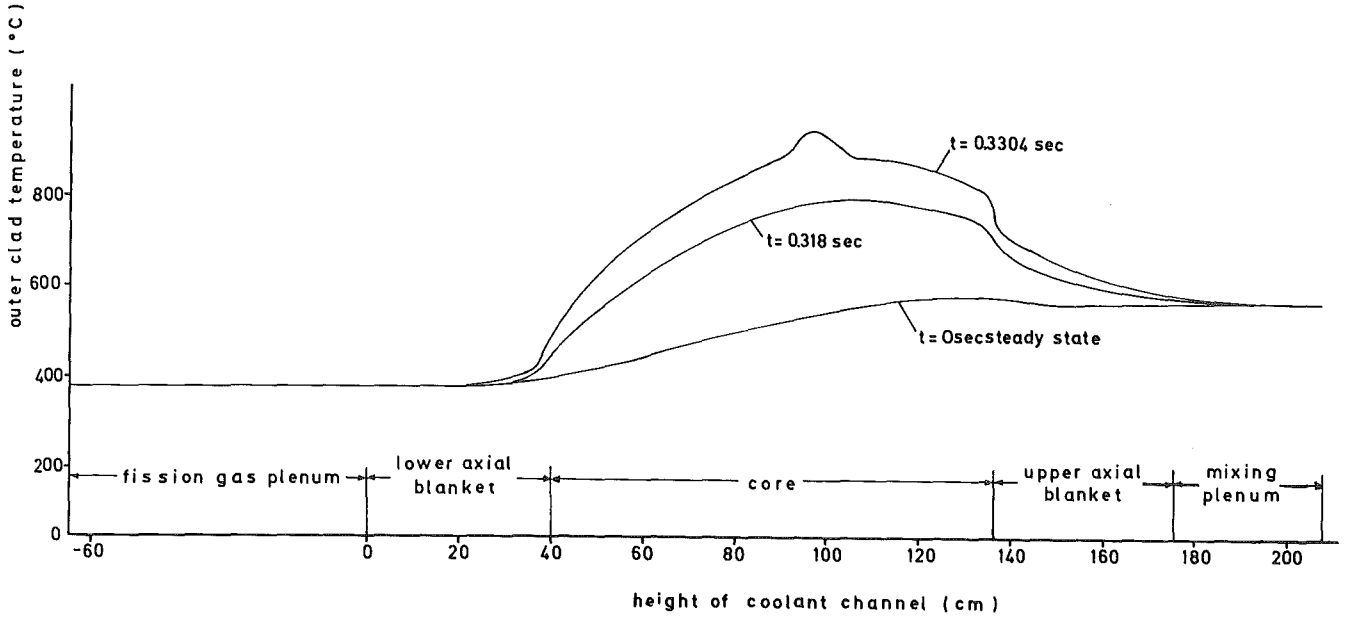

Fig:4.1.3.e Outer clad temperature in channel 1

5 $/sec reactivity ramp

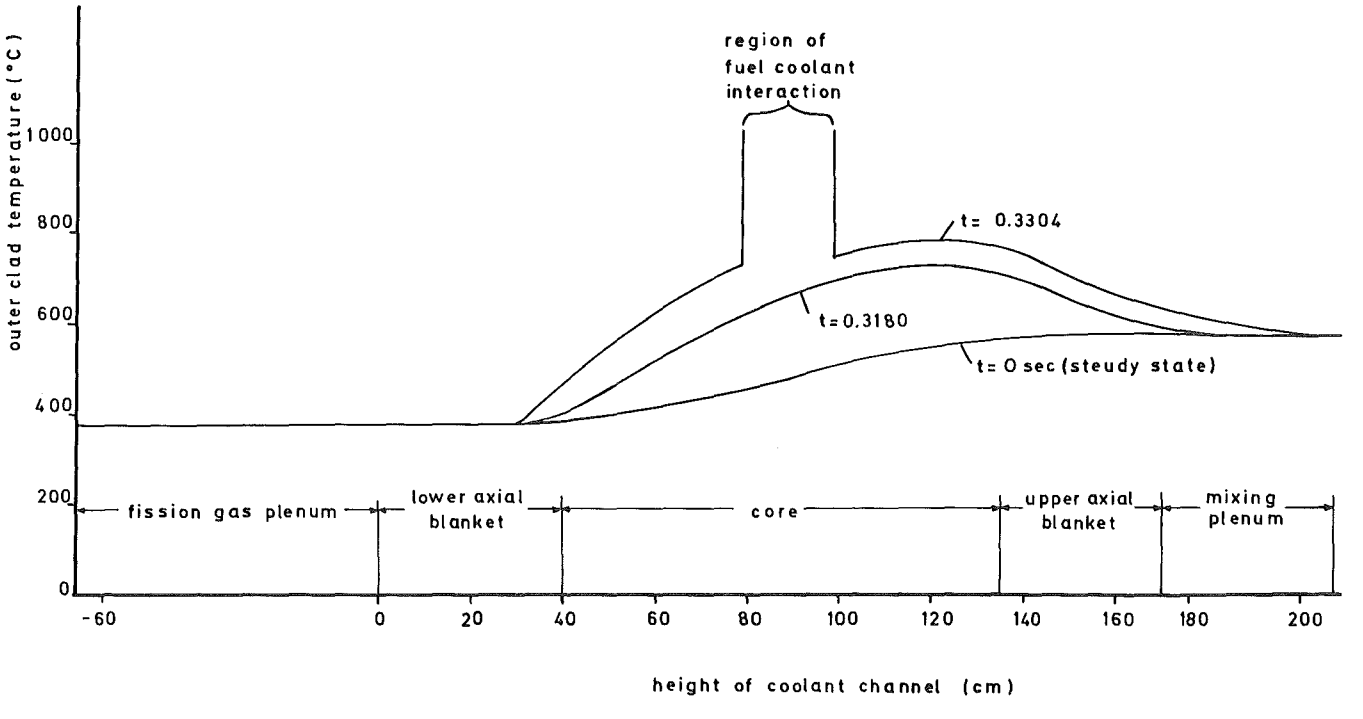

Fig: 4.1.3.f Coolant temperature in channel 1

5 $/sec reactivity ramp

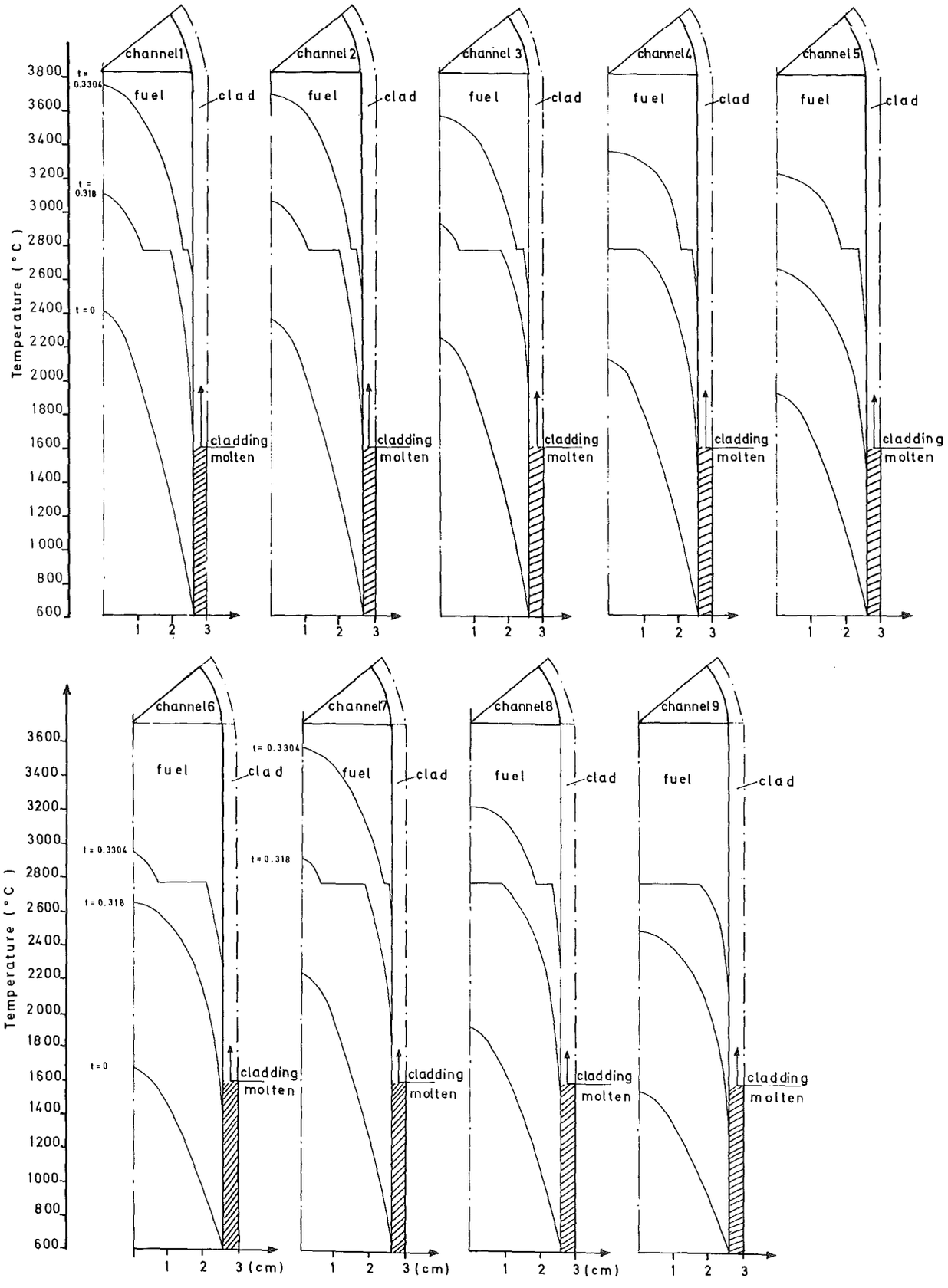

Fig. 4.1.3.g 5 $/sec reactivity ramp
Fuel temperatures (mid plane) as a function of time

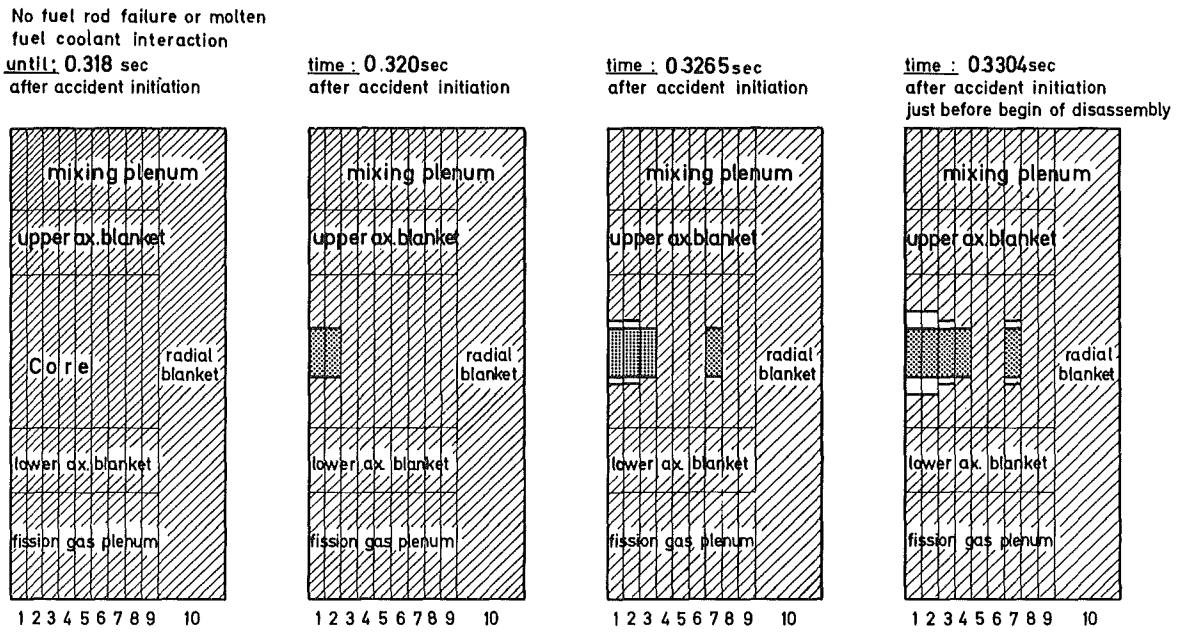

FIG: 4.1.3.h Boiling pattern during predisassembly phase
5 $ / sec reactivity ramp case

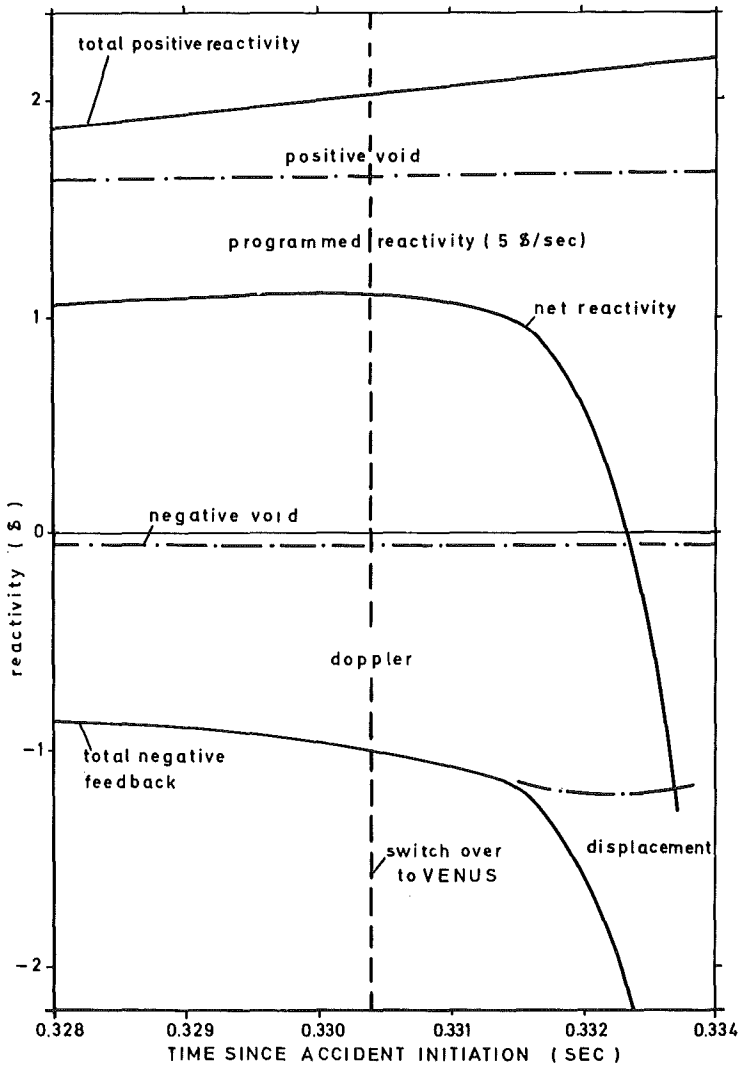

FIG: 4.1.3.i 5 $ / SEC REACTIVITY RAMP
REACTIVITIES IMMEDIATELY BEFORE AND DURING
THE DISASSEMBLY PHASE

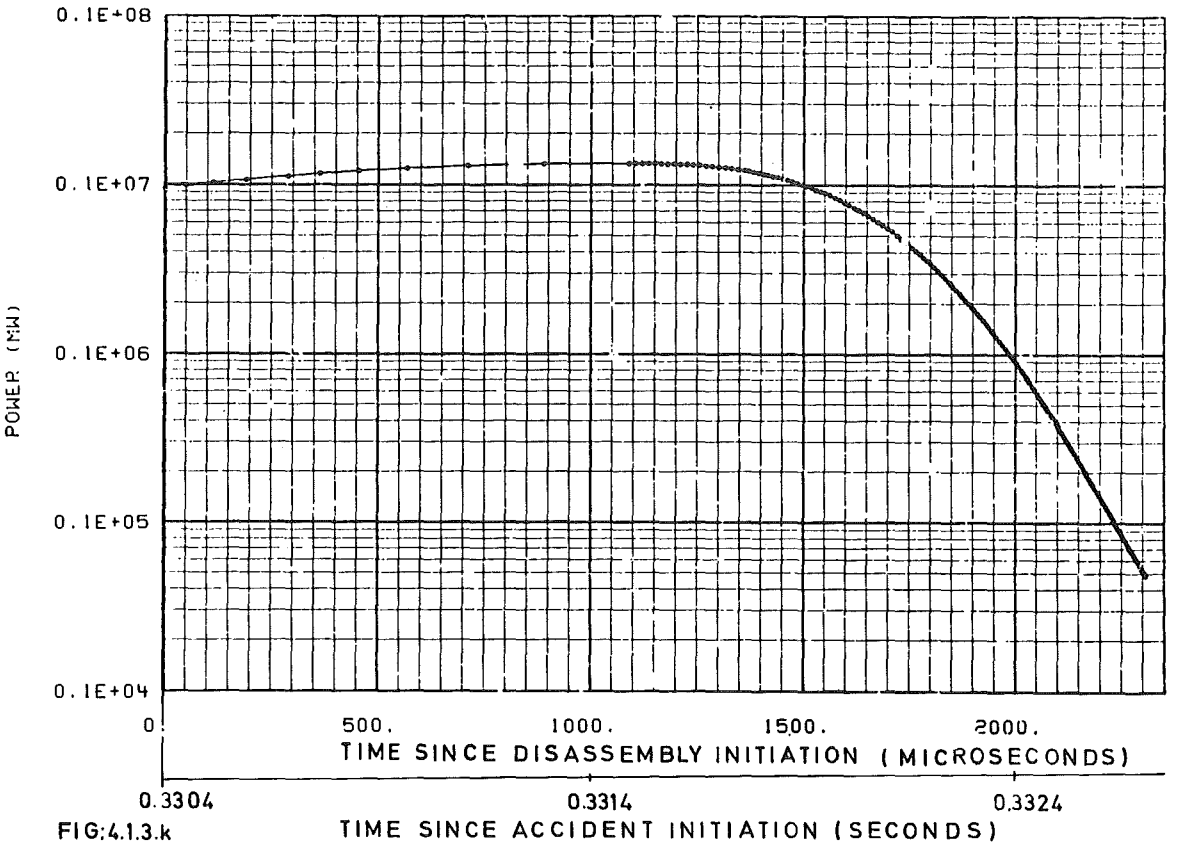

FIG:4.1.3.k
5 $/SEC REACTIVITY RAMP
POWER AS FUNCTION OF TIME DURING THE DISASSEMBLY PHASE

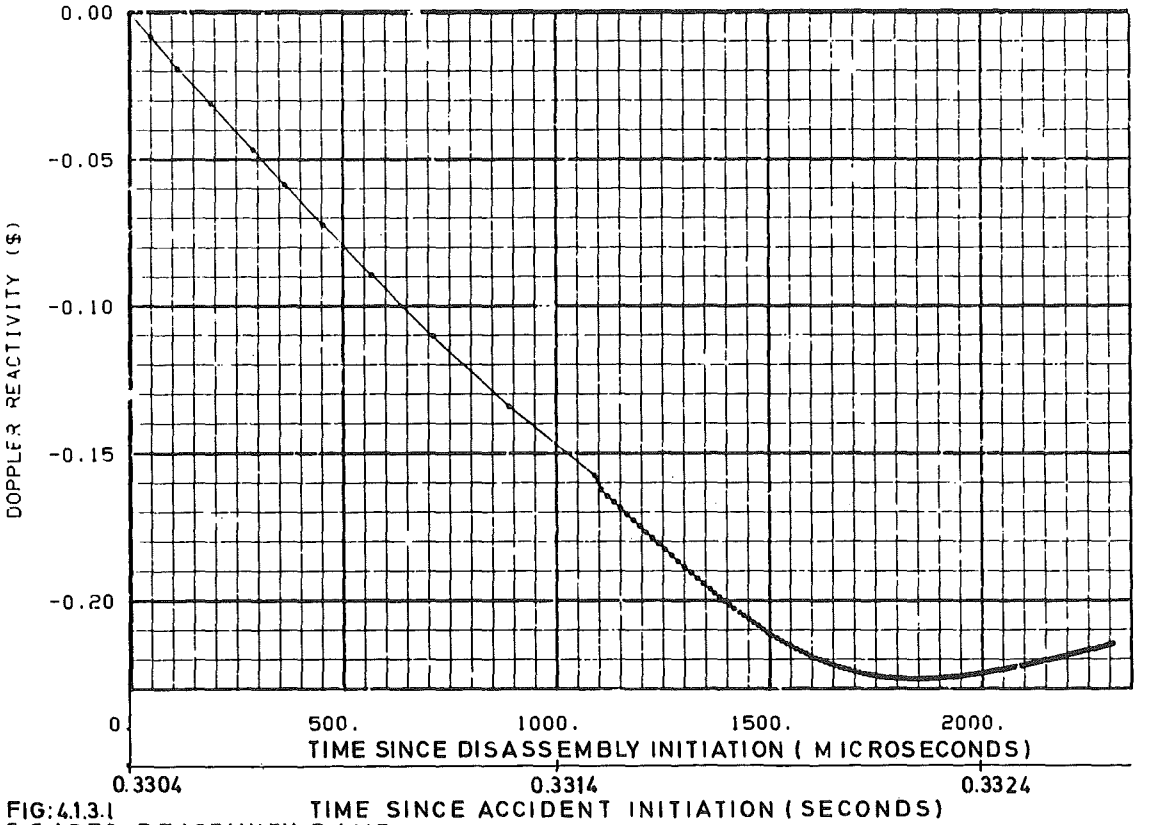

FIG:4.1.3.l
5 $/SEC REACTIVITY RAMP
DOPPLER FEEDBACK AS FUNCTION OF TIME DURING THE DISASSEMBLY PHASE

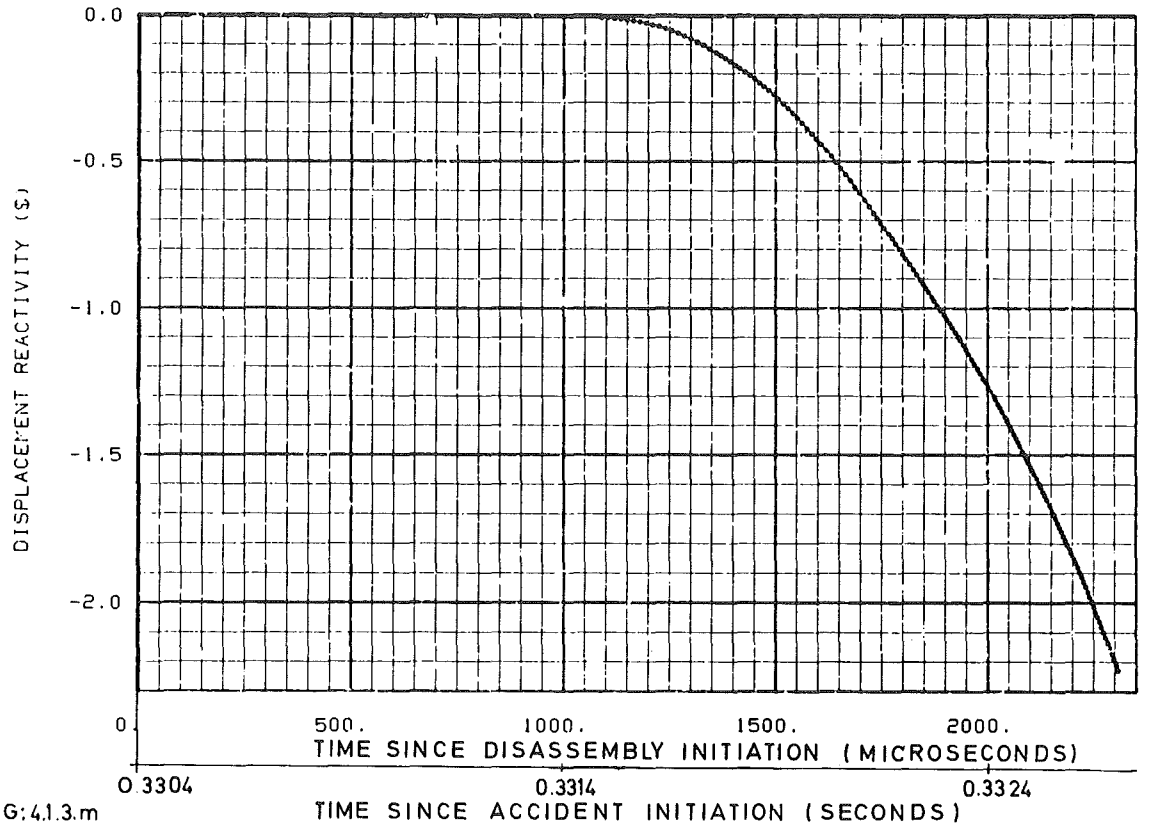

FIG:4.1.3.m
5 $/SEC REACTIVITY RAMP
DISPLACE MENT REACTIVITY AS FUNCTION OF TIME DURING THE DISASSEMBLY PHASE

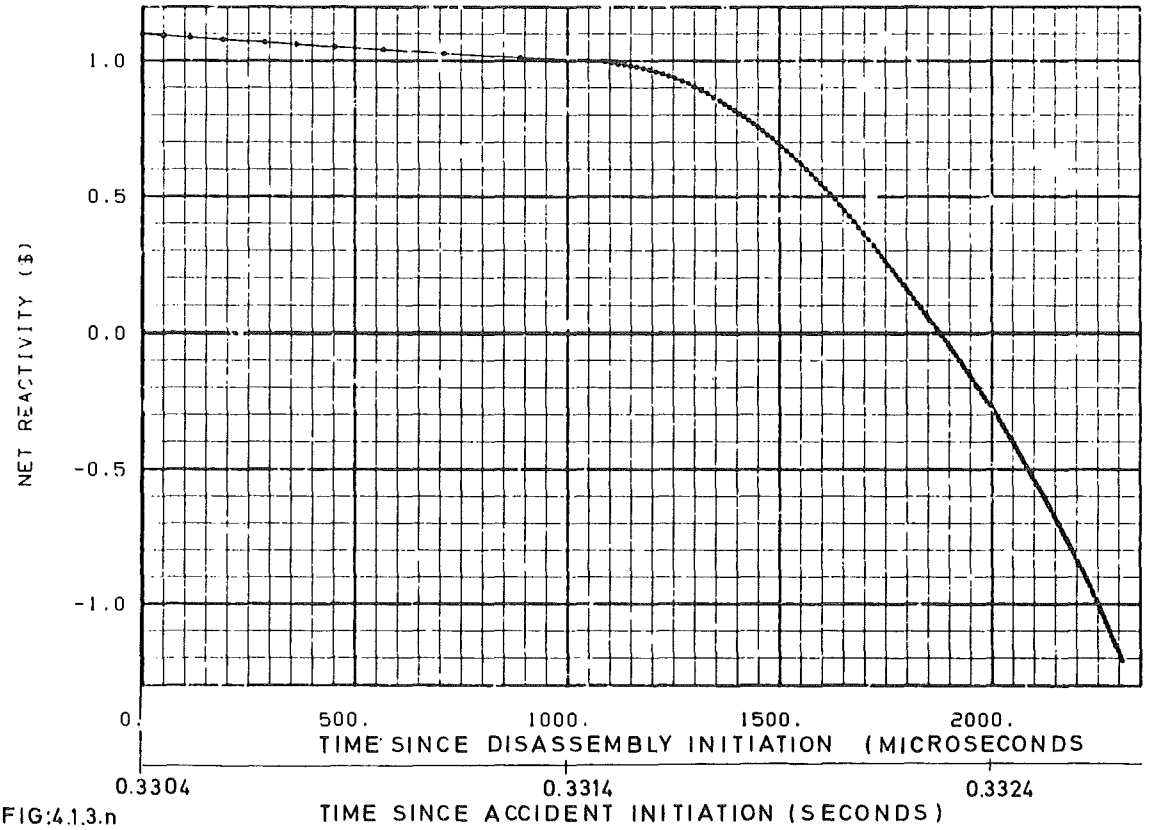

FIG:4.1.3.n
5 $/SEC REACTIVITY RAMP
NET REACTIVITY AS FUNCTION OF TIME DURING THE DISASSEMBLY PHASE

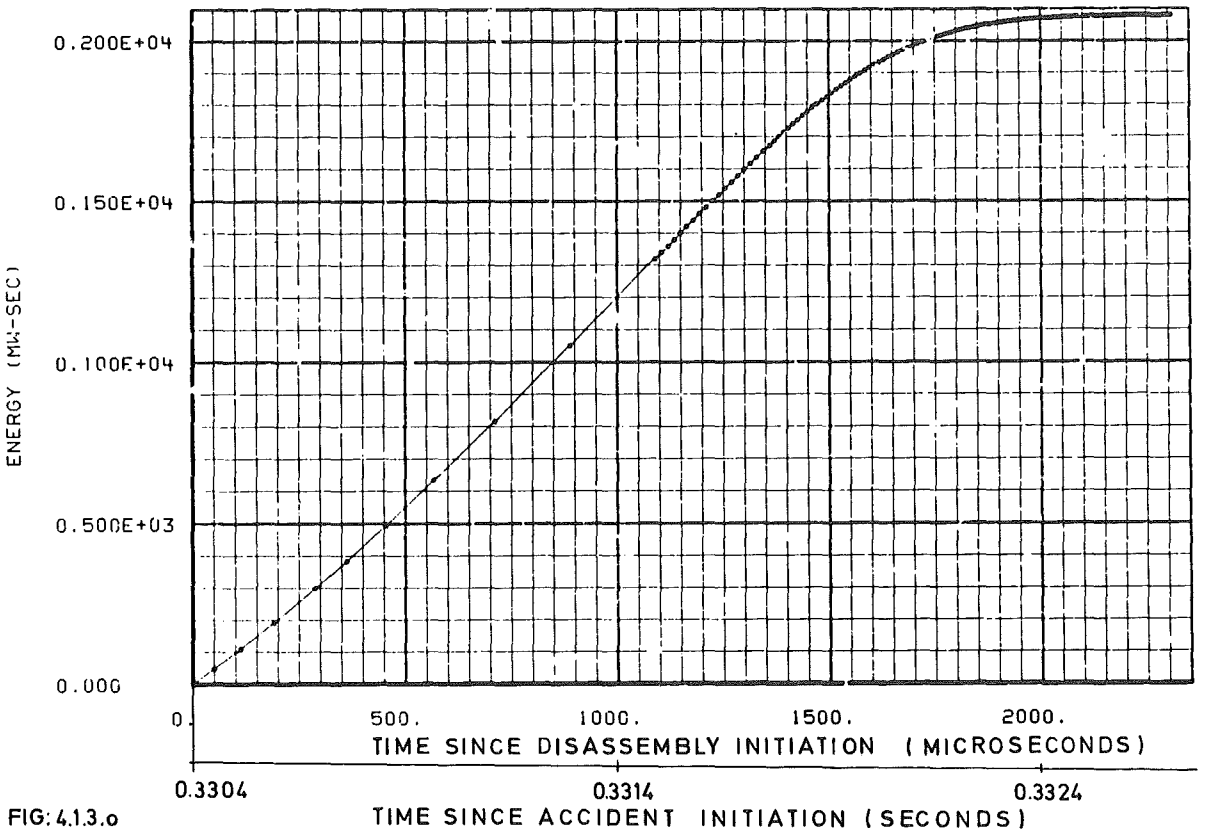

FIG: 4.1.3.o
5 $/SEC REACTIVITY RAMP
THERMAL ENERGY RELEASE DURING THE DISASSEMBLY PHASE

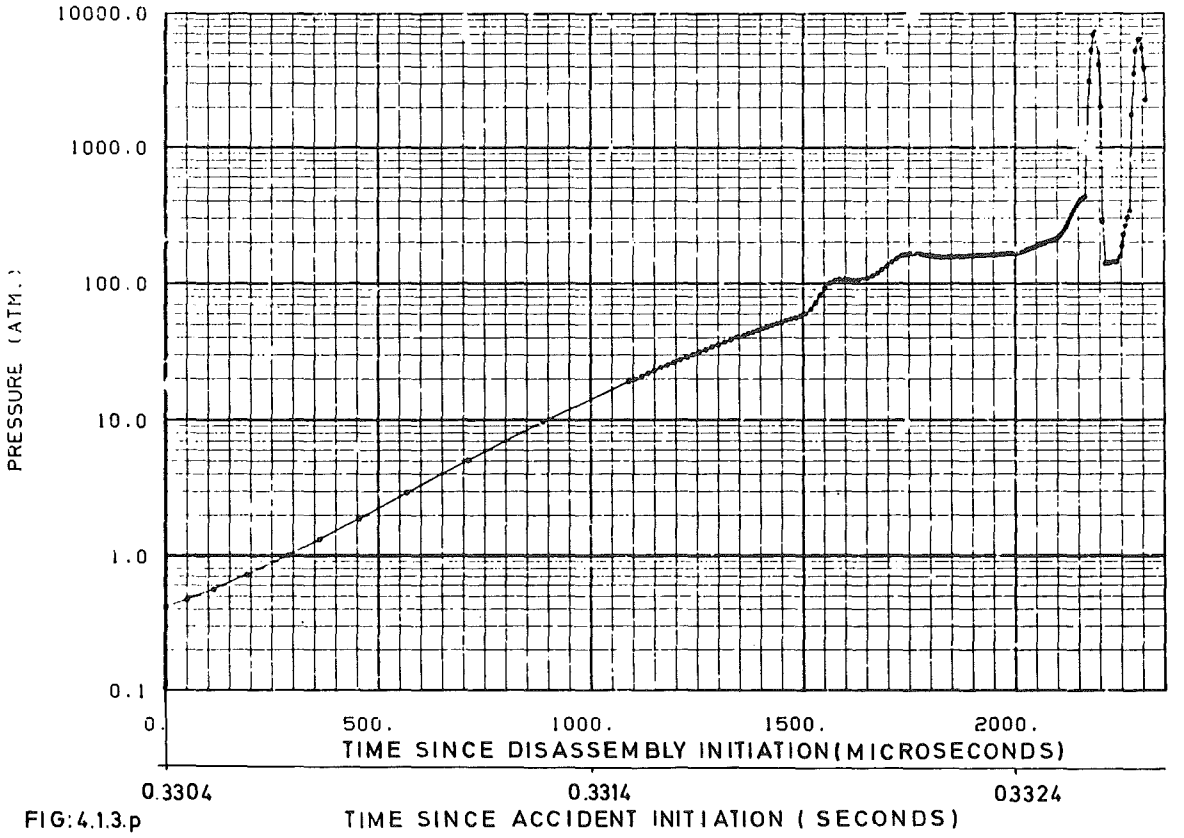

FIG: 4.1.3.p
5 $/SEC REACTIVITY RAMP
PRESSURE AT THE CENTRE OF THE CORE AS FUNCTION OF TIME DURING THE DISASSEMBLY PHASE

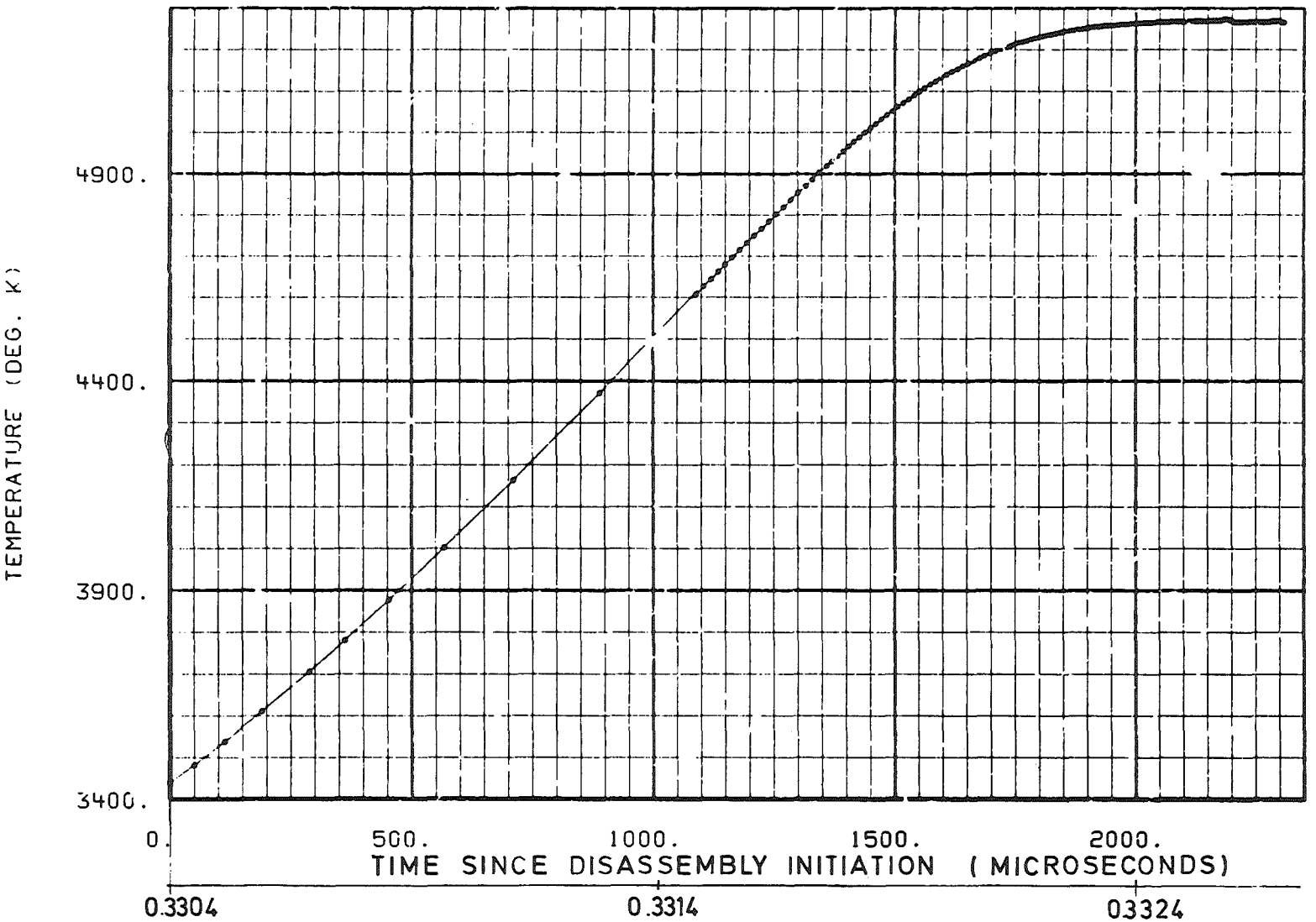

FIG:4.1.3.q

5 $ / SEC REACTIVITY RAMP

TEMPERATURE AT THE CENTRE OF THE CORE AS FUNCTION OF TIME DURING THE DISASSEMBLY PHASE

4.1.4 Reactivity accident (Ejection of an absorber rod)

The hypothetical case of the rapid ejection of an absorber rod has been discussed in section 1.
The reactivity time curve, determined in /3/ under very conservative assumptions, was employed for the SAS2A-VENUS calculations.

Fig. 4.1.4a shows the time curve of the reactor power from the initiation of the accident up to the end of disassembly. The reactor power, initially rises very slowly. Between o.1o sec and o.15 sec, however, the positive reactivity ramp of the axial absorber rod movement has its full impact causing the SNR-3oo core to become super prompt critical at o.15 sec. The consequence is an even steeper increase in reactor power which, however, can be accommodated for the time being by the build-up of fuel temperatures (fig. 4.1.4c) and the negative doppler feedback (fig. 4.1.4b) at about o.16 sec. Shortly afterwards the fuel begins to melt in the center of the central annular channel (fig. 4.1.4c and 4.1.4d). As a consequence of the continued addition of inserted reactivity, the reactor core becomes super-prompt critical a second time at approximately o.17 sec. Now the fuel temperatures increase very rapidly. The increasingly negative doppler reactivity can compensate the inserted reactivity only to such an extent as to keep the total net reactivity slightly below 1 $ (prompt critical).
At o.185 sec, approximately 6o% of the fuel pin cross section in the central annular channels 1 and 2 has melted (fig. 4.1.4c and 4.1.4d). The central temperature has risen to approximately 34oo^{o}C. A fuel pressure builds up in the fuel after 35oo^{o}C is reached. The temperatures of the cladding and the coolant, however, are only 8oo^{o}C in the center of the core (fig. 4.1.4e and 4.1.4f). The point of sodium boiling is not reached in the individual annular channels.

Now, as in section 4.1.3, the assumption is made that the fuel pin ruptures over a length of 3o cm in the center of the core under these temperature conditions. The total amount of molten fuel existing in the fuel pin over this length is assumed to mix with all the sodium contained in the coolant channel with a mixing and dispersion time constant of approximately 1o msec. This causes a rapid heat transfer from the molten fuel to the sodium accompanied by the build up of very high pressures. After pressure relief sodium vapour is produced which expells the columns of liquid sodium being above and below the reaction zone (fig. 4.1.4g). By the expulsion of the coolant additional positive reactivity is inserted.

As in section 4.1.3, the movement of fuel particles to areas of less importance is excluded. Again, the buildup of the sodium vapour pressure and the velocity of the sodium columns on top of the 3o cm long reaction zone are calculated by means of the Cho-Wright model /21/.
On the basis of the criteria listed above, the fuel pins in the individual annular channels fail in this sequence:

annular channel 1 at o.1852 sec
2 at o.1856
3 at o.1867

Successive voiding (fig. 4.1.4h) in annular channels 1, 2, and 3 very quickly builds up positive reactivity ramp contributions (fig.4.1.4b) with the result that prompt criticality is exceeded again and a transition is made into the disassembly phase (fig. 4.1.4a).

Taking into account reactivity ramp contributions due to sodium voiding, the maximum reactivity ramp shortly before and during the disassembly phase is approximately 4o $/sec (fig. 4.1.4b and 4.1.4i). Core disassembly starts at o.19 sec. Doppler and displacement feedbacks then cause the net reactivity to decrease below - 1 $ very quickly (fig. 4.1.4b, 4.1.4n). The reactor power decreases abruptly (fig. 4.1.4a and 4.1.4k) and the production of energy is stopped. As a consequence of bursting fuel pins, there is a thermal interaction between molten fuel and sodium even during disassembly, which give rise to a slight amount of fuel chilling and a minor increase in the doppler feddback curve towards the end of the diasssembly process (fig. 4.1.4l.)

On the whole, an additional 594 MWsec of thermal energy is released during this short disassembly phase of 2.4 msec which now is stored in a further increase in the fuel temperature (fig. 4.1.3q), buildup of fuel pressure (fig. 4.1.4p), and additional fuel melting. Fuel temperatures of 365o^{o}K are reached in the center of the core. As a consequence of the fuel-sodium thermal interaction pressures of 851 bar are generated within the core region (table 4.1.4A and 4.1.4B).
Approximately 13oo kg of fuel is molten or evaporated in the core central region and is able to transfer energy to the sodium coolant. In the outer core regions the fuel is merely molten and not able to transfer energy to sodium.In the axial and radial blankets, there has been no melting of the cladding or the fuel even during the disassembly phase.In core regions with fuel temperatures above the melting point there is a thermal interaction between molten fuel and sodium. The further coarse of accident will be dealt within section 5.

T_{max} = 365o°K ≙ 365 at Mesh Point /14,1/

22	3o2	3o1	3oo	281	281	253	252	23o	229	237	235	2o6	2o4
21	3o3	3o3	3o3	3o3	3o3	299	298	273	271	283	28o	247	243
2o	326	326	324	3o3	3o3	3o3	3o3	295	293	3o3	3o3	27o	266
19	336	335	333	322	324	3o3	3o3	3o3	3o3	3o3	3o3	284	279
18	344	344	342	32o	319	3o3	3o3	3o3	3o3	3o3	3o3	295	291
17	3o5	35o	348	322	321	3o3	3o3	3o3	3o3	3o3	3o3	3o3	3o1
16	358	357	354	327	325	326	326	3o3	3o3	3o3	3o3	3o3	3o3
15	361	36o	357	33o	328	326	324	3o3	3o3	328	325	3o3	3o3
14	365	365	363	331	329	324	322	216	313	32o	317	3o3	3o3
13	36o	36o	358	331	329	323	32o	312	3o9	317	314	3o3	3o3
12	357	357	354	329	327	321	318	3o6	3o1	315	313	3o3	3o3
11	353	352	349	324	323	319	316	3o6	3o2	214	312	3o3	3o3
1o	344	343	341	319	317	32o	317	31o	3o7	31o	3o8	3o3	3o3
9	333	335	332	312	31o	319	317	311	3o9	311	3o9	3o3	3o3
8	325	324	322	315	313	3o3	3o3	3o3	3o3	3o3	3o3	3o3	299
7	3o3	3o3	3o3	3o3	3o3	3o3	3o3	3o3	3o3	3o3	3o3	3o1	299
6	282	281	279	271	27o	262	26o	252	25o	264	263	227	226
	1	2	3	4	5	6	7	8	9	1o	11	12	13

Table 4.1.4A Rod ejection
Temperatures in each mesh of the core after the end of the disassembly phase

P_{max} = 851 bar ^851 at Mesh Point /12,7/

22		o	5	496	299	17	441	6	278	1	o	o	443	18
21		o	o	4	o	3	o	o	175	62	531	76	o	67
2o		21	2o	2o	o	o	778	175	2	363	1	o	o	o
19		22	22	22	3	123	217	1	o	o	1o1	o	3	o
18		25	2o4	25	11	6	o	o	6	126	292	18	1	234
17		28	26	1o6	211	312	565	o	425	91	396	o	24o	o
16		27	27	19o	261	419	7	33o	49o	441	14	96	222	o
15		29	142	27	8	415	1o	11	5	o	3	3	12	o
14		3o	459	147	8	8	286	323	272	33o	8	176	128	277
13		31	28	27	8	266	429	181	455	347	3o	427	1oo	9
12		35	27	27	9	213	328	851	281	16	12	335	1	1
11		26	26	25	8	239	677	36o	98	216	11	346	8	1
1o		27	62	2oo	286	161	99	279	8	266	11	158	81	3
9		25	22	21	1o9	77	4	368	398	535	287	218	o	3
8		2o	2o	19	2	2	598	6	232	72	461	11	173	198
7		o	2	5	196	13	o	557	o	638	o	o	22o	o
6		3o5	242	268	o	o	38o	668	2	1o2	294	4	o	o
		1	2	3	4	5	6	7	8	9	1o	11	12	13

Table 4.1.4B Rod ejection
Pressures in each mesh of the core after the end of the disassembly phase

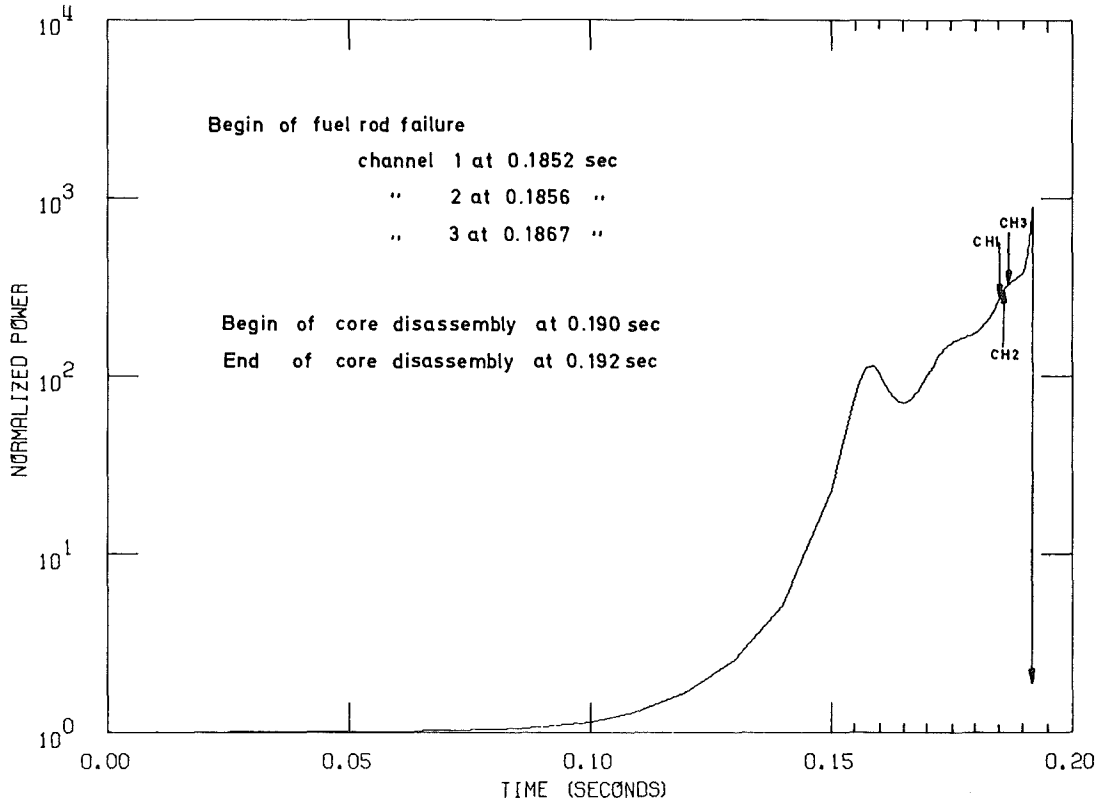

SNR ROD EJECTION

Fig.4.1.4.a Normalized power as function of time

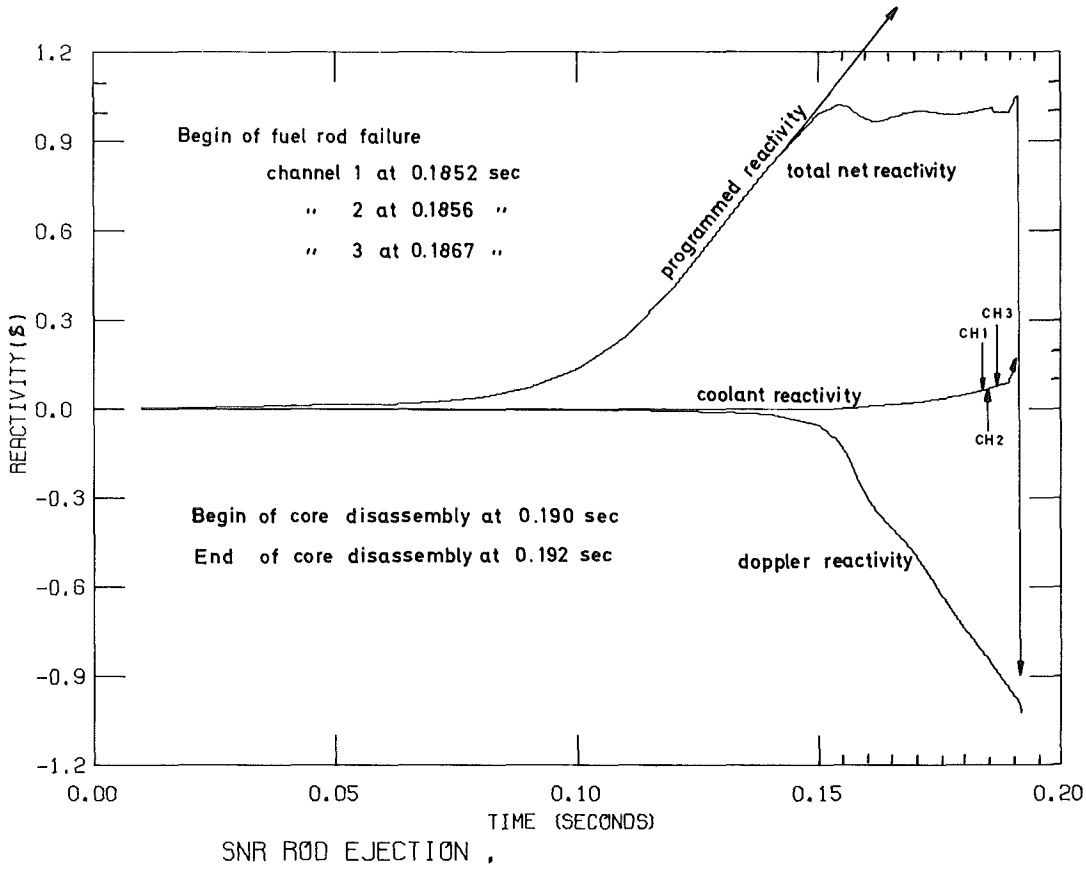

SNR ROD EJECTION ,

Fig 4.1.4.b Reactivity as a function of time

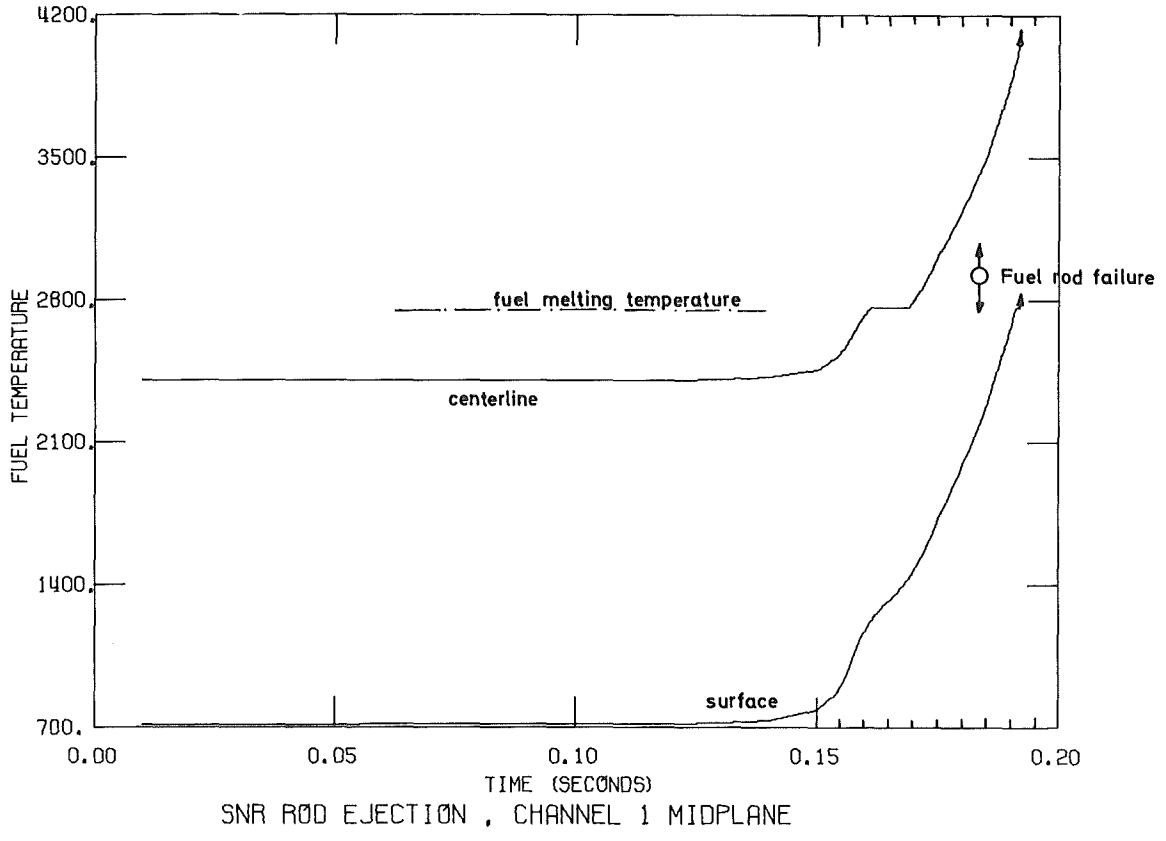

Fig 4.1.4.c Fuel temperature as a function of time

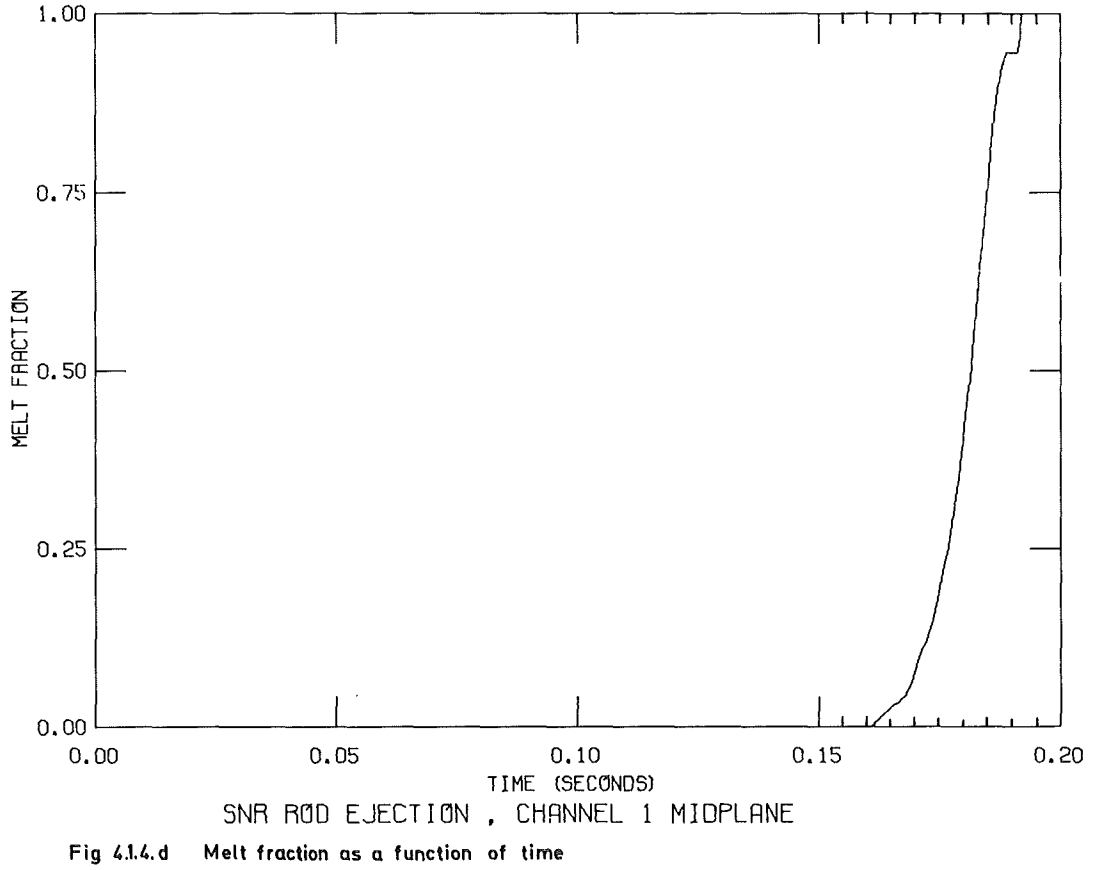

Fig 4.1.4.d Melt fraction as a function of time

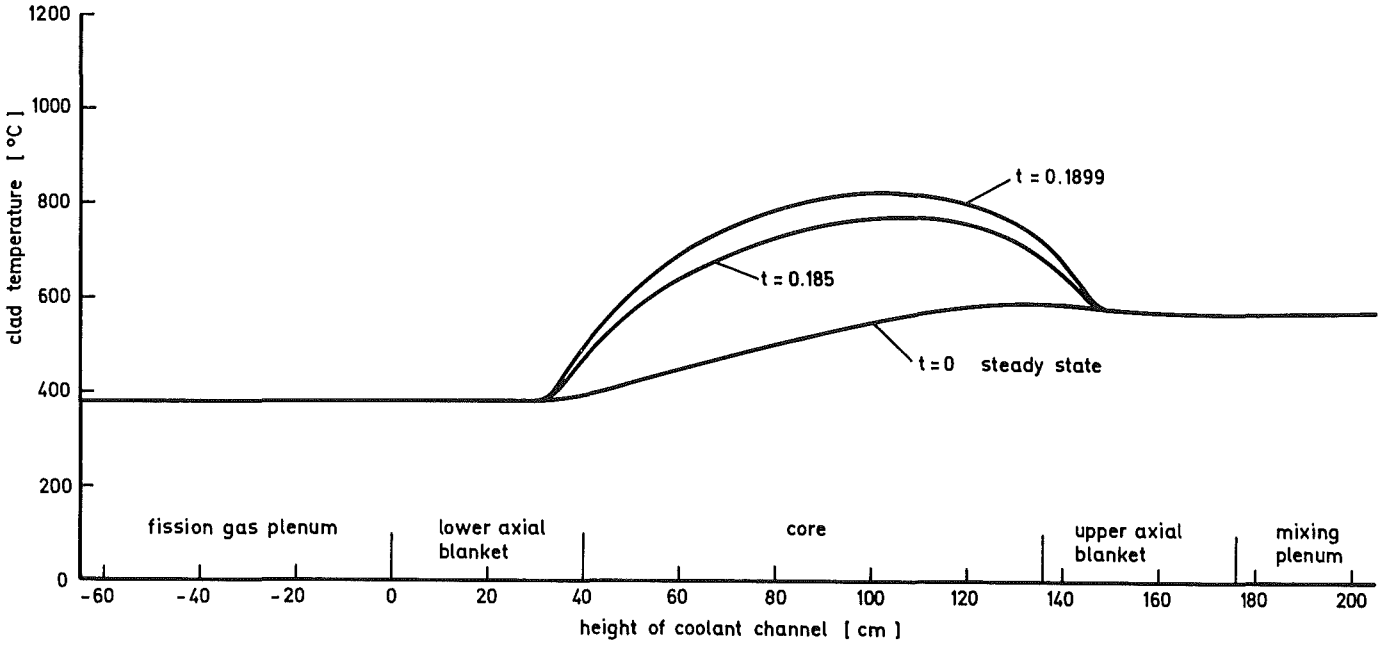

Fig. 4.1.4.e Rod ejection
Outer clad temperature in channel 1

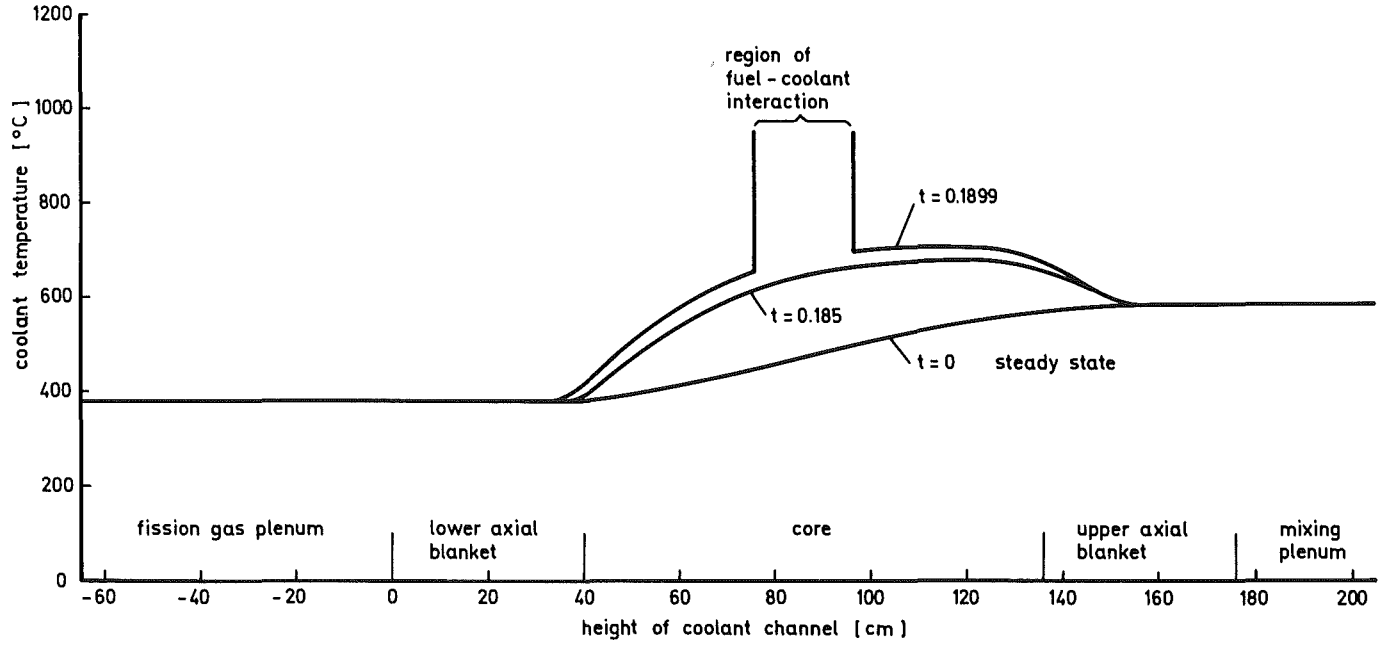

Fig. 4.1.4.f Rod ejection
Coolant temperature in channel 1

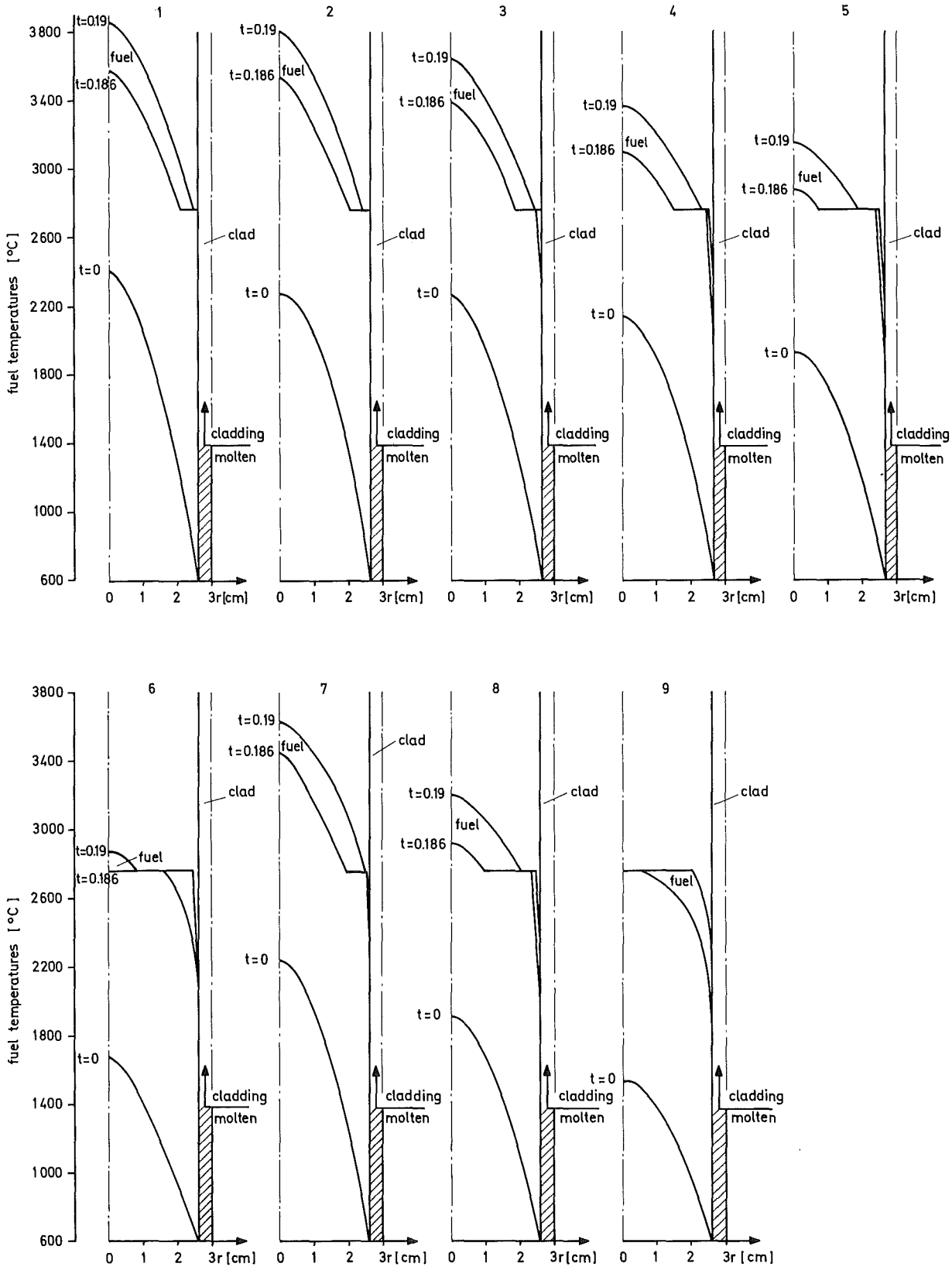

Fig. 4.1.4.g Fuel temperatures as a function of time
Rod ejection

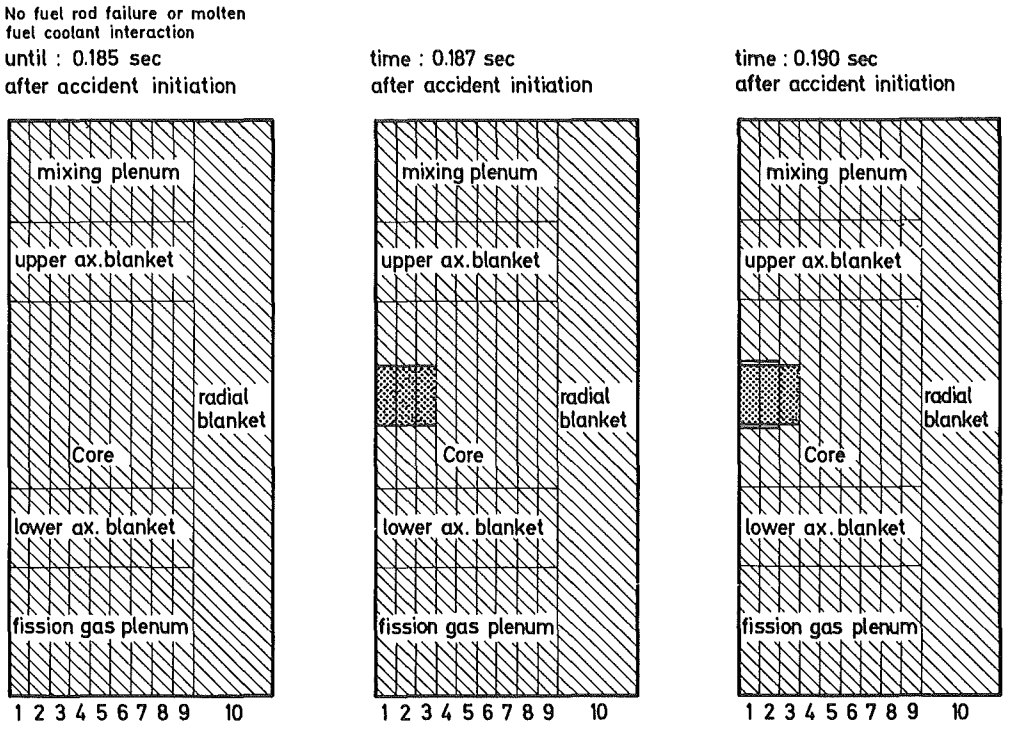

Fig. 4.1.4.h Boiling pattern during predisassembly phase
Rod ejection case

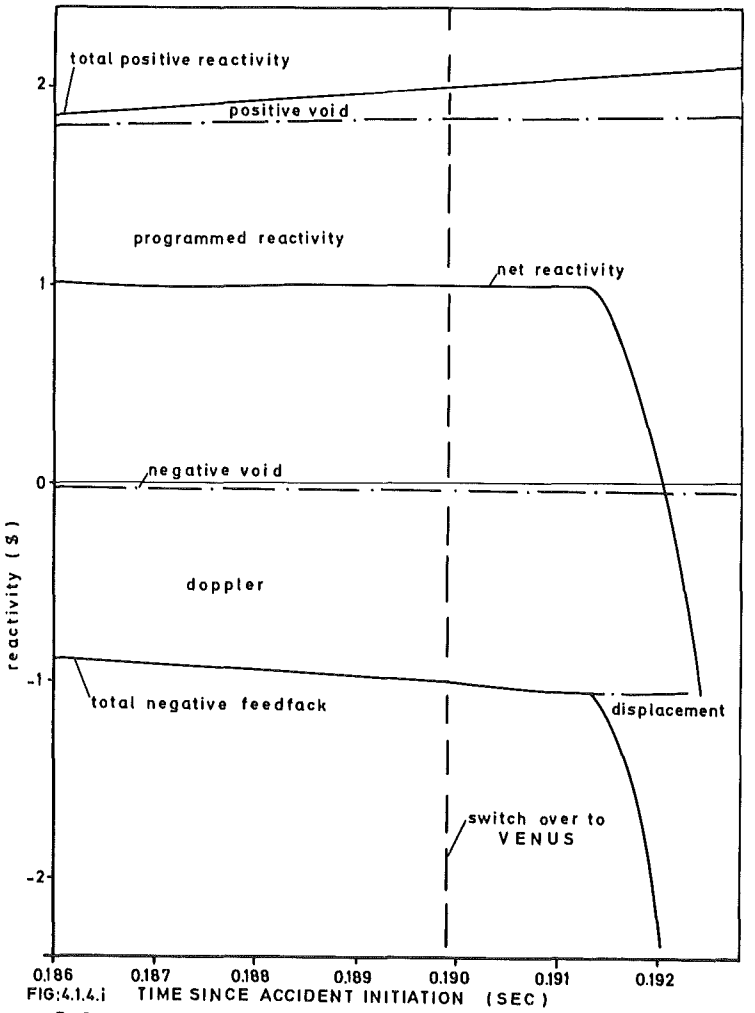

FIG:4.1.4.i RODEJECTION
REACTIVITIES IMMEDIATELY BEFORE AND DURING THE DISASSEMBLY PHASE

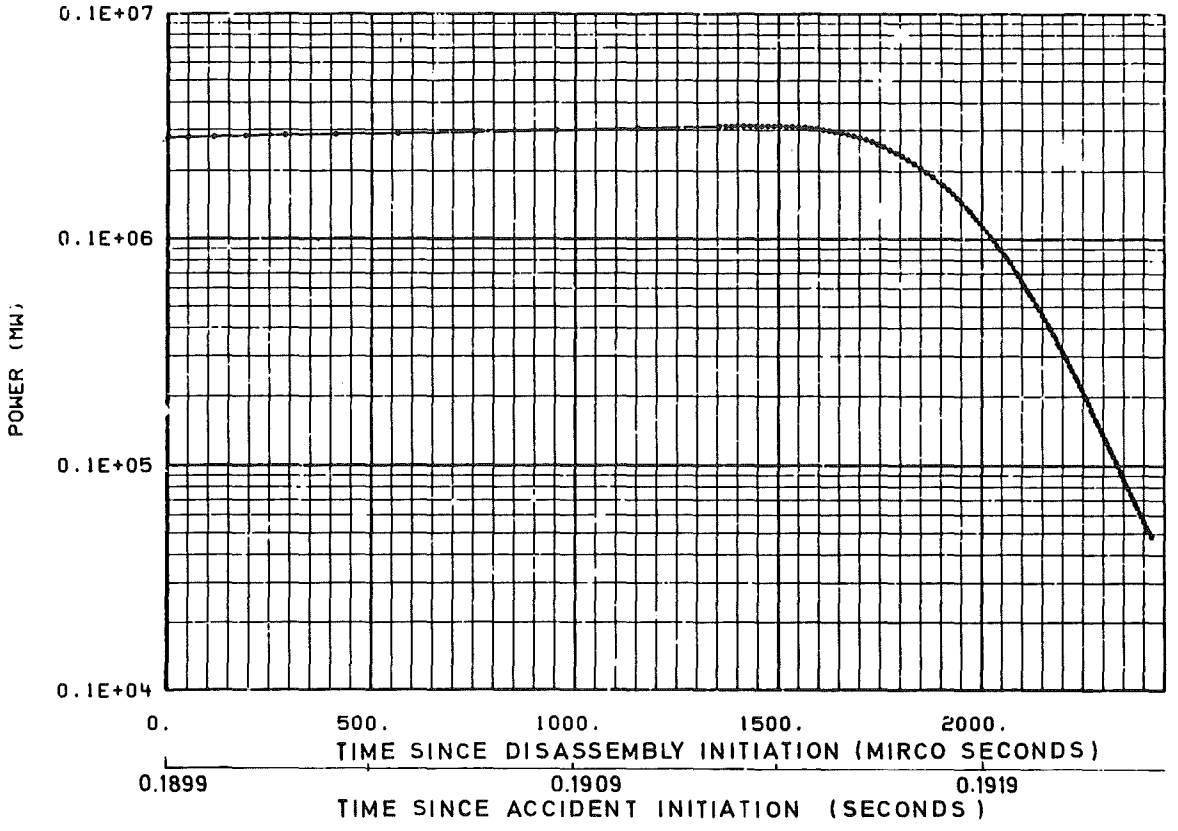

FIG.4.1.4k ROD EJECTION
POWER AS FUNCTION OF TIME DURING THE DISASSEMBLY PHASE

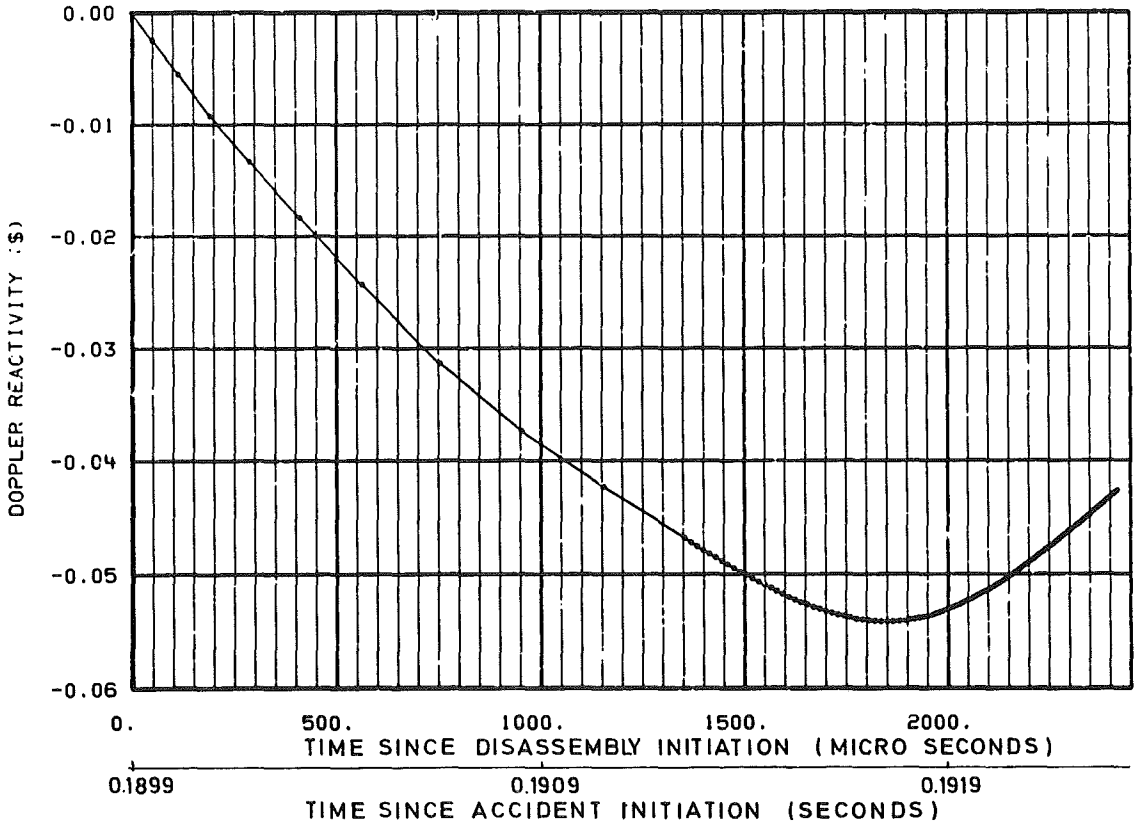

FIG.4.1.4.l ROD EJECTION
DOPPLER FEEDBACK AS FUNCTION OF TIME DURING THE DISASSEMBLY PHASE

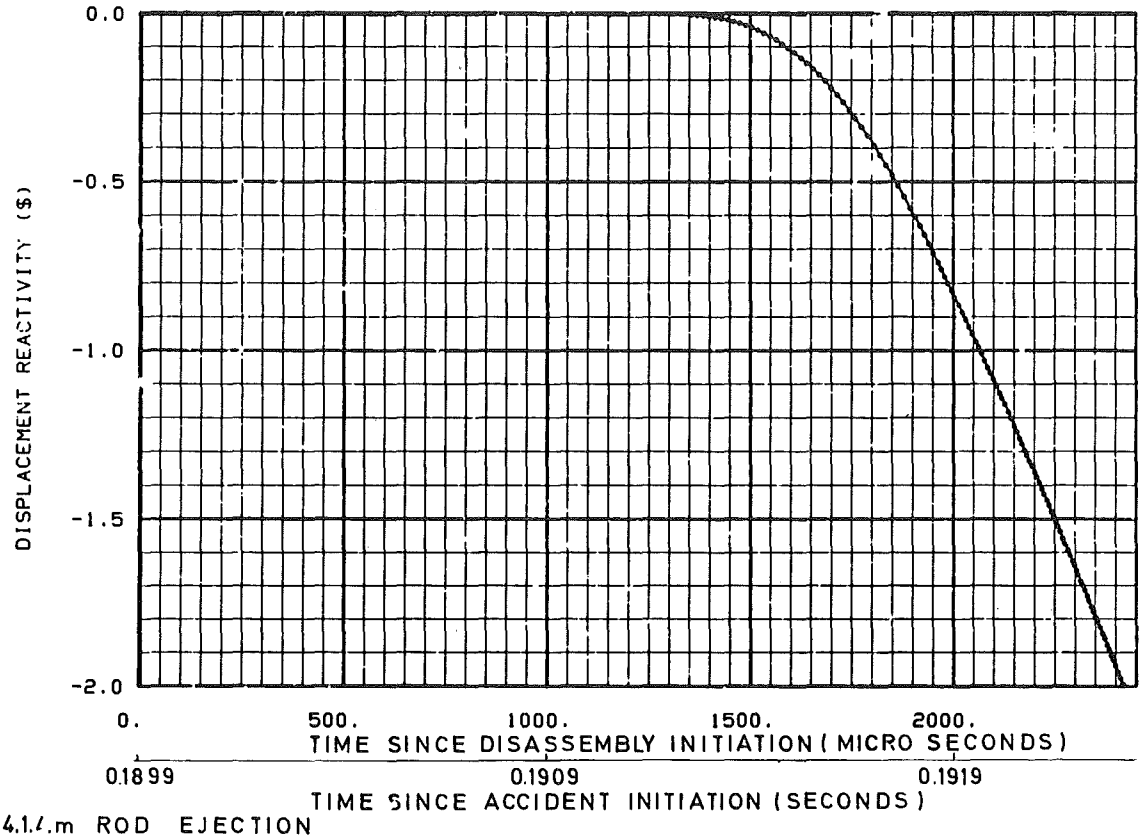

FIG. 4.1.4.m ROD EJECTION
DISPLACEMENT REACTIVITY AS FUNCTION OF TIME DURING THE DISASSEMBLY PHASE

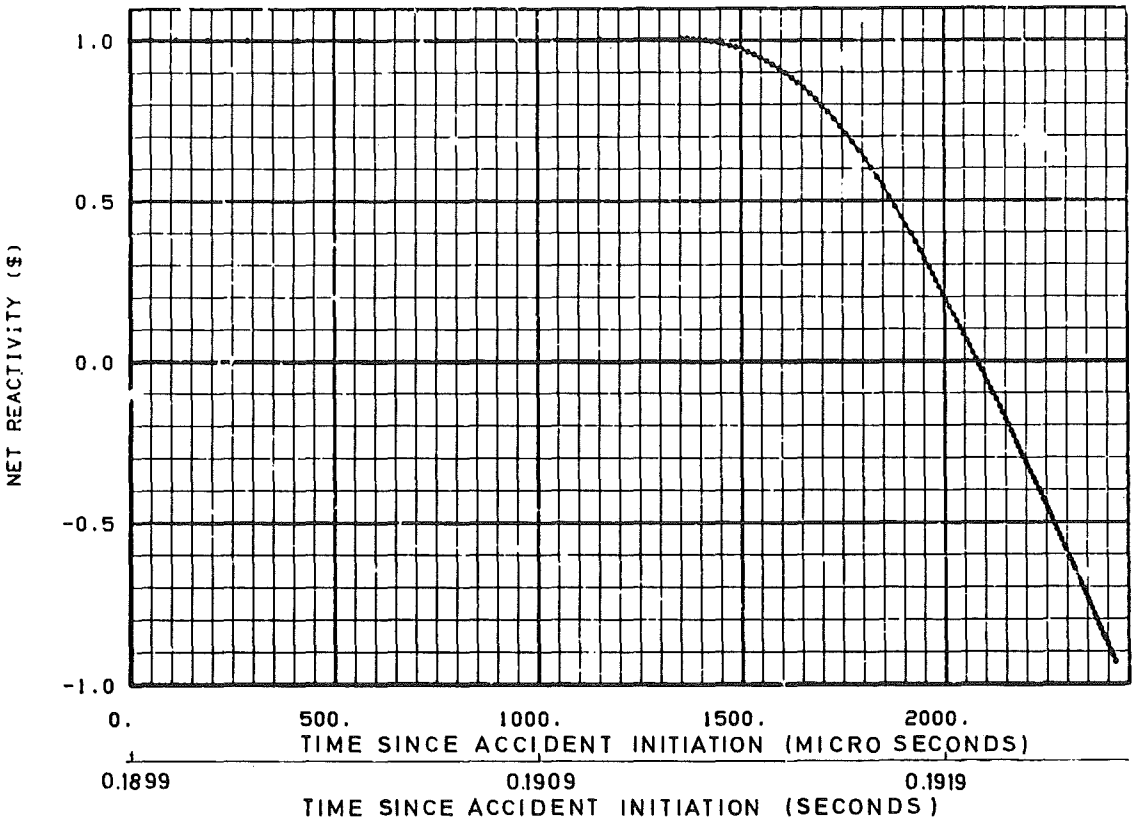

FIG. 4.1.4.n ROD EJECTION
NET REACTIVITY AS FUNCTION OF TIME DURING THE DISASSEMBLY PHASE

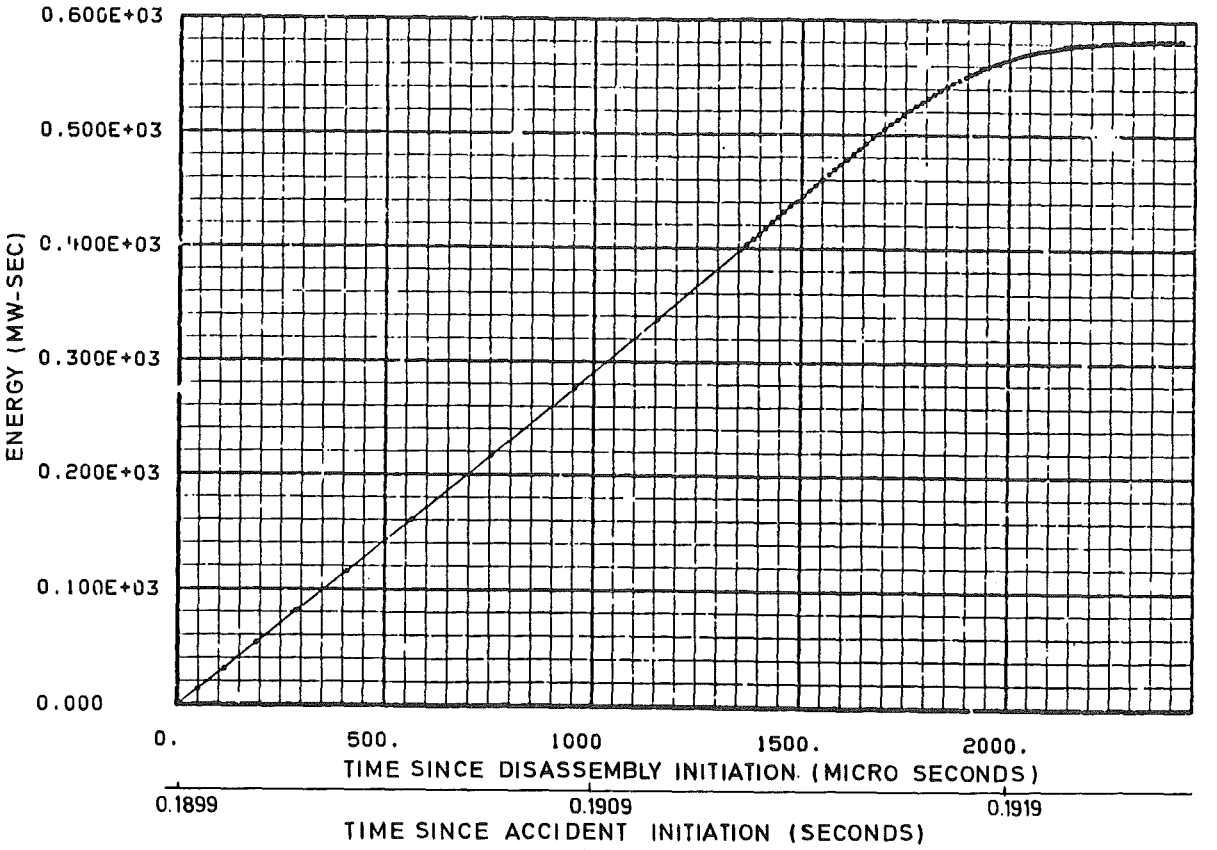

FIG: 4.1.4.o ROD EJECTION
THERMAL ENERGY RELEASE DURING THE DISASSEMBLY PHASE

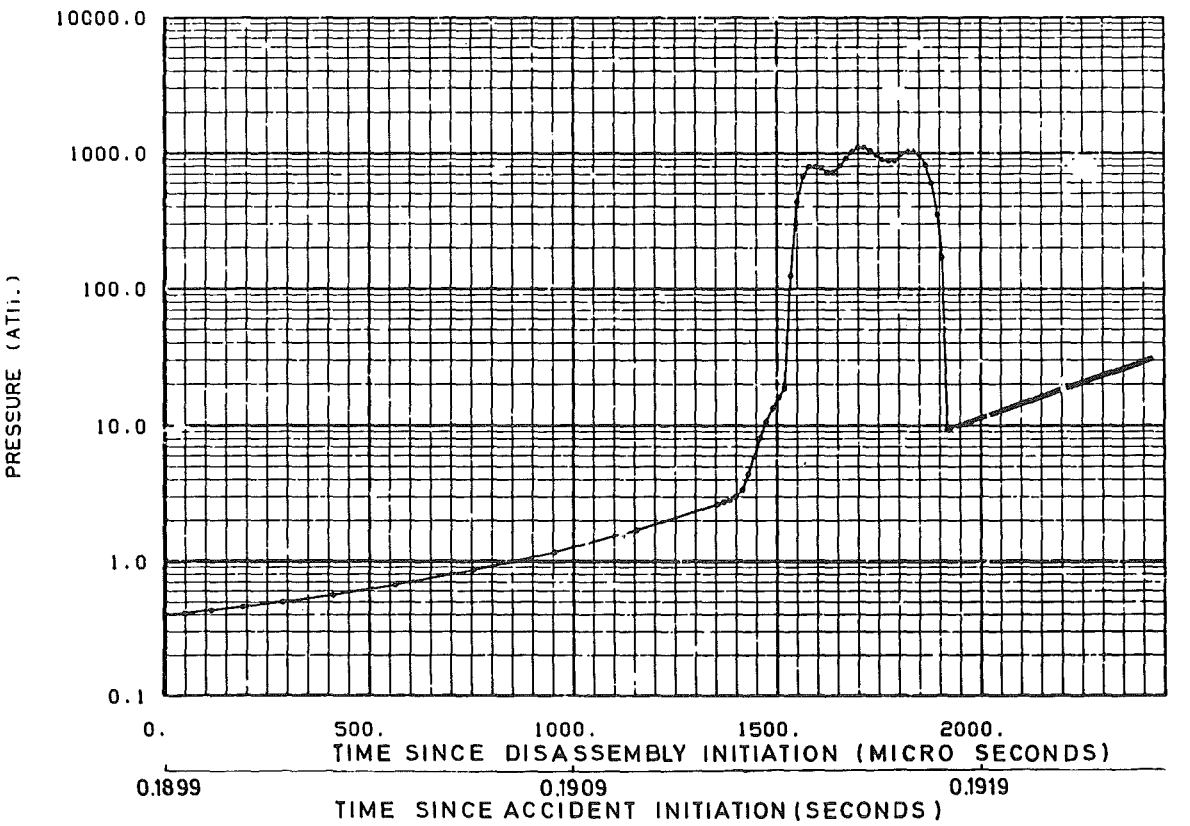

FIG.4.1.4.p ROD EJECTION
PRESSURE AT THE CENTRE OF THE CORE AS FUNCTION OF TIME DURING THE DISASSEMBLY PHASE

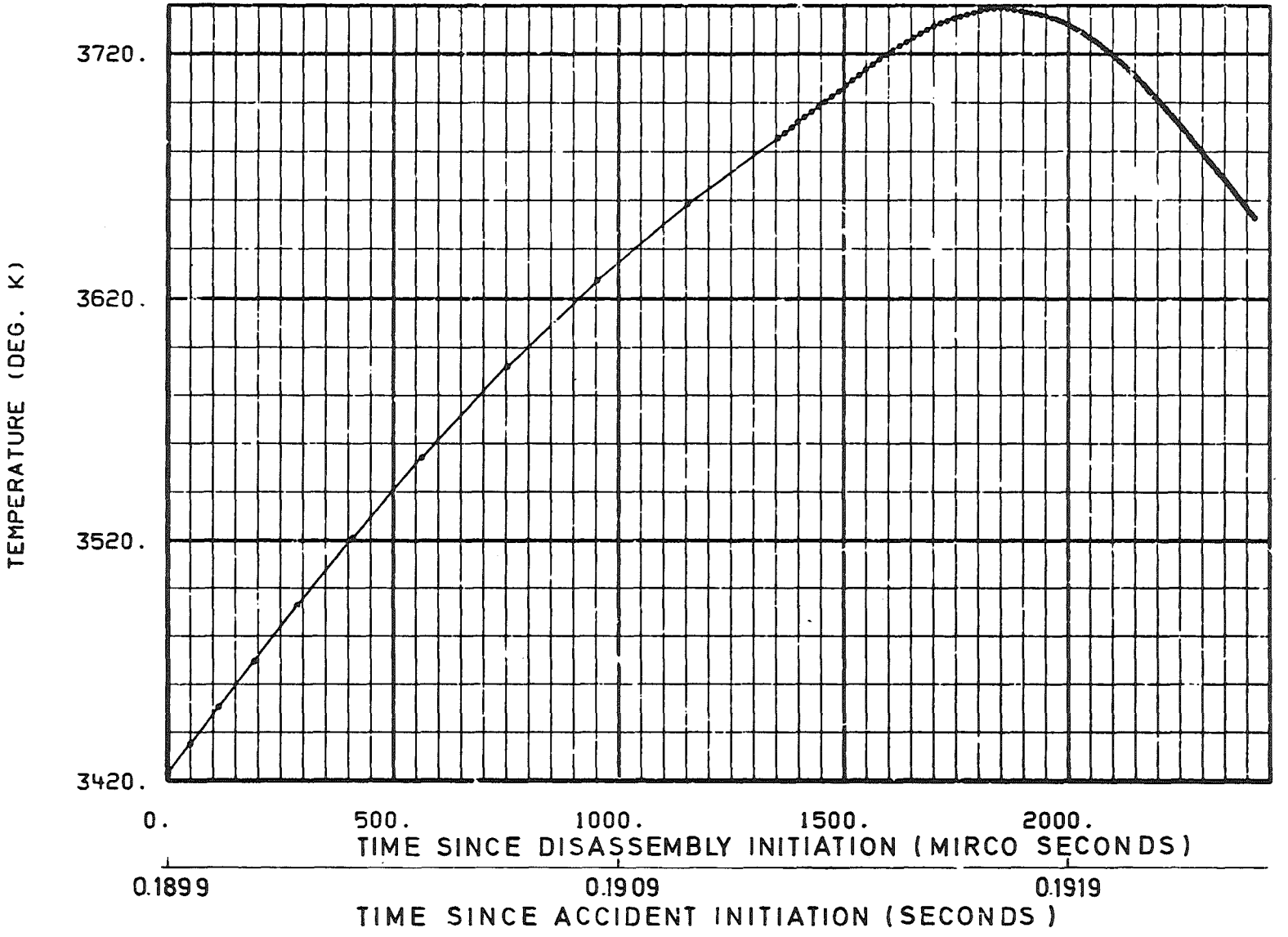

FIG. 4.1.4.q ROD EJECTON
TEMPERATURE AT THE CENTRE OF THE CORE AS FUNCTION OF TIME DURING THE DISASSEMBLY PHASE

4.2 Influence of parameter changes

In the case of reactivity ramp accidents described in chapters 4.1.3 and 4.1.4 a fuel coolant interaction is assumed to occur as a consequence of failing fuel pins. This causes sodium to be ejected from the core and gives rise to an increase in the initial reactivity ramp.

In obtaining the results of the previous sections the following assumptions were made:

a) The sodium fuel interaction and hence the ejection of sodium starts when 45% of the fuel in any mesh is molten (failure of the fuel rod). This assumption is very much on the conservative side. Fuel pin failure is not likely to occur until about 6o% of the fuel has become liquid; especially in this class of accidents where the cladding temperatures are only around 8oo^{o}C (fig. 4.1.3.e and 4.1.4.e).

b) All the liquid fuel of the 3o cm length reaction zone mixes with sodium. This assumption includes a particle diameter of 15o μ and a "mixing time" constant of 1o msec. However, most probably only 25-5o% of the fuel will participate in the interaction.

c) Fuel coolant interactions occur in major areas of the core (fig. 4.1.3.h) before the disassembly phase is initiated (coupling of SAS2A with VENUS) giving rise to pressures of approximately 5o atm. It was assumed that these pressures only result in the ejection of sodium from the core, while disa-sembly events and fuel particle movements generated by this process were not taken into account.

These are very conservative assumptions as has been shown by Kastenberg /13/. More advanced fuel rod failure models, recently developed by Fischer /23/ and Waltar /51/ can account for fuel movement in the coolant channel which leads to lower ramp rates during transition into core disassembly.

Under the very conservative assumptions listed above the sodium void ramp at the beginning of the disassembly depends on the following para-meters:

- time of pin failure or amount of molten fuel within the fuel pin at failure
- quantity of liquid fuel released from the pin
- time constant for the entrance of molten fuel into the coolant channel, and subsequent fragmentation and mixing with coolant
- size distribution of fuel particles during the thermal interaction between molten fuel and sodium

In table 4.2.1 results of calculations are shown for which the transition point for the coupling between SAS2A and VENUS calculations was artificially changed to show the influence of subsequent ramp contributions by bursting pins core core channels 1, 2, 3, 4 and 7. In case A the annular channels 1, 2, 3 and 4 contribute fully to the positive sodium void reactivity ramp given as input to the disassembly calculation (results of section 4.1.3). However, channel 7 can hardly contribute any more **during the predisassembly phase, since disassembly processes in most parts of the core have been started already.** In case B only the annular channels 1 and 2 give full positive void contributions and it is assumed that contributions from channels 3, 4 and 7 are already overshadowed by disassembly processes in the core. As can be seen, the input reactivity ramp for disassembly calculations is reduced from 55 $/sec (case A and section 4.1.3) to 24 $/sec (case B).

If it is assumed that only 5o% instead of 1oo% of the liquid fuel is mixed with sodium in the coolant channel (case C) then the reactivity ramp is further reduced to 18 $/sec.

Table 4.2.1 Results of VENUS calculations for different fuel rod failure conditions (5 $/sec initial ramp)

CASE	A	B	C
transition time /sec/ and temperature (fuel) /^{o}C/	o.33o4 325o	o.3265 278o	o.3265 278o
fraction of liquid fuel mixed	1oo%	1oo%	5o%
reactivity ramp at the beginning of the disassembly phase ($/sec)	55	24	18
duration of disassembly phase (msec)	2,3	7,6	1o
energy released in the disassembly phase (MWsec)	2o8o	198o	176o
mass of molten fuel at the^{+} end of the disassembly phase (kg)	2515	1372	946
average temperature of the molten fuel (^{o}K)	3756	32oo	3o9o

$^{+}$ available to transfer energy to sodium

By detailed analysis of the results of case B and C one can extrapolate, with good accuracy, that the resulting input reactivity ramps of 24 $/sec (case B) and 18 $/sec (case C) for the disassembly calculations are also valid for two additional cases. In these two extrapolated cases the fuel rods would fail only when about 6o% of the radial pellet cross section is molten in channels 1, 2, 3, 4 and 7. Since already 6o% or more of the pellet cross section is molten, the core is closer to disassembly as in cases B and C, and channels 5,4 and 7 can hardly contribute any more to sodium void ramps. The disassembly process starts quicker in the highly rated central parts of the core. Results of these considerations are discussed in /67/. However, a slight increase in the mass of molten fuel at the end of the disassembly phase, corresponding to 2oo MWsec additional energy release, in comparison to cases B and C, has to be taken into account. Similar results were found for the rod ejection case and a slight change in the fraction of liquid fuel mixed in the coolant channel have to be accounted for /67/.
In sections 4.1.3 and 4.1.4 a mean effective fuel particle diameter of 3oo μ and a mixing time constant of 3 msec were used as input data for the fuel-sodium interaction model incorporated in the disassembly code VENUS. Table 4.2.2 indicates results obtained for mean effective particle diameters of 5oo μ and a mixing time constant of 6 msec.

Table 4.2.2 Results of VENUS calculations for 5 $/sec initiating reactivity ramp,
Influence of different parameters for sodium fuel interaction during disassembly

CASE	B+	D	E
particle diameter (μ)	3oo	3oo	5oo
mixing time constant (msec)	3	6	3
duration of disassembly phase (msec)	7,6	8,6	8,1
energy released in the disassembly phase (MWsec)	198o	229o	217o
mass of molten fuel at the++ end of the disassembly phase (kg)	1372	1755	1625
average temperature of molten fuel (^{o}K)	32oo	3334	3275

+ Refers to case B of table 4.2.1

++ available to transfer energy to sodium

In order to obtain an indication of an upper limit to the results which can be achieved when using various fuel-sodium interaction parameters, VENUS-calculations were also performed for cases in which no fuel-sodium interaction was taken into account. The results of these calculations are shown in table 4.2.3. It is seen that the influence of the fuel-sodium interaction is particulary large in the absorber rod ejection case. This is due to the fact that only small parts of the core are voided in this case, when the disassembly phase begins. These cases, however, are inconsistent, since a fuel-sodium interaction is taken into account during the predisassembly phase but not during the disassembly phase.

Table 4.2.3 Results of VENUS calculations: with and without sodium fuel interaction during the disassembly phase

CASE	5 $/sec				rod ejection			
transition ramp ($/sec)	55[+]	55	24	24	4o[++]	4o	25[+++]	25
fuel sodium interaction	yes	no	yes	no	yes	no	yes	no
duration of disassembly phase (msec)	2.3	3.3	7.6	11.2	2.4	7.5	3.35	9.5
energy released in the disassembly phase (MWsec)	2o8o	272o	198o	267o	594	162o	544	198o
mass of molten fuel at the end of the disassembly phase (kg)	2515	32oo	1372	2o7o	1324	21oo	124	1664
average temperature of molten fuel (^{o}K)	3756	4o89	32oo	353o	3249	382o	3o9o	3456

+ Case A of table 4.2.1,described in section 4.1.3

++ Described in section 4.1.4

+++ Only annular channels 1 and 2 contribute to the positive void ramp

Concluding this discussion the following can be stated:

- the 5 $/sec reactivity ramp case, leading with a 55 $/sec transition ramp into the disassembly phase, yields the highest amount of molten fuel (2515 kg) with the highest average fuel temperatures (3756°K) after disassembly
- the above made assumptions are extremely conservative as has been shown in /13, 23,51/. These conservative assumptions were only made, because quantitative experimental results about fuel movement during a sodium fuel interaction in the coolant channel are not available yet
- The 55 $/sec transition ramp (case A), appears to be extremely conservative.
- since fuel-sodium interaction effects are already taken into account during the predisassembly phase it is also necessary to account for these effects during the disassembly phase. Therefore the cases of table 4.2.3 not dealing with fuel-sodium interaction effects during disassembly are unrealistic and inconsistent
- during the predisassembly phase a mixing time constant of 1o msec appears to be appropriate /64/, since during this accident phase the power is only changing slightly. In addition this mixing time constant describes the process of fuel rod failure, expulsion of molten fuel from the fuel rod into the coolant channel, mixing of molten fuel and coolant as well as the fragmentation process for the fuel
- a similar mixing time constant of only 3 msec describing these processes during disassembly appears also adequate since the reactor power is changing there by a factor 4oo times faster than during the predisassembly phase and much of the fuel is already mixed with sodium.

5. RELEASE OF MECHANICAL ENERGY AFTER CORE DISASSEMBLY

Tables 4.1.1A to 4.1.4A and 4.1.1B to 4.1.4B have indicated the final conditions of the core in terms of fuel temperatures and fuel pressures. Table 5.1A and 5.1B as well as 5.2A and 5.2B show the material velocities for the axial and radial directions after disassembly for the two characteristic cases of a

- pump failure (fresh core) and a
- 5 $/sec initial reactivity ramp

Since the energy production was abruptly stopped, the ultimate pressures and consequent accelerations of material are not increased further. The material displacements and velocities, however, will continue to change as a function of time and will make the core more subcritical.

Again, there are two typical cases on the basis of which the further sequence of accident events can be described:

a) In the case of pump failure the disassembly phase terminates with the core and the axial blankets voided. Only in the center of the core, fuel pressures of about 5o bars are attained. The central core contains a very hot fuel bubble which is surrounded by liquid fuel at lower temperatures. The outer core regions still contain solid core and fuel pin structures. Above all, the axial blankets have retained their original fuel pin structure. However, they are filled only with sodium vapour. The phase boundary between sodium vapour and liquid sodium is located in the upper mixing plenum. Because of the physical separation of liquid fuel and sodium, a direct sodium fuel reaction is not possible. Under certain conditions there may be minor fuel sodium reactions in the further coarse of the accident.

b) In all reactivity accidents (5 $/sec initiation ramp and absorber rod ejection), in which there is fuel pin failure prior to sodium boiling, the reactor core is still filled with sodium. Shortly before, and during the disassembly phase, the fuel pins fail because of high fuel and cladding temperatures or as a consequence of the very fast buildup of a fuel vapour pressure. Since the actual disassembly process will last for only a few msec in all these cases, liquid and vapourized fuel will be mixed under high pressure with sodium, cladding and structural materials. There is very fast heat transfer between the fuel and sodium within a very few msec, followed by generation of sodium vapour and the performance of mechanical work on the vessel structures.

Axial velocity $W_{a,max}$= 23.9 m/sec ≙ 239 at
Mesh Point /18,1/

22	32	31	28	17	3	o	o	o	o	o	o	o	o
21	84	84	76	61	5o	22	1	o	o	o	o	o	o
2o	141	136	126	98	58	29	6	o	o	o	o	o	o
19	196	186	176	139	79	41	11	4	o	o	o	o	o
18	239	227	215	224	175	62	45	27	6	9	7	4	1
17	21o	2o1	191	91	92	54	22	47	31	47	6o	24	o
16	158	15o	143	147	129	36	15	9	8	13	13	8	2
15	o	o	-3		-17	-8	1o	6	3	3	7	11	6
14	-73	-7o	-12o	-1o3	-11	-11	-4	-2	-1	1	4	3	o
13	-193	-184	-178	-38	2	-41	-16	-11	-6	-11	-15	-5	o
12	-2o5	-196	-186	-216	-178	-5o	-21	-12	-9	-14	-15	13	16
11	-225	-212	-198	-155	-98	-6o	-24	-16	-11	-2o	-26	-24	-3
1o	-174	-168	-153	-121	-78	-45	-2o	-12	-1o	-15	-19	o	o
9	-128	-121	-1o9	-86	-56	-32	-14	- 9	-7	-12	-15	-14	-9
8	-7o	-7o	-62	-48	-36	-2o	-9	-7	-5	-8	-1o	-7	-5
7	-22	-21	-19	-1o	-2	o	o	o	o	o	o	o	o
6	o	o	o	o	o	o	o	o	o	o	o	o	o
	1	2	3	4	5	6	7	8	9	1o	11	12	13

Table 5.1.A Flow coast down I (fresh core)

Axial velocity in any mesh of the core after the end of the disassembly phase

Radial velocity $W_{r,max}$= 34.8 m/sec ≙ 348 at
Mesh Point /14,5/

22	o	o	o	o	o	o	o	o	o	o	o	o	o
21	o	o	3	13	4	o	o	o	o	o	o	o	o
2o	o	1	11	38	14	23	o	o	o	o	o	o	o
19	o	4	21	7o	3o	58	1o	o	o	o	o	o	o
18	o	12	31	114	54	82	2o	2	1	o	o	o	o
17	o	23	44	145	176	1o1	29	24	o	o	o	o	o
16	o	33	58	157	216	125	39	23	2	-18	12	24	2
15	o	43	75	189	291	146	5o	27	6	-38	22	47	4
14	o	47	82	17o	348	154	56	31	4	-42	24	52	7
13	o	45	8o	219	226	151	56	32	4	-5o	24	59	8
12	o	4o	71	177	19o	137	51	28	3	-47	21	57	1
11	o	32	56	147	21o	113	41	21	3	-4o	16	3o	22
1o	o	22	43	14o	69	84	28	14	3	-31	12	15	15
9	o	12	29	89	45	51	17	8	2	-19	7	7	4
8	o	5	19	54	25	29	8	4	2	-11	4	-1	8
7	o	1	1o	28	11	9	3	1	o	-3	1	o	1
6	o	o	2	9	2	o	o	o	o	o	o	o	o
	1	2	3	4	5	6	7	8	9	1o	11	12	13

Table 5.1.B Flow coast down I (fresh core)

Radial velocity in any mesh of the core after the end of the disassembly phase

Axial velocity $W_{a,max}$ = 33.8 m/sec
Mesh Point /12,1/

22	79	84	11o	74	34	7o	76	87	88	67	59	39	8
21	274	214	1o1	1o4	15o	96	98	88	45	33	24	66	1o3
2o	182	2o3	171	177	172	98	63	62	9o	111	118	39	1
19	2o	55	22o	169	125	16o	1o7	112	97	99	45	67	65
18	66	1oo	72	117	148	148	112	76	117	78	87	72	43
17	253	169	134	2o9	181	7o	139	158	1o9	128	1o2	58	68
16	123	117	114	-6	23	167	137	144	93	82	1o5	72	13
15	135	38	-25	-66	21o	162	12o	9	52	9o	54	54	82
14	248	224	174	45	-115	-1o3	64	1o7	29	52	21	-33	27
13	-166	-327	-255	-19	7o	52	5o	34	16	51	-3	36	15
12	338	-136	38	-14	-152	-86	-1o	-118	-95	48	121	51	18
11	-1o6	-188	-79	21	38	-22	-161	-15	3o	-66	-92	-83	42
1o	-93	-74	-89	-3o	-9o	-67	49	-45	-56	-36	-52	1	-57
9	15	-8	-131	-222	-112	-4o	-66	-85	-133	-125	-43	-81	-1o1
8	-1o3	-1o6	-123	-116	-5o	-116	-172	-121	-93	-158	-215	-9o	-5
7	9	-25	-76	-161	-2o1	-228	-175	-96	-85	-91	-89	-98	-9o
6	8	-2o4	-181	-128	-1o7	-168	-143	-95	-98	-78	-55	-43	-69
	1	2	3	4	5	6	7	8	9	1o	11	12	13

Table 5.2.A 5 $/sec reactivity ramp
axial velocities in any mesh of the core
after the end of the disassembly phase

Radial velocity $W_{r,max}$ = 22.2 m/sec
Mesh Point /12,13/

22	o	8	-43	46	33	77	79	6	51	59	12	66	3o
21	o	66	-2o	91	11	82	33	64	76	1o3	o	44	5o
2o	o	127	63	-1o	155	9o	34	93	96	8o	3o	35	36
19	o	91	47	62	121	157	39	95	79	69	77	66	58
18	o	47	19	127	69	142	96	71	88	93	93	39	1o7
17	o	73	18	39	217	67	1o8	83	91	1o8	93	83	77
16	o	116	-9	121	145	89	31	155	115	74	128	1o8	92
15	o	14	75	38	32	75	8o	2o6	76	9o	129	136	88
14	o	57	14o	-61	94	55	123	121	96	116	131	17o	74
13	o	25	7o	-3	21	15o	37	78	132	133	152	145	166
12	o	18	42	21	51	73	43	19o	12	86	184	13o	222
11	o	-66	-34	91	94	62	114	84	52	3	214	158	111
1o	o	-17	-114	1o3	1o2	86	12o	27	62	67	176	145	67
9	o	-13	-51	19	154	-3o	156	77	57	51	137	174	126
8	o	3	2	-16	28	89	132	5o	92	7o	1o2	153	99
7	o	49	31	-45	18	128	7o	36	75	131	81	71	31
6	o	58	26	-54	123	-4	51	28	33	124	71	119	-14
	1	2	3	4	5	6	7	8	9	1o	11	12	13

Table 5.2.B 5 $/sec Reactivity ramp
Radial velocities in any mesh of the core
after the end of the disassembly phase

For the calculation of the possible mechanical energy generated in the SNR vessel, the model by Cho and Wright /21/ was used to describe phenomena occuring during the fuel-sodium interactions in the core region. According to this model, the mixing and fragmentation process of fuel is described by a fragmentation and mixing time constant.
A specific particle size distribution for the fuel is taken from experiments /53/. During an initial phase of a few msec, heat is transfered from the surface of the particles to the surrounding liquid sodium, thus causing high pressure peaks as a consequence of the thermal expansion of the liquid zone around the fuel particles. Any fission gas contained in this mixture can be taken into account. When the pressure peak has decreased to the saturation curve of sodium, that is to say, after the return of the reflected wave from the surface of the sodium column on top of the reaction zone, there will be pressure relief followed by sodium evaporation in the reaction zone. This incipient production of sodium vapour will move all the liquid and steel media surrounding the reaction zone. Heat transfer from the fuel to the surrounding sodium can be assumed for a specific period, as proposed by Caldarola /68/. Values for the heat transfer coefficient are taken from /69, 7o/.

5.1 Flow coast down accidents

Because of the physical separation between liquid fuel and sodium by sodium vapour, there can not be a direct interaction between liquid fuel and sodium. An estimate of the possible mechanical work performed by the evaporated fuel gives approximately 4o MWsec during isentropic expansion to 1 atm according to Padilla /59/ and the data of Booth /6o/. Only minor quantities of liquid fuel and sodium can be subjected to the thermal interaction. There will be a multitude of separate interactions with pressure buildup, when sodium comes back into the core region. However, it seems impossible for liquid or evaporated fuel to meet in a radially coherent contact front with sodium. Instead, the molten fuel will also transfer its thermal energy to colder steel and fuel structures in the lower blanket region and small quantities of sodium above the core will again and again contact the surface of molten fuel, evaporate and release this thermal energy into the upper vessel region.

Even if approximately 1/3 of the molten fuel were suddenly mixed with sodium, the resulting stresses upon the reactor vessel would in any case be smaller than in the cases outlined in the 5 $/sec ramp case. Hence as far as integrity of the vessel is concerned, this case must not be regarded as the critical one. It is however important for considerations on the cooling of these molten fuel masses over long time periods which leads to the problem of core catcher design /63/.

5.2 Reactivity accidents

In these cases, which have been described in sections 4.1.3 to 4.1.5, the reactor core and the blankets are still filled with sodium during and after disassembly. Fuel melting, fuel pin failure and a thermal interaction between molten fuel and sodium in the coolant channel occur before sodium starts boiling.
During the disassembly phase the fuel vapour pressure builds up from a few atmospheres to maximum values of a few hundred atmospheres within several msec. After failure of the fuel pin, molten fuel, steel and sodium will be mixed. The degree of mixing and the time constant of the fragmentation and mixing processes depend on the locally variable fuel pressure in the core.

At the point of maximum fuel pressure the mixing and fragmentation time constant will be on the order of msec; in the outer core regions with lower fuel pressures, the time constant will be on the order of 1o msec and above. Under these conditions, an assessment of the possible work due to the expansion of the fuel vapour according to Meyer-Wolfe /61/ or Padilla /59/ as in section 5.1 (pump failure) is no longer adequate because now, within a very few msec, the heat will be transfered very quickly from particles of hot fuel to sodium and sodium represents a better working medium for a conversion into mechanical energy /59/.

A large part of the reactor core may be regarded as a reaction zone for the thermal interaction between molten fuel and sodium, which is under a sodium column approximately 4.5 m high within the reactor vessel,and is surrounded at the bottom by the axial blanket, the grid plate and the inlet plenum. Within the reaction zone there is a locally variable field of pressures and temperatures; hence, the fuel dispersion and mixing processes described above will also occur with some local variability.
From the results of the VENUS calculation for the case of a 5 $/sec initiating ramp leading into a 55 $/sec disassembly ramp (table 4.1.3A, 4.1.3B), it is possible to derive a reaction zone with a radius of 73 cm and a height of 55 cm in which 2515 kg of molten fuel with an average temperature of 3756^{o}K is to be mixed with sodium in a ratio of 7.5:1.

A calculation on the basis of the fuel-coolant interaction model of Cho and Wright /21/ supplies the values of isothermal expansion work to 1 bar listed in table 5.2.1 for a field of parameters including the particle radius, heat transfer during the vapour phase and duration.

In calculating the release of mechanical energy, it is assumed in the Cho-Wright-model /21/ that after the end of the acoustic phase, there can still be heat transfer from fuel particles to sodium, with a heat transfer coefficient, for a certain period of time. The basic particle distribution is to be arrived at the end of a process of mixing and fragmentation. The distribution of particle sizes is taken into account by a mean effective particle radius.
Moreover, a time constant t_M, on the average, describes the time functions for the following processes:

- the generation of liquid fuel occuring from the beginning of the first pin failure to the end of disassembly
- the process of fuel pin failure with the mixture of fuel and sodium
- the process of dispersion of the fuel up to the final distribution of particle sizes.

The lower limit for this mean time constant t_M, was assumed to be 1o msec /64/. The data for the release of mechanical energy holds for an expansion of the sodium vapour to 1 bar and are meant to be symbolic values for comparison, because the ultimate pressure in the reactor vessel is far in excess of 1 bar. Measurements of the distribution of particle sizes are available from TREAT-experiments and a number of out of pile experiments /53/. The use of this distribution of particle sizes in a model to describe the thermal interaction between liquid fuel and sodium, according to Caldarola /62, 68/, shows that an effective particle radius of approximately 15o μ should be used for determining the release of mechanical energy.

Table 5.2.1 Mechanical energy release (MWsec) vapour expansion to 1 (atm)

effective fuel particle radius	15o μ	15o μ	3oo μ
heat transfer coefficient (cal/cm^2 sec ^{0}K)	o.1	o.2	o.2
time period for film boiling heat transfer (msec)			
o	55	55	8
5	11o	113	25
1o	185	223	47

Measurements of heat transfer coefficients during film boiling of sodium were performed by Witte /69/ and Farahat /7o/. They are clearly below the value of o.1 cal/cm^{2}sec^{o}K used in table 5.2.1. The time of heat transfer from the fuel particles to sodium after the acoustic phase, is shown in /62, 68/, is hardly longer then a few msec because by then the entire reaction zone will have been filled with sodium vapour. With these experimental results and conclusions in mind, values for the release of mechanical energy between 5o and 223 MWsec result (table 5.2.1). From the spectrum of the values possible, on the basis of different parameters chosen, two cases (17o MWsec and 1oo MWsec) were selected for the calculations described in section 6 determining the stresses upon the reactor vessel.

5.3 P-V-relationship for the calculation of the mechanical effects on the vessel structure

In the previous section only the worst cases were investigated and discussed with the aim of obtaining **an upper limit for the mechanical loads** on the vessel system; all the other cases have resulted in less grave results.

As already stated above the indication of the mechanical energy released during an expansion of the sodium vapour to 1 bar (given in table 5.2.1) has only symbolic character. This quantity is merely a possibility of comparing the individual cases.What is more important for the further calculations as outlined in section 6 with codes such as REXCO-H /27, 28/ or ARES /29/ and DRAP /3o/, are the time functions for the pressure in the reaction zone (reactor core) p (t) and the movement of the sodium column on top of the reaction zone. From both time functions, p (t) and v (t), it is possible to determine an equation of state H (v,p) = o for the coupling of results obtained in sections 5.1 and 5.2 with the REXCO-H or ARES-code calculation (fig. 2.1). This equation of state H (p,v) is represented in fig. 5.3.1 for three different cases. As already mentioned two idealized cases of 17o MWsec and 1oo MWsec energy release (symbolic expansion to 1 atm) were selected from table 5.2.1 and fig. 5.3.1 for further calculations. It is evident from the above discussion that the first value of 17o MWsec represents a pessimistic combination of parameters whereas the second value can be localized in the more realistic optimistic range of the parameter field.

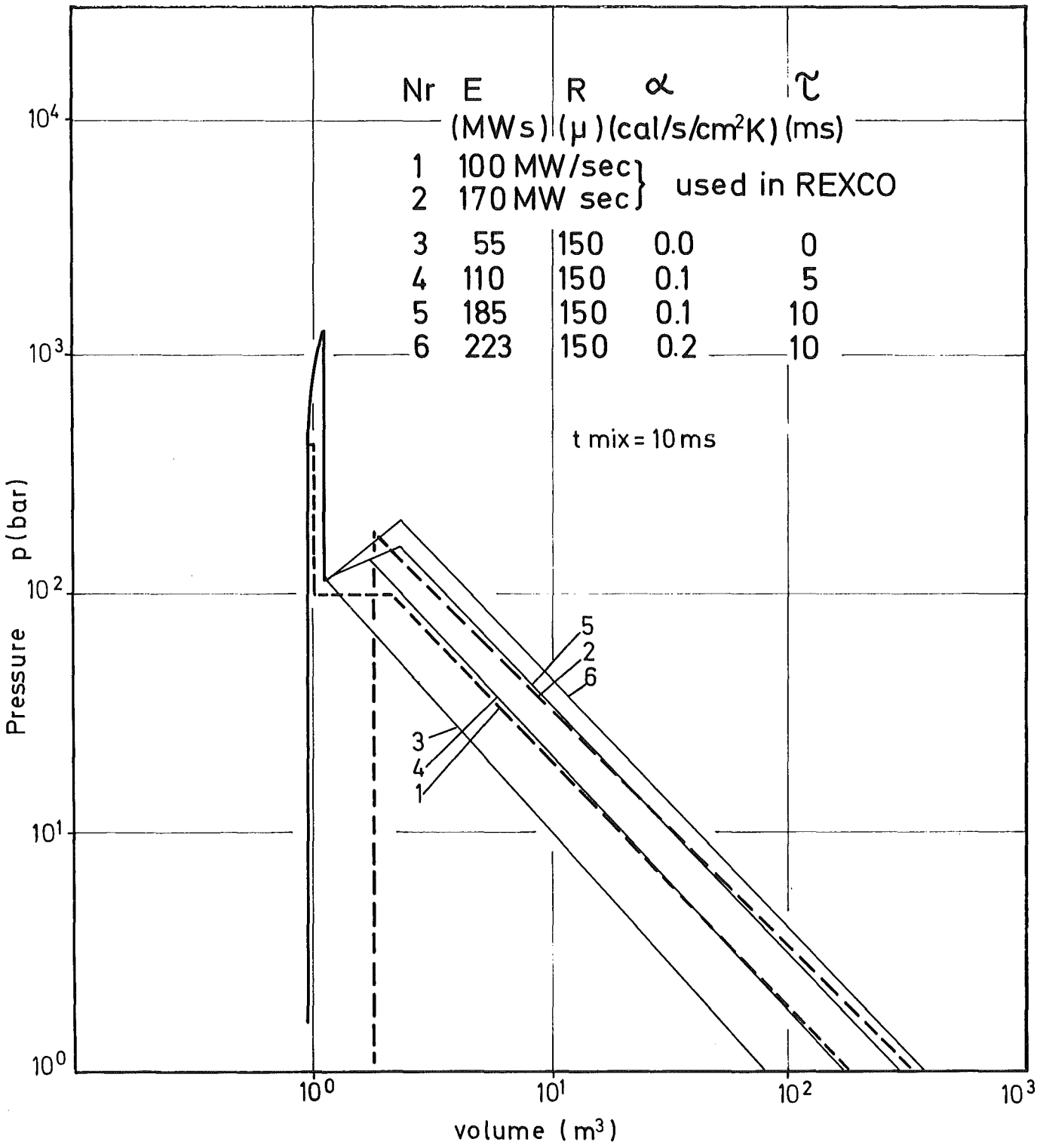

Fig.5.3.1 Pressure - volume relationships

6. MECHANICAL EFFECTS ON THE REACTOR VESSEL AND TOP PLUG

6.1 Description of the reactor vessel models

For all following calculations with REXCO-H /27, 28/, ARES /29/ and DRAP /3o/ the model of the reactor vessel system shown in fig. 6.1.1 has been used. The geometric dimensions of the reactor top structures and the material data used, are detailed in /3/ and /31/. The reactor core is surrounded radially, first by the structures of the core support and then by a thick shield tank with openings in the side which reduces the pressure stress on the external wall of the vessel. In the upper region of the vessel there is a perforated plate dipped into the sodium, transfering the liquid friction forces to the top structure and reducing the velocity of the sodium column which is accelerated towards the top. In this way, the so called "water hammer effect" on the top structure is reduced. In the lower region the core grid plate and its support on the outer reactor vessel are shown. The reactor top is clamped by stretch bolts.

For calculations with REXCO-H and ARES, flows and friction effects in the holes of the shield tank and the perforated dip plate can not be taken into account. Hence, calculations of two models were analysed. In model-1, the dip plate is simulated as a full plate firmly connected with the reactor top. In model-2 the dip plate is neglected. Both models are extreme cases.

The equation of state for the reaction zone in a pressure-volume relationship as shown in fig. 5.3.1 was used for the calculations with REXCO-H and ARES. For all other regions around the reaction zone, an equation of state of a Murnaghan type /65/ is used. The compressibility of materials used in all cases was that of liquid sodium because it is the most important compressible component.
The break down and size of meshes of the basic Lagrange grid was already shown in fig. 3.6 of section 3. The geometric configurations of model-1 (with dip plate) and model-2 (without dip plate) are given in fig. 6.1.2. Compared with fig. 3.6 an additional row of meshes (13 cm high) was introduced at the top which represents the sodium above the dip plate; the cover gas plenum with a height of 18o cm was also accounted for. The material densities for different regions are given in table 6.1.1. Structures having a strength are simulated by shells and slabs (table 6.1.2). Depending upon the position of the individual components relative to the core, stress-strain diagrams for embrittled or non embrittled material are used for the calculations (fig. 6.1.3, 6.1.4).

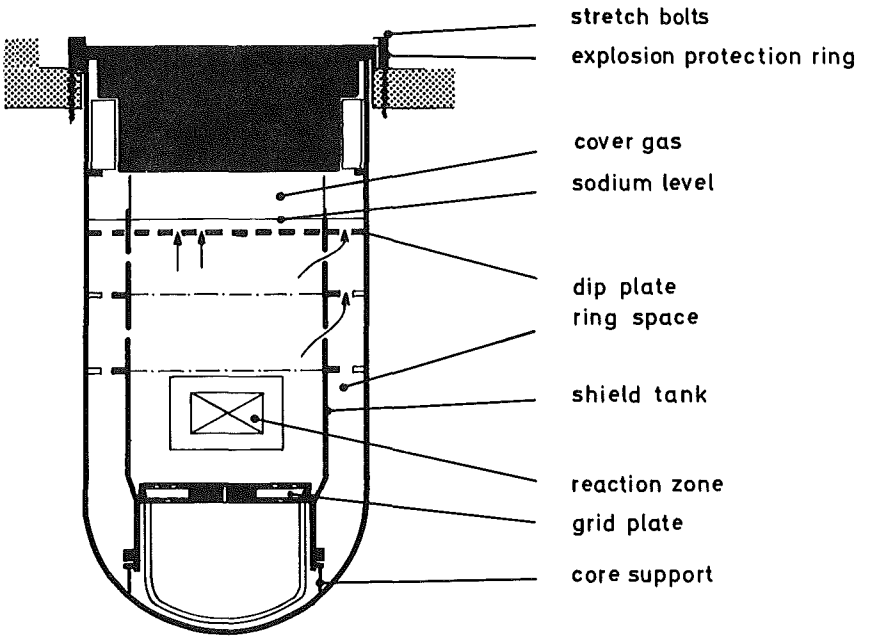

Fig.6.1.1 REACTOR VESSEL OF SNR-300

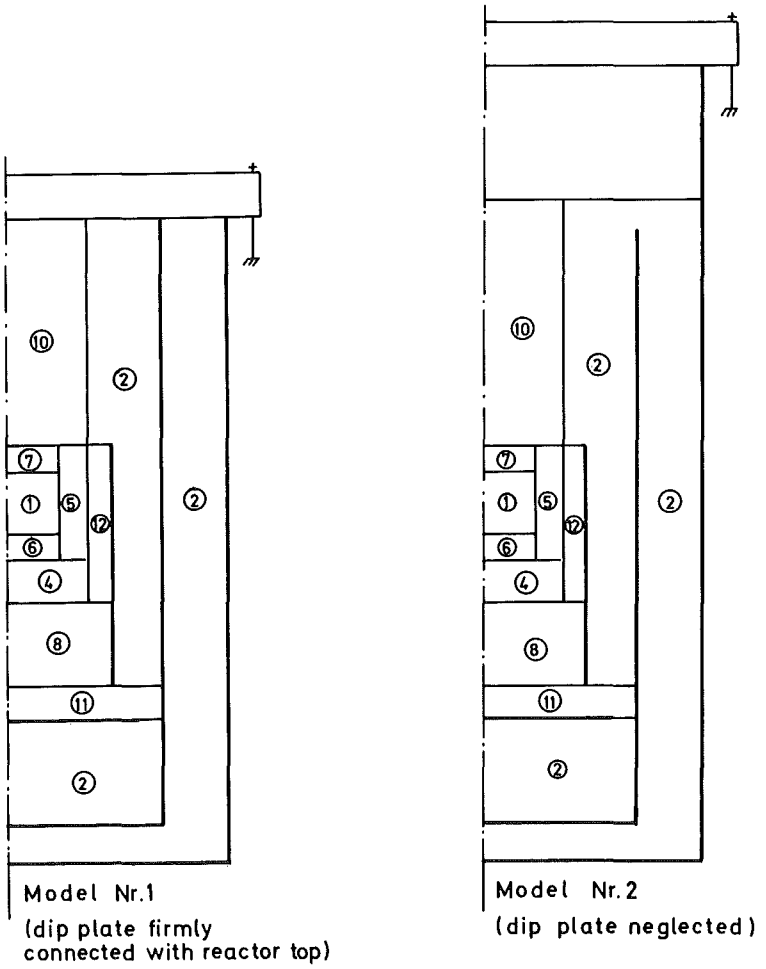

Fig.6.1.2 Vessel models used in REXCO calculations

Table 6.1.1 Distribution of regions and material densities used in REXCO-calculations

No.	region/material	density (g/cm^3)
1	active core	4.86
2	sodium	o.84
3	dummy	-
4	fission gas region	1.91
5	radial blanket	6.56
6	lower axial blanket	4.84
7	upper axial blanket	5.35
8	lower fuel element region and connecting tubes to grid plate	-
9	dummy	-
1o	region of the absorber guide tubes	1.oo
11	grid plate region	1.43
12	reflector	2.2o

Table 6.1.2 Different structures used in REXO-H and ARES-calculations

shells:

shield tank	thickness	
above grid plate region	8 cm	(irradiated)
below grid plate region (Simulation of high pressure plenum vessel)	4 cm	(unirradiated)
reactor vessel	4 cm	(unirradiated)
shell of core clamping	1 cm	(irradiated)

slabs:

bottom of shield tank (bottom of high pressure plenum vessel)	4 cm	(unirradiated)
bottom of reactor vessel	2.5 cm	(unirradiated)
grid plate	1o cm	(unirradiated)

reactor top plug 4oo to weight

plug clamping bolts:

number	11o
diameter	5.5 cm
lengths of expansion	55 cm

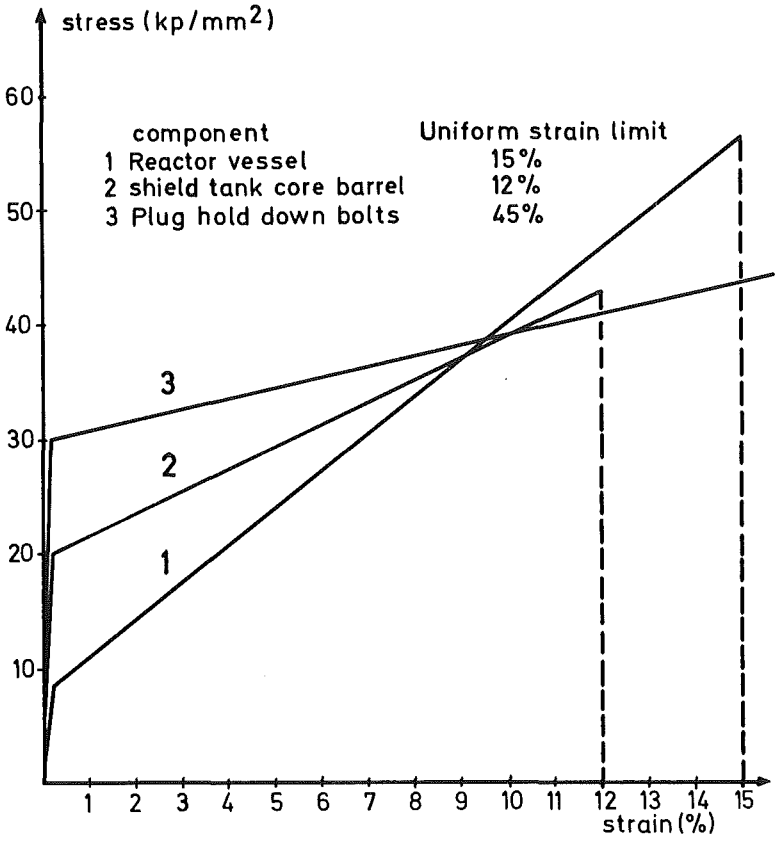

Fig. 6.1.3 stress-strain diagrams

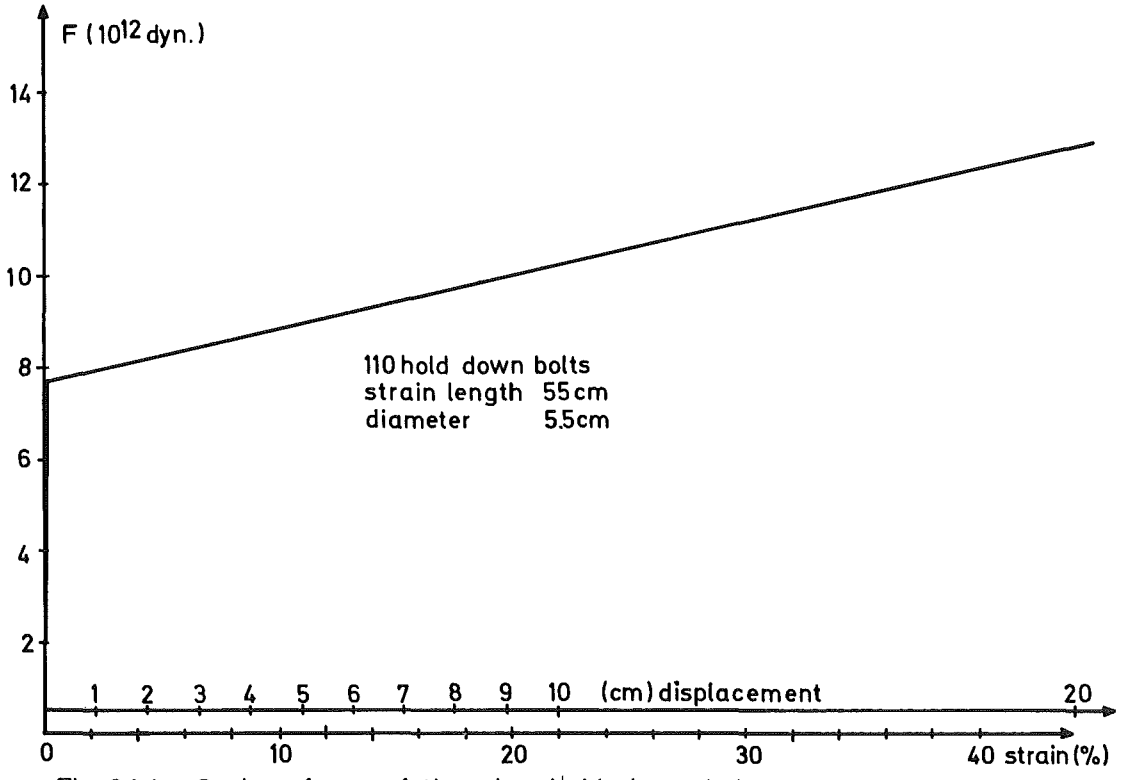

Fig. 6.1.4 Spring force of the plug hold down bolts

6.2 Results for a release of mechanical energy of 17o MWsec

Starting from the reaction zone in the core, the first component that can be stressed in a radial direction, is the cylindrical shell of the core clamping which, to a certain extent, also takes into account the strength of the structures inside (radial blanket). For this reason, the respective shell is assumed to fail only if the uniform strain limit of the embrittled material is exceeded. Fig. 6.2.1 shows the curves of angular strain of the cylindrical shell representing the core clamping system at the core mid plane for the model-1 and model-2 cases. The resulting strain is higher for the case without dip plate because more sodium is axially moved. Up to approximately 7 msec both curves behave identically.

Fig. 6.2.2 shows the angular strain of the shield tank and the reactor vessel at the core midplane as a function of time. These values determined by REXCO-H agree for both models: model-1 with dip plate and model-2 without dip plate up to about 7 msec. Afterwards, the strains become unrealistic for the model-1 case with the full dip plate because of the obstruction to axial movement of the sodium. (Sodium flow through holes of the dip plate and the shield tank is not taken into account by REXCO-H or ARES). From the results of fig. 6.2.2 it must be anticipated that 2-dim. REXCO-H calculations represent the true conditions up to about 7 msec. Afterwards, flow and friction phenomena in the reactor vessel tend to influence the development of the pressure. These phenomena are taken into account in the HEINKO /55/ and DRAP-code /57/. A similar conclusion can be drawn from results of fig. 6.2.3, where the pressure on the grid plate and four other places in the reactor vessel are shown. However, the longer the distance of these places is from the reaction zone the more different become the results for the model-1 and model-2 cases after about 7 msec.

For the calculations with HEINKO and DRAP the results for the first few msec were taken from the 2-dim. REXCO-H calculations and curve fitted. This requires a knowledge of the mean pressure accelerating the sodium column on top of the reaction zone in the shield tank. From hydrodynamic considerations, it is apparent that the changes of the axial kinetic energy of the sodium column as against the volume change of the reaction zone (dE_{kin}/dV) equals the mean pressure driving the column (fig. 6.2.4). This curve of dE_{kin}/dV was taken from the REXCO-H calculations as input to HEINKO and DRAP and used as a driving function.

Fig. 6.2.5 shows the pressure curves at various axial positions of the reactor vessel and the liquid pressure at the dip plate as calculated by means of the incompressible 2-dim. DRAP-code.

The pressure curve at the dip plate, determined by means of DRAP is compared in fig. 6.2.6 with results of the HEINKO-code. Compressibility effects and pressure oscillations cannot occur in the DRAP calculations (incompressible model). In addition it can be seen that the increasing pressure, as determined with HEINKO is about 2o% higher at 2o msec than determined with DRAP, because HEINKO cannot take into account the radial stress relief. It is however important that the pressure oscillations, as determined by HEINKO, are represented in a more or less quantitatively correct way by DRAP and that there is good agreement between the incompressible and the compressible treatments.
The further time behavior of the liquid pressure at the dip plate is influenced after a peak by the slowed down movement of the sodium column by the compression of the innert gas below the reactor top. The maximum expansions experienced by various components of the vessel top system are summarized and constrasted in table 6.2.1.

Table 6.2.1 Comparison of maximum expansions (%o) at the vessel top system for 17o MWsec

	REXCO-H		DRAP
	with full dip plate	without dip plate	with perforated dip plate
shield tank	5^{+}	2.4^{+}	1.4
reactor vessel (azimutal)	1.5^{+}	1^{+}	1.8
top clamping	-	-	o.5

The maximum values of the REXCO-H calculations (+) occur after about 15 msec. The maximum values of the DRAP calculations occur at about 2o msec. Since flow and friction effects have to be accounted for both results (REXCO-H and DRAP) cannot be fully compared.
The values in table 6.2.1 apply to an embrittled shield tank of 8 cm thickness. Since in DRAP calculations, the pressure release due to sodium flow through the holes of the shield tank is taken into account, the stress upon the shield tank is reduced and causes that of the reactor vessel to be higher than that determined on the basis of REXCO-H. For unembrittled material the maximum expansion of the shield tank would be 1.3%, the stress upon the dip plate and the reactor top is reduced correspondingly.
The mechanical energy of 115 MWsec, effective during the excursion, is thus accommodated by the vessel top structure and strain bolts.

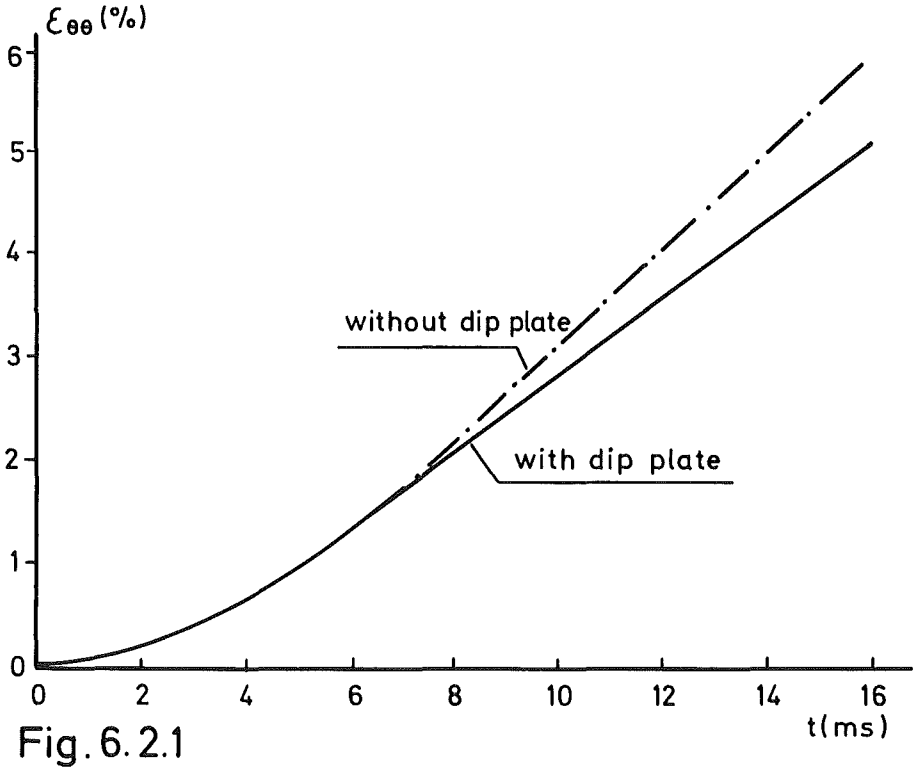

Fig. 6.2.1

REXO calculation for 170 MW_s
Angular strain of the core barrel at core mid plane

FIG. 6.2.2

ANGULAR STRAIN OF SHIELD TANK AND REACTOR VESSEL FOR THE 170 MWsec EXCURSION

(shield tank thickness = 8 cm)

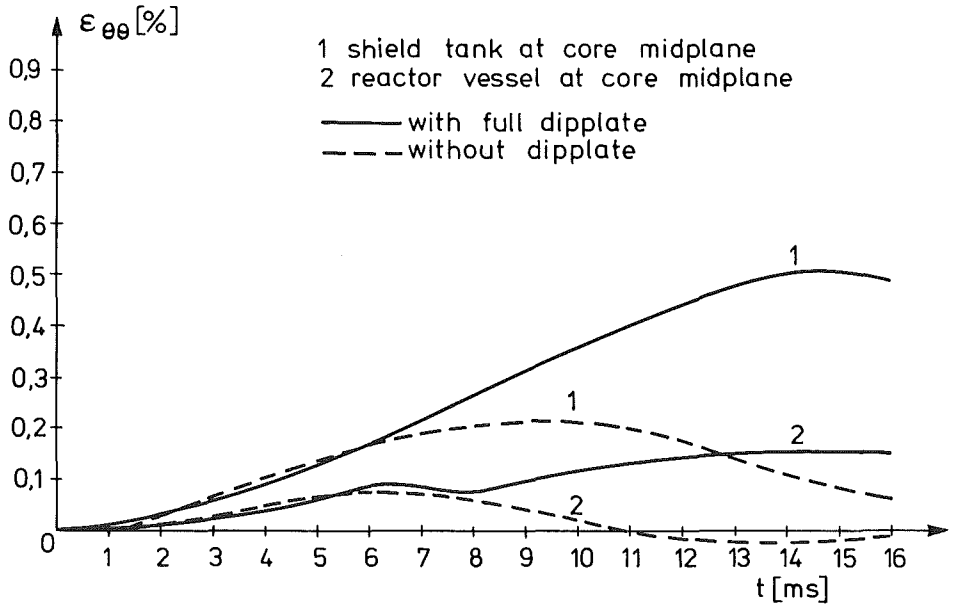

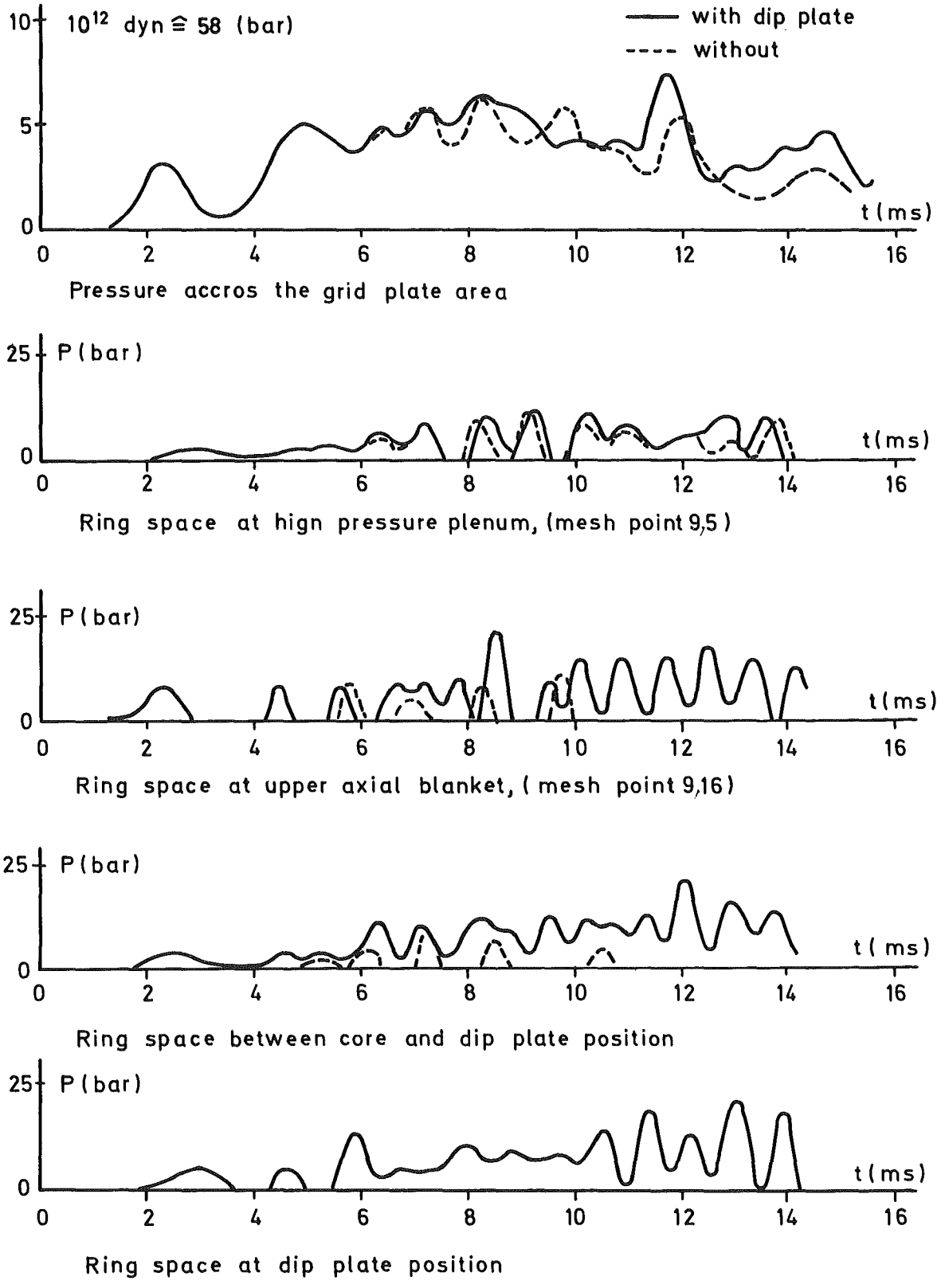

Fig. 6.2.3

REXCO calculation for 170 MWs
Pressures accross the grid plate area and in the ring space between shield tank and reactor vessel

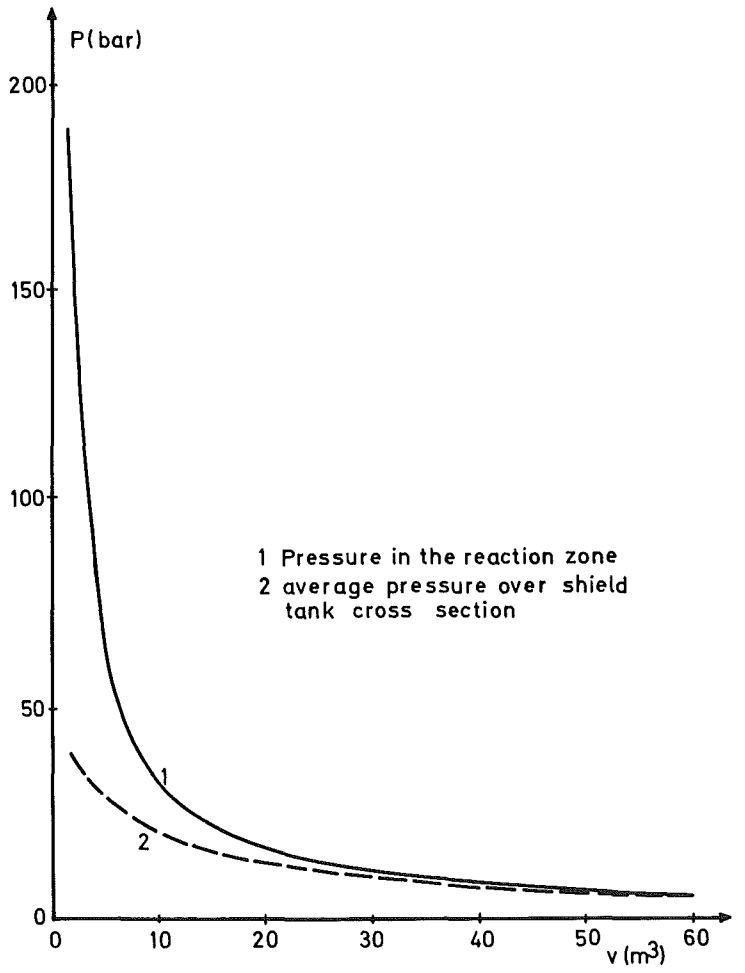

Fig:6.2.4 Pressure volume relationships for 170 MWsec

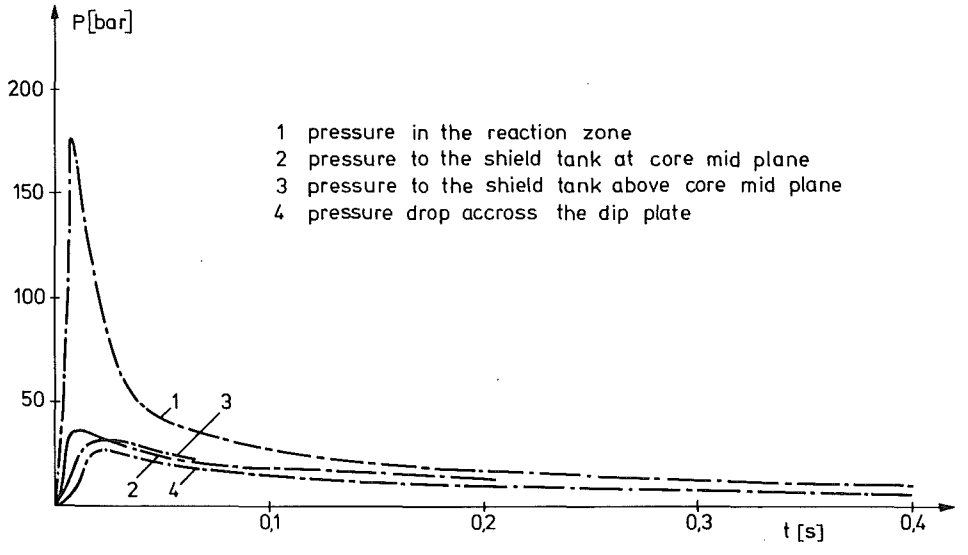

FIG. 6.2.5 PRESSURE-TIME-FUNCTIONS DRAP CALCULATION FOR 170 MWs

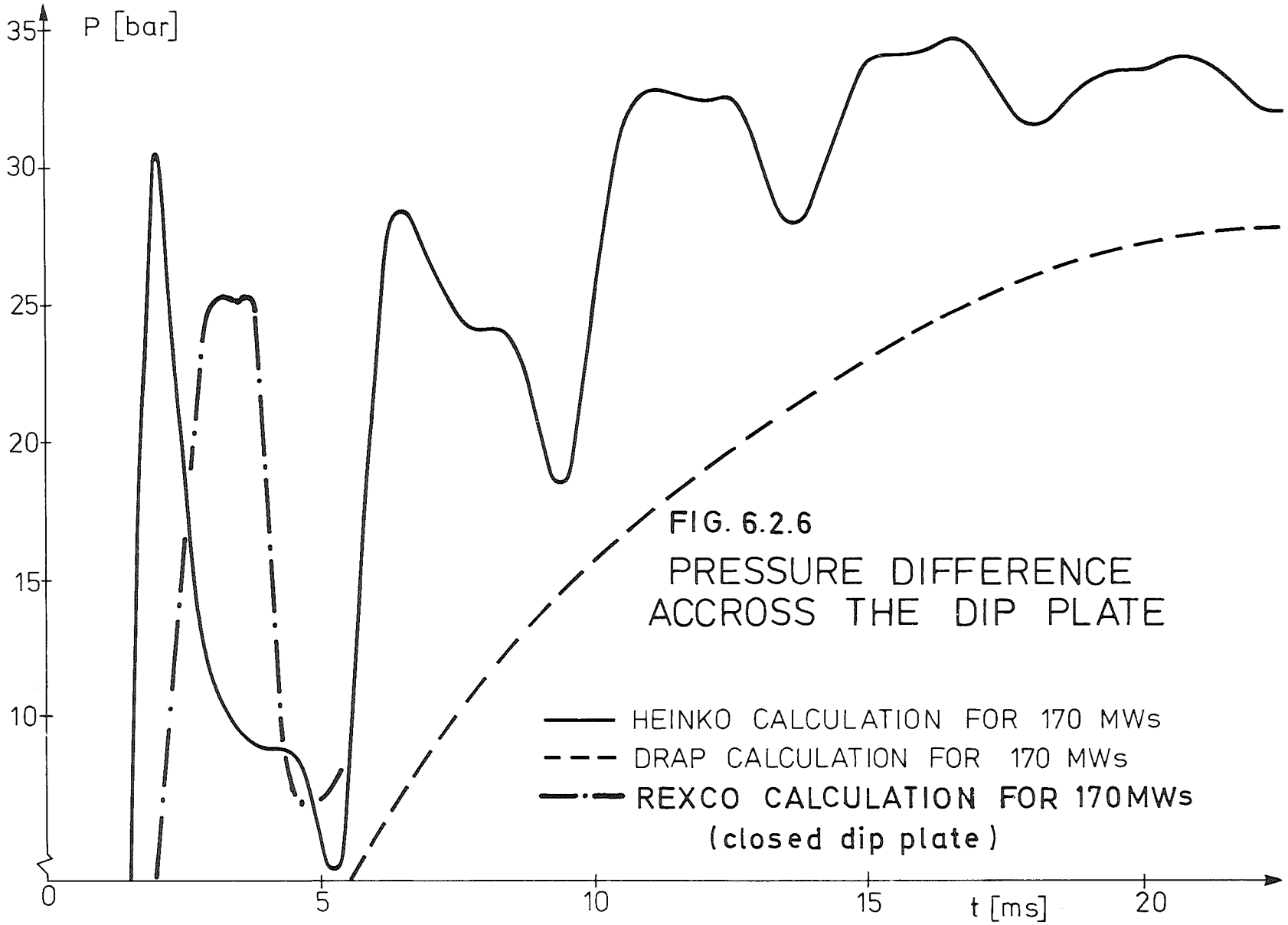

FIG. 6.2.6

PRESSURE DIFFERENCE ACCROSS THE DIP PLATE

6.3 Results of a release of mechanical energy of 1oo MWsec

The ARES-code was used for calculations of the initial phase of the dynamic stresses acting upon the vessel top system for this case. ARES and REXCO-H are equivalent and, as will be shown in /13/ and fig. 6.3.1, give the same quantitative results. The calculations for 1oo MWsec were performed in a similar way to those outlined in section 6.3, by inputing the pressure volume characteristics of fig. 5.3.1 in ARES.
The dynamical behavior of the vessel-top system was pursued with ARES for 8 msec. At the end of this phase the pressure in the reaction zone has decreased to approximately 77 /bar/ as shown in fig. 6.3.2. The reaction zone has expanded from original o.921 m^3 to 2.2o3 m^3. The average pressure, as calculated for the dipped plate, is given by fig. 6.3.3. A maximum pressure peak of about 34 bar occurs at about 2 msec.
After 8 msec, DRAP was used, employing the velocities and strains determined from ARES as initial values and the method outlined in section 6.1. These calculations were carried out over about 15o msec. As a result, fig. 6.3.4 shows the pressure curve at the dip plate as a function of time. The pressure waves cause oscillations in the reactor vessel, shield tank, vessel cover and clmaping systems. For example, fig. 6.3.5 shows the behavior of the stretch bolts of the vessel cover clamping system. The maximum stresses and strains occuring are summarized in tables 6.3.1 to 6.3.4. Fig. 6.3.6 indicates the different places in the vessel system where these strains and stresses occur during calculations with the DRAP-code. The values of tables 6.3.1 and 6.3.3 were obtained for a 5 cm thick, shield tank now provided for the design. The steel of the tank was considered unembrittled. Only at mid core level of the shield tank was a clear plastic strain (1.2%) seen in this excursion. 8o MWsec of mechanical energy is effective and is accommodated by the vessel top structure (shield tank 5 cm).

Table 6.3.1 1oo MWsec-excursion: maximum stresses and strains in the core support system:

location	ε /%o/	σ /bar/
AB	1.84	968.o
BC	o.32	173.7
BD	1.63	854.o
D1	1.45	759.o
D1U	1.81	948.o
D1O	1.21	632.5

For description of different locations see fig. 6.3.6.

Table 6.3.2 1oo MWsec: maximum tangential stresses and strains in the reactor vessel (location of segment described in fig. 6.3.6)

Segment-No.	ε /%o/	σ /bar/
1	o.465	197.6
2	1.o7	455.7
3	1.o8	458.1
4	1.o8	458.1
5	1.o8	458.1
6	1.o8	458.1
7	1.o8	458.1
8	1.o7	453.7
9	o.2o	99.7
1o	o.3o2	1.6

Table 6.3.3 1oo MWsec: maximum axial strains and stresses in tank wall (for description of location see fig. 6.3.6)

	ε_{ax} /%o/	σ_{ax} /bar/
between point 1 and 2	3.79	916.9
between point 2 and 3	3.68	913.3
between point 3 and 4	3.51	9o6.8
between point 4 and 5	3.4o	9o2.8
between point 5 and 6	3.3o	899.1
between point 6 and 7	3.21	895.2
between point 7 and 8	3.2o	87o.5
between point 8 and 9	3.27	897.6
between point 9 and 1o	1.71	713.1

Table 6.3.4 1oo MWsec: maximum stresses and strains in the shield tank and the top clamping systems

location	ε_{max}/%o/	σ_{max}/bar/
S1	12.o	1225.
S2	2.8	88o.
S3	1.94	83o.
DV	o.95	142o.

For description of location see fig. 6.3.6

FIG. 6.3.1 COMPARISON OF REXCO-H AND ARES COMPUTED PRESSURES WITH MEASURED VALUES

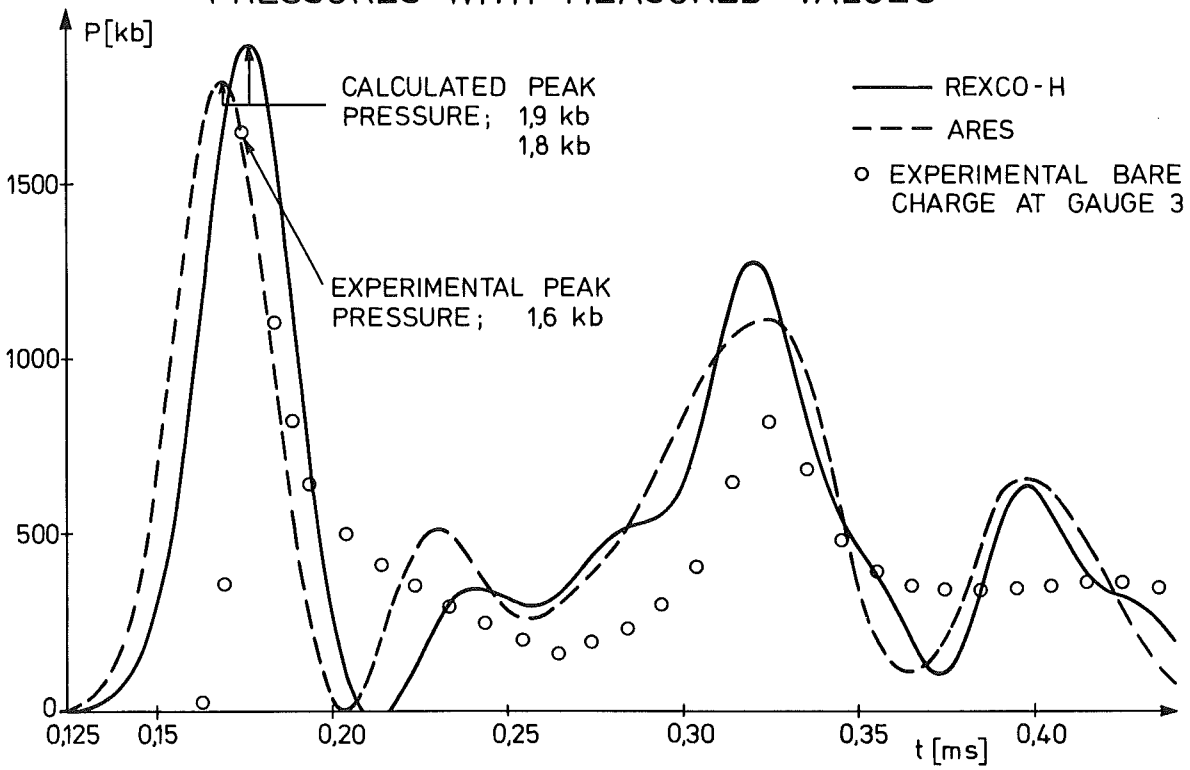

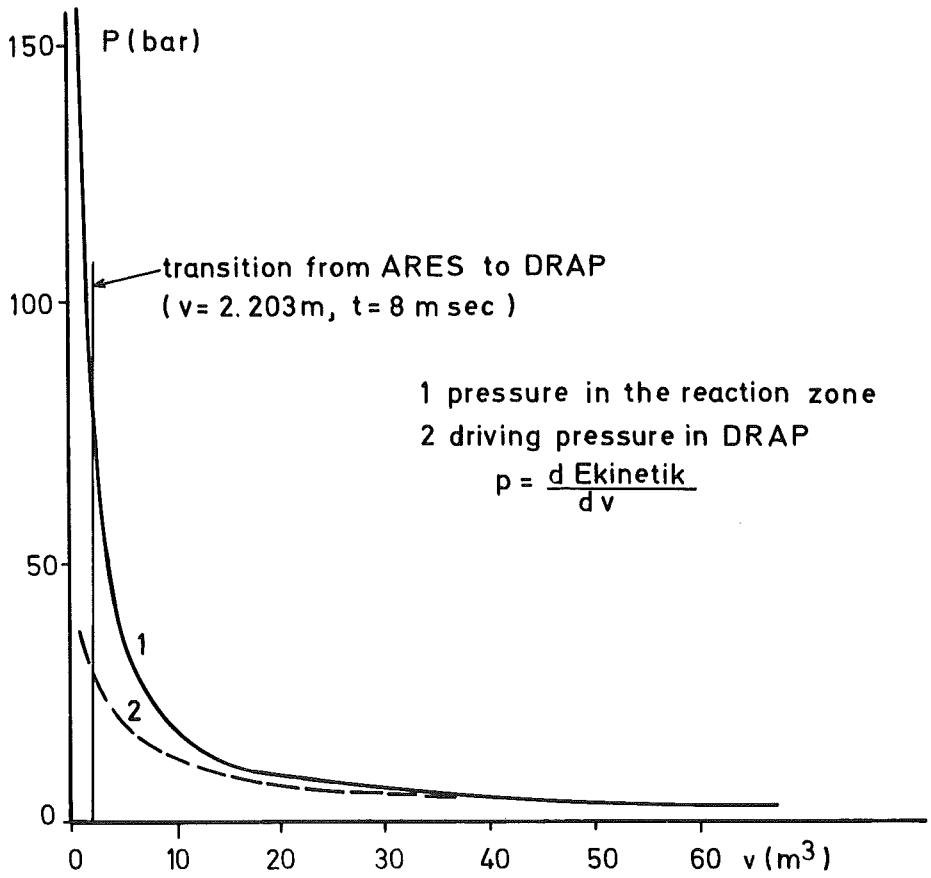

Fig.6.3.2 Pressure-volume-curve for ARES and DRAP (100MWs)

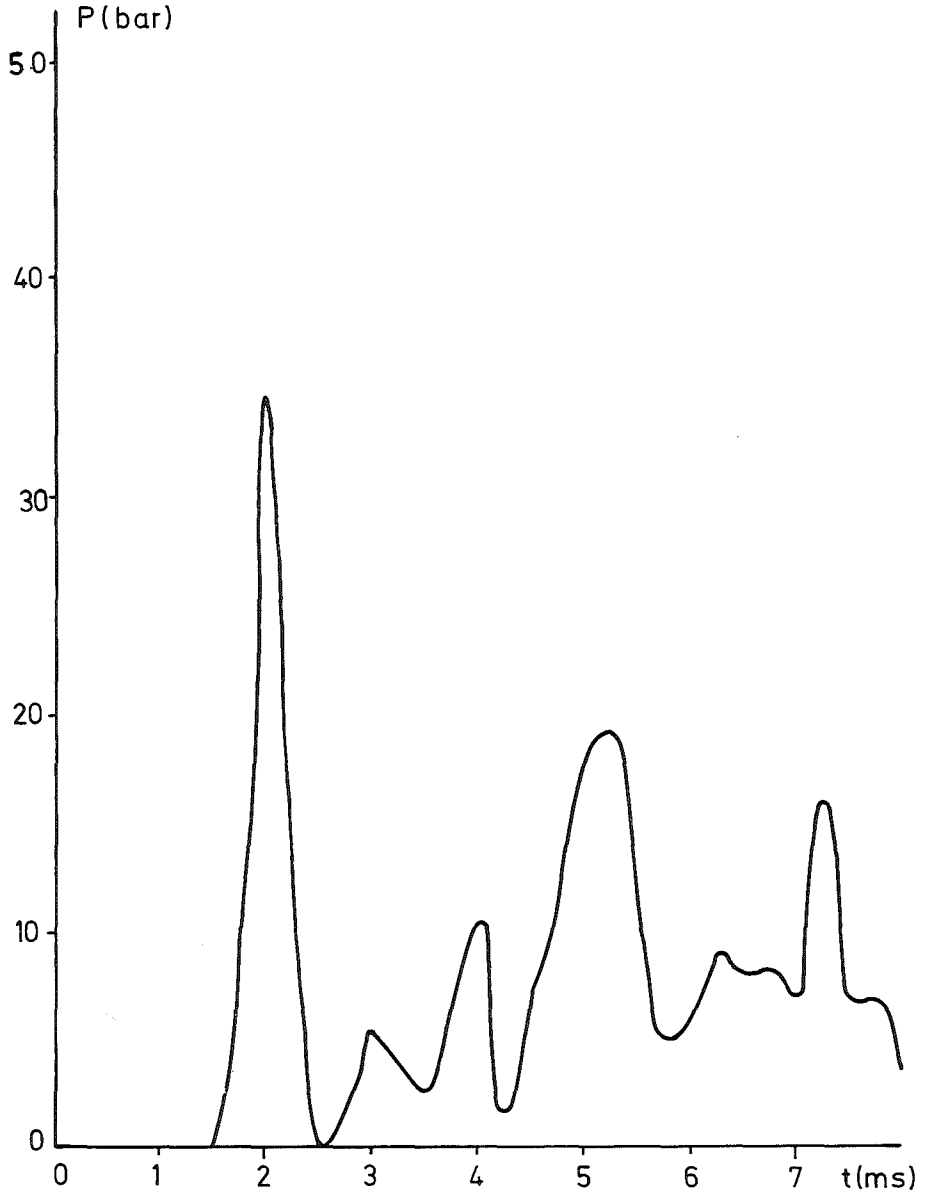

Fig. 6.3.3 ARES calculation for 100MWs
Pressure to the dip plate

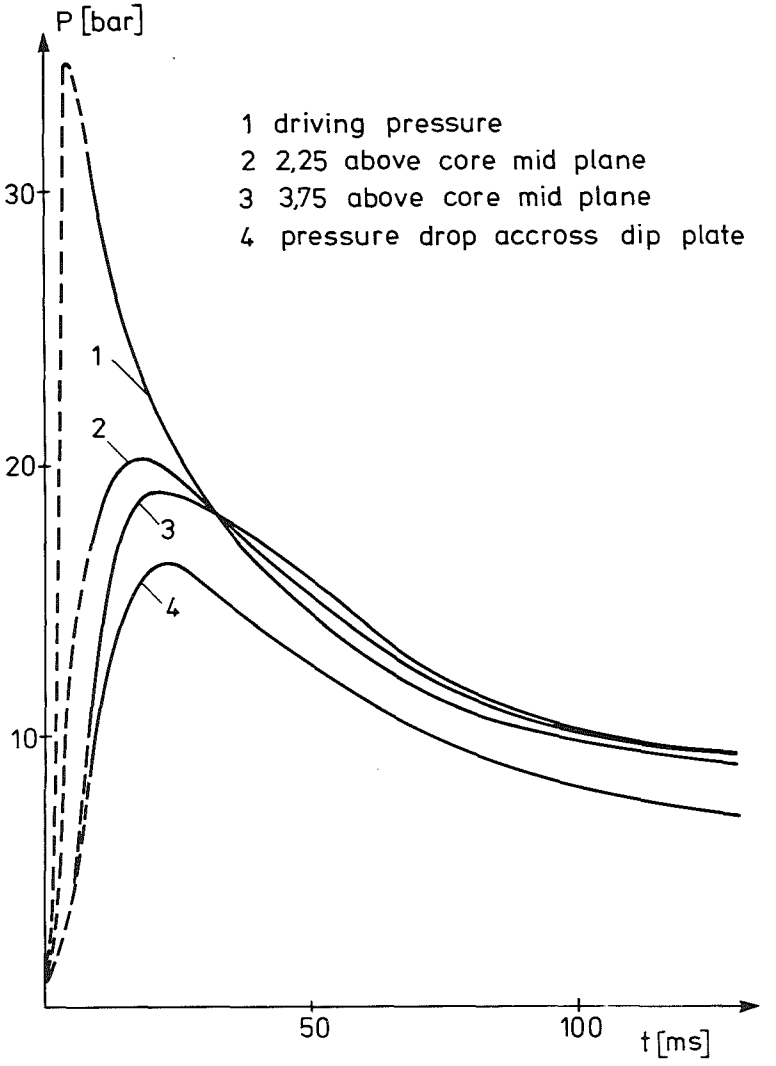

FIG. 6.3.4 PRESSURE FUNCTIONS
AT VARIOUS AXIAL POSITIONS
DRAP CALCULATION FOR 100 MWs

FIG.6.3.5

STRESSES, STRAINS AND STRAIN RATES FOR THE STRETCH BOLTS DRAP CALCULATION FOR 100 MWs

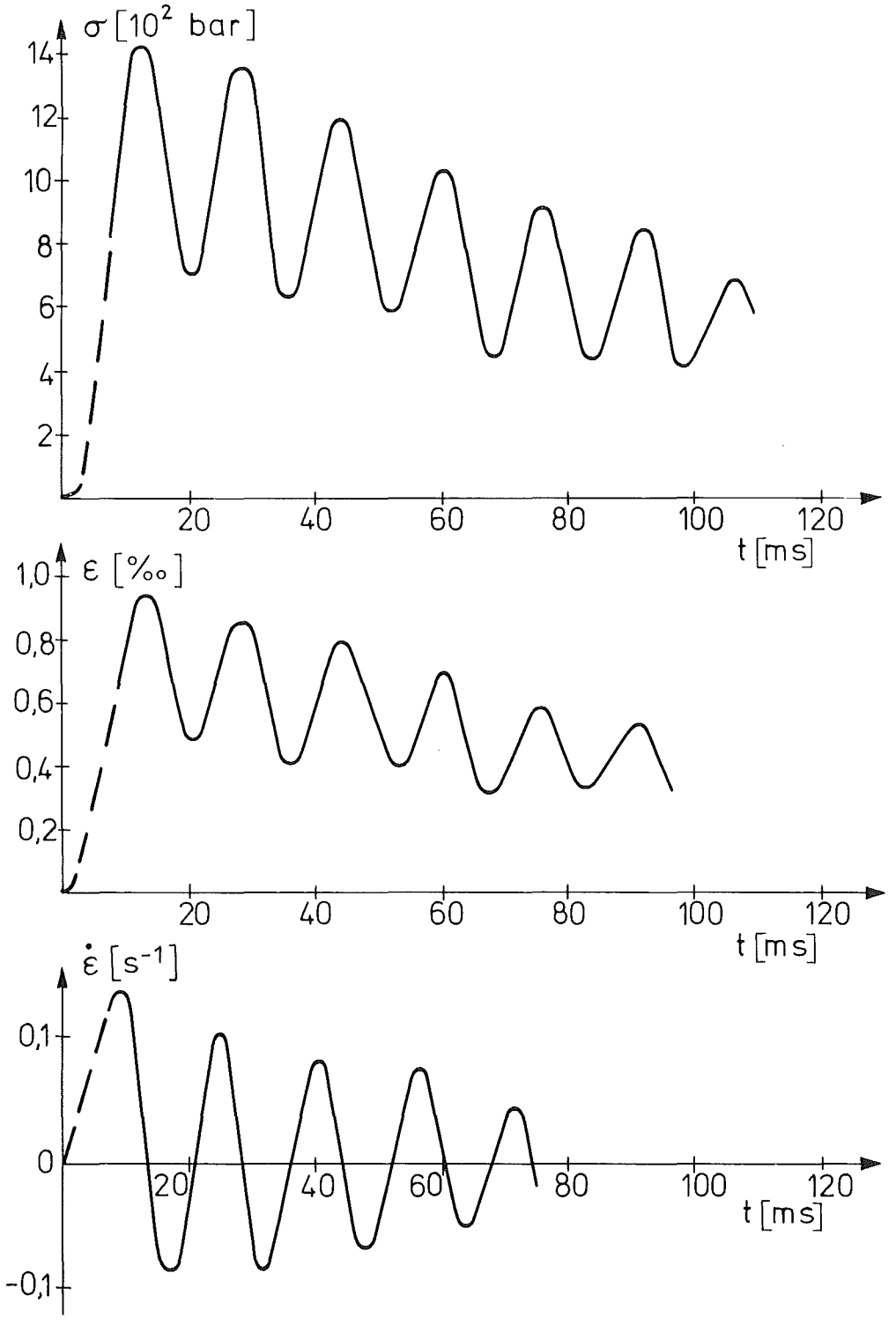

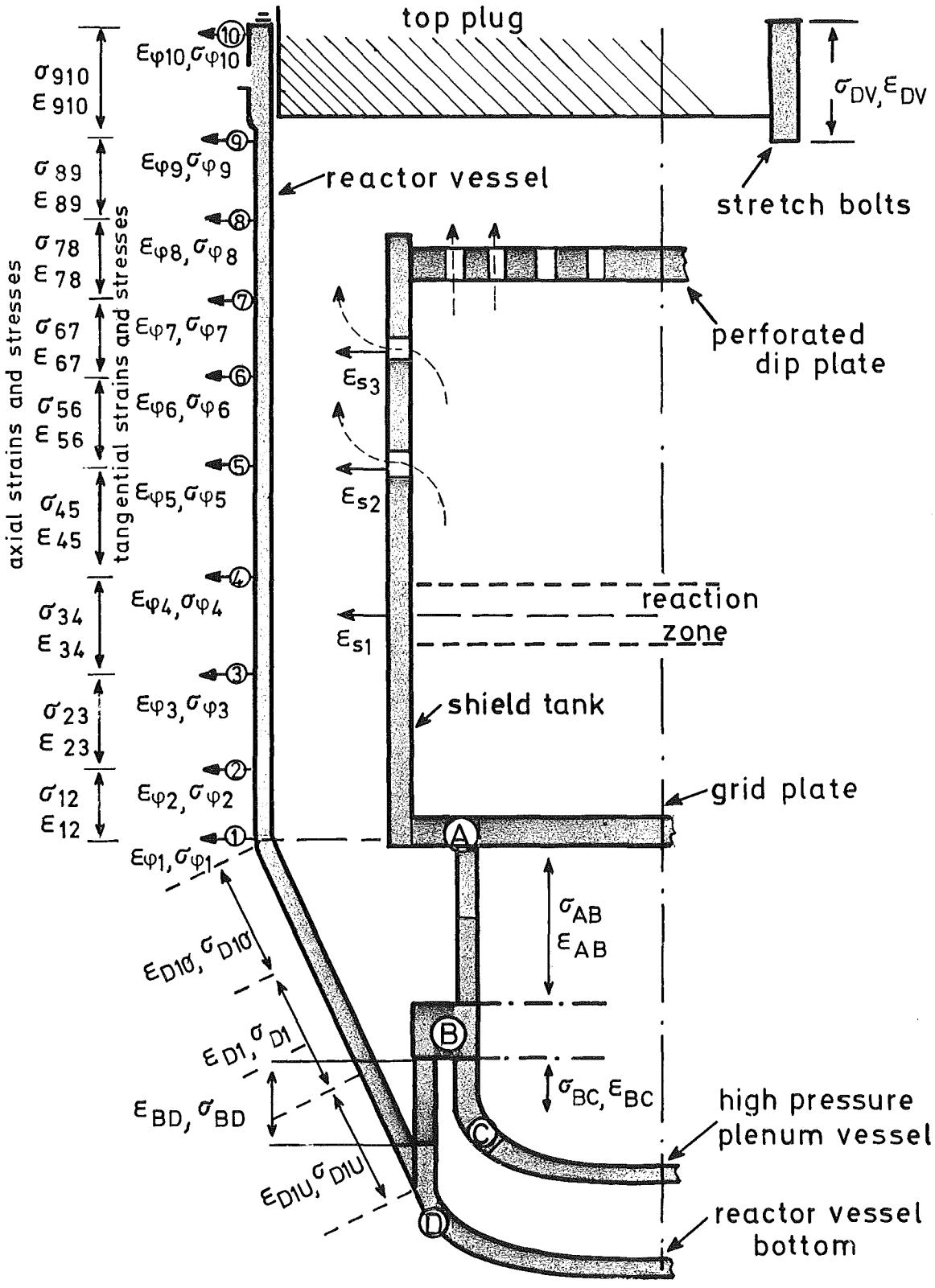

Fig.6.3.6 Distribution of sections and components for DRAP calculations

7. SUMMARY

The analysis of the coast down of all primary pumps and the simultaneous failure of the shut down systems by means of the SAS2A and VENUS-code showed that both in the case of the fresh core and of a core with a high burnup, sodium boiling followed by fuel pin slumping result in a destruction of the reactor core. In both cases, some 2100 kg of fuel was molten at the end of the disassembly phase. However, due to the physical separation between the molten fuel and the sodium there is only a sequence of less severe interactions between the liquid fuel and the sodium.

These do not give rise to maximum stresses acting upon the vessel. However, cooling of the molten core must be ensured. The analysis of the severe hypothetical reactivity incidents showed that under very conservative assumptions in the predisassembly phase, in case of a 5 $/sec reactivity ramp, the core will be mixed with the sodium still contained in the core. An assessment of the mechanical energy released in this fuel-sodium interaction using the model of Cho-Wright resulted in values in the range between 50 and 200 MWsec, depending upon the choice and combination of the most important parameters.
For calculating the stress acting upon the vessel 170 MWsec and 100 MWsec were selected from this field of parameters for analyses with the REXCO-H, ARES, HEINKO and DRAP-codes. For 170 MWsec and a shield tank 8 cm thick, a maximum strain of 1.3% resulted; approximately the same maximum plastic strain was calculated for 100 MWsec and a shield tank of 5 cm thickness. It can be concluded that the SNR-300 reactor vessel will withstand pressure loads arising from severe hypothetical accidents.

Acknowledgement

The authors wish to thank Drs. Wintzer and Bogensberger for their help in preparing the input data and Dr. W. Kastenberg for many usefull discussions and his enthousiasm in following this work.

References:

/1/ H.J. Otway, R.C. Erdmann:
A comparison of late mortality risks from reactor accidents
Nucl. Safety Vol. 11, No. 6, Dec. 197o

/2/ Die Sicherheit Schneller Natriumgekühlter Reaktoren am
Beispiel des SNR-3oo
Memorandum d. Konsortiums SNR, Bensberg 1972

/3/ Sicherheitsbericht SNR, Band 2, Konsortium SNR, Bensberg, INTAT-84a, 1971

/4/ A.E. Waltar, W.T. Sha:
An integrated model for analyizing disruptive accidents
in fast reactors
Nucl. Sci. + Eng., Vol. 44, p. 135, 1971

/5/ An appreciation of fast reactor safety (197o)
Safeguards Division, AHSB, Risley, Lancs. 197o

/6/ D.J. Stoker, R. Balent
Design of the Atomics Intern. Fast Breeder Demonstration Plant
Conf. on Fast Reactors, Palo Alto, Cal., 1971

/7/ G. Kußmaul et.al.
Super prompt-critical transients in SEFOR
ANS-Conf. paper, Las Vegas, June 1972

/8/ W. Häfele
Superpromptkritische Leistungsexkursionen in schnellen Reaktoren
Nucleonic Bd. 5, Heft 5, S. 2o1-2o8, 1963

/9/ D. Smidt, G. Heusener, G. Kessler et al.
Safety and cost analysis of a 1ooo MWe sodium cooled fast power reactor
Proceedings of the Conf. on Safety, Fuels and Core Design in Large
Fast Power Reactors
ANL 712o, Oct. 1965

/1o/ G.R. Pflasterer et al.
SEFOR-Development Program, 29th Quarterly-Report
GEAP 1oo-1o-29
May-Aug.1971

/11/ G.R. Pflasterer et al.
SEFOR-Development Program, 3oth Quarterly-Report
GEAP-1oo-1o-3o
Aug.-Oct. 1971

/12/ D.D. Freeman et al.
SEFOR experimental results and application to LMFBR's
Paper presented at Intern. Conf. on Eng. of Fast Reactors
for Safe and Reliable Operation, Karlsruhe, Oct. 1972

/13/ W. Kastenberg and E.T. Rumble,
On the analysis of the predisassembly phase of the unprotected overpower
transient accident for LMFBR's
Submitted to Nucl. Eng. + Design, Febr. 1973

/14/ B. Wolfe, personal communication, March 1971

/15/ J.C. Carter et al.
SAS1A- A Computer code for the analysis of fast reactor
power and flow transients
ANL 76o7, Oct. 197o

/16/ F.E. Dunn, G. Fischer et al.
A mutliplé bubble slug ejection model for coolant voiding
ANS Topical Meeting on new developments in reactor mathematics + applic.
Idaho Falls, March 1971

/17/ F.E. Dunn, G. Fischer et al.
The SAS2A-LMFBR accident analysis code
ANS Topical Meeting on new developments in reactor mathematics + applic.
Idaho Falls, March 1971

/18/ A. Watanabe, A.M. Judd
A computer code for predicting the behavior of oxide fuel
in accidents
ANS-Meeting, Miami, June 1971

/19/ F.E. Dunn et al.
Comparison of SAS2A sodium boiling analysis with experiment
ANS-Conf. paper, Las Vegas, June 1972

/20/ G.J. Fischer et al.
Progress analysis of severe accidents
Int. Conf. on engineering of fast reactors for safe and reliable
Operations, Karlsruhe Oct. 1972

/21/ D.H. Cho, R.W. Wright, R.O. Ivins
Pressure Generation by molten fuel-coolant interactions under
LMFBR accident conditions
ANS-Topical Meeting on new developments in reactor mathematics + applic.
Idaho Falls, March 1971

/22/ W.R. Bohl
Fuel slumping: Preliminary Analysis and Suggestions
ANL-report to be published, 1972

/23/ G.J. Fischer, M.G. Stevenson
Analysis of fuel motion after loss of integrity of pins (slumping)
ANL 7872, p. 8.2, 1971

/24/ W.T. Sha, T.H. Hughes
VENUS - A 2-dim. coupled neutronics-hydrodynamics
Computer Program for fast reactor power excursion
ANL 77o1, Oct. 197o

/25/ J.F. Jackson, R.B. Nicholson
Partial Voiding and Fission product gas in LMFBR Disassembly Calculations
ANS-Conf. paper, Miami, Nov. 71

/26/ J.F. Jackson, R.B. Nicholson
Disassembly Accident Analysis, including Computer Code Development and
Sensitivity Studies
ANL-Reactor Development Program Report RDP-1, Jan. 72

/27/ Y.W. Chang, J. Gvildys, S.H. Fistedis
Two-dimensional Hydrodynamic Analysis of
Primary Containment
ANL 7498, Nov. 1969

/28/ G. Cinelli, J. Gvildys, S.H. Fistedis
Inclastic response of primary reactor containment to high-energy excursions
ANL 7499, Nov. 1969

/29/ K. Doerbecker: ARES: ein zweidimensionales Rechenprogramm zur
Beschreibung der kurzzeitigen Auswirkungen einer hypothetischen un-
kontrollierten nuklearen Exkursion auf Reaktortank, Drehdeckel und
Einbauten, gzeigt am Beispiel des SNR-3oo
Reaktortagung Hamburg, 11.-14.1.1972

/3o/ L. Lange
Analyse des dyn. Verhaltens eines schnellen Reaktors nach einer überprompt-
kritischen Energiefreisetzung (DRAP)
Interatom-Arbeitsbericht 69/2, 23.1.1969

/31/ W. Häfele, G. Kessler
SNR: The German Benelux fast Breeder
Nucl. News, March 1972

/32/ E. Kiefhaber et al.
MOXTOT-Cross section set
Evaluation of critical experiments by recent methods and data
BNES-Conf., London, June 1969

/33/ G.R. Keepin
Physics of nuclear kinetics
Addison Wesly Publishing Company, Inc., 1965

/34/ H. Kämpf
Allgemeine Spaltgleichung für den Wärmedurchgang Brennstoff-Hülle
KFK 6o4, 1967

/35/ A. Gerken, H. Kämpf, G. Karsten
Theoretical and Computer Analysis on the behavior of fast reactor fuel pins and related parts of the core under operational conditions
KFK 878,1968

/36/ C.N. Craig, J.L. Krankota, W.E. Baily
Effective thermal conductivity of PuO_2-UO_2 at high burn-up
GEAP-137o3, March 1971

/37/ C.N. Craig, W.E. Baily
In-pile comparison of effective thermal conductivity of PuO_2-UO_2 mixed oxides
GEAP-5556, Jan. 1969

/38/ C.N. Craig, G.R. Hull, W.E. Baily
Heat transfer coefficients between fuel and cladding in oxide fuel rods
GEAP 5748, Jan. 1968

/39/ A. Pee
Stoffdaten von Natrium
KFK 924, Febr. 1969

/4o/ H. Blank et al.
Zwei- und Mehrstoffsysteme mit Plutonium
KFK 1o5, Juni 62

/41/ K.D. Cloß
Physikalische und mech. Eigenschaften von Hüllmaterialien
PSB-Bericht Nr. 1oo1 (Karlsruhe, Aug. 1968)

/42/ U. Schumann
MAPBLIB - Ein Programmsystem zur Bereitstellung von Stoffdaten für Rechenprogramme
KFK 1253, Sept. 7o

/43/ H. Böhm
Hüllwerkstoffe für schnelle Brutreaktoren
KFK 985, Juli 69

/44/ F.A. Comprelli, H.J. Busboom, M.F. Gebhardt
Mechanical properties of irradiated type 3o4 and type 316 stainless steel in fast reactors
GEAP 1oo62, June 1969

/45/ H. Kämpf, M. Elbel, K. Kummerer
Brennstabmodelltheorie
KFK 14oo, Okt. 71

/46/ T. Lauritzen, A. Withrop, G.P. Ferguson
Mechanical properties evaluation of austenitic stainless irradiated in EBR-II
GEAP-1oo66, June 69

/47/ G.F. Schultheiß, Experimentelle Untersuchungen des Siedeverzugs von Natrium an künstlichen Oberflächenrauhigkeiten
KFK 1332, Dez. 7o

/48/ D. Logan, C.J. Baroczy, J.A. Landoni, H.A. Morewitz
Effects of velocity, oxide level and flow transients on boiling initiation in sodium
AI-AEC-12939, Sept. 7o

/49/ D. Logan, C.J. Baroczy, J.A. Landoni, H.A. Morewitz
Studies of boiling initiation for sodium flowing in a heated channel
AI-AEC-12767, Sept. 69

/5o/ J.A. Landoni
Analysis of the statistical distribution of incipient boiling
AI-AEC-129o6, Dec. 69

/51/ A.E. Waltar et al.
Fast reactor safety implications of recent assessments of fuel pin transient behavior
Int. Conf. on engineering of fast reactors for safe and reliable operations
Karlsruhe, Oct. 9-13, 1972

/53/ D.R. Armstrong, F.J. Testa, R. Raridon
Interaction of sodium with molten UO_2 and stainless steel using a dropping mode of contact
ANL 789o, Dec. 71

/54/ W.E. Kastenberg, E.T. Rumble
Preliminary analysis of the predisassembly phase of the unprotected overpower transient accident for SNR-3oo
KFK 1782, Febr. 73

/55/ R. Hübner, W. Schnitker
Berechnung des Druckaufbaus in kompressiblen Medien bei Na-H_2O-Reaktionen
Reaktortagung Bonn, 3o.3.-2.4.71

/56/ K. Doerbecker
ARES: Ein 2-dim. Computerprogramm zur Berechnung der kurzfristigen Auswirkungen einer hypothetischen nuklearen Exkursion eines schnellen natriumgekühlten Kernreaktors auf das primäre Containment
Interatom-Notiz 35.95.2, 22.1o.71

/57/ L. Lange
Erweiterung des DRAP-Codes unter dem Gesichtspunkt der neuen Sicherheitsphilosophie bei einer Bethe-Tait-Exkursion
Interatom-Notiz 35.42.9

/58/ L. Lange
Dynamisches Verhalten der Kernhaltestruktur bei einer Nuklearexkursion
Interatom-Notiz 35.1o2.1

/59/ A. Padilla
Lecture Series on Fast Reactor Safety and Technology:
Chapter xvu: Energy release mechanisms
BNWL-SA 3o93 (197o)

/6o/ D.L. Booth
The thermodynamic properties of UO_2 and sodium
TRG-Report 1971 (R/X), 1969

/61/ R.A. Meyer, B. Wolfe, N.F. Friedman, R. Seifert
Fast Reactor meltdown accidents using Bethe-Tait-analysis
GEAP 48o9 (1967)

/62/ L. Caldarola, personal communication 1972

/63/ J.C. Hesson, R.H. Sevy, T.J. Marciniak
Postaccident heat removal in LMFBRs: In-vessel considerations
ANL-7859, 1971

/64/ A.W. Cronenberg
A thermodynamical model for molten UO_2-Na-interaction
certaining to fast reactor fuel failure accidents
Dissertation, Northwestern University

/65/ F.D. Murnaghan
The compressibility of media under extreme pressures
Proc. Natl. Acad. Sci. 3o, 244-247 (1944)

/66/ Y.W. Chang, Argonne National Laboratory
Privat Communication

/67/ G. Heusener, G. Kessler et al.
Analysis of hypothetical accidents for SNR-3oo
Int. Conf. on eng. of fast reactors for safe and reliable operation
Karlsruhe, Oct. 1972

/68/ L. Caldarola
A theoretical model for the molten fuel-sodium interaction in a
nuclear fast reactor
Nucl. Eng. + Design, Vol 22, p. 175, 1972

/69/ Stevens and Witte
Transient film and transition boiling from a sphere
Int. Journal Heat and Mass Transfer, Vol. 14, p. 443.45o, 1971

/7o/ Mohamed K. Farahad
Transient boiling heat transfer from spheres to sodium
ANL 79o9, 1972

/71/ T.C. Chawla, B.M. Hoglund
A study of coolant transients during a rapid fission gas
release in a fast reactor subassembly
ANL 7651, Jan. 71